



The
University
Of
Sheffield.

Faculty of Engineering / Department of Mechanical Engineering

**Characterization of blanking induced magneto-mechanical
cut edge defects in non-oriented electrical steel**

By:

Ammar Dawood Ghali Al-Rubaye

A thesis submitted to the Department of Mechanical Engineering,
University of Sheffield in partial fulfilment of the requirements
for the degree of Doctor of Philosophy

Academic supervisors:

Dr. Hassan Ghadbeigi (MEC)

Prof. Kais Atallah (EEE)

July 2019

Abstract

Electrical steels play a vital role in the generation and use of electricity as they are widely used in a range of electrical equipment for industrial and domestic appliances. The material is usually manufactured in the form of cold-rolled thin strips that are stacked together to form the laminated stacks used to form the stator and rotor parts of electric motors. As the individual layers are made mostly by blanking and piercing processes the quality of the final product directly affects the performance of the electrical machines. The blanking process results in local plastic deformation and texture modification in electrical steels which will affect the magnetic and mechanical performance of the electric motors and transformers. Therefore, the main aim of the project is to obtain a better understanding of the global and local magneto-mechanical properties of the sheet material at the cut edge and vicinity area to optimise design parameters used for the final products.

An experimental investigation was designed and implemented to study the mechanism of blanking operation and local magneto-mechanical properties of thin strip electrical steels at the cut edge. The deformation at the cut edges was identified regarding main blanking parameters such as deformation rate, material thickness and sheet orientation at a specific clearance. The thickness of individual laminates plays a critical role in the magnetic performance of the manufactured power units. However, the thinner gauges introduce challenges to the manufacturing and processing of the material, especially in the high-speed cutting operations. Therefore the study was considered using two different thin gauge thickness with different grain orientations of electrical steel with nominated thickness 0.2 mm and compare results with those for 0.35 mm sheet thickness.

A novel blanking experiment together with Digital Image Correlation was designed in order to identify local strain distribution in laminates of both the used thicknesses during the blanking process. That was done to achieve a better understanding of deformation induced microstructural damage in the vicinity of the cut edge. Also, a bespoke single sheet magnetic tester was designed and built to determine the effect of blanking induced cut edge damage on magnetic properties in the form of hysteresis losses and quantify magnetic deterioration in the produced laminations. The microstructure of cut edge deformation and the fracture surface was observed using both optical and

scanning electron microscopes. Furthermore, Nano-indentations tests were implemented in the deformed area at the cut edges to characterize local deformation.

The results showed that the cutting process parameters have a significant impact on the mechanical and magnetic properties and the cut edge quality. The reduced thickness also introduced a great challenge in preparing samples for all the tests that were done. Sheet thickness had a significant role on the hysteresis loss and extension of deformation and strain amount. The results also showed that the blanking speed also has an important influence on blanking results and thereby more affected in mechanical and magnetic properties. However, it was observed that the thickness of the laminations plays an important role due to the small number of grains in the thickness direction causing the individual grains to have a significantly high effect on the local properties of the produced parts. The change in the cutting location regarding the grains could cause different deformation state. This variations in the blanking deformation make it very difficult to determine the extension of deformation or give clear trend to the blanking behaviour effects upon the mechanical and magnetic properties.

The achieved results can be used to enhance our knowledge and be practically implemented through the interconnection between the inputs of the cutting process and the outputs represented by the edge quality and affected properties. This investigation can also be incorporated in improving the manufacturing process in order to manage magnetic property deterioration, thereby exploiting the full potential of the magnetic materials; as a result, improving the machine's performance.

Declaration

Described in this dissertation is work performed in the Department of Mechanical Engineering, the University of Sheffield between October 2014 and October 2018. I hereby declare that no part of this work has been submitted as an exercise for a degree at this or any other university. This thesis is entirely the result of my own work and includes nothing which is the outcome of collaboration, except when stated otherwise. This thesis contains 127 figures and 10 tables and about 50,000 words.

Dedication

To my parents Father and mother,

To my family, wife and children Rusul and Mohammed,

To my brothers and sisters

I dedicate this work.

Ammar

Acknowledgements

First of all, I would like to thank Almighty Allah for everything in my life.

This research project would not have been possible without the support of many people;

Initially, I would like to express my deep sincere gratitude to my supervisor, Dr Hassan Ghadbeigi for his support and guidance throughout the project and for the knowledge that I received from him and his great amount of time and effort he spent to help me to accomplish this project,

I would also thank my second supervisor Professor Kais Atallah for the valuable information that he gave me and his support during my study,

I would like to thank the Ministry of Higher Education and Scientific Research in Iraq to nominating me to the scholarship and financial support to complete my high education.

I also want to thank all the technical staff in the Mechanical, Electrical, and Materials Engineering Departments at the University of Sheffield, who helped me to carry out my experimental work and providing laboratory facilities,

I also thank all my friends and colleagues for their supporting and cooperation,

I would like to express my gratitude to my family whose have always given me their support for the duration of my studies, my wife and my children,

Finally, I would like to thank from all my heart, my parents for their encouragement, and continue praying for me, and for supporting me spiritually.

Nomenclature

Symbols

μ	Permeability, tesla/A/m
μ_0	Permeability of free space, $4\pi \times 10^{-7}$
Φ	Quantity of flux, weber
ρ	Resistivity, $\Omega\cdot\text{m}$, ohm metres
A	Area, m^2
B	Induction, tesla
f	Frequency, Hz
H	Applied field, A/m
HC	Coercive force, A/m
I	Current, amps
J	Intrinsic magnetisation (B–H), tesla
N, n	Number of winding turns
R	Resistance, ohms
T	Temperature (Celsius)
t	Time
V	Voltage, volts
W	Power, watts

Abbreviations

ES	Electrical steel
GO	Grain orientation
NGO	Non grain orientation
SST	Single Sheet Tester
DW	Domain wall
ASM	American Society for Metals
ASME	American Society of Mechanical Engineers
ASTM	American Society for Testing and Materials
COE	Cube-on-edge
DC	Direct current
AC	Alternative current
DIC	Digital image correlation
FCC	Face-centred cubic
HAZ	Heat-affected zone
DAZ	Deformation affected zone
SEM	Scanning electron microscopy

Contents

Abstract	I
Declaration.....	III
Dedication.....	IV
Acknowledgements.....	V
Nomenclature.....	VI
Symbols	VI
Abbreviations.....	VI
List of Figures	X
List of Tables	XV
1 Introduction.....	1
1.1 Introduction.....	1
1.2 Problem Description.....	2
1.3 Research objectives and novelty	4
1.4 Thesis Outline	5
2 Literature review	6
2.1 Introduction	6
2.2 Electrical Steel (E.S)	7
2.2.1 Electrical steel applications	7
2.2.2 Classification of electrical steel	8
2.2.3 Material isotropy and grains orientation.....	9
2.2.4 Metallurgical properties.....	11
2.2.5 Methods for manufacturing electrical steels.....	13
2.3 Magnetic properties of ES.....	16
2.3.1 Ferromagnetic domains and magnetic properties	16
2.3.2 Domain structure and domain walls motion	17
2.3.3 Parameters of magnetic properties and hysteresis phenomena.....	19
2.3.4 Magnetic power losses.....	22
2.4 Measuring magnetic properties of electrical steel sheets.....	24
2.5 Methods for cutting laminations	27
2.6 Blanking process	35
2.6.1 Mechanism of the blanking process.....	36
2.6.2 Analysis of applied stresses during the blanking process.....	37
2.6.3 Influence of various process parameters on blanked edge quality	39

2.6.4	Effect of blanking parameters on the cutting force and cut edge quality .	40
2.6.5	Effect of sheet thickness on the cutting force and cut edge quality.....	43
2.6.6	Effect of blanking speed on the cutting force and cut edge quality.....	45
2.6.7	Strain fields measurement.....	47
2.7	Effect of plastic deformation and residual stress on the magnetic properties..	50
2.8	Effects of blanking on the magnetic properties.....	56
2.9	Characterization of local deformation using hardness variations	59
2.10	Summary	61
3	The experimental methodology	64
3.1	Introduction	64
3.2	Material selection	65
3.3	Measurement of mechanical properties	66
3.3.1	Tensile tests.....	66
3.3.2	Tensile strain measurement using DIC	68
3.3.3	Blanking dies setup	70
3.3.4	Blanking dies design	71
3.3.5	Blanking parameters	72
3.3.6	Blanking force assessments	74
3.3.7	In-situ strain measurement during blanking using DIC	74
3.4	Nano-indentation tests.....	78
3.5	Magnetic tests using the single sheet tester.....	82
3.5.1	Design of the new SST apparatus	83
3.5.2	Determination of magnetization curve and hysteresis loss.....	86
3.5.3	Uncertainty and limitations of determination the magnetization curve and complete hysteresis loop.....	89
3.6	Microstructural analysis	90
3.6.1	Samples preparation.....	90
3.6.2	Microstructure examination	92
3.7	Summary	93
4	Experimental results.....	94
4.1	Introduction	94
4.2	Characterization of mechanical properties.....	94
4.2.1	Tensile tests.....	94
4.2.2	Strain distribution in uniaxial loading	96
4.3	Blanking process results.....	103

4.3.1	Blanking load stroke	103
4.3.2	Strain distribution in the blanking process	105
4.3.3	Characterization of local deformation using Nano-indentation.....	115
4.4	Magnetic properties outcomes	120
4.4.1	Effect of uniaxial deformation on magnetic properties	120
4.4.2	Effect of induced blanking deformation on magnetic properties	125
4.5	Microstructural analysis of the cut edge	131
4.5.1	Investigation of the induced cut edge fracture surface	131
4.5.2	Deformation analysis of cut edge fracture	140
4.5.3	Estimation of the depth of cut edge deformation.....	146
4.5.4	Estimation of the grain size and number over the sheet thickness	148
4.6	Summary	149
5	Discussions and statistical analysis	151
5.1	Introduction	151
5.2	The critical influences of the cut edge microstructure	151
5.3	Plastic strain and magnetic properties under uniaxial tension	154
5.4	Defects evolution during the blanking process	156
5.5	Blanking local strain and the depth of deformation.....	158
5.6	The effects of blanking plastic deformation on magnetic properties	162
5.7	Statistical Analysis	164
5.7.1	Interaction between parameters and response	165
5.7.2	Analysis of Variance (ANOVA).....	165
5.7.3	The impact strength of the maximum equivalent strain versus sheet thickness, blanking speed, and sheet orientation.....	166
5.7.4	The impact strength of the maximum cutting force of the full die versus sheet thickness, blanking speed, and sheet orientation.....	168
5.7.5	The impact strength of the maximum hysteresis loss versus thickness, blanking speed, sheet orientation	169
5.8	Summary	171
6	Conclusions and future works.....	172
6.1	Conclusions	172
6.2	Recommendations for future work.....	174
	References.....	177
	Appendix A.....	187
	Appendix B	188

List of Figures

Figure 2.1: Main applications of ES: a) electrical motor, b) electrical transformer	8
Figure 2.2: Types of magnetic materials	8
Figure 2.3: Electrical steel grains orientation system: (a) B.C.C lattice, (b, c) the anisotropy of ES due to the oriented texture	10
Figure 2.4: Micrograph of NGO electrical steel etched in 2% Nital	11
Figure 2.5: Effects of some elements on iron properties, a) material resistivity, b) Magnetic and electrical properties	12
Figure 2.6: Phase diagram of Fe-Si alloys and the effect of Si on the material structure	12
Figure 2.7: Electrical steel making outline	14
Figure 2.8: The Production route of fully processed GO electrical steel	15
Figure 2.9: The Production route of fully processed NGO electrical steel	15
Figure 2.10: Typical domain structures observed in ferroelectric material	17
Figure 2.11: Schematic of spin rotation in a 180° domain wall	18
Figure 2.12: Observations of domains at grain boundaries in NGO steel	18
Figure 2.13: Initial magnetization curve and permeability for iron	20
Figure 2.14: Typical magnetization and hysteresis curve	21
Figure 2.15: a) Differences between the AC and DC magnetization on the hysteresis loops, b) Effect of applied current and flux density on the hysteresis loops	22
Figure 2.16: Lamination sheet and inter-laminar eddy current	24
Figure 2.17: Magnetic measurement methods used to determine magnetic properties and iron losses in electrical steel sheets	25
Figure 2.18: Single sheet tester fixtures for measuring magnetic properties	25
Figure 2.19: Lamination cutting methods, a) blanking, b) Wire EDM, c) Laser cutting, and d) water-jet	28
Figure 2.20: Effects of different sheet cutting processes on the cut edge	30
Figure 2.21: Cut edge surface roughness produced by different cutting methods	30
Figure 2.22: Blanking process mechanism	35
Figure 2.23: Punching, blanking, and piercing operations	35
Figure 2.24: Blanking process deformation stages	36
Figure 2.25: Deformations zones of the cut edge: a) characteristic edge in blanking process, b) blank side-scheme areas	37
Figure 2.26: Forces distribution in the workpiece during blanking process	38
Figure 2.27: Typical load-stroke curve of a blanking	38
Figure 2.28: Parameters affecting the blanking process	39

Figure 2.29: a) Effects of clearance on the deformations zone and vicinity areas, b) Vickers hardness contours expressing the cold working in the shared region	40
Figure 2.30: Effect of clearance and tools radii on deformations of cut edge	41
Figure 2.31: The principle of the DIC measurement method based on the differences between the target subset and the reference subset	48
Figure 2.32: TEM micrographs of Fe 3% Si under tensile loading	51
Figure 2.33: Hysteresis loops of elastically and plastically deformed samples for uniaxial tensile stress and magnetic flux density in RD and TD	52
Figure 2.34: Effect of various stresses on the energy loss	53
Figure 2.35: Hysteresis loops measured at elastic and plastic tensile stresses	55
Figure 2.36: Deformation and strains visible at the edge, induced by blanking process	56
Figure 3.1: Outline of the research structure	65
Figure 3.2: Size and orientation of tensile samples in both RD and TD according to the sheet rolling direction.....	67
Figure 3.3: Material under tension at different strain states	67
Figure 3.4: Tensile tests at different plastic extensions.....	68
Figure 3.5: Macrograph of the tensile test sample with random speckle pattern.....	68
Figure 3.6: Full blanking die (Type A)	70
Figure 3.7: One side free blanking die (Type B)	71
Figure 3.8: A virtual representation of the blanked samples to illustrate sample size, orientation, and test locations regarding the sheet rolling direction.....	73
Figure 3.9: Blanking tools, machine control, and Lavisoin DIC system.....	75
Figure 3.10: Schematic of blanking and DIC test setup.....	77
Figure 3.11: DIC and specimen setup for deformation area measurement of the ES.....	77
Figure 3.12: Nano-indentation system.....	79
Figure 3.13: (a) Elastic-plastic deformation at the maximum applied load, (b) Plastic deformation after releasing the load	79
Figure 3.14: Load-penetration curve of the Nano-indentation test.....	80
Figure 3.15: Determination of the actual position of the indenter in the Nano-indentation system.....	81
Figure 3.16: SST system design and coils arrangement.....	84
Figure 3.17: (a) Flux path in closed double yoke system, (b) Flux coil path in ES sheet.....	85
Figure 3.18: SST equipment parts connections and electrical circuit.....	85
Figure 3.19: Full design of new single sheet magnetic tester	86
Figure 3.20: Determination of hysteresis loss: (a) entire hysteresis curve, (b) absorbed energy area w_1 , (c) dissipated energy area w_2	87
Figure 3.21: Arrangement of the cut samples in the cold mounting.....	91

Figure 4.1: Tensile rate sensitivity at different test speeds, a) 0.2 RD, b) 0.2 TD, c) maximum UTS and yield stress values with standard deviation error bars.....	95
Figure 4.2: Tensile rate sensitivity at different test speeds, a) 0.35 RD, b) 0.35 TD, c) maximum UTS and yield stress values with standard deviation error bars.....	96
Figure 4.3: Stress-Strain curves for 0.2, 0.35 in RD, TD samples at 10 mm/min test speed.....	97
Figure 4.4: Macrograph of tensile samples at different plastic extensions	97
Figure 4.5: The strain error analysis for the tensile samples determined with DIC	98
Figure 4.6: Maximum normal strain distribution of tensile samples at different stages of extension during the tensile tests of 0.2 RD.....	99
Figure 4.7: Maximum normal strain distribution of tensile samples at different stages of extension during the tensile tests of 0.2 TD.....	100
Figure 4.8: Maximum normal strain distribution of tensile samples at different stages of extension during the tensile tests of 0.35 RD.....	101
Figure 4.9: Maximum normal strain distribution of tensile samples at different stages of extension during the tensile tests of 0.35 TD.....	102
Figure 4.10: Blanking load-stroke displacements for 0.2 and 0.35, RD and TD samples.....	103
Figure 4.11: Maximum load stroke at different blanking speeds for full die.....	104
Figure 4.12: Maximum load stroke at different blanking speeds for the die type B.....	104
Figure 4.13: The strain error analysis for the blanking samples determined with DIC.....	105
Figure 4.14: Maximum equivalent strain distributions during the blanking process in different stages at 100 mm/min for 0.2 RD 100 sample.....	108
Figure 4.15: Maximum equivalent strain distributions during the blanking process in different stages at 500 mm/min for 0.2 RD 500 sample.....	108
Figure 4.16: Maximum equivalent strain distributions during the blanking process in different stages at 1000 mm/min for 0.2 RD 1000 sample.....	109
Figure 4.17: Maximum equivalent strain distributions during the blanking process in different stages at 100 mm/min for 0.2 TD 100 sample.....	110
Figure 4.18: Maximum equivalent strain distributions during the blanking process in different stages at 500 mm/min for 0.2 TD 500 sample.....	110
Figure 4.19: Maximum equivalent strain distributions during the blanking process in different stages at 1000 mm/min for 0.2 TD 1000 sample.....	111
Figure 4.20: Maximum equivalent strain distributions during the blanking process in different stages at 100 mm/min for 0.35 RD 100 sample.....	112
Figure 4.21: Maximum equivalent strain distributions during the blanking process in different stages at 500 mm/min for 0.35 RD 500 sample.....	112
Figure 4.22: Maximum equivalent strain distributions during the blanking process in different stages at 1000 mm/min for 0.35 RD 1000 sample.....	113

Figure 4.23: Maximum equivalent strain distributions during the blanking process in different stages at 100 mm/min for 0.35 TD 100 sample.....	114
Figure 4.24: Maximum equivalent strain distributions during the blanking process in different stages at 500 mm/min for 0.35 TD 500 sample.....	114
Figure 4.25: Maximum equivalent strain distributions during the blanking process in different stages at 1000 mm/min for 0.35 TD 1000 sample.....	115
Figure 4.26: General effects of blanking speeds and sheet thickness, orientation regarding max. equivalent strain.....	115
Figure 4.27: Nano-hardness distribution as a function of the distance from the cut edge for 0.2 RD 1000 sample, a) 3D distribution of hardness values b) SEM image of indents locations regarding the cut edge.....	116
Figure 4.28: Nano-hardness distribution as a function of the distance from the cut edge for 0.35 RD 1000 sample, a) 3D distribution of hardness values b) SEM image of indent locations regarding the cut edge.....	117
Figure 4.29: The average Nano-hardness value of the material.....	117
Figure 4.30: The distributions of Nano indentation values for 0.2 mm sheet thickness at different blanking speeds.	118
Figure 4.31: The effect of the blanking parameters against the hardness values of 0.2 ES sheet thickness.....	119
Figure 4.32: The distributions of Nano indentation values for 0.35 mm sheet thickness at different blanking speeds.....	120
Figure 4.33: The effect of the blanking parameters against the hardness values of 0.35 ES sheet thickness	121
Figure 4.34: Hysteresis loops of 0.2 RD of ES samples at different elongations of tension ...	122
Figure 4.35: Hysteresis loops of electrical steel type 0.2 TD samples at different stages of elongations of tension	123
Figure 4.36: Hysteresis loops of electrical steel type 0.35 RD samples at different stages of elongations of tension.....	124
Figure 4.37: Complete hysteresis loops of electrical steel type 0.35 TD samples at different stages of elongations of tension.....	125
Figure 4.38: Maximum flux density at different stages of elongations of tension for the different electrical steel samples categories.....	126
Figure 4.39: Hysteresis loops of electrical steel type 0.2 RD samples cut by blanking process at different blanking speeds.....	127
Figure 4.40: Hysteresis loops of electrical steel type 0.2 TD samples cut by blanking process at different blanking speeds.....	128

Figure 4.41: Hysteresis loops of electrical steel type 0.35 RD samples cut by blanking process at different blanking speeds.....	129
Figure 4.42: Hysteresis loops of electrical steel type 0.35 TD samples cut by blanking process at different blanking speeds.....	130
Figure 4.43: Hysteresis losses of electrical steel samples cut by blanking process at different blanking speeds.....	131
Figure 4.44: Standard error bar for the maximum flux density at different blanking speeds for the different electrical steel samples categories	132
Figure 4.45: SEM image for induced blanking cut edges of 0.2 RD samples at different blanking speeds, A) 100 mm/min, B) 500 mm/min, C) 1000 mm/min.....	133
Figure 4.46: Microstructure at higher magnification of some selected areas in Figure 4.45 a,b) At shear and fracture zones, c,d) At rollover and shear zones.....	134
Figure 4.47: EDS analysis for the square part indicated in the Figure 4.46d.....	135
Figure 4.48: SEM image for induced blanking cut edges of 0.2 TD samples at different blanking speeds, A) 100 mm/min, B) 500 mm/min, C) 1000 mm/min.....	136
Figure 4.49: Microstructure at higher magnification of some selected areas in Figure 4.48 of 0.2 TD samples. a,b) At shear and fracture zones, c) at fracture and burr zones, d) At rollover and shear zones.....	137
Figure 4.50: EDS analysis for the square part indicated in the Figure 4.49d.....	137
Figure 4.51: SEM image for induced blanking cut edges of 0.35 RD samples at different blanking speeds, A) 100 mm/min, B) 500 mm/min, C) 1000 mm/min.....	138
Figure 4.52: Microstructure at higher magnification of some selected areas in Figure 4.51 of 0.35 RD samples. a) At shear and fracture zones, b) At rollover and shear zones.....	139
Figure 4.53: SEM image for induced blanking cut edges of 0.35 TD samples at different blanking speeds, A) 100 mm/min, B) 500 mm/min, C) 1000 mm/min.....	140
Figure 4.54: Microstructure at higher magnification of some selected areas in Figure 4.53 of 0.35 RD samples, a) At shear and fracture zones, b) At rollover and shear zones.....	140
Figure 4.55: SEM image for cut edge surface induced by EDM method used to prepare ES samples	141
Figure 4.56: Cut edge fracture surface for 0.2 RD sample at different blanking speeds.....	143
Figure 4.57: Cut edge fracture surface for 0.2 TD sample at different blanking speeds.....	144
Figure 4.58: Cut edge fracture surface for 0.35 RD sample at different blanking speeds.....	145
Figure 4.59: EDS analysis for the square parts indicated in the Figure 4.58 IIIb.....	146
Figure 4.60: Cut edge fracture surface for 0.35 TD sample at different blanking speeds.....	147
Figure 4.61: Optical micrographs for induced blanking cut edges of 0.2 RD samples at different blanking speeds, a) 100 mm/min, b) 500 mm/min, c) 1000 mm/min.....	148

Figure 4.62: Optical micrographs for induced blanking cut edges of 0.2 TD samples at different blanking speeds, a) 100 mm/min, b) 500 mm/min, c) 1000 mm/min.....	149
Figure 4.63: Optical micrographs for induced blanking cut edges of 0.35 RD samples at different blanking speeds, a) 100 mm/min, b) 500 mm/min, c) 1000 mm/min.....	149
Figure 4.64: Optical micrographs for induced blanking cut edges of 0.35 TD samples at different blanking speeds, a) 100 mm/min, b) 500 mm/min, c) 1000 mm/min.....	150
Figure 4.65: Optical micrographs for the (a) 0.2 mm and (b) 0.35 mm electrical sheet thicknesses at low magnification of 20X.....	151
Figure 5.1: Magnetic hysteresis losses and the induced blanking strain regarding blanking conditions.....	165
Figure 5.2: Effect of blanking and material factors on the induced equivalent strain	169
Figure 5.3: Effect strength of blanking and material factors on the induced cutting force	171
Figure 5.4: Effect strength of blanking and material factors on the hysteresis losses	172
Figure 0.1: local strain coordinate system	189

List of Tables

Table 2.1: Comparison of the performance of lamination cutting methods	34
Table 3.1: Electrical steel chemical composition	66
Table 3.2: DIC setting parameters for tensile tests	69
Table 3.3: Categorization of blanking samples.	73
Table 3.4: DIC setting parameters for blanking tests	76
Table 5.1: ANOVA model for plastic strains versus blanking parameters.	167
Table 5.2: ANOVA model for the cutting force versus blanking parameters	168
Table 5.3: ANOVA model for the hysteresis losses versus blanking parameters.	169
Table 5.4: ANOVA model summary of the factors' impact strength on the blanking results...	170
Table 0.1: Grains size calculations for both ES thickness 0.2 and 0.35 mm.....	188

1

Introduction

1.1 Introduction

Improving production processes and product quality is a very important issue and ongoing concern for researchers seeking to enhance the quality of products as part of a global trend towards reducing energy consumption along with achieving high machines performance [1]. The laminations of core are one of the main components of transformers or the stator and rotor parts of electric motors. The blanking process is used to cut the sheet material to the required shape by mass production at low cost and therefore remains the most commonly preferred cutting process for producing laminations [2].

Electrical steels are widely used as lamination materials in the electrical industry because of their superior electrical properties such as high permeability and low magnetic losses and the low cost [3]. However, the blanking process induces plastic deformation and local damage at the cut edge which in turn causes negative effects on material properties and the cut edge quality. Among all features of the final product, the produced magnetic properties are extremely important for blanked electrical steels because these are directly correlated to the performance of electrical motors. Magnetic properties are influenced negatively by cut edge distortion and texture modification that are considered as sources of stress concentrations and poor properties in the material [4].

It is essential to detect, quantify, and when possible eliminate the edge deformation through optimisation of the blanking parameters in order to produce high-quality final blanked electrical steels. Therefore, this research focuses on the effects of

blanking parameters on magneto-mechanical properties at the cut edge of thin sheet electrical steels, to understand the local properties of the sheet material at the cut edge and the vicinity area.

1.2 Problem Description

Blanking is the preferred process for producing electrical steel laminations for electrical machines and transformers. Ideally, this process should take in ES sheets and deliver perfect blanked parts with the same properties as the feedstock used. However, in practice, a range of defects can arise during the blanking operation. The presence of edge and vicinity area defects remains the most serious problem in the blanking process; this is because they interfere with the performance of the final product [4].

During this cutting process, the material is plastically deformed and residual stresses are generated, especially at the cutting edge and the vicinity area. The induced deformation can affect the mechanical and magnetic properties of the electrical steel sheet due to modifying of the material's features and edge surface profile in the deformation zone. Distortion in local cut edge grains occurs due to the exposure of the cut zone to diverse stresses such as tension, compression, and shear [3]. In such a process, plastic deformation occurs due to the movement of an edge dislocation across the crystal lattice under a shear stress. The presence of a dislocation can lower the shear stress required to cause slip [4]. The dislocations can become entangled and interfere with each other, whilst barriers such as grain boundaries, impurities in the material may cause impediments. The increased shear stress required to overcome these entanglements and impediments results in an increase in the overall strength and the hardness of the metal or, as it is known, strain hardening. The greater the deformation, the greater the number of entanglements and hence the higher the increase in the metal's strength. The dislocation density increases proportionally to the plastic strain, thereby affecting the material's permeability and flux density in the edge region [5].

The blanking process can cause a number of defects in the metal crystals such as micro-voids and cracks. Mechanical and electrical properties of metals, such as yield stress, fracture strength, electrical conductivity, and magnetic losses can adversely be affected by these imperfections [5]. The other important issue is the generation of burrs, which inevitably occurs when displacing metals mechanically such as by blanking, causing burrs to be formed on the cut edge. Much effort is expended to restrain burr

effects. The burr size relates to the appropriate die design regarding the material properties [1]. The deterioration of magnetic properties may occur due to crystal deformation; where the disrupted crystal lattice will produce a region of locked-in stresses and dislocations due to the cold work [6]. These sites pin domain walls, impair permeability and increase power loss [3].

Analysis of the blanking process is very complex because this process includes multiple factors that simultaneously play a role in the generation of defects. For example, since the speed of the cutting operation relates directly to the economics of lamination production, a high cutting rate is preferred. Also, thinner sheets may have better magnetic performance but require more laminations to give stack height. The mismatch between the punching parameters could cause changes in the geometrical shape of the cut edge. Typically, as the region of disruption spreads some distance from a sheared edge, using appropriate die parameters will minimize process damage at the cutting area. Cutting the small parts such as stator lamination teeth will increase the effect of the process due to the convergence of the effect of the edges. The blanking die contains a lot of parts. However, designing new blanking ideas may eliminate some parts, such as the stripper plate and feeding control, depending on the experience with using the process and the required aims. The analysis of cut edge deformation is very difficult because of the small size of the deformation zone and the process deformation takes place in the closed area inside the die cavity. The challenge of the test is increased when the used sheet material thickness is very thin.

The research problem can be summed up in terms of the analysis of the blanking process using new techniques and strategies to investigate the mechanisms of blanking and cut-edge formation of thin sheets of electrical steel to achieve a better understanding. In addition, it involves linking the affected mechanical and magnetic properties and the affected edge features regarding the process parameters. Because of the interactions among the various process factors, improving the quality of the final product could depend on considering all these factors and the corresponding results simultaneously.

1.3 Research objectives and novelty

Blanking processes involve a lot of variables and phases and their interactions make the cutting mechanism system extremely complex. An experimental investigation was adopted to emulate the actual blanking tests. It has become known that the blanking process results in a local plastic deformation and generated stresses concentrate at the cut edge and extend to the vicinity area of deformation zone, which causes deterioration of the magnetic-mechanical performance of electrical steels.

Therefore, the project focused on investigating blanking mechanisms and local magneto-mechanical properties of thin sheet non-grain oriented steels at the cut edge concerning deformed or damaged material.

One of the main novelties of this research is represented by using new techniques and strategies to investigate the mechanisms of blanking through such as implementing the high-speed digital image correlation technique (DIC) to visualize cut edge damage during the blanking process on an in-situ blanking rig. Moreover, to illustrate the failure mechanism of the material and give a clear view of the material's behaviour on crack initiation and propagation during the cutting process. Furthermore, a new small single sheet magnetic tester (SST) was designed and utilized to accommodate a specific flat specimen and measure magnetic properties to determine the general magneto-properties and specific hysteresis losses. That could lead to the development of a production strategy regarding the microstructure and mechanical properties of the material that improves the quality of the final blanked material.

The project aimed to use of a new generation gauge of electrical steel. It might be the first time that the thin sheet (with thickness 0.2 mm) steel has been used to analyse and measure the deformation and damage during blanking and link it to the magnetic properties and comparing the results with those for 0.35 mm steel. In line with the industrial trend to increase machine efficiency and reduce the total losses.

The project also attempts to evaluate the effective weight for the process parameters such as blanking speed, material thickness, and sheet orientation regarding the magnetic losses. Finally, one of the major research thrusts involves finding connections among blanking process parameters and the mechanical, magnetic, and microstructure properties regarding the deformed cut edge of electrical steel.

1.4 Thesis Outline

The thesis is organized in six chapters with the following content:

- **Chapter 1:** This, the current chapter, gives a brief introduction about the scope of the thesis, the aims and novelty of this research.
- **Chapter 2:** This presents the literature review and gives a general introduction to the electrical steel material and its industrial manufacturing method. A simple comparison is made between popular lamination materials and cutting methods. In addition, the physical magnetization process is explained and typical measurement methods for iron losses in the single sheet of electrical steel are discussed. The blanking process mechanism and cutting parameters affecting the cut edge features and affecting magneto-mechanical properties are introduced as well. Finally, a summary is provided of the main knowledge gap.
- **Chapter 3:** Gives an overview on the empirical methodology followed in this study, including the selection of research material and the new practical methods and techniques that are used, along with presentation of illustrative designs and tools. The measurement setup developed in this project is also described in this chapter.
- **Chapter 4:** Determines the effects of blanking operation on local magneto-mechanical properties at the cut edge through the study outcomes. Characteristics of mechanical properties including tensile, Nano-indentation, and strain measurements are evaluated. Furthermore, it evaluates the possibility of using the measured results to characterize the magnetic properties losses in ES due to the influence of the cutting process. Also, the microstructure and local material features at the cut edge and the fracture surface are examined.
- **Chapter 5:** Discussion and comparison are conducted of the measured results in order to identify and interpret their causes and consequences. Simple statistical results analysis is also carried out to establish direct relations between the blanking parameters and induced deformation and the blanked properties.
- **Chapter 6:** Provides a brief conclusion of the main results of this thesis and presents proposals for future activities to investigate the cut edge deformation induced by magneto-mechanical cut edge defects in electrical steel.

2

Literature review

2.1 Introduction

Blanking process is a manufacturing operation where sheet metals are cut into specific geometries using the interaction of blanking die and punch sets. In this operation, the material experiences a large localized deformation where the cutting edges of the die-punch meet in order to shear away boundaries of the products. This localized deformation could adversely affect micromechanical and microstructural properties of the parts at the vicinity of the cut section which is called the cut edge. The blanking process induces damage in parts of the cut edge; this deformation becomes more critical when the cut area and sheet thickness are small [1, 3]. Steel grades with a high percentage of Si content are widely used in electrical applications and mostly referred to as Electrical Steel (ES). These materials are usually provided as very thin sheets ready to be blanked in specific complex geometries for use in applications such as the stator and rotor of electromotor cores, or the laminations of transformers. The presence of high Si content in ES together with their small thickness makes them prone to severe cut edge defects such as localized deformation and excessive burr which in turn result in the loss of magnetic efficiency in the final products. Therefore, this chapter will deal with the ES material in some detail and clarify the blanking mechanism and steps. In addition, it will explain the main principles of the magnetic properties and power losses to convey how blanking deformation affects the material's properties. Moreover, it will refer to the techniques and tests used in analysis by relevant studies and the results of those researches.

2.2 Electrical Steel (E.S)

Electrical steel is a type of low carbon steel, sometimes referred to as lamination steel, silicon steel, or transformer steel. However, the term electrical steel has become the most popular and indicates a magnetic material formed of cold rolled sheets with a high percentage of silicon element. These sheets, called laminations, are assembled to form the cores of transformers or the stator and rotor parts of electric motors. Laminations may be cut to desired shapes either by a blanking process in mass production or by laser and wire erosion for smaller quantities [1, 3]. The magnetic performance of ES sheets is increased through reducing their thickness as this reduces the generated eddy current loss [1, 7]. For this reason, a new generation of classical electrical steels has been developed, for example, the steel with a thin gauge of 0.2 mm used in the current study [8].

2.2.1 Electrical steel applications

Electrical steel sheets are used in a wide range of equipment, from the simplest domestic appliances to the modern technologies such as the core of the traction motors of electric vehicles (EV) and hybrid electric vehicles (HEV). The continued demand for smaller, lighter, more powerful and efficient motors is the driving force for investigating and developing methods for enhancing the performance of electrical steel sheets [7].

There are some other magnetic materials such as Nickel and Cobalt iron alloys which could be used in similar or particular electrical applications [3, 9]. Cobalt steels are used primarily in aircraft applications where size and weight are critical [10], whereas Nickel steels are used with a high frequency ranging from 500 to 50000 Hz in inductors, transformers and communication equipment [1]. However, electrical steel sheet is the most commonly used ferromagnetic material due to its relatively high magnetic properties such as high permeability and lower loss in addition to its good formability and lower cost compared to other materials [11]. [Figure 2.1](#) shows the main applications and their component ES laminations.

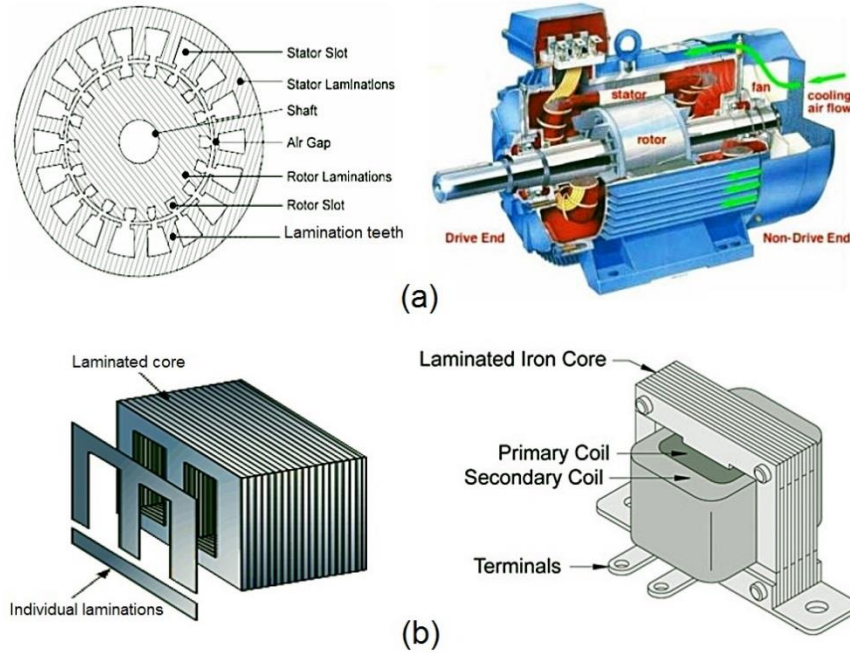


Figure 2.1: Main applications of ES: a) electrical motor, b) electrical transformer [1, 12].

2.2.2 Classification of electrical steel

Magnetic materials include ferromagnetic and ferri-magnetic materials that can be categorized into three types including; soft magnetic materials, hard magnetic materials, and semi-hard magnetic material based on their magnetization and demagnetization processes. ES is considered as a soft ferromagnetic material; the different types of magnetic material are shown in Figure 2.2 [8].

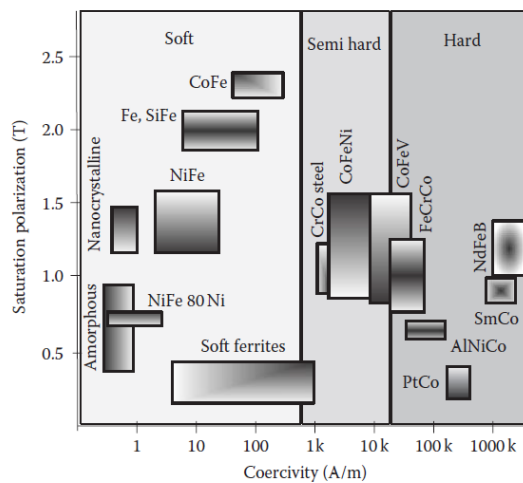


Figure 2.2: Types of magnetic materials [8].

Soft magnetic materials are typically used for applications in which small magnetic fields are applied to switch the magnetization direction, whereas hard magnetic materials (or permanent magnets) are used in applications where the magnetization does not change unless relatively large magnetic fields are applied, such as in speakers and microphones [9]. ES materials can be divided into the following categories according to their magneto-mechanical and microstructural properties [1, 3]:

1) Non-Grain Oriented (NGO): In which the magnetic properties are assumed to be approximately the same in different directions of the material; therefore, it is used in rotational applications such as electrical motors.

2) Grain Oriented (GO): In which the magnetic properties are most powerful toward the rolling direction, but it has inferior properties in other directions; therefore, this type is preferred for stationary applications such as transformers.

2.2.3 Material isotropy and grains orientation

At room temperature, the electron spins are spontaneously aligned within iron crystal to give self-saturation, whilst some directions can be much more easily magnetized than others [8]. The material is considered to have isotropic magnetic properties if its properties do not change regarding grains orientation and to have anisotropic properties if its properties are affected by the texture orientation.

Non-oriented electrical steels have different grains orientation, these differences in direction can make the magnetization of the material much easier at low saturation levels. There are two complex systems of slip directions; plane orientations (100, 110, and 111), and planes orientations (001 and 011). [Figure 2.3](#) shows the case when the grains orientations of (001) or (011) planes parallel to the plane direction of the sheet of the (100). In case of oriented electrical steel, the grains orientation is controlled toward the rolled direction (called the cube-on-edge (COE) or Goss texture) so that the axes of planes (001) and (100) are identical [7, 9]. Modification of texture can be achieved by applying a complex series of cold rolling and heat treatment operations that causes the grains to grow in such a way that makes the material easy to magnetize in sheet rolling direction. This process will enhance the magnetic properties in the rolling direction but produces relatively poor magnetic properties in the transverse direction (90°) [1]. The figure also shows the iron lattice and grains orientation system. The (100) direction is the

easy cube edge direction; (110) is the hard cube face diagonal direction; (111) is the hardest cube body diagonal direction [3].

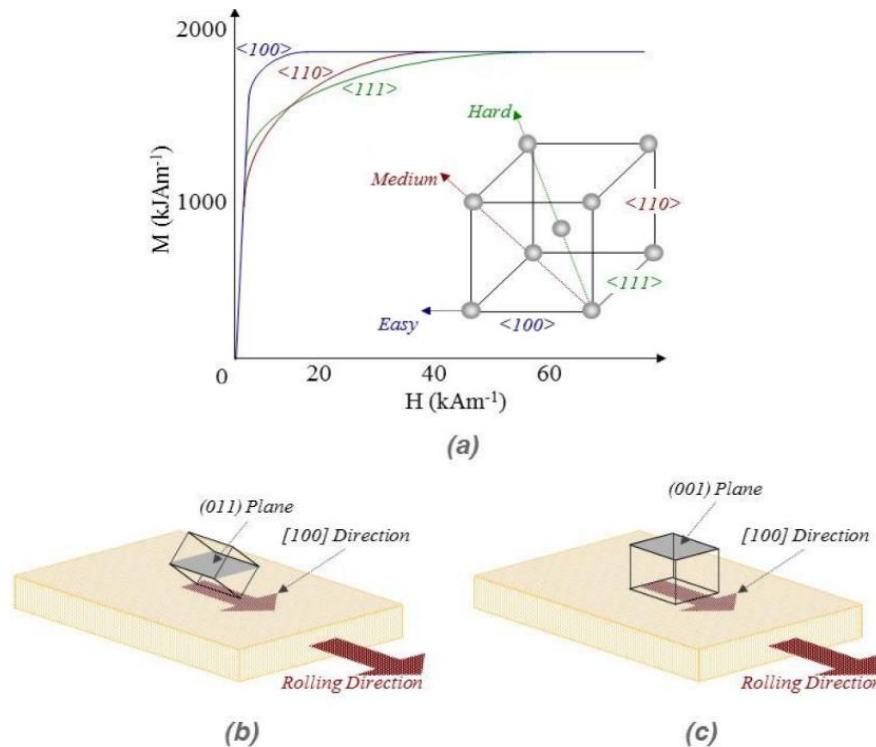


Figure 2.3: Electrical steel grains orientation system: (a) B.C.C lattice, (b, c) the anisotropy of ES due to the oriented texture [3].

Magneto-crystalline anisotropy means that more energy is needed to magnetize material in a certain direction, either RD or TD. Additionally, tensile stresses ease the process of magnetization and reduce the power loss. Conversely, compressive stresses interfere with the magnetization process negatively [13]. The excitation of the material is affected by the sheet grain orientation; thereby the magnetic properties become sensitive to the grain's direction. It is notable to mention that although the material is assumed to be isotropic, the magnetic properties are reported not to be identical in the RD and TD directions of the material [14].

2.2.4 Metallurgical properties

Electrical steels have a structure of body centred cubic crystals [15], which contains several elements such as Silicon, Manganese, Aluminium, and carbon in small percentages. Electrical Steel's microstructure is similar to that of low-carbon sheet steels; the microstructure of a typical motor lamination steel is shown in [Figure 2.4](#) [16]. The non-oriented grades contain minor amounts of cementite and inclusions and low sulphur levels, often below 0.01%; in the oriented grades sulphides and nitrides are used to improve grain orientation by promoting secondary recrystallization [1, 3].

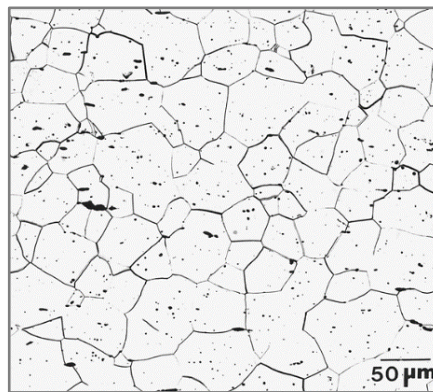


Figure 2.4: Micrograph of NGO electrical steel etched in 2% Nital [16].

Silicon is used as the main effective additive element because it causes increasing the electrical resistivity and decreases the induced eddy currents, thus lowering the power core loss [3, 7]. Electrical steel may have from 0-6.5% Si, whereas commercial alloys have silicon content of up to 3.2% [2]. Very high silicon content (e.g., >4.0%) may result in lowering of induction permeability saturation density, as well as potentially changing the alloy phase or mechanical properties in the form of increasing the brittleness. Depending on the type of product, aluminium and manganese are added in amounts of less than 1.0%, in order to gain the benefits of increased resistivity, obtaining an optimal grain size, and reducing the impurity content. It is worthy of notice that increasing the grain size will reduce the core losses up to a certain grain size [9]. [Figure 2.5](#) shows the influences of some elements on the resistivity of iron (A), and percentage of silicon (B) in proportion to the magnetic and electrical parameters.

2.2.5 Methods for manufacturing electrical steels

The initial ES production steps are similar to those for carbon steel. Firstly, as in the initial stage for steel making, the steel is melted in a blast furnace and continuously poured to make slabs, then hot rolling from the initial casting ingot to small gauge thickness of about few millimetres, followed by cold rolling to the desired thickness up to 0.1 mm [18], and to achieve good surface conditions. Before cold rolling, the coils are exposed to heating, side-trim and pickling processes to remove scale and provide a surface suitable for cold rolling. The sheets are heat treated to homogenize the internal structure of the metal and achieve the required characteristics and finally coiled up and side trimmed [3].

As a result of these processes, the steel crystals are stretched and flattened in the same direction of rolling. That will reduce the grain size and increase the grain boundary. The grain boundary is considered as a boundary of a big domain or small polarization zones, which contain many small domains. Therefore, a reduction of the domain size produces lower core losses; this can be accomplished by reducing grain size or by applying tensile stress in the rolling direction [9]. Electrical steel can be produced in two states: first, fully-processed, in which case the material is completely developed with all the final properties, and second, a semi-processed state, where the material is produced to the final thickness without full annealing heat treatment. The users need to adapt the heat treatment according to the required magnetic properties [1, 9]. [Figure 2.7](#) shows the technological path of ES sheets production according to the Cogent Power Company (the supplier of electrical steel material for the current study) [18].

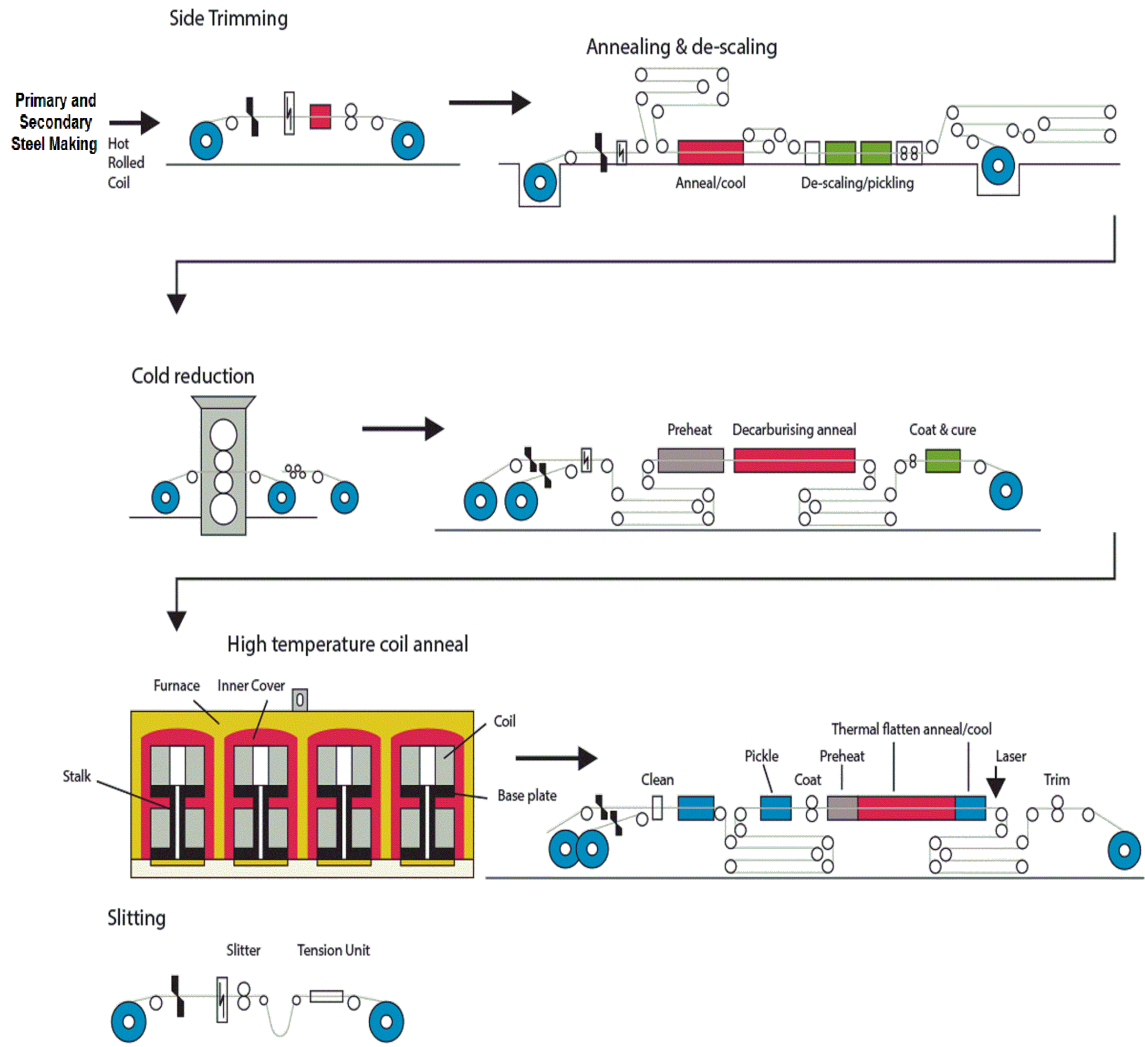


Figure 2.7: Electrical steel making outline [18].

The following two typical routes in [Figure 2.8](#) and [2.9](#) show the main differences in production of two electrical steel types which are essentially related to the alignment direction of grains and heat treatments.

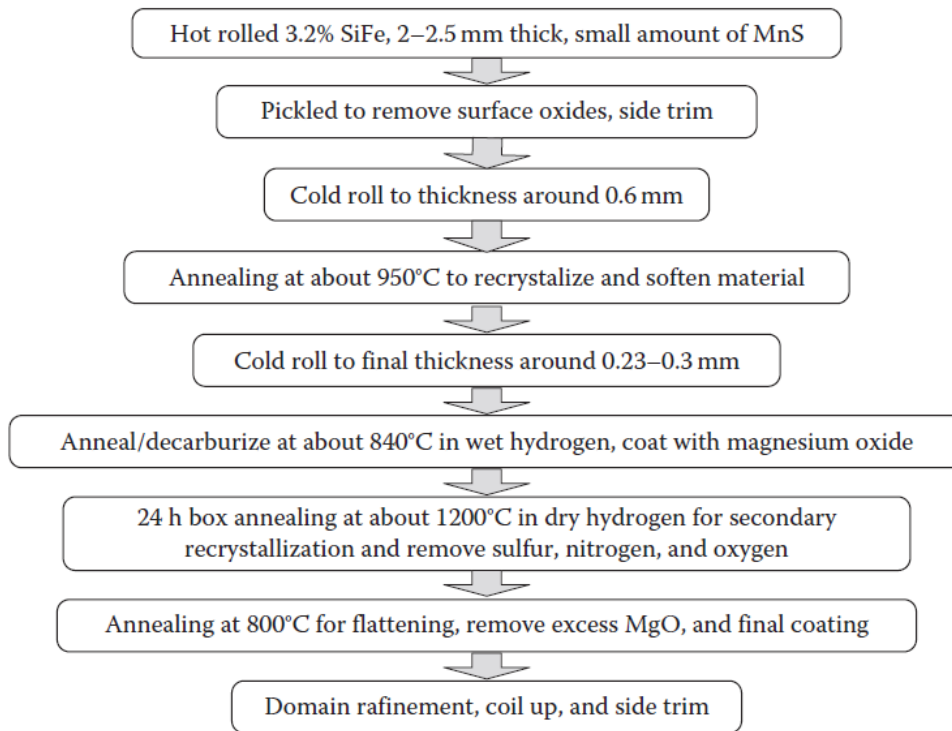


Figure 2.8: The Production route of fully processed GO electrical steel [3, 8].

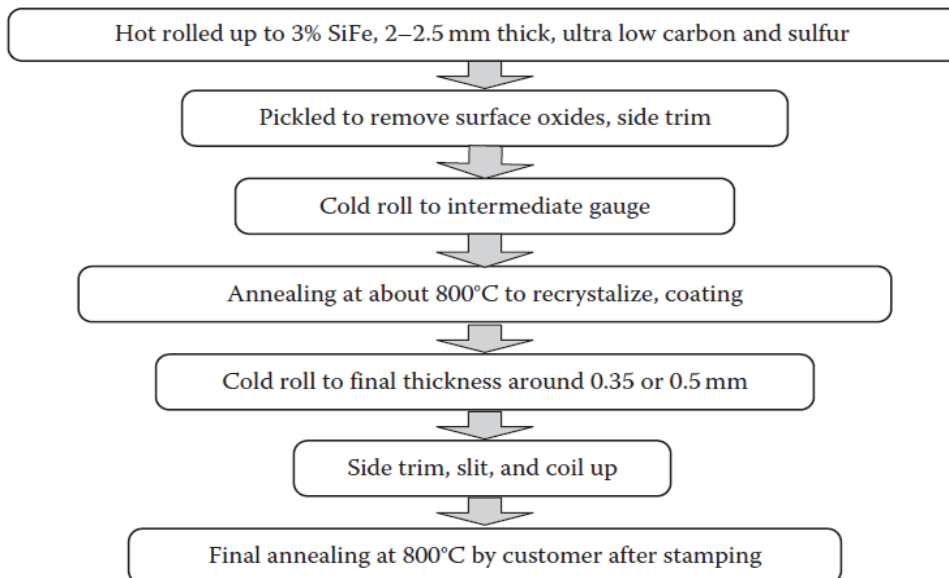


Figure 2.9: The Production route of fully processed NGO electrical steel [3, 8].

2.3 Magnetic properties of ES

When a ferromagnetic sheet is placed within an external magnetic field, the material's structure is affected because of electron movement in the atoms. A rearrangement of the domain structure takes place, mainly due to domain wall movement. The domains energetically tend directionally to the applied field direction. Therefore, it is essential to understand the principles of the magnetic domain structure and factors influencing the magnetic properties in order to understand the behaviour of the material during the diverse deformations and the reasons for improvement or deterioration in these properties. In addition, it is important to identify the terms used to describe and quantify magnetic materials such as hysteresis loops and induction and including the magnetic field and flux density.

2.3.1 Ferromagnetic domains and magnetic properties

Soft ferromagnetic materials such as ES can be easily magnetized and demagnetized [7]. This unique property of ferromagnetic materials lies in the ability of small externally applied fields to organize domains in the crystal structure, which can greatly influence the switching to the magnetization state [9]. The magnetic domain structure can be explained starting from the atom structure in the material. At the centre of an atom there is a nucleus around which electrons orbit in a complicated manner. Each electron has an electric charge generated as a result of its spin or rotation around itself. Also there is a magnetic moment caused by its rotation around the nucleus. The atom has a large number of electrons. Therefore, the resultant magnetic moment tendency is associated with the overall directions of the electrons. The number of electrons which are effective in contributing to the atomic magnetic moment is called the Bohr magneto number [3, 19].

The magnetization process in ferromagnetic materials comes from the electrons' movements in orbit. Small polarization zones with a micro field, known as domains, are generated inside the materials. The boundaries between domains, called domain walls or Bloch walls, become mobile when a sufficient field is applied [9]. The grains in the material have many domain areas. Therefore, each grain will have special behaviour on the axis of magnetization. These grains could have irregular directions, and thus the whole material consists of a large number of magnetized areas in a random direction, as shown in [Figure 2.10](#). When all the electrons' movement aligns with the external field direction,

a powerful overall directionally coordinated magnetic field is generated. This internal spontaneous magnetic field that aligns the electron spins could stop at the grain boundary of the metal [3].

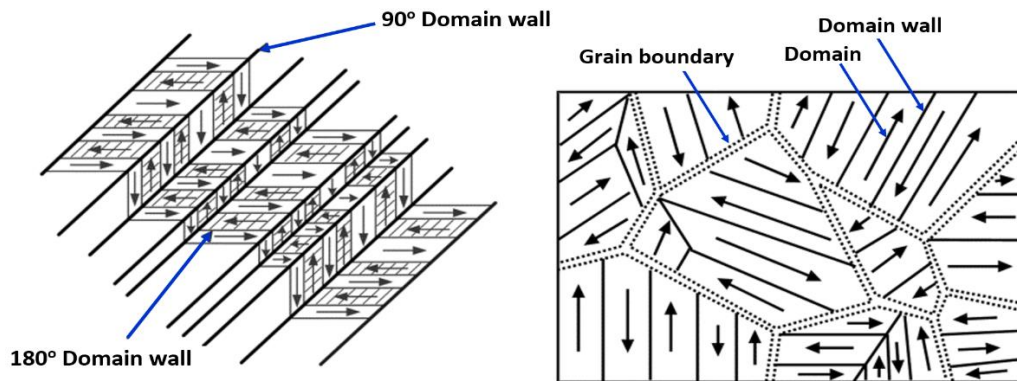


Figure 2.10: Typical domain structures observed in ferroelectric material [20].

In ferromagnetic material such as ES, when a large enough field is applied, all the atomic moments become aligned preferentially along the applied field direction, in what is known as the saturated state [9]. The saturation state of magnetization depends on the number of atoms per unit volume and the Bohr number. The arranging of atomic magnetic moments in parallel to the applied direction can occur only at low temperatures. The higher temperatures can cause random movements, which increase up to a value called the Curie temperature (T_c), where the thermal agitation overcomes the effect of the coupling forces; thereby the material loses its ferromagnetic properties [19].

2.3.2 Domain structure and domain walls motion

During the magnetization process, an internal magnetic field is generated opposed to the aligning of the electromagnetic atomic spins. Consequently, created a localized region contain pairs that equal in value and opposite in charge direction, called dipoles. The dipoles make a gradual transition from the first domain alignment to the second through the domain walls. Figure 2.11 shows a schematic diagram of the domain wall movement and spin dipoles. If a single crystal of iron is magnetized, the crystal will be in a high potential energy state, but magnetization of an increased number of crystals or domains will reduce the energy in ferromagnetic polycrystalline material [21].

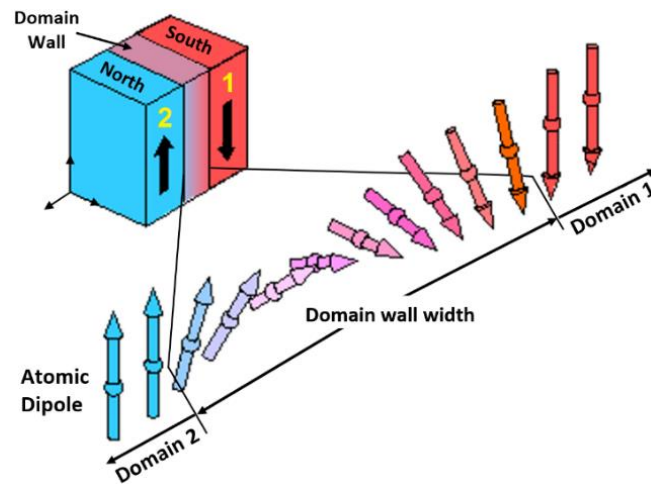


Figure 2.11: Schematic of spin rotation in a 180° domain wall [21].

The process of domains alignment follows the easy axes of the material anisotropy based on the displacement of domain walls and the rotation of the dipoles inside the domains [22]. The domain pattern is dependent on the grain boundary regarding the applied field. [Figure 2.12](#) shows the effect of grain boundaries on the domains' movement when the magnetization field in non-oriented silicon steel material is applied. The figure illustrates how the random domain patterns begin to organize gradually from the low field ([Figure 2.12a](#)) to the high field ([Figure 2.12d](#)) where the domains are clearly seen stops at grain boundaries.

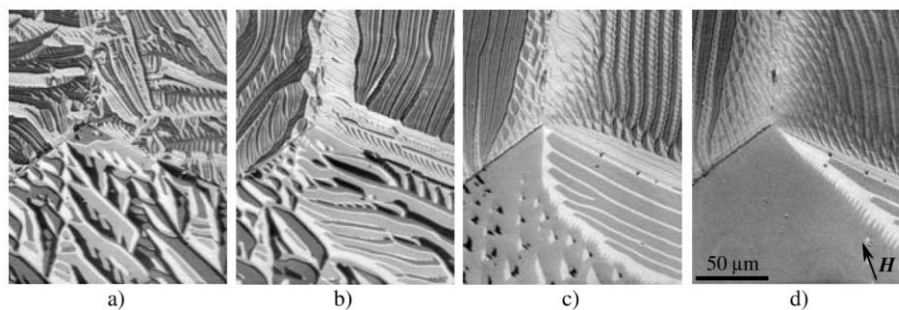


Figure 2.12: Observations of domains at grain boundaries in NGO steel [22].

The distribution of local domain walls in NGO electrical steel sheet is very complicated and depends on many factors such as grain structure and size, material impurities, local stress, and local potential energy [8, 20]. Pinning of these domain walls by small oxide precipitates and strain fields is considered as the main cause of reduction

of magneto-static energy inside the precipitates. If the magnetic field is increased to a certain extent, the domain exhibits various movements in addition to its natural movement, including:

- 1) The domain wall twists or jumps on encountering obstacles that are formed because of plastic deformation or precipitations. These domain wall jumps are called Barkhausen jumps and cause ferromagnetic hysteresis due to the absorption of one of the neighbouring domains [19]. The domain walls have been observed to move in curved lines around the precipitates in non-oriented steel [17].
- 2) The domains can rotate in preferred directions close to the field, the final alignment occurs in the main field direction by the continuous raising of the field [19].

2.3.3 Parameters of magnetic properties and hysteresis phenomena

The presence of a magnetic field strength H , sometimes called magnetic field intensity, in an area A , can generate a magnetic flux Φ . The magnetic flux density B , also known as magnetic induction, depends on the magnetic properties of the medium described by permeability (μ) and the magnetization of material [3, 8]. H is measured in units of Amperes per meter, Φ is measured in units of Wb or Weber, and B is measured in Tesla units or Weber per meter. The related parameters between them are the permeability μ or (B/H) , hysteresis losses $(H \times dB/dt)$, and polarization J or $(B - \mu_0 H)$.

When a piece of steel is brought near a magnet or subjected to a magnetic field, the magnetization in the iron process is described by a magnetization curve or $B-H$ loop. This curve can be obtained by plotting the magnetic induction B against the field strength H . The $B-H$ curve is a fundamental relationship for describing the essential information regarding the magnetic properties of materials [23]. The permeability of free space (μ_0) is equal to $4\pi 10^{-7}$ [H/m]. [Figure 2.13](#) shows the relationships between the flux density, magnetic field, and the permeability.

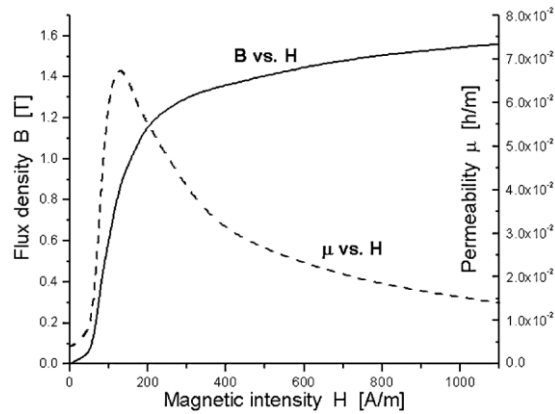


Figure 2.13: Initial magnetization curve and permeability for iron [24].

Magnetic hysteresis is a physical property of ferromagnetic materials that results in the dissipation of wasted energy in the form of heat energy that is proportional to the area of the magnetic hysteresis loop, in what is known as hysteresis loss [2, 25].

Figure 2.14 shows a typical magnetization curve (B - H curve) to explain the behaviour of a ferromagnetic core. When the core is un-magnetized, both B and H start from zero (point 0) of the curve. When the current increases in a positive direction, the magnetic field strength and flux density increases linearly (o-a curve) until reaching the saturation state. When any further increase in the magnetic field strength has no effect on the value of B , this point on the graph is called Magnetic Saturation or core saturation. Saturation occurs when the random arrangement of the domain structure within the core material reaches the ideal alignment that induces a maximum flux density. Then, when the magnetizing current and magnetic field reduced to zero, the flux will not reach zero due to the residual magnetism present within the core (a-b curve).

This retaining of some magnetism is called retentivity or remanence and the remaining of flux density is called residual magnetism (B_r). That occurs because of some of the tiny molecular magnets do not return completely to the original state. The way of zeroing the flux density is by reversing the direction of the current to make the value of the magnetic field negative. This effect is called a Coercive Force (H_c). The reverse of the magnetic field will cause re-arranging the molecular magnets of the core until becomes un-magnetized (at point c). The increase in the current and magnetic field in the reverse direction will cause reach the core to the saturation point but in the opposite direction (point d) which is symmetrical to point a.

If applying the same procedure but with reversing the magnetizing current flowing through the coil, the second half of the loop will be reached, i.e. (d-e-f-a) curve. The fully B-H curve representing the magnetic hysteresis loop. Soft ferromagnetic materials such as silicon steel have very narrow magnetic hysteresis loops. Soft magnetic materials can be magnetized using AC and DC currents, the magnetic properties are varying in these two conditions. In the AC condition, the magnetic losses occur due to the continuous reversing the direction of magnetic poles. DC magnetization also incurs hysteresis losses as magnetic poles are alternately reversing directions of one cycle and can show behaviour similar to that of AC. The shape of the hysteresis loop depends on the used material type [7, 26].

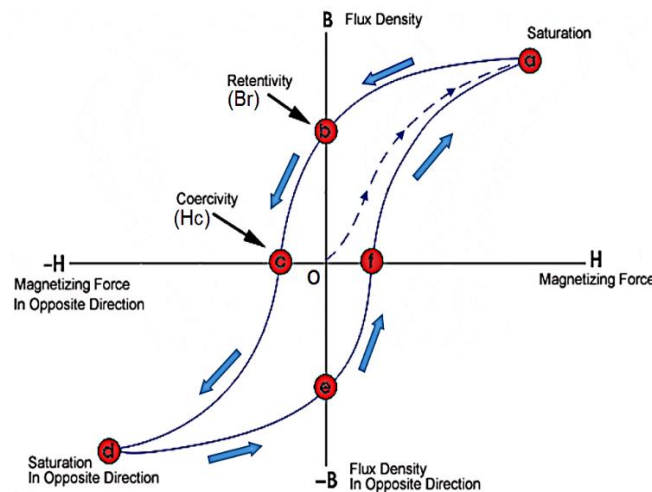


Figure 2.14: Typical magnetization and hysteresis curve [21].

A. Krings and J. Soulard [27] explained that the change in magnetic losses in both AC and DC magnetization occurs due to the movement of domain walls. Also, hysteresis losses could arise at DC due to the fact that even though the magnetization change is very slow, the local magnetization inside the domains changes rapidly. Figure 2.15a, illustrates the differences between AC and DC magnetization in the hysteresis loop states. The solid curve is the DC hysteresis loop. The loop becomes wider at the higher frequency which means more losses as shown by the dotted lines. Therefore, it is evident that B_r and H_c may change with frequency even for the same B_m . However, at any frequency, the hysteresis loss is proportional to the area of the B-H loop. Increase in loop area with frequency is usually attributed to flow of eddy currents. Figure 2.15b shows that the flux density is also proportional to the applied current for a given frequency. Increasing the

number of turns of the magnetization coil leads to increase in the current and thereby an increase in the magnetic field. Therefore, the largest loop corresponds to the highest applied current at maximum flux density B_m . If the effective current is reduced, a smaller B-H loop results, with lower flux density B_m . When the current is reduced further, lower flux density is reached as in B_{m2} and B_{m1} [28]. The saturated state can be reached by applying sufficient current and magnetic field depending on the material type and size.

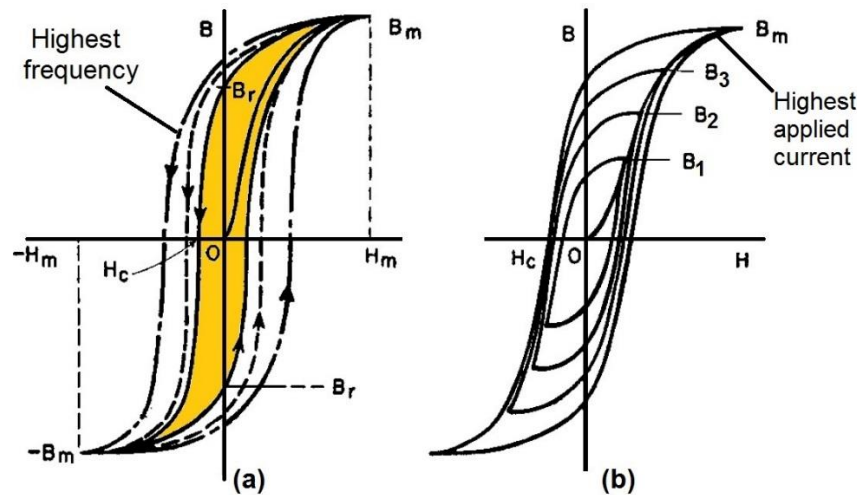


Figure 2.15: a) Differences between the AC and DC magnetization on the hysteresis loops, b) Effect of applied current and flux density on the hysteresis loops [28].

2.3.4 Magnetic power losses

The difference between the supplied and the output magnetic power is called the power loss [7]. It can also be defined as dissipation of energy as heat. The power loss is a very important property in determining the material's quality because of its contribution to total losses in machines, usually given as loss per cycle or watts per kilogram for a specific frequency. Permeability in ES applications is a secondary quantity and it is inversely related to the magnetic loss at the fixed magnetization condition [22]. The power energy loss can be generated from the following three sources [1, 26]:

- 1) Core losses or magnetic losses, which include hysteresis losses, eddy current, and anomalous losses of motor components [29].
- 2) Mechanical losses, which result due to friction and winding losses or copper losses.
- 3) Stray load losses are the losses which are caused by variation in load.

Usually, thin sheets of electrical steel are preferred for use in the manufacture of the stator and rotor cores, to reduce eddy current losses in the iron core as a result of the alternating flux induced during operation [7]. Hysteresis loss occurs due to the irreversible nature of the magnetization process of a magnetic material when an external field is applied, whereas eddy loss occurs due to the currents flow in the opposite direction to the electromotive force (emf) induced in the material due to the magnetic field [29]. One means of limiting the energy losses of ES steel sheet is by lowering the sheet thickness to reduce eddy current losses [30]. The power loss generally decreases at a certain thickness because the eddy current loss component tends to decrease in spite of the hysteresis loss component tending to increase with decreasing thickness. The eddy current loss decreases linearly with reduction in thickness [31].

Several factors appear to be responsible for the reductions in energy losses with decreasing thickness of ES sheet. The main reason for reducing loss is the change in the material's permeability. The other factor influencing the energy losses of thin sheet is the dependence of 180° domain wall spacing on sample thickness [30, 32]. Also, the concentrated electric fields at domain boundaries in thin sheets could contribute to increasing the eddy current losses [30]. There is a discrepancy between the sum of hysteresis and classical eddy current loss when compared to the specific total loss in a material. This difference is due to the anomalous losses. The increase in the number of domain walls because of increase in the grain numbers and grain boundaries at lower thickness results in reduced domain wall velocity for the same magnetization response because of reduction in the domain widths [29].

The inter-laminar eddy currents may occur between core laminations, as shown in [Figure 2.16](#) [1]. Therefore, the lamination is insulated by a coating layer on one or both sides to prevent circulation of currents between the sheets. Also, insulation increases electrical resistance between laminations to reduce eddy currents and to provide resistance to corrosion or rust [1]. There are numerous types of coating, organic and inorganic, that can be selected depending on the application [7]. The eddy current loss is proportional to the square of the thickness of flat-rolled magnetic materials, which indicates that reducing the lamination thickness by half could reduce the eddy current losses by one-fourth. The contribution of eddy-current loss to the total loss is less than that of the hysteresis loss at low frequency. However, the hysteresis loss becomes greater

than would be expected based on power-frequency considerations alone. Thus, hysteresis loss plays an important role at high as well as low frequencies [33].

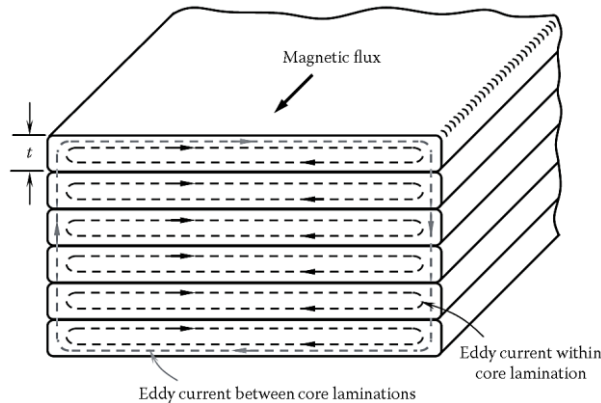


Figure 2.16: Lamination sheet and inter-laminar eddy current [1].

2.4 Measuring magnetic properties of electrical steel sheets

There are different standard tests for investigating and evaluating the magnetic properties and iron losses of lamination steels. Some are used to test the stack of laminations or the whole core before windings are applied and mounted into motors, such as the ring test as shown in [Figure 2.17a](#). In this test method the core assembly steps such as welding, riveting, and bolting need to be considered. Another testing method is used to test individual sheets to measure and characterize the sheet material's properties and is called the single sheet tester SST. Normally this test method is applied to measure power loss and define the magnetic property of ES. Such measurements play an important role in supplying valuable data on magnetic parameters and the quality of products. The best known method is called Epstein frame measurements and is a test that uses three layers of four ribbons with 25 cm length and 3 cm width, squarely placed and overlapping at the corners [3]. The Epstein test is considered as a general standard for comparing lamination properties among different manufacturers, despite having drawbacks relating to sample size and errors due to the overlapping corners as shown in [Figure 2.17b](#).

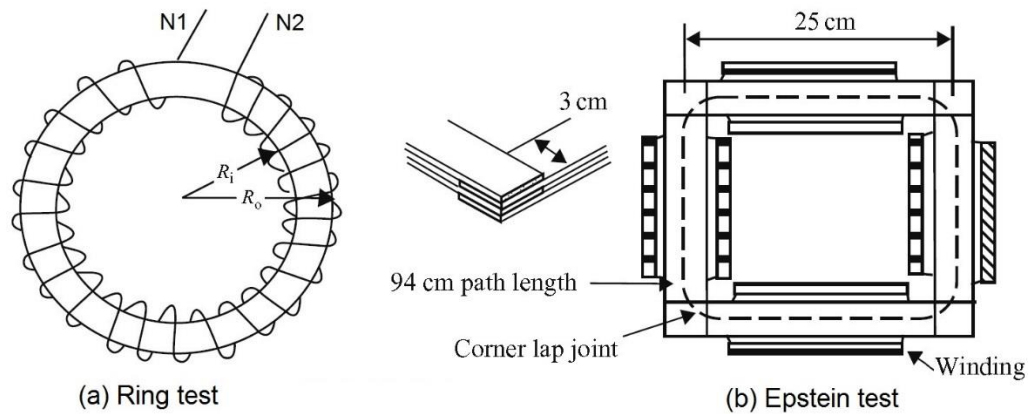


Figure 2.17: Magnetic measurement methods used to determine magnetic properties and iron losses in electrical steel sheets [3].

With the Epstein frame, measurements are taken using wide samples and it is thus not suitable for loss investigations in small sheet parts [27]. The drawbacks of the Epstein test can be avoided by using the single sheet tester. The SST method is used in a wide range of magnetic circuits in different configurations. For example, it may be used with or without closure yokes and with or without H-coils for direct sensing of the magnetic field strength [3]. However, the use of two-sided yokes is preferred to cancel the eddy current pools which add to measured losses and which may form in the strip at the limbs of one yoke. Some SST fixtures are shown in Figure 2.18.

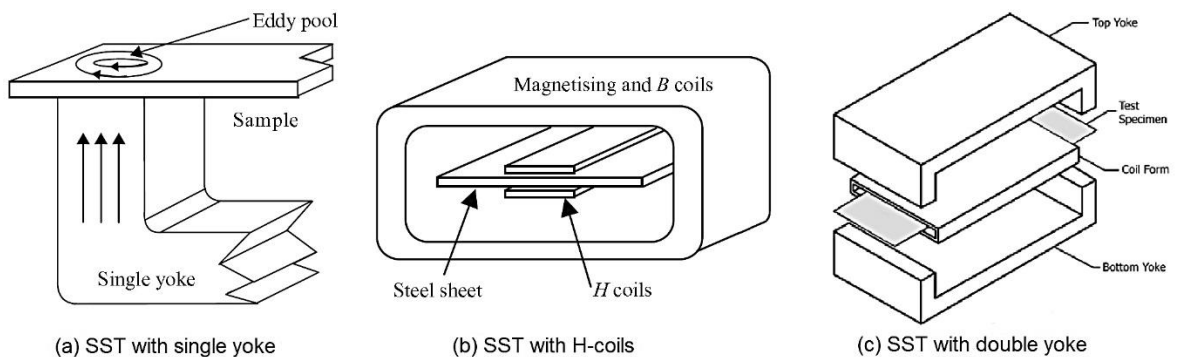


Figure 2.18: Single sheet tester fixtures for measuring magnetic properties [3].

M. Mikulec [34] investigated the accuracy of H-coil methods by evaluating the total measurement errors made by the single sheet testers (SST) in relation to the magnetic

properties. It was found that the causes of the measuring errors depended on the method of determining magnetic field strength in the specimen and measuring equipment. B. NAAS [35] evaluated the magnetic field strength using the single sheet tester for individual square sheet ($500 \times 500 \text{ mm}^2$) materials. The measurement efficiency was tested under unidirectional and sinusoidal flux density. It was found that the primary current did not have an effect because the frame shape was very complex and distant from the field, so two tangential coils were used to increase sensing of the magnetic field strength and obtain measured quantities. J. P. Schlegel [36], on the other hand, examined methods of measuring the magnetic properties and losses of individual non-oriented electrical steel sheets. The study examined three common types of test: single sheet tester, Epstein frame, and ring test.

A comparison was conducted to show the value and the efficiency of each measurement method, taking into account industrial considerations such as cost, time, complexity and accuracy of measurement. The ring test was found to be less expensive and more accurate than the other two types. In another study, E. Usak [37] studied the qualities of the double yoke type of single sheet tester. A magnetization field was applied by means of four magnetizing coils to a small specimen consisting of electrical steel strips. Test parameters such as the magnetization of field strength and flux density from the induction coil were measured. The measured quantities were compared with the results gained by the standard Epstein test method. The study found that the results differed between the two test methods and that it is important to calibrate the magnetizing circuit individually for each specimen. However, even with calibration, the magnetization curves were different from sample to sample. T. Nakata [38] investigated the efficiency of single sheet testers on the magnetic properties and iron losses measurement. SST was tested in different positions regarding the yoke position and the specimen material's dimensions and type. The study found that when using the closure yoke in the horizontal position loss measurement was highly influenced by the specimen width. Also, it commented that the accuracy of measurement at the horizontal position is less compared to the vertical type. N. Takahashi [39] examined a new method of testing magnetic properties for different sample sizes and geometries. The new technique included using an electromagnet and a specific probe with a very small active area. The test demonstrated the possibility of measuring the magnetic properties of a sheet or cylindrical shapes of soft electrical steel materials.

Moreover, the new test produced similar results in comparison with the conventional SST. H. Matsuo and M. Enokizono [40] used the single-sheet tester system to measure magnetic properties and losses for ES under DC power condition in both grain orientations. A comparison between magnetic hysteresis loops was conducted at a variety of magnetic flux densities. The research showed the possibility of using SST efficiently. Measurements indicated that the loss was dependent on the flux density and increased with increasing the indication flux. N. Takahashi [41] used the single sheet tester with two excitation coils in order to measure the magnetic properties of individual laminations of grain-oriented electrical steel. For accurate measuring, the SST was applied using diagonal exciting coils under high flux condition in arbitrary directions. The flux density, field strength and iron losses were measured under alternating rotating magnetic flux excitation. The results showed that there was an error between the two orthogonal coils of the B and H coils and clockwise excitation was different from that under counter-clockwise excitation, so the average value of the loss was obtained to conduct comparison with the ordinary Epstein tester measurements. Many investigations have been carried out of single sheet testing in relation to measuring magnetic properties. Each magnetic tester has specific features and the selection of tester type will depend on the required accuracy of measurement, sample size, the measurement position, and excitation type.

2.5 Methods for cutting laminations

There are many steps in the manufacturing of any machine core, including cutting the ES laminations, stacking, welding or sticking, and riveting. Any of these steps could have a significant negative effect on the resulting magnetic properties of the final product [3, 5]. The cutting process, which involves cutting the material and producing the final geometry of the electrical steel sheets, is a highly important procedure in the manufacturing of iron cores of electrical machines. It could cause modification of the material's texture at the cut edge, which could then influence the original magnetic properties and lead to an increase in the iron losses [3]. Several cutting methods are available, such as punching (blanking or piercing), laser, wire EDM, and jet water, as shown in [Figure 2.19](#). Method selection depends on several factors including production rate, cost, edge quality, and application type [5].

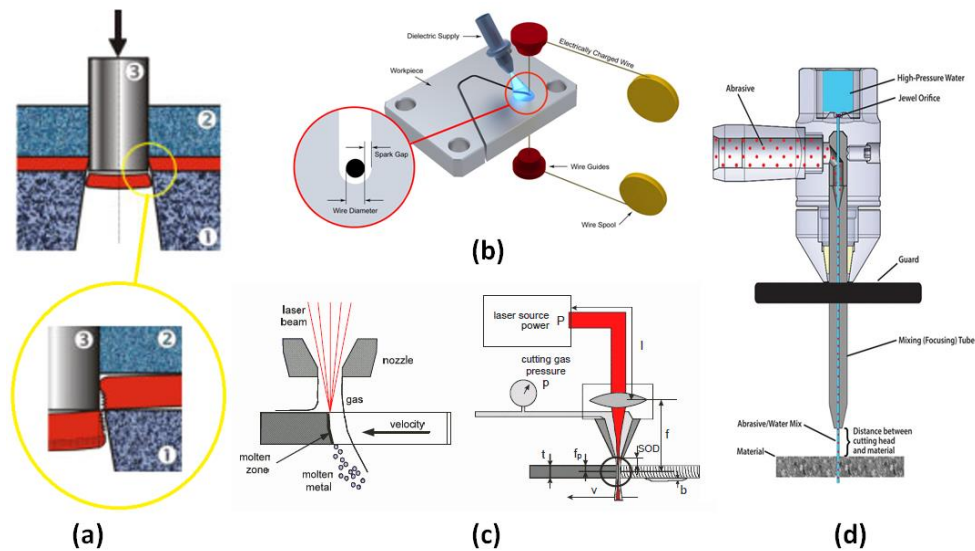


Figure 2.19: Lamination cutting methods, a) blanking, b) Wire EDM, c) Laser cutting, and d) water-jet [5, 42, 43].

The punching process shown in [Figure 2.19a](#), is performed by applying shear force using two tools called punch and die. The blanking method, which is the one adopted in the current study, requires specific dies to be made for the particular lamination geometry. Tool surfaces and the sharp edge can be affected by continuous production due to wear processes. Sometimes, both the stator and rotor laminations are cut simultaneously from the same sheet in order to reduce the amount of waste material and the time consumed by the cutting process [44]. The most important problem encountered during stamping cutting is burr formation at the lamination edges. These burrs may form electric paths for inter-laminar eddy current under assembly pressures. Consequently, the stamping operation must be carefully designed and controlled in order to keep the stamping burrs as small as possible [1]. The concepts and parameters of the blanking cutting process will be discussed in detail in the following section.

The electrical discharge method (EDM), sometimes called spark erosion, is shown in [Figure 2.19b](#). In this process, an electric spark is used to separate the work piece from the material by applying a pulsating electrical charge of high-frequency current through the electrode to the work piece. There are two types of EDM processes, one of which uses a formed electrode and the other uses a continuous moving wire electrode (Wire- EDM). EDM operations create surfaces with a relatively high roughness value of about 0.8 to 1.3

μm . Wire -EDM operation is commonly used to produce the prototypes of cores, pins, and stamping dies in small quantities [46].

In the laser cutting process shown in [Figure 2.19c](#), a laser beam is used as a thermal source to cut the material in different thicknesses. This method is applied to large-size laminations for which the stamping process may not be suitable [46]. This technique is also suitable for fast fabrication of motor prototypes because of its flexibility and its good dimensional accuracy. The drawbacks of laser cutting are the low productivity, and the higher cost compared to the blanking process. Changing the laser blanking speed can affect the cut edge quality. During laser cutting, an oxide film is generated on the burr, thereby reducing the conductivity of burr contact and reducing inter-laminar losses [1].

The abrasive water-jet (AWJ) machining process shown in [Figure 2.19d](#), uses a high-pressure water flow mixed with abrasive particles. The material is cut by spraying a jet of high-speed water from the nozzle onto the material surface. There is no heat generated in this process and it leaves no burrs or rough edges. It is a versatile machining process that is usually used for edge finishing and de-burring operations. Water-jet cutting can be an easy and efficient way of producing prototype parts. The main disadvantage of water-jet cutting is the limited number of materials that can be cut economically, and the time taken to cut parts can be very long and very costly. Also, thick parts such as stacked laminations cannot be cut with dimensional accuracy, and rough and wavy patterns may form on the cut surface. Moreover, the use of high-pressure water with abrasives requires special pressure intensifiers and sapphire nozzles that are costly and have limited flow capacity [45].

The effects of these processes on the magnetic properties of individual lamination electrical steels have been studied and compared to identify the preferred cutting method. Y. Demir et al. [46] studied the influence of punching, wire EDM, and laser-cut on stacked laminations for the rotor and stator of electrical motors. All tests were performed under the same conditions. The results of the comparison between the motor performances showed that the motor with wire-cut sheets produced the nearest results to the designed data compared to other methods. Also, microscopic observation of the effect of the cutting methods on the cut edge microscopically indicated that the blanking process produced a less affected edge, as shown in [Figure 2.20](#) a, b, and c.

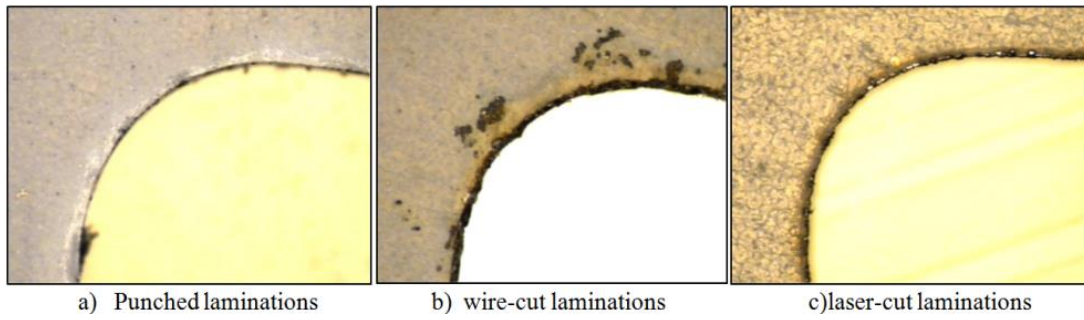


Figure 2.20: Effects of different sheet cutting processes on the cut edge [46].

S. Bayraktar and Y. Turgut reported similar results, using 0.5 mm of NGO laminations cut with different cutting methods and tested under AC current conditions. The authors found that the water-jet cutting resulted in the highest magnetic loss. The cut edge showed a higher amount of plastic deformation when using punching and AWJ, while the laser and EDM methods caused thermal degradation of the material.. The study also found that higher motor efficiency is achieved in cutting methods which produce lower average surface roughness (Ra), which is the case with punching, whereas in AWJ it is high, as shown in [Figure 2.21](#) [47].

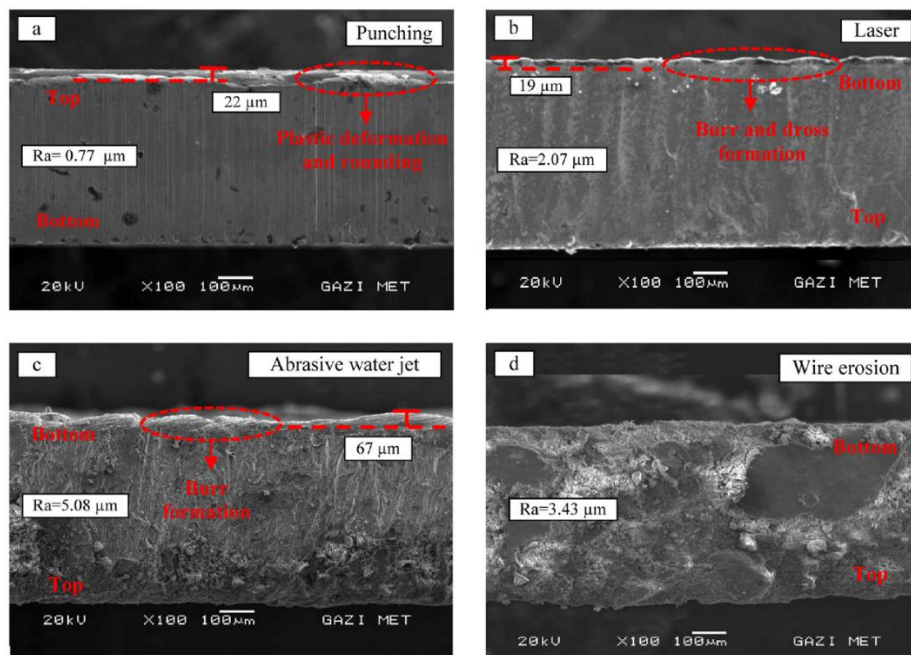


Figure 2.21: Cut edge surface roughness produced by different cutting methods [47].

V. Manescu [48] investigated the induced magnetic loss due to the laser and water jet cutting methods for ES with the thickness of 0.65 mm. The study found that the hysteresis losses were less for water jet than the laser cutting and depend on the impurities of the material. Because the laser method produced thermal stresses and local damages of the crystalline lattice and thereby affected the magnetic properties. This was explained according to domain wall impeded by the dislocation networks. Also, the permeability was influenced by both cutting processes [48]. The extension of deformation was approximately 0.3 mm, the extent of the affected area was less in the punching process than the laser cutting. Regarding the grains orientation, the differences in losses results were less than 10% between rolling and transverse directions, while differences in permeability were above 20%. Y. Kurosakia [49] also investigated the magneto properties of Non-grain oriented electrical steel (0.5mm thick and 2% Si). Blanking, laser cutting, and Wire EDM were used to produce ring shape sheets. The results showed the deterioration in magnetic properties due to the EDM method was lower than with the blanking and laser processes. Also, the hardness values at the cut edge were less in EDM than with blanking or laser, a finding which the researcher attributed to the porous surface produced by WEDM cutting.

Each of the cutting processes affects the cut edge quality and the mechanical and magnetic properties of the material. Therefore, many studies have been done to investigate the deformation effect at the cut edge. H. Naumoski et al. [50] investigated the influence of laser, EDM, and punching cutting on the magnetic properties of non-oriented electrical steel with a thickness of 0.35 mm and 2.8% silicon. The study indicated that all cutting processes induce stresses inside the material close to the cut edge and these stresses cause deterioration of magnetic properties. The EDM and laser processes produced straight cut edge profiles, while punching induced a typical burr and plastic deformation. The maximum permeability was decreased by about 35% and the losses were increased by 20% by using the punching technique. In addition, the observation test of domain wall displacement showed the domain structure changed over the first two to three grain rows near the edge. The domain wall movement could be the main reason for the changes in magnetic properties.

S Steentjes et al. [51] analysed the impact of material degradation on iron losses due to punching and laser cutting for non-oriented electrical steels of thickness 0.3 mm (2.4 % Si). Many 120 mm × 120 mm sheets were cut into smaller stripes in an attempt to investigate the local magnetic properties. The measurements showed increases of the hysteresis loss and decrease in magnetic permeability. The researchers explained that the

magnetic properties were affected as a result of the local modifications in the edge texture and stress state of the material; for example, dislocations and residual stresses during the punching process or thermal deterioration across the heat-affected zone in the case of laser cutting. T. Bulin et al. [52] described changes in magnetic properties after punching, laser, and spark cutting for toroid shaped samples of ES sheets M470-50A with thickness 0.5 mm (1.7% wt Si). The ring core magnetic test measurements showed that the sample that underwent EDM cutting exhibited the best magnetic parameters. In contrast to laser cutting, an important increase in total losses was observed in comparison with the punched samples. The study did not observe any changes in grain sizes in any sample, but plastic deformation was seen near the cut edge of the punched sample. Magnetic measurement also demonstrated that heat stress can cause significant changes in the material and its properties.

René Siebert et al. [53] investigated the effect of punching and laser cutting on the magnetic properties under both DC and AC conditions. Two electrical steel sheets with thicknesses of 0.35 and 0.5 mm were cut as strips in different widths from 5-30 mm. The study indicated that different cutting techniques under any power supply conditions can affect the structural features of the cutting edge. In the mechanical cutting, the plastic deformation appeared in the zone near the cutting line and caused a drop in the magnetic flux in the region. While cutting by laser process induced thermal stress which caused a decrease in the magnetic flux over the sheet width.

A. Belhadj et al. [54] investigated both the magnetic properties and the microstructure of non-oriented electrical sheets with a thickness of 0.65 mm. The study indicated that the mechanically cut samples retained better magnetic properties compared with the laser cut samples because residual thermal stress drawbacks caused an increase in the coercive field and a drop in the permeability. The laser process led to a drastic change in the texture of the HAZ along the cut edge. In addition, the study referred to the main factors which affect the magnetic domains' distribution and wall motions; for example, the texture obstacles which could pin the domain walls, such as grain boundary, precipitates, and dislocations. They also found that the mechanical cutting process generates a deformation affected zone (DAZ) less wide than the heat affecting zone (HAZ) produced in the laser cutting process.

M. Emura et al. [55] studied the magnetic properties for NGO electrical steel with 0.485 mm sheet thickness and 2% Si content using punching, laser, and EDM processes

with and without heat treatment. A plastic deformation was observed at the punching cut edge that extended about 0.3 mm, while the laser technique did not deform the grains and produced a sharp edge. The study showed that the cutting process had more effect on the magnetic permeability than on the magnetic induction losses. The differences between processes were less than 10% for losses and more than 20% for permeability. Also, it was found to be preferable to conduct annealing before rather than after the cutting process.

R. Roumaine et al. [56] tested NGO electrical steel with 0.65 mm thickness using both punching and EDM techniques. The researchers observed a plastic deformation near the cutting edge induced by punching methods. On the other hand, the EDM method did not induce mechanical stresses in the cutting edge zone because of the absence of contact between the material and cutting element. The deterioration of the magnetic properties was higher in the case of the punching method. This deterioration was interpreted according to the domain wall pinning resulting from the material dislocation network. The study also explained that the area affected by cutting is located around the core lamination teeth, and the accumulation of the effects of a group of teeth could result in a strong impact on the overall behaviour of the machine.

E. Gomes Araujo et al. [57] discussed the effect of the microstructural changes resulting from mechanical and laser cutting on the hysteresis losses of non-oriented electrical steel with 0.5 mm thickness. Plastic deformation was visible near to the mechanical cutting line, whereas laser cutting did not induce clear changes in the sheet surface morphology. The investigation also found that the magnetic losses became worse at large grain size. According to P. Lazari et al. [58], the resulting microstructure features were quite different between the mechanical and laser cutting methods, although both caused worsening of the magnetic properties of the tested electrical steels. The damage caused by the laser method was more extensive than that caused by the blanking process due to the temperature gradient during the process resulting in a substantial permeability reduction.

G. Loisos and A J. Moses [59] confirmed that changes occur in the microstructure of the material near the cut edge through using both blanking and laser methods to cut flat rectangular plate of electrical steel sheets 0.5mm. The study attributed the high magnetic loss after laser cutting to the rapid heating and cooling causing thermal stresses, despite the fact that high temperatures may cause grain growth which is sometimes beneficial for the magnetic properties. In addition, the induced plastic deformation in the

blanking process affected the magnetic flux distribution which in turn influenced the magnetic domain structure and domain wall motion during the magnetization process. P. Baudouin et al. [60] conducted a comparison between laser cut technique and punching cutting for three grades of ES with 0.31 thickness and 2.98% Si. Their results tended to indicate the superiority of mechanical cutting for the larger samples, whereas the laser cutting gave more satisfactory results for the smaller samples. The laser cutting technique caused more deterioration, although it was difficult to make a clear evaluation of the effect of the internal stresses on the magnetic properties of the electrical steels following cutting.

Each method is still selected for use in industry depending on the particular application and influence of the material [43]. However, it is generally accepted that the punching process is the most preferred method and the most desirable for producing core laminations from electrical steel sheets. This is because it can be used for mass production at lower cost and with acceptable cut edge quality compared to the others methods. Therefore, this method is adopted in the present study to achieve the study purpose of quantifying local deformation of blanking induced magneto-mechanical cut edge defects in electrical steel. Table 2.1 presents a general comparison of the performance of the different cutting methods in terms of the most important factors:

Table 2.1: Comparison of the performance of lamination cutting methods [43, 46].

	Punching	Wire EDM	Laser cutting	Jet water
Production size	Mass production	Prototype laminations only	Prototype and large-size laminations	Prototype and de-burring operation
Cost and time consumed in large-scale production	Fast, low cost	Very slow and high cost	Very slow and high cost	Very slow and high cost
Product shape flexibility	Dies cannot be changed easily	Flexible geometry design	Flexible geometry design	Flexible geometry design
Defects at cut edge	Plastic deformation Residual stress, edge burrs, no thermal distortion	High thermal stress, Burn coating layer	High thermal stress, Formation of oxide film, Burn coating layer	No burrs or thermal distortion, rough and non-straight edge for thick sheet

2.6 Blanking process

Blanking is a process used to cut sheet material to the required shape. The process is usually performed using a set of cutting tools called a die and punch as shown in [Figure 2.22](#). When the material is sheared during the blanking process, a plastic deformation occurs and stresses are generated in the sheet at the cut edge that cause work hardening. The strengthening of the metal occurs because of dislocation movements and dislocation within the crystal structure of the material.

The sheet is cut along the shearing line in one step to separate it from the surrounding material. If the cut part is the desired product, then the process is called blanking. Whereas, if the original sheet is the product and the cut part is scrap, then this method is referred to as piercing. Both are sometimes referred to as punching, as shown in [Figure 2.23](#). The process is performed at room temperature. Occasionally, if the sheets are extremely thick or high strength material is used, then warm or hot stamping is performed to decrease the forming force and increase formability [4, 61].

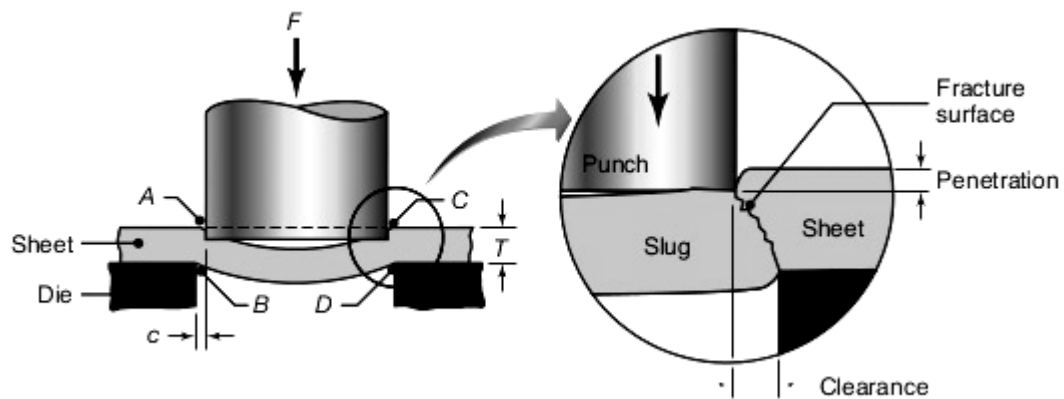


Figure 2.22: Blanking process mechanism [5].

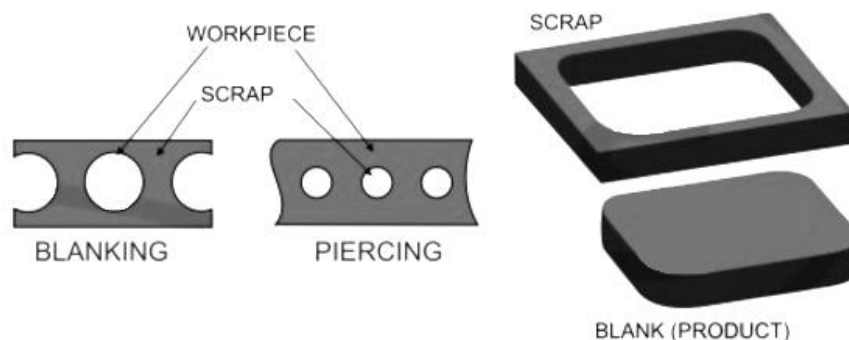


Figure 2.23: Punching, blanking, and piercing operations [5].

2.6.1 Mechanism of the blanking process

The blanking method consists of four sequential deformation stages that complete the cut cycle, as seen in Figure 2.24. Shearing generally starts when the edges of the die and punch come into contact with the top and bottom edges of the workpiece. In the second stage, the punch moves down and pushes the material against the die cutting edge to form the rollover zone. Then the punch moves more and penetrates further inside the material to produce a shearing surface. Finally, cracks are formed on points A and B, and C and D as shown in Figure 2.22. Cracks propagate to meet each other and complete separation, with the fracture surfaces resulting due to these cracks. If proper clearance and precise alignment are achieved, the fracture lines on the opposite sides will meet, resulting in a straight cut edge and smooth surface separation of the workpieces [61, 62].

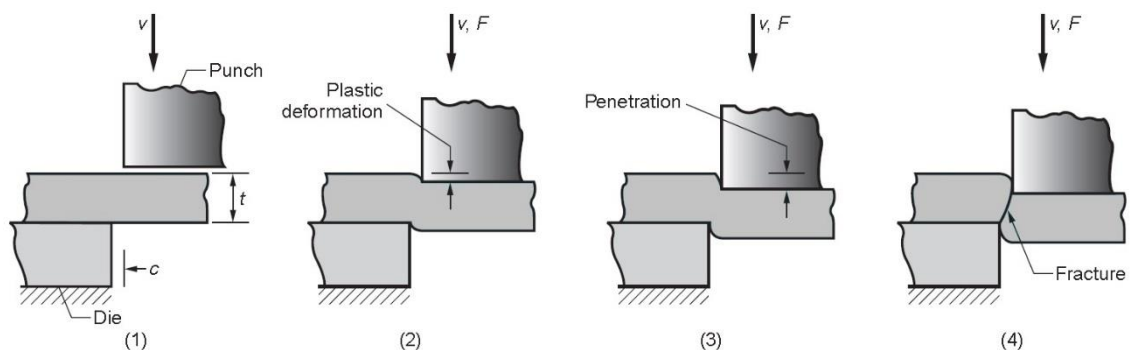


Figure 2.24: Blanking process deformation stages [61].

Different zones called rollover, shear, fracture and burr zones are generated in the cut edge surface of blank sections during the blanking operations; the size of each zone is dependent on process parameters such as tool condition and material properties. The ratio between these areas represents the quality of the cut edge; usually, large shear zone and smaller burr zone represent good edge quality [64]. The cut edge zones are shown in Figure 2.25 and defined as follows:

- Rollover zone (Z_r): Initial plastic deformation that forms at the top of the cut surface due to the first entry of the punch into the sheet material.
- Shear/burnish zone (Z_s): Smooth and shiny area resulting from material shearing due to the penetration of the punch into the work before fracture begins. Two areas could be generated if the cracks do not grow toward each other.

- Fracture/rupture zone (Z_f): Below the burnish is the fractured zone, a relatively rough surface of the cut edge. The depth of crack penetration (D_{cp}).
- Burr zone (Z_b): An extended area of material at the bottom of the edge caused by plastic elongation of the metal during the last separation of the metal.

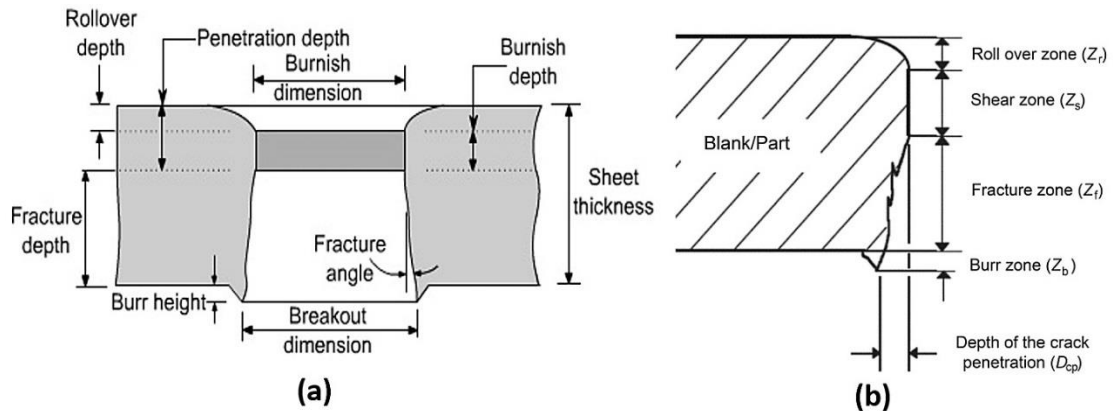


Figure 2.25: Deformations zones of the cut edge: a) characteristic edge in blanking process, b) blank side-scheme areas [63].

Blanking can cause further effects when a mismatch occurs between the punching strategies used and the material's properties. Burr is an important feature that can arise when displacing metal during the blanking process. Burr is a sharp edge that forms at the cut edge. Appropriate selection of blanking parameters, for example, sharp tools, suitable clearances, and high blanking speed, could reduce the burr size [4, 63].

2.6.2 Analysis of applied stresses during the blanking process

The cutting forces have two components: vertical (F_v) and horizontal (F_H). Affecting both is nonlinearity near to the cutting edge because of the existence of the distance l between the vertical compression forces. Thus bending stresses are created and lead to tilting of the sheet, as shown in Figure 2.26. In addition to these forces, there are frictional forces ($\mu F_{v \text{ or } H}$) between the workpiece and the die and punch tools which increase the required cutting force [4, 63].

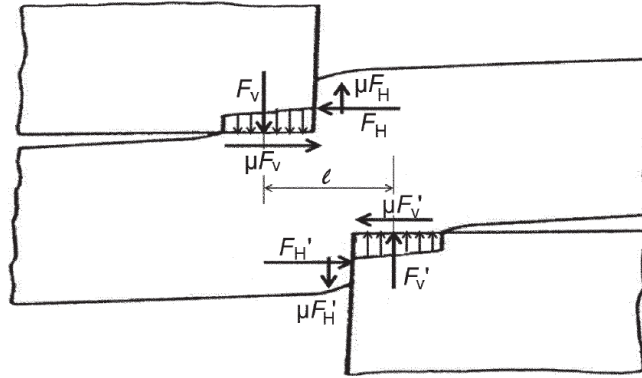


Figure 2.26: Forces distribution in the workpiece during blanking process [63].

The following equations can be used to estimate the cutting force and stress required to conduct the blanking process:

$$F = L \times t \times S_s \quad (2.1)$$

$$S_s = \frac{F}{A_p} \quad (2.2)$$

Where F is the force required for blanking, l is the perimeter of the cut, t is the sheet thickness, S_s is the shear strength of the material, and A_p is the cross-sectional cutting area. The blanking quality is assessed according to the zones formed at the cutting edge, and these areas directly relate to the punch movement steps during the process, each step corresponding to load value. Figure 2.27 shows a typical force-time diagram of the punch movement during operation.

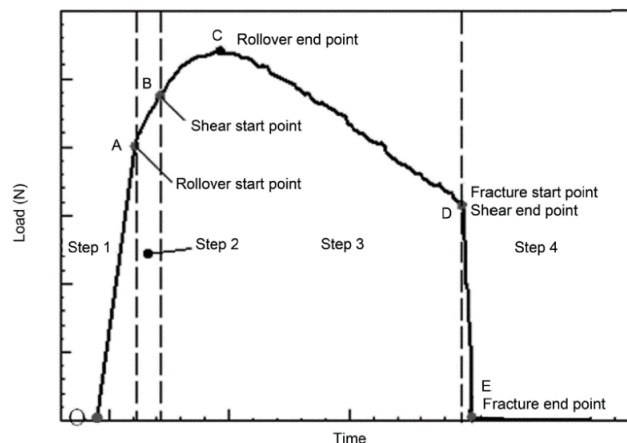


Figure 2.27: Typical load-stroke curve of a blanking [4, 63].

At step 1, an elastic deformation occurs. Then, in step 2, the material is flowing and this may cause a strain hardening, in which the force existing here increases up to the maximum load. At this stage, the cross-section is not reduced, and shearing has not started. The increased pressure at the cutting edges at step 3 prevents the material from flowing,

and shear starts. The blanking force decreases because of decrease in the cross-section, despite the strain hardening of the material. In the step 4 an initial crack is generated in both contact sides between the sheet and tools and fracture starts and then grows until complete separation occurs; because of the limit of material formability exceeding the cutting, the force will decrease rapidly during this phase [63].

2.6.3 Influence of various process parameters on blanked edge quality

There have been several research on the effects of blanking parameters on the process results and the sheared edge quality. Figure 2.28 shows an infographic of the possible parameters affecting the blanking process according to E. Al-Momani [65].

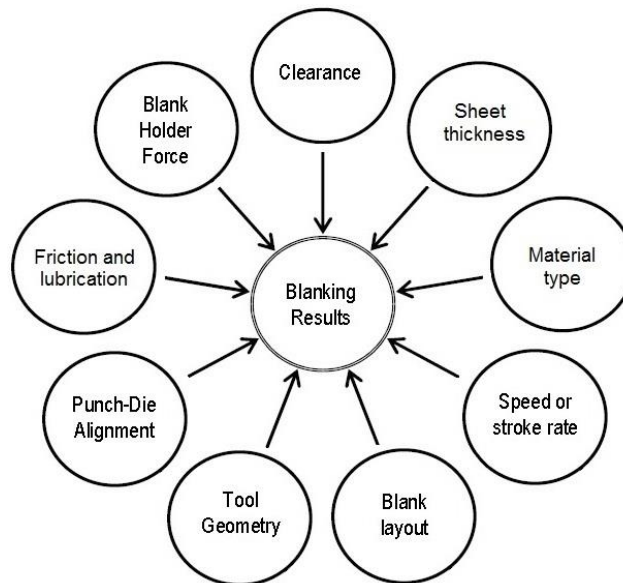


Figure 2.28: Parameters affecting the blanking process as indicated in [65].

As the material undergoes severe plastic deformation and shearing during the blanking process, the micromechanical properties of the sheets close to the cut edge are adversely affected by the blanking process and thereby the material properties are changing negatively during the cutting process. These changes occur due to shearing stresses and crystal deformation [50, 62].

It was reported [63] that the blanking parameters effects are interlinked therefore it is very difficult to study their effects individually; for instance, tool wear increases with a large punch and die edges radius and could cause height burr. Additionally, tool wear is increased by increasing the clearance; therefore, sometimes lubrication is necessary to reduce punch wear [63]. Therefore, most studies showed the parameters in a way that

demonstrate their effect on one of the process output such as the required process load or the sheared cut edge quality with specific process settings. For example; the effect of clearance on the cutting force and the geometry of the shared edge profile regarding the sheet thickness and material properties, or tool wear and tool life, or blanking speed and production rate with blanking load [66]. Also, the quality of the cut edge is dependent on blanking parameters, therefore the optimization of the blanking process depends on the required part quality and production rate. However, according to the studies related to the blanking process, there is a strong dependence between the geometrical quality of the blanked part and the magnitude of the force applied on the tool as well as the variations in the process factors [66].

2.6.4 Effect of blanking parameters on the required cutting force and cut edge quality

Clearance refers to the space between the die and the punch and it directly affects the blanking performance regarding the quality and shape of the cut edges of sheet material. The clearance is one of the key parameters affecting the blanking performance and cut edge quality. The clearance is one of the key parameters affecting the blanking performance and cut edge quality. Its value mainly depends on the type of material to be cut as well as the sheet thickness and estimated to be at approximately 5-20 % of the thickness [4,5]. When clearance increases the material tends to be pulled into the die rather than being sheared and the zone of deformation zone becomes bigger with a rough sheared edge [5]. That can lead to an increase in the shear zone and a decrease in the rupture zone [5, 63]. [Figure 2.29](#) shows the effects of clearance and strain hardening at the shared area.

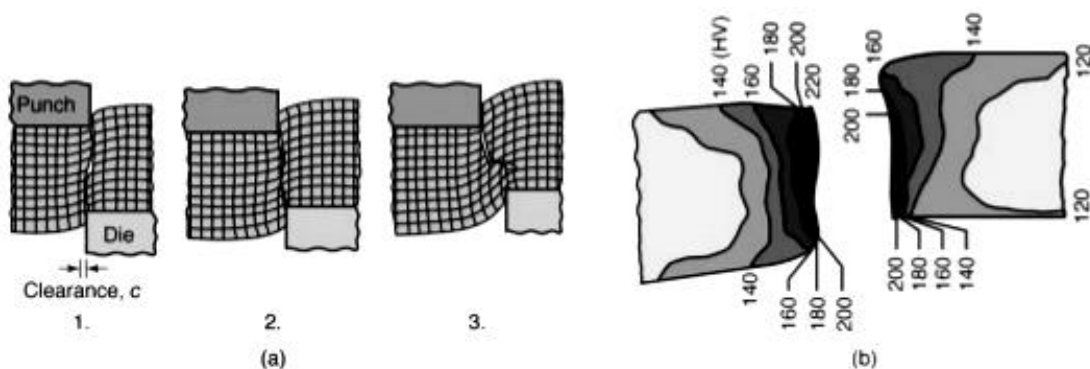


Figure 2.28: a) Effects of clearance on the deformations zone and vicinity areas, b) Vickers hardness contours expressing the cold working in the shared region [5].

According to [4] for blanking of 0.58 mm sheet thick, that when the clearance between the punch and die increases, the rollover zone, fracture zone, fracture angle and burr increase while the shear zone decreases. Excessive clearance causes large plastic deformation and lowered tool life. While using insufficient clearance produces secondary shear i.e. the cracks originating at the punch and die do not meet and cause further material stressed and thereby expending more energy. The impact of factors clearance and tools radii regarding cut edge zones are shown in Figure 2.30.

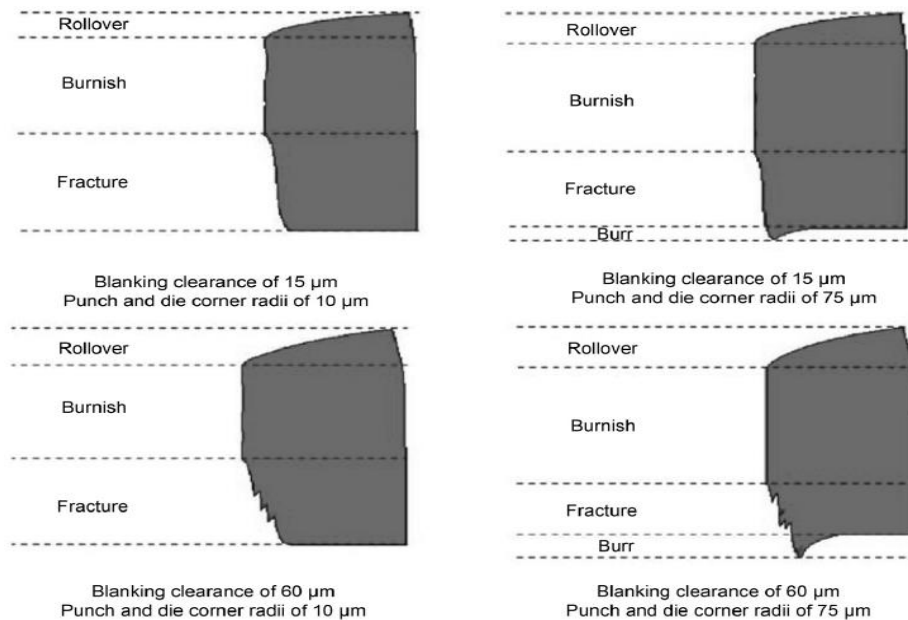


Figure 2.30: Effect of clearance and tools radii on deformations of cut edge [4].

C.Husson et al. [67] conducted blanking simulations of a copper alloy of sheet thickness 0.58mm and compared it with experimental results. The effect of punch-die clearance on the part edge quality was studied in the range of 2.5 -19 %t during blanking of 3.5mm diameter holes. It was found that rollover and shear edge increase and fractured edge decreases with increase in blanking clearance. The fracture angle increases significantly with clearance.

R.Wiedenmann et al. [68] conducted blanking studies on steel with 1.4mm thick. The effect of clearances on part edge quality in the range of 5-20%t was studied during blanking of 10mm diameter holes. It is reported that the size of roll over and fracture zones increase with clearance while the shear zone decreases with clearance.

Some studies have focused on the influence of the main blanking factors on the quality of the cutting edge and the required energy or load applied. For example, S.

Subramonian [69] investigated the influence of tool wear and stresses generated on the tool life, the study showed that the induced blanking stress was decreased with increasing punch radius. S.K. Maiti [70] conducted analysis of the blanking process of thin sheet mild steel to examine the impacts of die clearance, friction, and material thickness on the required process load. The achieved results showed that blanking load increases with reducing the tool clearance and when the coefficient of friction is increased.

Moreover, the change in the clearance did not affect the growth of the plastic deformation zone. A. Zaid [71] reviewed the effect of some blanking parameters including die and punch clearance, tool edge radius, and the effect of punch and die wear on the force and energy required for the operation as well as on the quality of the products. The study found that, at the low blanking speed of about 5 mm/min, the sharp tool edge with small radius produced better blanking quality. The blanking force and energy were found to decrease with increasing punch radius and possibly affect the tool life. Moreover, increasing the profile radius caused enlargement of the shear zone and delay in crack formation.

R. Hamblin [66] attempted to optimize the interaction between the clearance, tools wear, and sheet thickness on the cutting force and the geometry of the sheared edge profile. The results also demonstrated a complex variation in the process parameters. Moreover, there was strong interdependence between the blanked geometrical quality and the force applied by the tool. It was found that higher energy was required to cut thicker sheets whereas the blanking energy decreased with increasing clearance to-sheet thickness ratio c/t . Shim, et al. [72] conducted experimental studies in thin sheet metal blanking to investigate the effect of punch speed, lubrication, and tool clearance on the sheared surface and fracture locations during the deformation process. It was shown that an increase in punch–die corner radius causes an increase in the burr height and expansion of the effective sheared surface and early crack initiation. A.M. Govaerts [73] attempted to determine the stress relation for large strains in the localized shear zone by conducting tensile testing to characterize the criteria. The study found that characterization of the blanking stresses using tensile results is not valid because of the large strains in the localized shear zone. Greban et al. [74] investigated the effects of both sheet microstructure and process parameters upon the cutting edge quality. The quality of sheet metal blanking was quantified according to the relative ratio of the known four cut edge zones. A better blanking quality was identified by a small fracture zone and a larger

shared zone with lower burr height. The study showed that the burr size depended mainly on the blanking clearance and the material type rather than the rate of work hardening. In addition, the roll-over zone was influenced by the geometry of the blanking process, whereas the shared and fractured areas were mainly influenced by the mechanical properties of the sheet. Usually, the blanking process is performed at room temperature. However, Qin et al. [75] conducted the blanking process on Non-oriented electrical steel at a different temperature of about 100 °C. The microstructure results showed that increasing punching temperature or refining grain size can improve the ductility and punch-ability of the material, but affect the edge quality by producing larger burrs at the cut edge.

2.6.5 Effect of sheet thickness on the required cutting force and cut edge quality

The Increasing demand to improve the magnetic properties by means of reducing the eddy current loss led to reducing the thickness of the sheets used in the blanking process. However, reducing the sheet thickness can affect the grain size cross the thickness sheet area. In addition to the affecting the cut edge zones such as the fracture and shear areas. The increasing the sheet thickness will increase the blanking load, as the cut area will increase [76].

As the sheet thickness reduces, the effects of grain sizes (size effect) increase and the understanding of the blanking process becomes more complex. Thus, the deformation behaviour of the blanking process not only relates to the blanking parameters but also relates to the grain size of ES sheet. This is mostly due to the fact that few grains exist through the thickness of the sheets leading to large variations not only in the cut edge profile but also in blanking deformation distribution. Therefore, the grain size has a significant influence on the blanking process [76].

Joo, et al. [77] studied the size effect in the punching process. The study indicated that when there are only a few grains cross the sheet thickness, the conventional ductile fracture by crack initiation and propagation does not occur and the shear deformation is dominated along the cutting line. Blanking tests of the thin sheet were conducted by Xu, et al. [76] to investigate the influence of die clearance and grain size on the deformation and fracture behaviour of thin sheet material. The results showed that the deformation depth decreases with an increase of specimen thickness. Based on the experimental results

of the blanking process, the shear deformation is concentrated with just a few grains that confined by the punch and the die. The distribution and crystal orientation of grains also play a decisive role in shear deformation observed in sheet metal blanking process. With the decrease of sheet thickness, the number of grains in the cross section of the sheet decreases and the effect of anisotropy of grain becomes more visible.

The slip and coordination of grains during the shearing deformation is a very complex system, as mentioned in the literature [78], where the distribution of sheared edge was still remained rollover, burnish, fracture and burr. However, the fracture mechanism could change from ductile fracture to slip and separation with the decrease of length scale because of the existence of a few grains in the thickness direction. That makes the orientation of these grains very important, especially for the cutting direction. The grains having an extremely unfavourable orientation towards the blanking direction leads to more difficult shear deformation and coordination. The results also showed that the blanking force decreased with the increased relative blanking clearance ratio.

It is reported that the sheets with coarser grains could show a strong variation not only in maximum blanking force but also in the cut edge profile [76]. It is shown that for the sheets having larger grain sizes the geometry of the cross-section significantly varies not only in the profile of blanking edge but also in the distribution of rollover, burnish, fracture and burr zones. These extreme differences can be related to the variation of deformation behaviour during the blanking process where only a few systems are available to define the deformation mechanics. However, for the case of sheets having fine-grained microstructures, there could be more random grain orientations some of which would be in favour of applied deformation and stresses, therefore, the effect of grains orientation will be smaller having more favourable grain sliding systems. In the blanking process of coarse-grained sheet specimen, the grain crystal orientation varies and the sliding systems are oriented differently with the blanking direction.

The material deformation during blanking is not only related to the blanking parameters such as clearance, but also to the grain size of the sheet. Therefore, the ratio of blanking clearance to grain size may considerate as one of the main factors to influence the deformation behaviour of blanking.

2.6.6 Effect of blanking speed on the required cutting force and cut edge quality

Punch speed can be expressed as the number of strokes per time or punch moving distance per time [5]. The sheared edge can undergo severe cold working due to the high shear strains involved, and when the blanking speed is increased, the heat generated by plastic deformation may be limited to a narrower zone creating adiabatic heating conditions [5].

Blanking can be performed at different blanking speeds depending on the blanked part application and the available machine capacity and blanking conditions such as tool life, parts accuracy, material properties and thickness, and production rate. Blanking is sometimes performed at very high speed when large numbers of products and high precision are required, such as in the case of electronics parts. High-speed blanking is usually run at speeds of around 2000 strokes per minute. Cutting forces change very rapidly during material breakthrough. These forces can affect the tool life of dies and parts quality [4]. Increasing blanking punch speed can improve edge quality by means of lowering the altitude of burr and rollover zones while the shear zone increases. In addition, higher the blanking speeds can reduce production costs and energy consumption [79]. The blanking speed may rise to a very high value called ultra-speed wherein the punch velocity can reach more than 5 m/s. UHS blanking can provide very high cut edge quality to produce a fine blanking product at a lower cost. At ultra-speed, materials go through the different blanking phases including elastic, plastic, and fracture.

Moreover, different cut-edge zones may form and may omit the formation of rolled edges and burrs. The conversion of mechanical work into the thermal energy and presence of adiabatic heating conditions results in an increase of the temperature in the deformation zone during a very short period of about 100 μ s. The heat generated will not dissipate as quickly as it is being produced, which leads to instant softening of the material. The kinetic energy of the moving parts and potential rebounds may also affect the generated deformation and stresses in the cut edge [4]. The generated heat is distributed to the vicinity of the cut area by thermal conduction. In high punch velocities, the limited balancing of temperature causes concentrating temperature at the deformed cutting edge. In contrast, at slow punch velocity, the heat is dissipated out of the shearing zone because there is enough time for thermal conduction to occur [80]. The velocity of blanking has a significant influence on the forces generated in blanking such as [81].

There are conflicting data concerning the effects of shearing speed on the energy requirement for shearing [82]. Depending on the strain rate and the flow strength of the material, there could be a reduction in the energy required for shearing [82]. However, there are three available potential explanations; first, when the strain rate becomes sufficiently high, thermal softening effects that outweigh work hardening may occur in the shearing zone [81]. Another possible explanation is that the elastic compressive forces stored in the punch during blanking are released more rapidly at higher speeds [81]. The other possible explanation is that the quick impact of punch speed can apply high kinetic energy and cause quick crack initiation and propagation in the material; this reason could apply to the normal blanking speeds.

Several studies of the blanking process have been proposed to assess the influence of blanking parameters, but only a few are concerned with the punch velocity regarding the blanking cut edge deformation as it usually describes regarding the blanking load. Marouani et al. [83] conducted experimental and numerical investigations of the sheet metal blanking process to study the influence of punch speed (strain rate) and the clearance on the punch force, punch penetration and the shape of the cut edge. A 0.65 mm thick sheet of non-oriented electrical steel was used. A range of die clearance and punch velocity of 23 to 123 mm/s were applied. The results showed that the maximum punch force increases when the clearance decreases. Additionally, it was found that the shape of the cut edge is affected by the strain rate (punch velocity) where the sheared zone increases with the punch velocity. In addition, the clearance is shown to affect the punch penetration at fracture, and consequently, the shape of the cut edge.

Grunbaum et al, [84] investigate the blanking process for different materials at clearances ranging from 5 - 20% T sheet thickness. 12.7mm diameter holes were blanked. Experiments were conducted at different blanking speeds ranging from 0.15- 3.6 m/sec. according to the reported findings, the length of the shear zone is in direct correlation with the blanking velocity while it decreases with an increase in clearance for all materials. Hirsch et al. [85] conducted experiments to measure punch loads in high-speed blanking for various stroke rates 100, 300, 500 and 1000 strokes per minute for 0.29 mm sheet thickness. The results showed that the measured blanking force was increased with increasing cutting speed a bit and caused high vibrations of the stripper plate. Goijaerts, et al. [86] described the effect of punch speed on the blanking process for punch velocities from 10 mm/s up to approximately 1 m/s. The results showed a drop in the maximum

blanking force at larger punch speeds. This is reported to be a due to an increase in the thermal softening effect for the blanking process at larger punch speeds. Gaudilliere, et al. [87] measured the blanking force at different speeds for different sheet thicknesses of 2-4 mm. The measured of maximum force was decreased with increasing punch speed. The study showed that the specimen fracture takes place earlier for a lower penetration depth of the punch when the punch speed increases. Also, according to the authors, thermal softening of the material can play a key role compared with the strain and strain rate hardening. This is partly supported by the stud from Grunbaum, et al. [88] who investigated variations in the effects of different levels of blanking speeds on the blanking force and energy. The results at very high blanking speed showed a very high temperature concentration in a narrow shearing zone. In addition, the kinetic energy at high speeds was much higher than the energy required for the normal blanking speed. Moreover, results of part quality investigations have demonstrated the positive influence of high blanking speeds on the quality of the part edge. S.Krrabaj et al. [89] investigated the effect of blanking speed on the blanking performance using different punch-die clearances at different blanking speeds. The study found that conducting the process at higher speeds caused reduction in the punching force and improved the quality of the part edge as represented in a larger shear zone, smaller burr height, and rollover area. The study showed that the speed of the deformation significantly affects the blanking force. Also, it was concluded that at a specific blanking speed, the relationship becomes nonlinear between the speed and force. Meanwhile, at different blanking speeds, the cut material can show different behaviour which can result in a diverse cutting force [89].

2.6.7 Strain fields measurement

The traditional extensometers are used to measure the strain. However, they are limited to measure the average strain on a selected length. Even though this technique is accurate, but it is complex to operate especially for very small deformation area with a non-axial flow direction of the material [90]. All of these drawbacks of using the extensometer can be avoided by using the Digital Image Correlation or DIC technique. The DIC can measure the full-field strain distribution in the material during various deformations conditions [91]. The studies demonstrated that DIC is an accurate and reliable approach for taking strain measurements. The non-contact optical technique is well suited for characterizing the mechanical properties of the material in both elastic and plastic ranges.

DIC method includes acquiring images for the specimen surface before, during, and after deformation. The distribution of displacement vectors is obtained by recognition of kinematic changes in the surface patterns feature [92]. The measurement of displacement in DIC can be determined by solving nonlinear simultaneous equations of the subset deformation. Strains are obtainable by differentiating the measured displacements of the new position of the subset of the reference image in the deformed image, as shown in Figure 2.31[93].

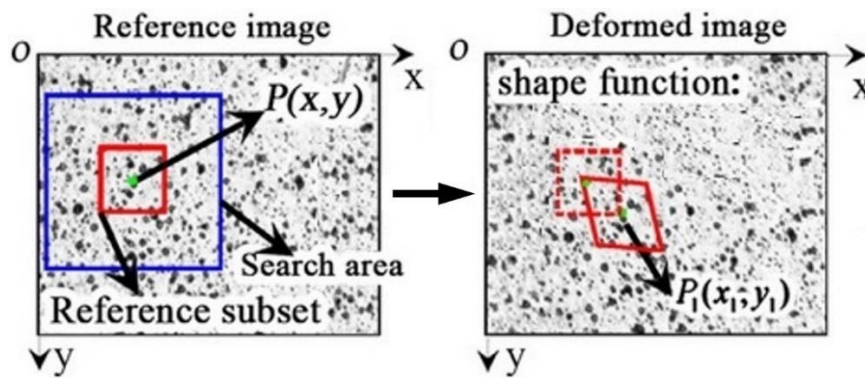


Figure 2.31: The principle of the DIC measurement method based on the differences between the target subset and the reference subset [94].

The natural features of the surface pattern can be used as a reference pattern, or random speckles can be created artificially using spray paint, usually by making two layers, white background with black speckles, or vice versa [93]. According to S. Yoneyama [93], using a small subset size increases measurement accuracy. The appropriate subset size depends on the number and size of the speckles or features in the random pattern regarding the deformation area.

The selection of DIC camera and focusing lens depends on the application rate and deformation zone size. For example, high-speed blanking requires a camera with a very high recording rate because of the short duration of the process and low thickness of the sheet [93]. The DIC camera is placed in such a way that the optical axis is perpendicular to the sample surface. The system can be coupled with microscopy to reveal the micro-scale measurement [13]. To achieve more contrast with high image resolution, zooming of the lens should be avoided [93].

The system has advantages represented by high accuracy of providing a whole field of true strain measurement. Also, DIC can measure strains at any point in the specimen or local strain, in addition to measuring the average strain or global strain by

applying the strain gauge across the gauge length [95]. However, DIC method also has some disadvantages; for example, the sample surface should have clear features, the measurement depends on the quality of the imaging system, and this technique cannot be applied only on exposed surfaces [13].

Practically, there have been few previous attempts to conduct strain measurement during the blanking process. That is because many technical challenges can appear when implementing full-field techniques such as DIC to measure local strain in the material during blanking operation, including the limited access to the deformation zone and the high speed of deformation, and very thin sheet such as electrical steel sheets [90, 92]. Goijaerts, et al. [96] conducted DIC at low blanking speed on stainless steel sheet with a 1mm thickness. The study located markers of the surface features to use as the random pattern. The results proved that the DIC method was suitable for observing the local strain fields in a blanking. Chen, et al. [90] investigated the strains distribution during operation of the Punch-stretch method. This work included using the 3D digital image correlation test to evaluate the strain distribution only for the area around the punch when the sheet was stretched. The cameras were attached to the hole in the upper die and the punch was travelling at a very low speed of about 0.5 mm/s. The study found that the DIC technique could provide accurate data for investigating the strain behaviour. According to the study, the specimens with lower width were exposed to fracture faster because the strain path is prone to uniaxial tension and change in the formability of the material. Moreover, the DIC cameras should not be attached to test tools because vibration and instability of the camera could affect the image quality and measurement accuracy. V. Bratus et al. [97] investigated the stamping process using electrical steel sheets with a thickness of 0.5 mm. System images followed the speckles during deformation with a CCD camera, and spray paint was used to create the speckles on the sample surface. The results focused on the profile of the round cutting edge in different directions. According to the study, the shear strain had no influence on the diversity on the final profile of the cutting edge.

Liutkus, et al. [91] conducted a 3D DIC for a punching experiment to investigate the plastic deformation of a sample in a tubular die having two narrow slots on opposing sides to allow two cameras to view the rear surface of the specimen. Three different punches tip geometries were used in these experiments. The obtained images were processed with a commercial software from Correlated Solutions (VIC) to calculate the full field measurements on the rear surface of the thin disk specimen. The material showed

significant strain hardening. In addition, the material's behaviour changed at high temperature, with the material showing decreasing flow stress with increasing temperature. Slavic et al. [98] used an in-situ blanking apparatus to identify the effect of blanking on electrical steel sheet with 0.5 mm thickness. Small holes were produced to study blanking parameters such as load, speed, punch-die misalignment, and temperature. The blanking speeds ranged from a very slow 0.1 m/s up to 4.5 m/s. Laser displacement and a thermal camera were used to measure the velocity and temperature of the sheet metal during the blanking process. The results showed that the punch-die misalignment changed the maximum force by up to 4%. Furthermore, the temperature of the sheet surface was increased by approximately 20°C and the research supposed that the hot-spot temperature inside the shear zone could be several times higher. The blanking force decreased slightly with an increase of the blanking speed, which the researcher attributed to the softening of the sheet metal because of the increase of temperature in the shear zone. Another reason could be inertia or the acceleration of the punch during blanking which was found to significantly affect the identified blanking force.

Wang and Wierzbicki [99] implemented the DIC test in blanking of high strength steel sheet with a thickness of 1.6 mm. The test was interrupted to study the crack formation and propagation during the blanking. The tests were performed at a very low cross-head speed of 0.01 mm/min. The results showed that two cracks were formed when blanking with a small die clearance, while only one crack arose when a large clearance was used and this caused formed the burr feature. Wang, et al. [100] conducted a similar study to compare the DIC results with the traditional method using an extensometer. Both were conducted simultaneously during a tensile test, with the front surface of the specimen measured by DIC and the back side of the specimen measured by the extensometer. The average results were convergent. However, the DIC measured the full-range strain distribution during the tensile test, while the extensometer measured only the average tensile strain. The studies demonstrated that DIC is an accurate and reliable approach for taking strain measurements.

2.7 Effect of plastic deformation and residual stress on the magnetic properties

When removing the applied elastic stress will permit the metal to return to essentially a stress-free condition and the magnetic properties will recover their original state.

Therefore, the measurement should be carried out during the applying of the loads when investigating the effect of elastic stress on the magnetic properties.

At plastic deformation, the material will retain permanent strain even though the loads are removed and elastic stresses are relaxed [3, 23]. In this case of deformation, the measurement can be performed after the test on the deformed samples. A complex of plastic deformation occurs due to the blanking process at cut edges of ES sheet when producing teeth and slots of the laminations. The impurities, residual stress, and grain boundaries could increase the effect of the deformation, causing a significant impact on the pinning of domain wall movement and thereby on the loss as explained in the previous sections. The average domain wall velocity will decrease and cause slower transverse energy due to pinning of domain wall movements that will result in an increase in losses compared to uniform wall motion, as the magnetic energy loss is proportional to the square of the wall velocity [23].

Dislocations of crystal lattice consider as the major pinning centres for domain wall movement [13]. Therefore, increase in the dislocation density will cause more hindering of domain wall movement and result in a large increase of energy loss at plastic strains. Generally, the dislocations stop at grain boundaries or precipitates in the material, however, increasing applied stress will lead to these pinning points tearing off and expansion of the dislocations [13]. [Figure 2.32](#) shows the microstructure during a tensile test of silicon steel from un-deformed state to the different stages of plastic deformation. The figure illustrates the effects of increasing plastic deformation in the forms of development of simple dislocations into clusters and then into wavy slip bands concentrated at grain boundaries [13].

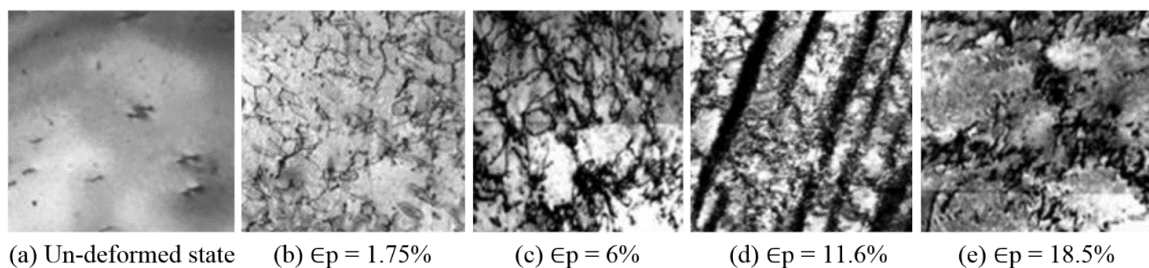


Figure 2.32: TEM micrographs of Fe 3% Si under tensile loading [13].

Leuning et al. [101], studied the effect of elastic and plastic tensile mechanical loading on the magnetic properties of NGO electrical steel with 0.5 mm sheet thickness.

Particular attention was paid to the effect of magnetic anisotropy, or the influence of the direction of applied mechanical stress with respect to the rolling direction. Three samples for both directions (RD and TD) were exposed to different mechanical loadings above yield strength. The plastic deformations are characterized according to the resulting strain or elongation that corresponding to externally applied mechanical stresses. , thereafter, separately characterized magnetically using SST tester. The plastic deformations showed a strong effect on the shape of the hysteresis loops and thereby the magnetic properties, such as coercivity H_c and the magnetizability as shown in Figure 2.33. Also, the research showed that the iron losses behave analogously to the change of coercivity and magnetization. The applied mechanical stresses affect hysteresis losses due to its strong relation to the material microstructure. The losses increased with increasing the plastic tensile stress. Small plastic deformations lead to a significant increase of required magnetization field strength and coercivity. However, it was observed that elastic stress caused a very low loss or sometimes improvement in the magnetic properties. The explanation of the effect of the elastic mechanical stresses was caused by homogeneous elongation across the entire specimen by deviating atoms of the crystal lattice from their equilibrium position. After having the mechanical load are removed, the domain restructured and the initial state is restored.

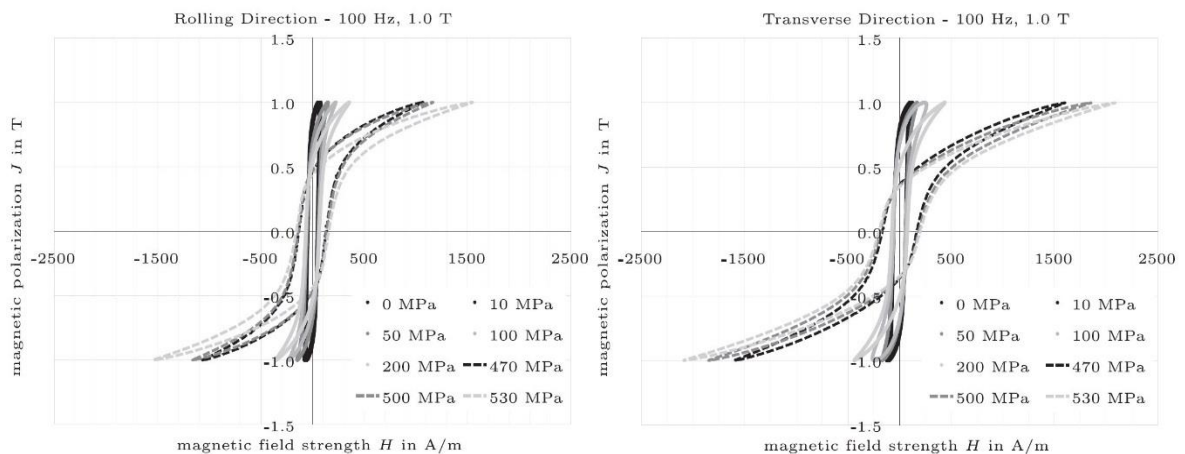


Figure 2.33: Hysteresis loops of elastically and plastically deformed samples for uniaxial tensile stress and magnetic flux density in RD and TD [101].

Generally, plastic stresses lead to harmful effects by causing a degradation of magnetic properties. The only exception, to some extent, is in the case of tensile stress. The standard explanation is related to the interaction between domain walls and the

dislocations produced by the deformation, which led to a proposal that hysteresis loss is proportional to the square root of the dislocation density [102]. The magnetic properties of electrical steels are especially sensitive to the stress arising from the stamping process of electrical steel. This effect occurs because of the distortion of the crystals in the strained metal. This distortion of the crystals affects the magnetization characteristics of the material [3].

Permiakov [23] applied mechanical loads in the rolling direction of NGO electrical steel sheets of two different thicknesses, 0.50 and 0.65 mm. The results showed that the area enclosed by the BH loops under tension reduced in comparison with the stress-free condition, but further increase of the tensile stress resulted in only a little change in the BH loops, as shown in Figure 2.34. While the compressive stresses led to a considerable deterioration of the magnetic properties. Also, the area of the B-H loop under compression stress is larger than those of stress-free condition. On the contrary, the tensile stress improves the magnetic properties especially in the direction of the apply stress.

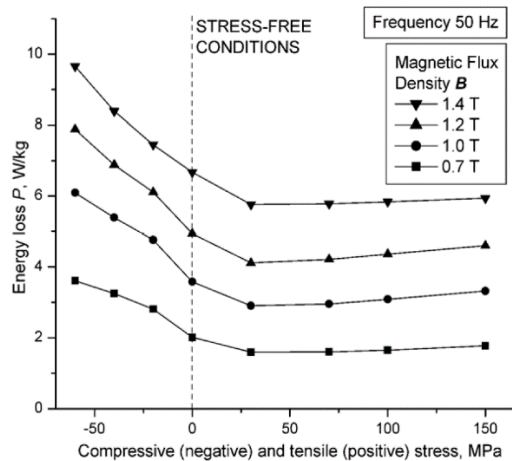


Figure 2.34: Effect of various stresses on the energy loss [23].

Also, the investigation of the grain size effect has shown that larger grains are less sensitive to the applied tensile stress than the compression stress [7, 23]. The magnetic properties of a non-oriented electrical steel sheet with 0.5 sheet thickness were tested under compressive stress using a single sheet tester. It was found that the permeability decreased in both RD and TD directions as the compressive stresses applied [23]. Also, the hysteresis loss in the rolling direction increased more than the transverse direction when applied compressive stresses. Iordache and Hug [103] investigated the influences

of strains deformation on magnetic material's properties. Magnetic hysteresis loops were achieved under tensile deformation for NGO electrical steel sheets using a single sheet tester. The results showed a linear relationship between the magnetic properties and plastic distortions and the internal stresses. The study concluded that a further increase of applied stress or plastic strain could cause a progressive degradation of the magnetic behaviour due to a drop in maximum permeability and maximum flux density, in addition to the pinning effect of dislocations.

Fukuhara et al. [104] investigated the deterioration of magnetic properties due to modified texture because of large plastic deformation. A compressive stress created by rolling was applied on the non-oriented electrical steel sheets. Electron backscatter diffraction (EBSD) and Scanning Electron Microscope (SEM) were used to understanding the structure and crystal orientation of materials. In addition to the single-sheet tester to characterize the magnetic properties. The results showed that with increasing plastic deformation, the value of flux density gradually decreased because of the effect of modified crystallographic texture. This deterioration of magnetic properties was linked to the deformation causing an increase in dislocation density, which would pin the domain walls and limit their movements during magnetization of the material, giving rise to a state of increasing residual stresses in the crystal lattice. Similar results were obtained by Landgraf, et al. [105] when investigating the permanent distortion impact on the induction field of the GO sheets in both RD and TD of sheet orientations, with the study finding that a small deformation induced a significant increase in magnetic losses. In addition, an effect of deformation on the domain structure was indicated.

Makar and Tanner [106], studied the effect of plastic tensile deformation and residual stress on the magnetic properties including characteristic changes in the shape of the hysteresis loops and the permeability curve. The measurements were made after the samples were uniaxial plastically deformed and the applied stress removed so that the samples only experienced residual stresses and plastic deformation. The results indicated that the plastic deformation was more effective than the residual stress, which has been attributed to the generation of pinning sites during the plastic deformation process. The study also concluded that the applied stress has more effect than the resulting strain on the magnetic parameters and there is a linear response of the coercive field (H_c) to the applied stress. However, the change in (H_c) did not imply a direct relationship with the

numbers of pinning sites because of the differences in pinning between domain walls due to the anisotropic of the dislocations during plastic deformation.

The effect of residual stress on the magnetic behaviour was also studied as an in-situ experiment while the sample remained under stress [106] examined [107]. These included the influence of stresses before and after the yield point on the magnetic properties of high strength steels by means of hysteresis loops, permeability curves, and magnetostriction loops. The results observed the change in magnetic behaviour before yield and this raises when a sample is approaching the yield point. The changes in the coercive field and remnant magnetisation were complicated when applying the low field. While, at the high field, the magnetisation decreases continuously with increasing strain. At low field magnetisation, below and near the knee of the curve are initially increases before decreasing at higher stress levels and there is no visible change in the straight section of the curves as shown in [Figure 2.35](#).

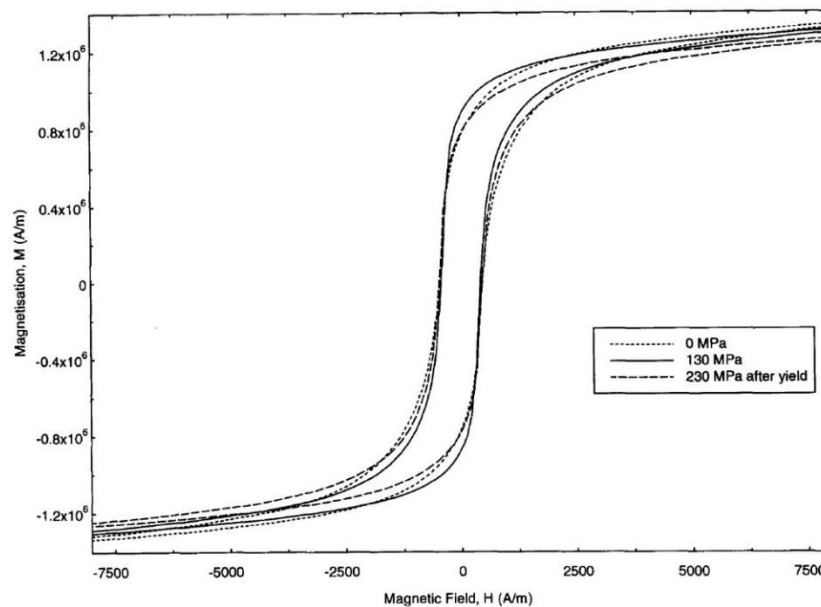


Figure 2.35: Hysteresis loops measured at elastic and plastic tensile stresses [107].

Kuleev et al. [108] also studied the influence of plastic deformations on the changes in the shapes of hysteresis loops and permeability of low carbon ferromagnetic steels. The results showed that there is a reduction in the hysteresis loops of low carbon steel after its plastic deformation due to the residual stresses because the distortion of the grains. The study also focused on the material anisotropy at the level of individual grains of the polycrystalline under external actions of fields and stresses. When the samples are

plastically deformed, and the load is reduced the loops decrease and this depends on the type of domain structure.

2.8 Effects of blanking on the magnetic properties

During the blanking process, ES laminations are exposed to various mechanical stresses which produce a plastic deformation resulting from the distortion of the crystal structure and modification of the material texture. The applied yield stress on an individual grain in a metal sample depends in part on its crystallographic orientation and that therefore different grains in a sample are likely to undergo different amounts of yield for a given stress.

One of the effects of the residual stress of steels is on the magnetic properties [106]. The influence of these stresses often results in drastic deterioration of the magnetic properties of the sheet at the cut edge and the vicinity area. It is important to quantify the effective stresses that cause this deterioration of the magnetic properties in order to obtain the desired magnetic performance [3, 23]. Figure 2.36 shows a micrograph of the cut edge of the NGO electrical sheet resulting from the blanking process. The deformation bands may present visual evidence of plastic deformation and stresses generated by punching, seemingly bending in the direction of movement of the punch. Increasing the extension of the deformed area could express more deformation of the cut edge [2].

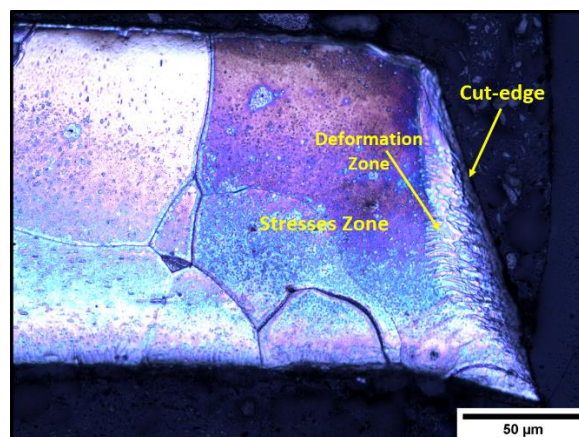


Figure 2.36: Deformation and strains visible at the edge, induced by blanking process.

Besides deformation of the material's crystals at the cut edge and the generation of shearing stress in the vicinity area, blanking defects can also include changes in the sheared edge geometry and production of burrs [3, 4]. Schoppa et al. [109] investigated

the effects of manufacturing steps on the motor core performance. The study concluded that the induced stresses of stamping NGO electrical steel sheets are one of the main factors in increasing the material's magnetic loss. Also, the deep extension of the residual stresses from the cut edge can cause more deterioration of the magnetic properties. A similar conclusion was obtained by Singh et al. [110].

The blanking process can cause a negative effect on the flux distribution and domain pattern in the cutting region. Senda et al. [111] studied the affected flux density due to the stamping process using NGO sheets with a thickness of 0.5 mm. The study found that the domain patterns changed due to the punching process at the vicinity area of the sheared edge, which implied the existence of a strong strain effect. In addition, the degradation of the flux density in the affected region increased with a decrease in the magnetic field. The width of the degraded region was less than 1 mm. Peksoz et al. [112] also studied the deterioration of flux distribution in the cutting region using the same material and measuring system. The observed results showed that the punching process caused a significant drop in localized flux density in a region up to 10 mm from close to the cut edge. Moreover, a remarkably large variation in deterioration of magnetic properties was found with respect to the grain size.

The lamination teeth design can also increase the effect of the blanking process on the magnetic loss. Kedous et al. [113] investigated the influence of punching on the magnetic behaviour in the stator teeth of the electrical motor. The study found a high degradation in terms of magnetic loss was induced by the teeth punching of NGO electrical steel with 0.65 mm sheet thickness. The study indicated that the influences of punching can increase due to the lamination teeth geometry. Their large number and small size could cause convergence in the cut edge deformation. According to the study, the small tooth can constitute a small part of the magnetic circuit that could distort the flux path. Also, punching caused an alteration in the material texture.

Usually, the effect of punching on the magnetic loss is measured using a large sheet; then the sheet is cut into strips and the magnetic loss is measured according to the cut line length. Moses et al. [114] described some effects of punching on the flux distribution and power loss of NGO electrical steel with around 0.5 mm sheet thickness. The sheet material was cut into 2, 4, and 8 strips and then the magnetic properties were measured by SST. The cutting into narrow strips showed an increased the power loss of up to 30%, with a significantly change in the B-H loops. Similar degradation of the B-H

curves was found at frequencies of 50 and 400 Hz. The study stated that the flux density at all locations tended to increase due to the build-up of stress at the increasing number of cut edges. A similar study by Schoppa et al. [115] investigated the deterioration of flux density in the vicinity area of the cutting edges. The magnetic loss was measured for a large sheet of NGO electrical steel, then for the same sheet size with a cut from the middle. The study indicated deterioration in the magnetic properties because of the induced mechanical stresses due to cutting. Also, increasing the cutting length caused an increase in core loss.

It has been reported that grain size has a significant influence on the cut edge deformation type, which in turn causes variation in measurements of the resultant effect of blanking. Rygal et al. [116] investigated the influence of cutting stress on the magnetic field and flux density distribution in non-oriented electrical steels. The study implemented two grades of ES sheets with 0.5 and 0.35mm sheet thickness. According to the obtained data, the investigation identified a significant variation in the extent of the degradation due to differences in grain size. The study also indicated that the cutting caused a reduction in permeability of the area close to the cut edge.

Weiss et al. [117] investigated the influence of the residual stresses induced by punching on the magnetic properties. NGO electrical steel with two sheet thicknesses of 0.35 and 0.5 mm was used. The study used a micro-hardness test for analysis of the cut edge area and SST to identify the magnetic properties. The sample was cut into a number of strips. The study results indicated that the shearing process generally causes a deterioration of magnetic properties and steepening of the $B-H$ Hysteresis loop. The magnetic losses increased with increasing cutting line length and were highly dependent on the flux distribution in the crystallographic texture. In addition, the stress and hardness distribution values were not constant along the extent of the deformation or throughout the blank thickness. Moreover, it has been found that grain size has a significant impact on the crystalline material deformation that may lead to considerable deviations in results used in the analysis of the cut edge surface. Sheet thickness and cutting parameters alter the stress state and the structure near the cut edge, whilst blanking speed also can affect the hysteresis losses, especially at low speeds.

2.9 Characterization of local deformation using hardness variations

Hardness testing is one of the most important methods used to characterize the mechanical properties and quantify the local deformation of material. During cold work such as the blanking process, the sheet metal can be exposed to plastic deformation due to the applied mechanical loads. This can alter the mechanical properties of material and cause strain hardening at the cut edge and the vicinity area [117, 118]. The determination of mechanical properties from the hardness values could be considered as a reverse engineering, and is used for analysis to find the equivalent properties for the deformation state [119].

Generally, hardness testing is considered as a non-destructive technique and use to assess the material's resistance to plastic deformation through measuring mechanical properties such as strength, ductility, and fatigue resistance [120]. The hardness test can be based on various scales, for example, Macro, Micro, or Nano scale. Hardness values could be affected by material composition, impurities, grain morphology and boundaries. Therefore, hardness testing could produce varying values for the same surface [119].

Nano-indentation is sometimes called instrumented indentation or Nano-hardness. The main advantage of Nano-indentation is that it provides information about mechanical properties such as hardness, elastic modulus, and yield strength through the load and displacement curve measured during loading and unloading tests [121].

There are two known indenters used in Nano-indentation: Berkovich and cube corner. The Berkovich indenter is a three-sided pyramid with a face angle of 65.3° with the vertical axis [122, 123]. The cube corner is also a three-sided pyramid and represents precisely the corner of a cube. The indents produce very small projection area; therefore, with optical microscopy it is not possible to observe the indents. The most accurate way to measure the distance between the indents' location and the cut edge is by using SEM observation.

Studies that have exploited the hardness tests to identify the local deformation of blanking process include the work of H. Cao et al. [118] who used Nano-indentation and the punching process to study the distribution of residual stress and magnetic domain structure of non-oriented electrical steel with 0.5 mm sheet thickness. The residual stress calculation was determined according to the hardness values. The results showed the residual compressive stress generated around the sheared edge and the width of the stress affected zone was almost equal to the material thickness. The results demonstrate that it

is feasible to estimate the residual stress by Nano-indentation method. A similar study, done by Pulnikov et al. [124], investigated the induced stresses due to the mechanical cutting of NGO electrical steels with thickness of about 0.65 mm. The micro-hardness analysis showed strongly fluctuating values but with a decreasing trend starting from the cut edge area and extending less than 1 mm. Moreover, BenIsmail [125] implemented the inverse analysis methods by using the Nano-indentation tests to determine the cut edge zone affected by the blanking process. The Nano-indentation measurements were used to compute the yield stress near the cut edge of NGO material with thickness of about 0.65 mm. The study found that the determination of material characteristics and their equivalency requires a comprehensive understanding of the affected part of the material.

Some research has explored the relationships between hardness values and the other mechanical properties; for example, Oliver and Pharr [126] presented an analysis technique to improve the method for determining mechanical properties from indentation load-displacement data. The obtained data for six tested materials showed that the indentation load-displacement curves is not linear; therefore, data were derived to determine mechanical properties. Shen and Tan [127] investigated the correlation between hardness and yield strength using Nano-indentation. Their study served to provide a baseline understanding of the relationship between indentation hardness and overall yield strength for multi-layered elastic-plastic materials.

Furthermore, Giannakopoulos and Suresh [128] identified a general theoretical framework for instrumented sharp indentation and used the inverse method to extract material properties through instrumented indentation. The method provided a theoretical correlations between penetration depth and true contact area for a sharp indenter, without the need for visual observations. This study also illustrated that the ratio of plastic work to total work from the area under the indentation curve may give sufficient information to find the required properties. These results have been evaluated by Venkatesh et al. [129] where the study attempted to assess the validity of the existing theoretical framework in two ways: first, by direct analysis, where the characteristics of the $B-H$ curve are predicted from known material properties, second, by applying inverse analysis, where the material elastic-plastic properties are estimated from the measured loading and unloading P-h responses. The study showed that the Young's modulus and hardness of a wide variety of materials can be extracted from the P-h response with good accuracy. Poon et al. [130] reassessed the various assumptions used in extracting the linearly elastic

material properties in an elastic-plastic indentation. In addition, the study proposed a new methodology to extract the yield stress of materials using Nano indentation by directly measuring the projected contact area. In another study, Heinrich et al. [131] compared the results of using two different Nano indenter tips. The study led to a new methodology that included the friction between the indenter and the material for extracting material properties of an unknown elastic-plastic material using Nano-indentation.

The hardness values can be affected by the material grain size as it is shown by Zhang et al. [132] who studied the relationship between the mechanical properties of the material by applying the hardness test to materials of different grain size. The study found that coarse-grained and ultrafine-grained materials produced quite different results in terms of the relationship between strength and hardness. Also, it was found the ratio of hardness to UTS is lower than 3 in the materials with high ductility and this ratio could increase to a high level in brittle materials.

2.10 Summary

The literatures showed that the blanking process is the preferred method for producing the laminations of cores of electrical steel sheets (ES), due to the high production rate, good dimensions, and low cost. Nevertheless, the blanking process results in local plastic deformation and stresses at the cutting edge and the vicinity area, which can affect the mechanical and magnetic properties of electrical steel.

The appropriate selection of a lamination material depends on the material's final application. Non-grain oriented silicon steel material is a highly efficient and low-cost material that is widely used in industry. Therefore, it has been chosen for this research. Since the electrical steel application is related to its electrical and magnetic properties, therefore, considering these properties to the blanking condition and cut edge quality could provide valuable knowledge that may lead to better understanding of how to improve product performance.

The blanking process involve a lot of variables and phases, and their interactions make the cutting mechanism extremely complex. Many studies have investigated blanking variables from different viewpoints to understand the cutting process regarding the cut edge quality. However, more investigations are need to extend the knowledge in blanking parameters and material behaviour on the mechanical and magnetic properties

of the blanked sheet. Nonetheless, the most reliable way to improve blanking process performance is to acquire further experimental data.

Blanking speed has been reported as one of the most important blanking parameters, as it can affect both mechanical and magnetic properties. Nevertheless, no direct correlation for the influence of blanking speed on the magnetic properties has yet been provided, certainly not in relation to different grain orientations. It has been found that the cutting speed was only studied relative to the cutting force and the quality of the cut edge. Moreover, blanking speed usually implemented in different speeds depending on the production rate, therefore it is difficult to determine its impacts.

When studying non-grain-oriented (NGO) electrical steels, Particular attention should be paid to the effect of magnetic anisotropy, i.e., the influence of the direction of applied mechanical stress with respect to the rolling direction because in rotating electrical machines a homogeneous and isotropic magnetic field in all rotation directions is necessary to ensure consistent behaviour at all times, in every planar direction. Therefore, each experiment is performed in rolling direction (RD) as well as transversal direction (TD) to enable comparison and to ensure comprehensible considerations.

Considered as a whole, it has been observed that most of the previous studies conducted by Electronic and Electrical Engineering (EEE) groups were concerned with the effects resulting from deformation through the cutting process on the magnetic properties and power losses of Electrical steel (ES), often of thickness less than 0.5 mm, without focusing on mechanical aspects and die design. Conversely, mechanical engineering researchers tended to focus on the effects of blanking process parameters and die design on the blanked quality for different materials, mostly of thickness no less than 1 mm, but tended not to study the impact of product quality on the magnetic properties. In addition, previous research has indicated that reducing the thickness of the sheet leads to improved magnetic properties by reducing losses of eddy currents. However, reducing the thickness of the sheet will lead to a change in mechanical properties due to the rolling process. This effect become noticeable in the blanking process, especially for very thin sheet, where the number of grains will significantly reduce along the thickness of the sheet. This in turn makes the features of a single grain play a key role in determining the deformation of cut and the quality of the cut edge. Also, the changing of the cutting location could lead to change the type of distortion caused by the cutting process. Thereby, that can result in difficulties of determination the extent of the deformation from

the cut edge to the rest of the material. Therefore, studying the effect of the cutting process on the thin sheet may result in change in the basics of the known cutting mechanism. Therefore, the current research focused on the use of blanking process in thin sheet with 0.2 mm thickness and compared the results with 0.35 mm sheet thick.

Using new techniques to investigate and analysis the blanking process may lead to finding more detailed information that contributes to the development of the process and the quality of the product. For examples, DIC identified as an effective tool for identifying local deformation. Although, some research attempts to implement DIC during the blanking process. However, all of these studies were conducted at low blanking speed and high sheet thickness. Therefore, implementing high-speed DIC on much thinner sheet may give new and wider picture of deformation by the high blanking mechanism. Due to the occurrence of cold forming and strain hardening at the cutting edge, micro hardness measurement was used for identifying the local edge deformation. The applying of Nano-indentation tests in the current study could provide a valuable data on the random distribution of the cut edge deformation. The single sheet magnetic tester is an appropriate method for measuring the magnetic properties and power losses for an individual sheet of electrical steel. However, different sample shape and size required a different magnetic tester system, especially for small-size. The next chapter will explain in detail the new techniques and tool designs utilized in this study.

To conclude, investigating the blanking process and blanked quality of thin ES sheet from both mechanical and magnetic aspects regarding the deformed cut edge at different cutting conditions such as such deformation rate, material grain orientations and sheet thickness that could make a good contribution in terms of developing the process design of the final product of the blanking process.

3

The experimental methodology

3.1 Introduction

This chapter focuses on the methodology adopted for all the experimental works undertaken in the present study. The chapter provides details of the materials used, samples preparation, testing and analysis techniques, and the blanking procedures including dies design. The design, fabrication and testing conditions of a new magnetic single sheet tester (SST) are also reported in this chapter. The newly developed magnetic testing rig was used to assess the blanking induced defects in the magnetic properties of the selected materials. [Figure 3.1](#) presents a flowchart outlining all the experimental works and characterization methods used in this research.

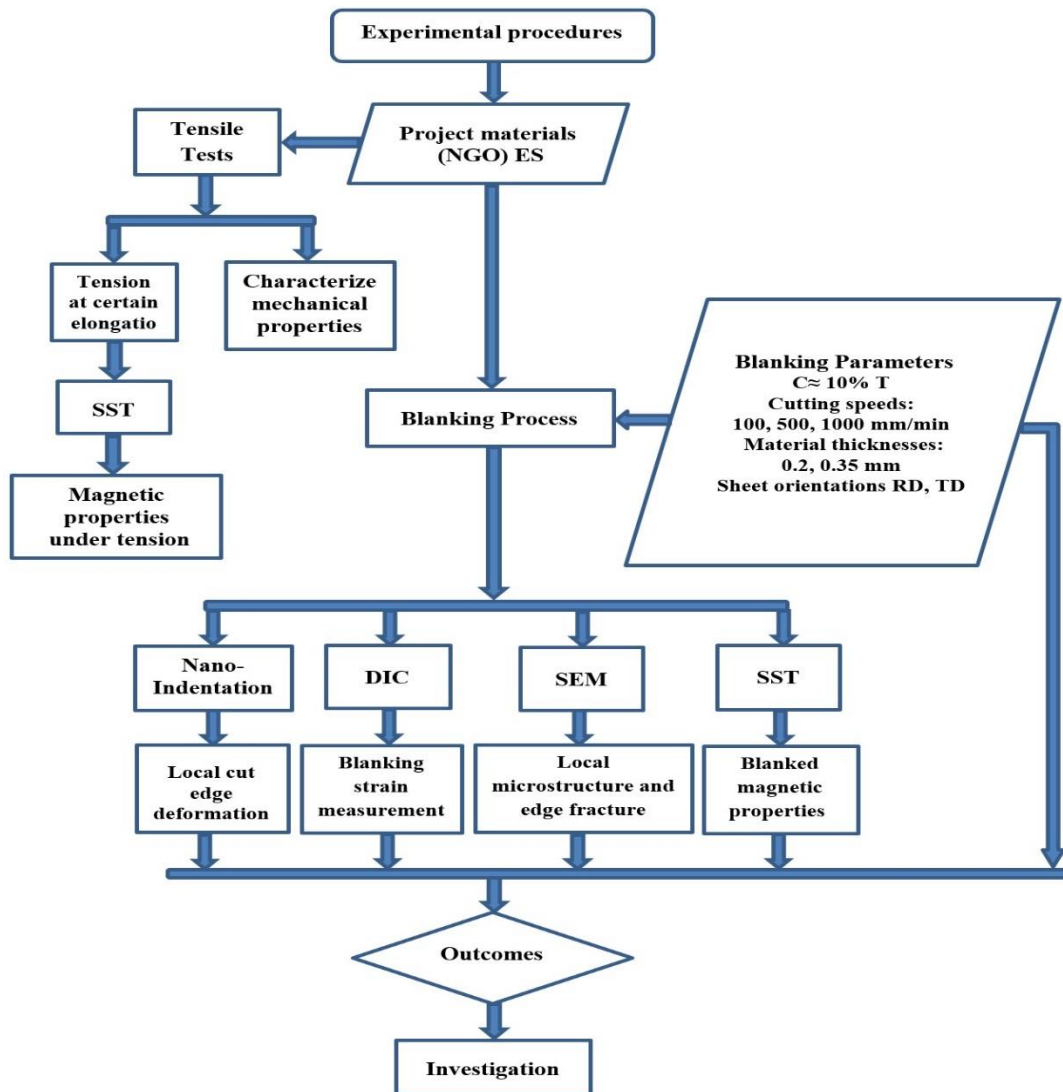


Figure 3.1: Outline of the research structure.

3.2 Material selection

Two cold rolled non-grain orientation grades (CRNGO) of fully processed electrical steel sheets were used in this research. The grades were NO20 and NO35 according to the company standards of the supplier, Cogent Power- TATA steel Company. The materials have a silicon content of about 3wt. % Si, and the chemical composition is shown in [Table 3.1](#). Two different nominal thicknesses of 0.2 and 0.35 mm have been adopted to show the thickness impact upon the cut edge type and magneto-mechanical properties. It is worth mentioning that the selected 0.2 mm electrical steel grade thickness (NO20) is

considered as a new generation of ES developed by the provider company as an attempt to enhance the efficiency of material used for higher rotational speed motors.

Table 3.1: Electrical steel chemical composition.

Element	C	Si	MN	P	Cr	Ni	Cu	Al
Mass percent (wt. %)	0.0039	3.15	0.18	0.019	0.029	0.014	0.026	1.09

Material texture isotropy and grains orientation are among the most important parameters for determining the magnetic properties of steel sheets because these features can affect the magnetization process and power losses. The non-oriented ES magnetic properties in rolling (RD) and transverse (TD) directions may differ according to the cutting plane direction due to differences in the material's grains direction at the cutting edge. Therefore it is important to study the effect of blanking in both RD and TD direction on magneto mechanical defects generated by the cutting process. To that end, the study cases were categorized into 0.2RD, 0.2TD, 0.35RD, and 0.35TD groups. These cases were applied for all tension and blanking processes tests, where 0.2 and 0.35 were the material thicknesses and RD and TD the grain orientations. Subsequently, the results were also divided into four fully parallel paths. The selected material was cut using the wire EDM method (at blanking speed of 6 mm/min with 0.25 wire diameter) to produce both standard tensile test samples (bone shape) and blanking implementation samples.

3.3 Measurement of mechanical properties

3.3.1 Tensile tests

Standard tensile test samples were prepared according to the ASTM standard [133] to carry out the tensile tests. DIC technique was also implemented during the tensile test. The tensile test was conducted in a 25kN electro-mechanical Tinius Olsen H25KS test frame. The sub-size of the tensile sample was used to reduce the amount of material consumed and to ensure it would fit in the magnetic tester. The standard tensile samples' dimensions are shown in [Figure 3.2](#).

investigate the effect of plastic deformation on the magnetic properties. The increment extension was 1mm between each sample until the maximum possible extension without fracture. In front of each elongation, a maximum strain value is provided, and the UTS that caused it. The real stress-strain values were obtained using the DIC technique during tensile tests, as illustrated in [Figure 3.4](#).

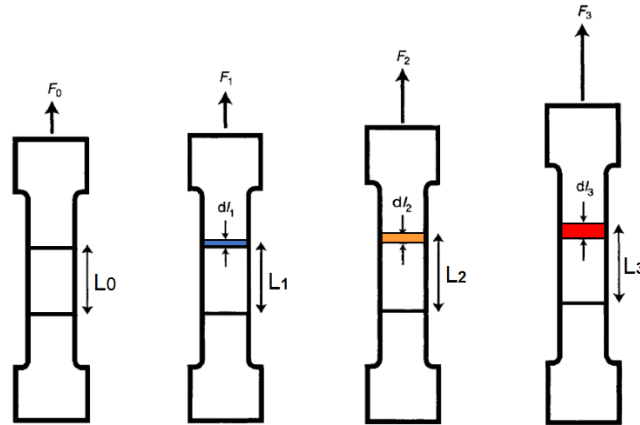


Figure 3.4: Tensile tests at different plastic extensions.

3.3.2 Tensile strain measurement using DIC

Digital image correlation technique can be used to measure strains deformation in a test specimen during tensile, shear, or compression tests [135]. Therefore, the DIC technique was used during tensile tests to measure both local and global strain distribution across the tensile samples. Before the test, the tensile specimens were painted with a white background and then with a random black speckle pattern to enable data capture by DIC camera. The airbrush technique was used to produce the required pattern of speckles on the surface of the sample. [Figure 3.5](#) shows a macrograph of the tensile test sample with a speckle pattern.

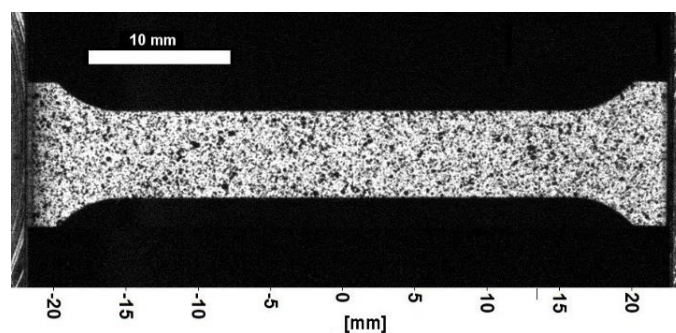


Figure 3.5: Macrograph of the tensile test sample with random speckle pattern.

The DIC system from LaVision was used with Davis 8.4 image correlation software for analysis the tension deformation. Maximum normal strain components were extracted for all stages of the extension during the tensile tests because of the tensile strain in the thin sheets is affected in one direction parallel to the applied load direction.

To calculate the strains, the images are divided into subsets were using larger subsets increases the strain resolution but lowers the spatial resolution, i.e. the distance between two measurement points. The subsets are separated by steps that are the physical distance between the centres of two adjacent subsets. The. While reducing the step size increases the spatial resolution but lowers the strain resolution [136]. A sensitive study was done to determine the most optimum DIC parameters such as the subset size and step size led to select the accurate calculation mode with subset 23 and step size 9 as a DIC set-up for processing the captured images. Table 3.2 present the DIC parameters setting used to gain the correlation data regarding both hardware and software DIC system.

Table 3.2: DIC setting parameters for tensile tests.

Technique	Digital image resolution (DIC)
Software	Davis 8.4
Subset size	23 pixel (≈ 0.55 mm)
Step size	9 pixel (≈ 0.21 mm)
Camera	LaVision Image E-lite
Lens	Tonkina AT-X PROD 100 mm F2.8
Image resolution	2480 x 2073 pixel
Scale factor	42.0544 pixel/mm
Field of view	104160 x 87066 (Resolution x Scale factor)
Frame rate recording	10 image/s
Spatial Resolution	$(1/42.0544) * 9 = 0.214$ mm (step size x Scale factor)

The image acquisition frequency was increased to 10 Hz to give more visualization details of the material behaviour during the test. The camera was placed at the same level as the sample using a tripod, and the optical axis was aligned to be normal to the centre of the gauge length with a sharp focus. The region of interest was selected in such a way that it covered the sample gauge length. In addition, to extract the force and crosshead extensions of the tensile machine, two channels were connected between the tensile

machine and DIC system across the acquisition card. This helped to synchronize the machine data with the DIC results such as the number of image and strain value at each step of the test.

3.3.3 Blanking dies setup

Two kinds of blanking die sets were designed and manufactured to perform in-situ strain measurement during blanking and run a full cut on the samples to study the affected magnetic properties of the blanked samples with known cutting conditions.

Die design concepts were based on the sample size, quantity, and the edge quality. The first type was a fully closed die (die type A) as shown in Figure 3.6, and the second was a die with one open side (die type B) as shown in Figure 3.7. Since two material thicknesses, 0.2 and 0.35 mm, and two orientations, RD and TD, were used in the study, four blanking tools (two of die type A, and two of die type B) with appropriate punches that would fit a clearance of around 10% of the thickness of the ES sheets needed to be made. The new insight into the blanking process enabled by the new experimental blanking tools may allow a more detailed understanding of the blanking process and potentially lead to the developing of better products.

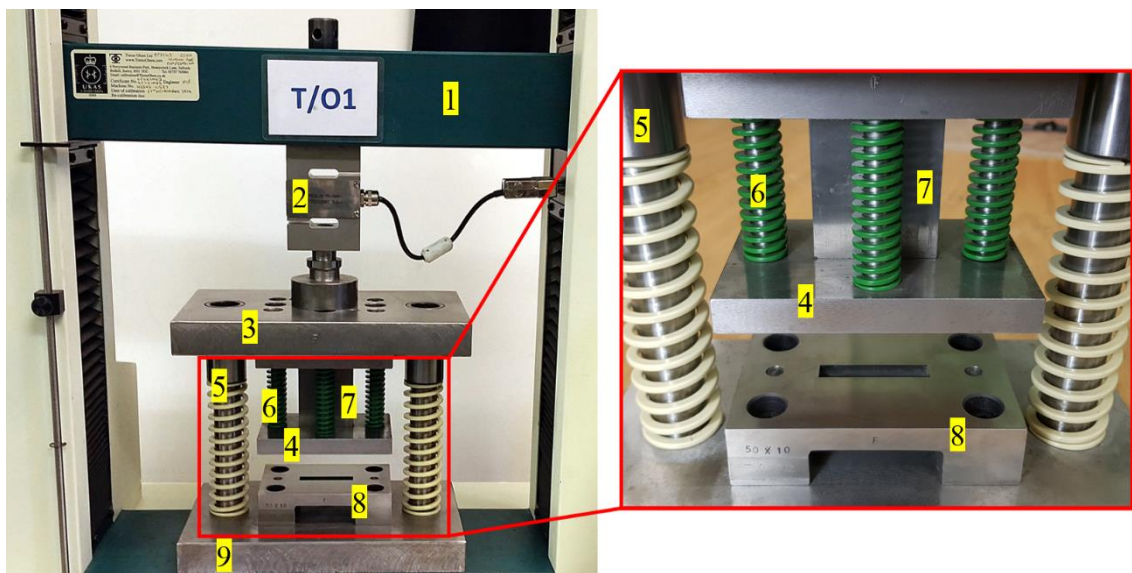


Figure 3.6: Full blanking die (Type A), 1) Machine ram, 2) load cell, 3) upper plate, 4) blank holder, 5) bushings and pillars, 6) spring, 7) punch block, 8) die block, 9) lower plate

Although the die type A can emulate industrial dies, it normally operates in a closed area which would have prevented investigation inside the cutting deformation

zone. Therefore, one side was removed from the die type A as a new blanking method that would allow measuring of local sheet strains during blanking using the DIC technique at the different blanking parameters including blanking speed, thickness, and material sheet orientation.

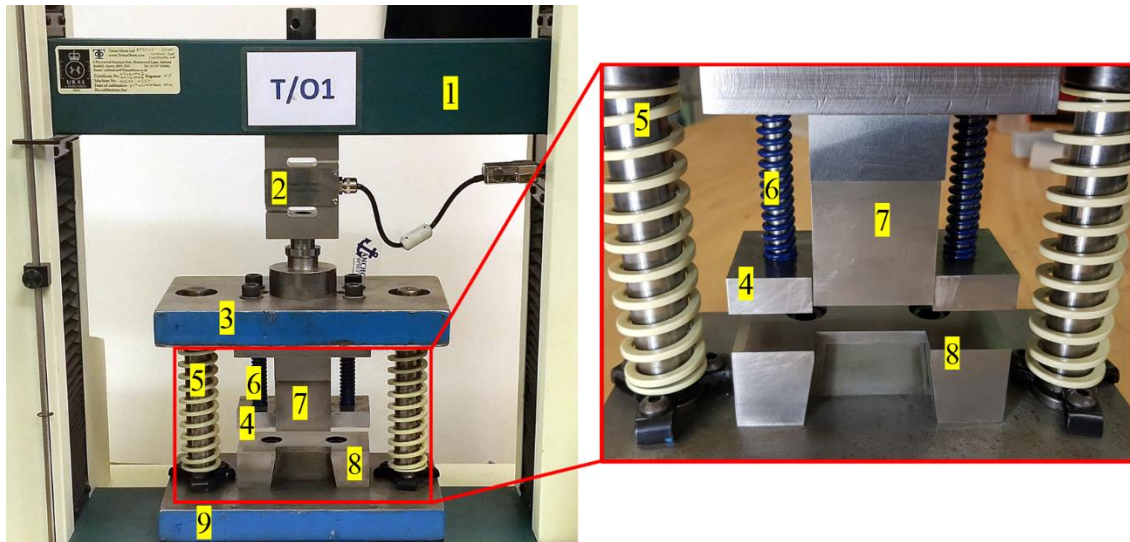


Figure 3.7: One free blanking die Type B, 1) machine ram, 2) load cell, 3) upper plate, 4) blank holder, 5) bushings and pillars, 6) spring, 7) punch block, 8) die block, 9) lower plate

3.3.4 Blanking dies design

The ideal blanking die needs to incorporate many parts including die- set, die- punch blocks, die- punch holders, guide bushings and pillars, stripper, pilot and finger stop for automatic stop, and fasteners parts such as screws and dowels. However, some supplementary parts of the blanking tool were dispensed with because they were not needed for the investigative purposes of the current study [62].

Tools steel material for cold work that heat-treated to a hardness of 59HRC was used for manufacturing both die and punch because its characteristics of high hardness and resistance to abrasion make it ideal for manufacturing blanking tools. Tool steel can be classified in terms of alloys, heat treatment, and applications. While the remaining die parts and support plates were made from mild steel, the die opening concept was given special consideration in order to facilitate the exit of the blank from the die. The clearance between the punch and die was applied to be approximately equal for all used dies for both material thicknesses, 0.2 and 0.35 mm.

Due to the light load required to accomplish cutting of a thin sheet, a centre post die-set was chosen of a size that would fit the designed blanked part, to help align the tool and ensure that the punch head and the die would share the same middle plane. All parts of the blanking die were assembled and built within the die set. The bushing and guidepost require particular attention as they could affect the precision of the cutting process.

Blanking dies were designed to cut the thin sheets of electrical steel and produce project samples of rectangular shape ($50 \times 10 \text{ mm}^2$) that were cut from the previously prepared samples. Punches were connected to the punch holder and then to the upper plate of the die set. The machine ram was moved down to push the punch down until it cut the material inside the die cavity. During the process, the cutting force was recorded by the load cell between the machine's ram and the blanking die. On the opposite side, the die blocks were mounted on the lower plate of the die set which was fixed on the test machine's lower platform. Three springs were used to fasten the sheet material to the blank holder plate during the blanking process. The stripper plate is able to travel up and down on the shank of the punch. All die parts were fastened together using socket head screws and threaded holes. The cutting tests were implemented using the Tinius Olsen H25KS tension-compression machine.

3.3.5 Blanking parameters

The blanking process was implemented at three different blanking speeds, 100, 500, and 1000 mm/min, with 1000 mm/min being the maximum speed for the machine. The electrical steel sheets samples prepared using wire EDM were made with an additional 10 mm on all sides so that they would be larger than the produced rectangle blanked to size $50 \times 10 \text{ mm}^2$. All the sheet samples, for the 0.2 and 0.35 mm thicknesses and the RD and TD orientations, were cut using the blanking process. [Figure 3.8](#) shows the schematic of the virtual shape of the blanked samples to illustrate the sample size, orientation, and test locations regarding the sheet rolling direction. The samples produced by die A were used to investigate the cut edge quality, local deformation using Nano-indentation, and magnetic properties using the SST because this type emulates the real samples produced in the industry. On the other hand, the samples produced by die type B were used only to implement DIC technique during the blanking process for measuring the local strain in the cut edge and vicinity area.

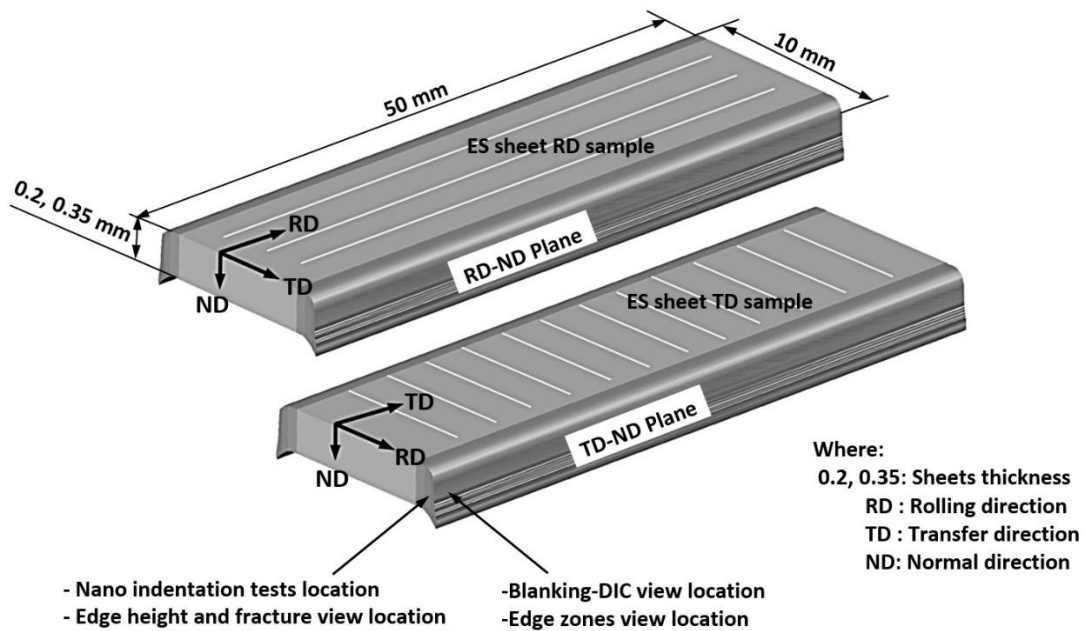


Figure 3.8: A virtual representation of the blanked samples to illustrate sample size, orientation, and test locations regarding the sheet rolling direction.

Table 3.3 presents classification of the studied blanking cases according to the four samples categories, 0.2RD, 0.2TD, 0.35RD, and 0.35TD. Subsequently, the results would be further divided into four fully parallel paths. These cases were applied both to die type A and type B.

Table 3.3: Categorization of blanking samples.

Sample case	Groups	Sample code	Sheet thickness (mm)	Material sheet orientation	Blanking speed (mm/min)
1	Group 1	0.2 RD 100	0.2	RD	100
2		0.2 RD 500	0.2	RD	500
3		0.2 RD 1000	0.2	RD	1000
4	Group 2	0.2 TD 100	0.2	TD	100
5		0.2 TD 500	0.2	TD	500
6		0.2 TD 1000	0.2	TD	1000
7	Group 3	0.35 RD 100	0.35	RD	100
8		0.35 RD 500	0.35	RD	500
9		0.35 RD 1000	0.35	RD	1000
10	Group 4	0.35 TD 100	0.35	TD	100
11		0.35 TD 500	0.35	TD	500
12		0.35 TD 1000	0.35	TD	1000

3.3.6 Blanking force assessments

The blanking force can be defined as the force required to penetrate the sheet material with the punch [137]. Blanking forces were measured and used to compare the performance of the cutting action under the selected conditions. Blanking forces can be estimated theoretically according to the sample cut size and material type. However, the theoretical calculation of force needs to be increased by 20-40% because it is affected by cutting and material conditions [64, 137]. The current study adopted the experimental results to determine the actual force values during the blanking process. Also, the blanking force was calculated theoretically to confirm the results.

The critical value of the blanking load occurs when the force increases up to the maximum magnitude because this represents the ultimate resistance of the material to the applied load, in addition to its importance in determining the required machine capacity.

Blanking force was tracked throughout the blanking operation to record the load-stroke of the punch movement. During the downward movement of the punch, the force values jump to their maximum when the punch contacts the sheet surface and then the force rapidly decreases on complete separation because of the decrease in the cross-section and the limit of material formability exceeding the cutting [138]. Therefore, the beginning of the sudden change of values was considered as the starting point of the actual sheet cut. All the values at this stage were subtracted from the values derived from the earlier steps.

3.3.7 In-situ strain measurement during blanking using DIC

The new laboratory blanking apparatus (Die type B) in [Figure 3.7](#) was designed in such way that the specimen can be observed by the DIC camera and avoid blocking the view by blanking tools (the punch and die) during the test. Therefore, the main feature of this die is that one cutting side was opened up to expose the cut edge to outside view and allow the camera to capture images throughout the cutting stages. In blanking tests of thin ES sheets, major challenges are presented by the very small deformation zone represented by the thickness of the sample (0.2 and 0.35 mm), as well as the high-speed movement of the punch during the blanking process associated with this test.

The deformation of the specimen was recorded by camera and processed through DIC method and measuring the sheet local strain during blanking process. To obtain the required resolution, a micro-lens with a high magnification was used. The full DIC system arrangement is shown in Figure 3.9.

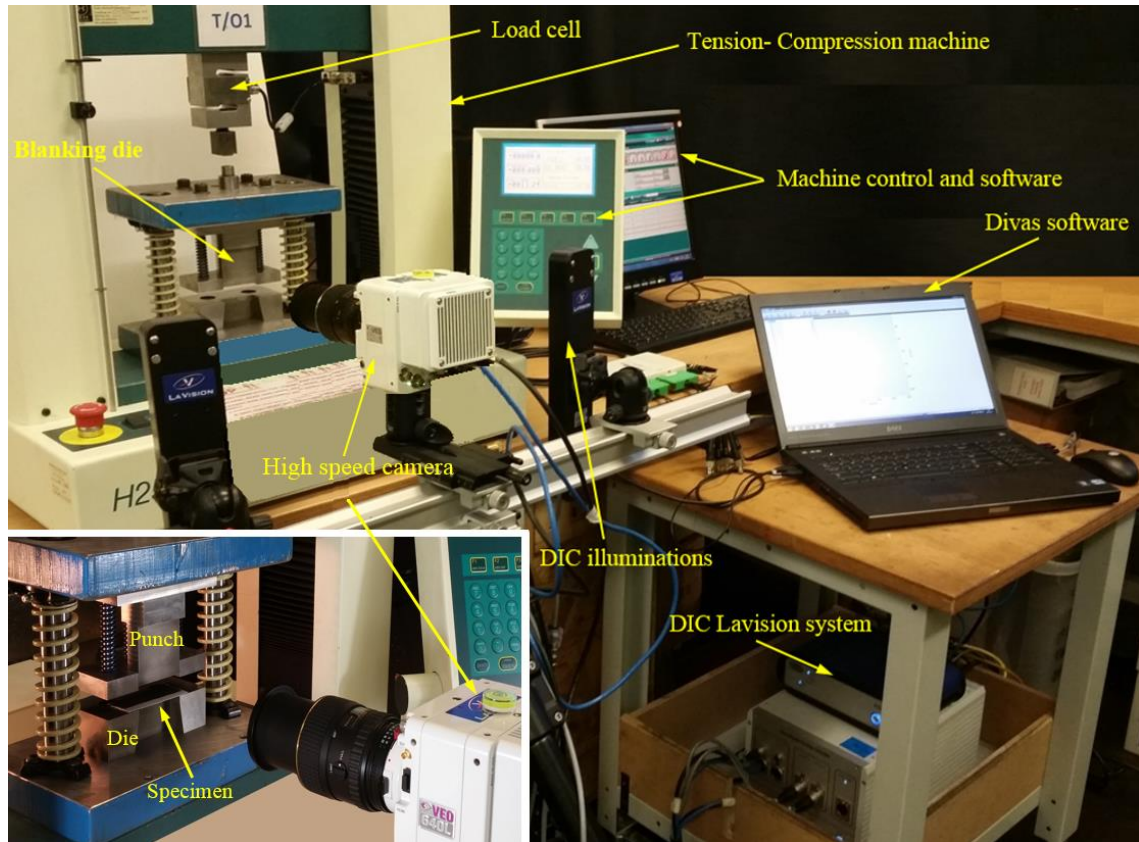


Figure 3.9: Blanking tools, machine control, and Lavisson DIC system.

A sensitive study was done to determine the most optimum DIC parameters such as the subset size and step size led to select the subset 11 and step size 4 with accurate calculation mode as a DIC set-up for processing the captured images. Table 3.4 present the DIC parameters setting used to gain the correlation data regarding both hardware and software DIC system. Maximum equivalent strains were extracted for blanking samples because during the process, the material exposes to the tension, shear, and compression. Therefore, the strain values transform at each point and the local shear values may minimize or maximize due to the turning of the coordinate system of the principle strain mode (see Appendix A). Thereby, the equivalent strain could better express the strain in blanked material than the normal stain as it is a resultant of both principle and shear strains.

Table 3.4: DIC setting parameters for blanking tests.

Technique	Digital image resolution (DIC)
Software	Davis 8.4
Subset size	11 pixel (≈ 0.095 mm)
Step size	4 pixel (≈ 0.035 mm)
Camera	High speed Phantom
Lens	Tonkina AT-X PROD 100 mm F2.8
Image resolution	1280 x 608 pixel
Scale factor	115 pixel/mm
Field of view or Image size	147200 x 69920 (Resolution x Scale factor)
Frame rate recording	2000 i/s
Spatial Resolution	$(1/115) * 4 = 0.0347$ mm (step size x Scale factor)

A high-speed camera (Phantom) was used to capture images during the test. However, with such kind of camera, there is limited image storage capacity. Therefore, the image resolution was reduced to increase the number of recorded images and thereby increase the recording time. The actual time taken to cut a 0.2 mm sheet thickness with 1000 mm/min punch speed is 12 ms. To reduce the light captured by the sensor, the exposure time or shutter speed was reduced to be 316 μ s. Also, the saturation of the sensor dynamic range was avoided using the intensity calibration to reduce the image noise. The distance between the camera and the specimen surface was around 20 cm. The maximum camera temperature 35 C°.

In order to guarantee capturing images of the deformation area, high attention was given to the instant of starting recording image and beginning of blanking test. Both were starting exactly at the same time, as a result, images were acquired before, during, and after finishing the test. Later the images when the punch touches the surface of sample and even cut the sample were selected for processing and analysis by DIC software.

Figure 3.10 illustrates the blanking test setup with DIC and camera position. The distance between the camera and the cut edge depends on the size of the region of interest and can affect the image quality. Figure 3.11 shows the region of interest for the specimen and the setup of the blanking tools. The airbrush technique was used to produce the required speckle pattern in the side section of the samples. Despite the considerable

challenge faced in creating an acceptable number of speckles in this small area of the specimen, approximately 15 speckles were obtained along the thickness.

A random speckles pattern was applied to carry out the DIC strain measurement. The use of a common spray can did not give enough speckles; therefore, an airbrush was used in association with a magnifier lens to create the required number of speckles. An airbrush and fluid acrylic black and white paint conforming to the standard [139] were used to create a much finer speckle pattern.

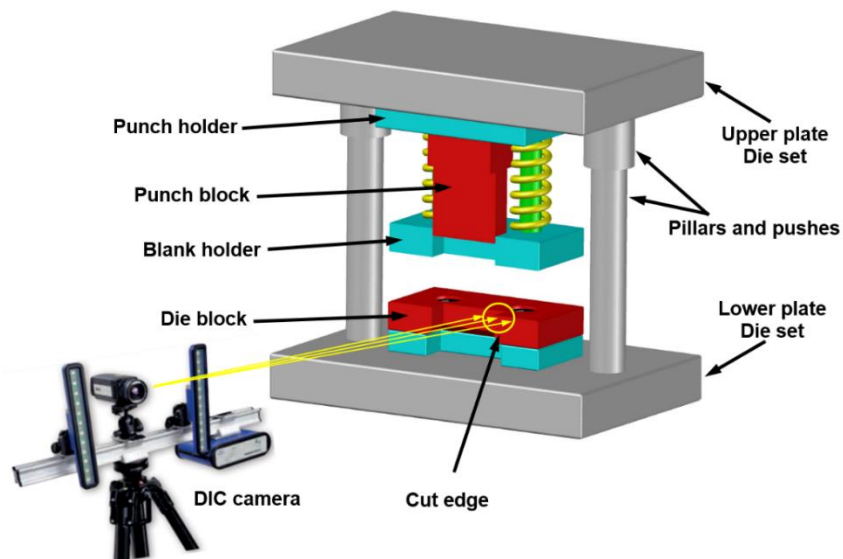


Figure 3.10: Schematic of blanking and DIC test setup.

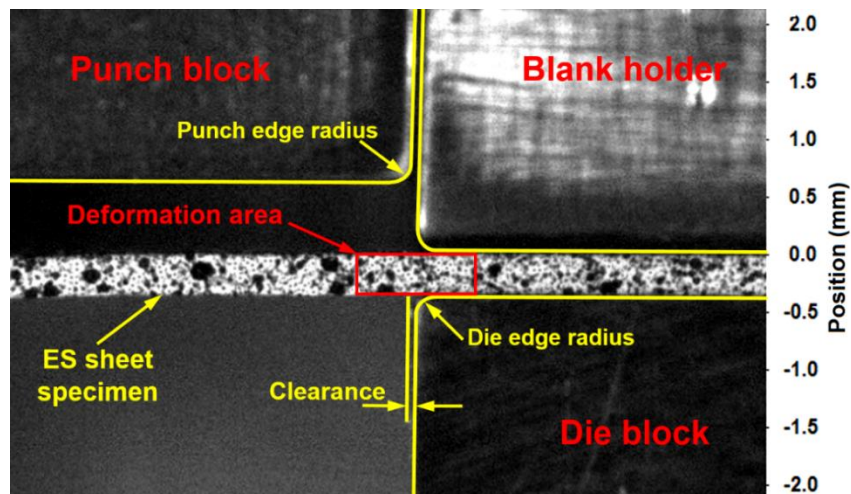


Figure 3.11: DIC and specimen setup for deformation area measurement of the ES.

3.4 Nano-indentation tests

The Nano-indentation test was implemented for the thin sheet electrical steel material at the cut edges and vicinity area to measure material properties and show the distribution of residual stress on the sheared edge and the nearby area. It is known that there is a strong relationship between the hardness and tensile strength. Therefore, the deformation could be estimated based on the specific hardness test results. Finding the hardness values for the material involves forward analysis of the mechanics of indentation, while extracting material properties from results through instrumented indentation can be considered as inverse analysis [119]. Using the theoretical framework for instrumented indentation enables the determination of elastic and plastic properties of materials based on the correlations between the indenter penetration depth and true contact area.

In addition to the advantages of high resolution, this test allows estimation of the mechanical properties and the residual stresses based on the theories of characterizing indentation at different size scales. Also, Nano indentation allows the investigation to be conducted very close to the end of the cut edge.

Nano-indentation testing was implemented using the Triboscope Nano-mechanical test instrument supplied by the Hysitron Corporation, as shown in [Figure 3.12](#). The test was carried out in the form of two areas of indents starting from the cut edge until stability of the hardness value was achieved. Each area contained 25 indenters that were distributed in the form of a matrix with five rows and five columns with a space between the indenters of 10 μm . A fixed load of 5000 μN was applied to each single indent with trapezoid load and un-load function and 15S dwell time. Two indents arrays were conducted in order to cover most of the affected deformation area because the maximum scan area (scan size) for the single test was 50 μm . The Berkovich indenter tip was used in the current test, with a total included angle on the tip of 142.3 degrees, and with a half angle of 65.35 degrees [122].

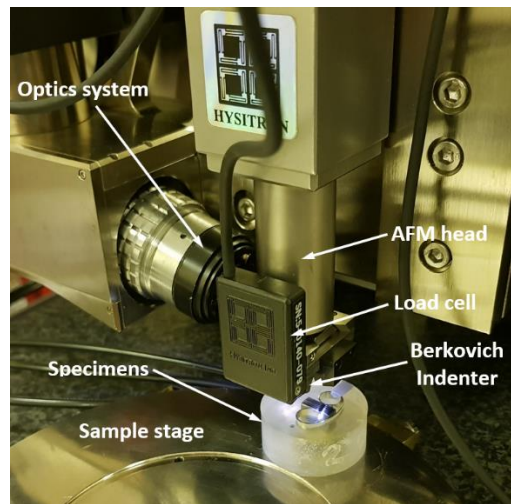


Figure 3.12: Nano-indentation system.

In the Nano indentation test, the indenter is pushed into the surface of the sample to produce both elastic and plastic deformation of the material, as illustrated in [Figure 3.13](#). The main difference from macro or micro-indentation tests is that in the Nano indentation machines, the displacement h and the load L are continuously monitored with high precision.

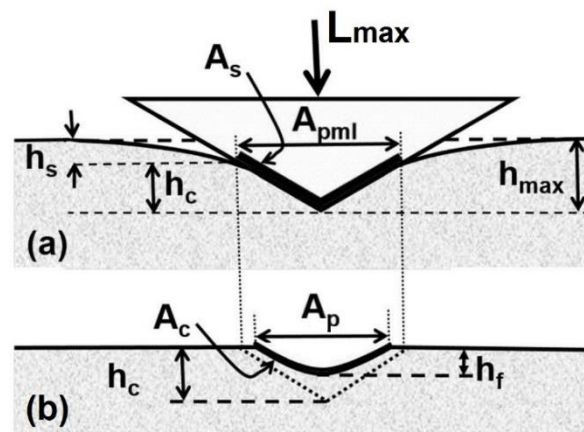


Figure 3.13: (a) Elastic-plastic deformation at the maximum applied load, (b) Plastic deformation after releasing the load [120].

Nano hardness values were calculated by analysis of the produced curve of the load P as a function of the depth of the indenter's penetration inside the material h . The P - h curve data can give details about material properties such as Young's modulus and yield strength. [Figure 3.14](#) shows the schematic of the load-penetration depth (P - h) curve for the Berkovich indenter at the cut edge for one of the cut samples of electrical steel sheet used in the current study.

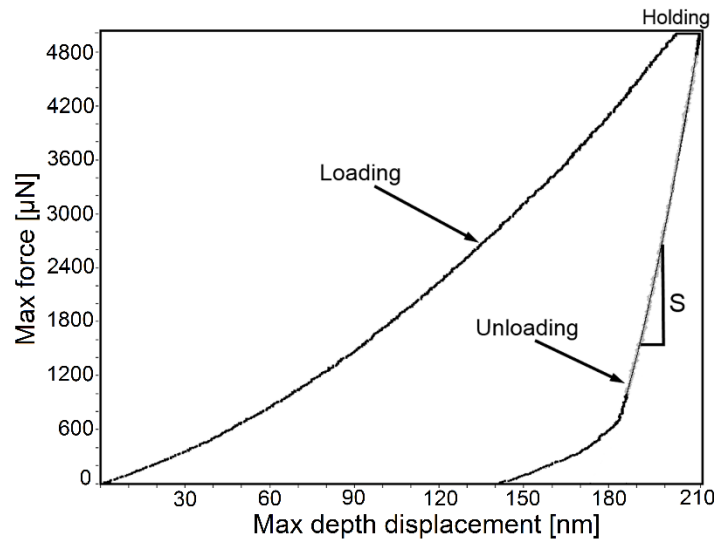


Figure 3.14: Load-penetration curve of the Nano-indentation test.

The Nano-indentation test includes applying and removing a single load for each indent. The total load is applied in a cycle, firstly, the load reaches maximum value followed by holding and then unloading. During loading, the curve follows the equation 3.1. Where P_{max} is the maximum indentation load that causes the h_{max} depth and creates the projected contact area A_{max} on the indented surface and C is the indentation curvature which is a measure of the resistance of the material to indentation. While in the unloading part of curve is used to find the hardness value H from the equation 3.2. The slope S of the unloading curve is used to calculate E from the equation 3.3 [128,129].

$$P_{max} = C \cdot h_{max}^2 \quad (3.1)$$

$$H = \frac{P_{max}}{A} \quad (3.2)$$

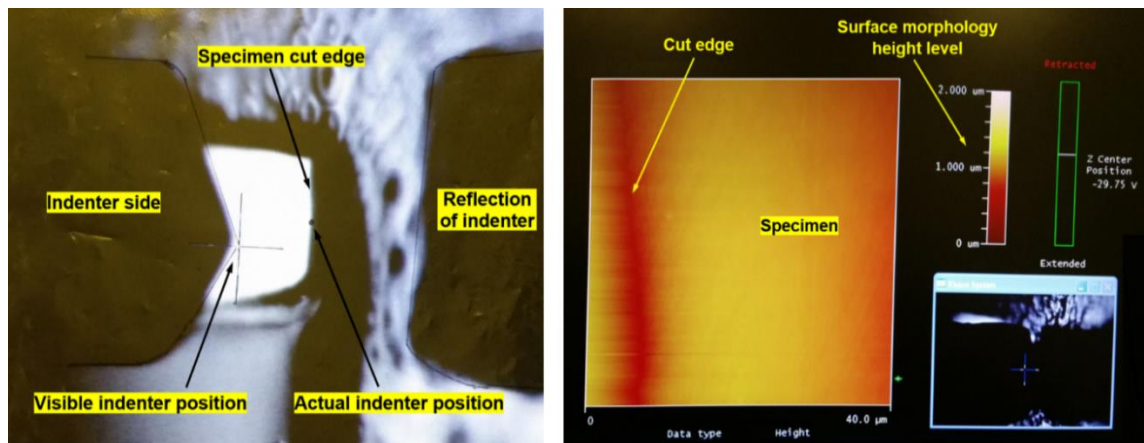
$$E = \frac{S \sqrt{\pi}}{2 \sqrt{A_{max}}} \quad (3.3)$$

The induced plastic deformation of the cutting process is a consequence of the tension, compression, and shear stresses. Thereby the induced strain due to the blanking process may exceed the tensile strain. Also, the hardness values in the cut edge deformation area could be much higher than the ultimate tensile strength. Therefore, characterization using a tensile test may not be suitable to express the local strain in the blanked sheet because of the limited strain data in the tensile test [86, 140].

During the Nano-indentation test, it was quite a big challenge to locate the indenter at the end of the cut edge because of the difficulty to determine exactly the end of the cut edge according to the test vision.

In addition, the cold mounting causes shrinkage between the material edges that may cause a difference in surface level between the sheet material and the mounted material. Thus the surface topography becomes greater than the maximum vertical movement of the indenter, which should not exceed 3.5μ vertically. So, it is not possible to conduct the test exactly at the edge (i.e. Zero edge coordinate) and instead it should take place in a nearby area but still within the deformation zone. Moreover, cold mounting can cause some discharge of static electricity at the material surface that may affect the test in the form of causing unclear AFM images.

Figure 3.15 shows how difficult it is to determine exactly the cut edge position before implementing the actual test even when using Nano-scope AFM images (Atomic force microscopy AFM is a very-high-resolution type of scanning probe microscopy SPM used to indicate material topography). The dark red line in the figure represents a low height level area because of shrinkage in the polymer of the cold mounting. The only way to measure the indents' location was after the test by using SEM observation.



(a) Vision system

(b) Nano-scope AFM image

Figure 3.15: Determination of the actual position of the indenter in the Nano-indentation system.

3.5 Magnetic tests using the single sheet tester

Power loss is the most important magnetic property in relation to ES, followed by the permeability of the steel during magnetic analysis. The thickness and material grain orientation are directly linked to the power loss. The Epstein test is usually used for measuring magnetic properties for electrical steel sheets; however, this apparatus has certain limitations. For example, the test is not suitable for small samples. Also, an accurately dimensioned square is needed, and when the material is thin, air gaps may open up at the corners of limbs and some weights may be required. Use of the single sheet tester (SST) can overcome these drawbacks. Therefore, in the current study, SST was adopted to measure the magnetic properties of the deformed samples of electrical steel sheets. The device was designed and fabricated proportional to the sample conditions and size.

The results of measurement of the power loss in single sheet test specimens usually correlate with the Epstein frame results. However, power loss measurements gained by the single sheet method are entirely independent of the Epstein frame. Accordingly, the results from the single sheet tester may differ from those of the Epstein frame even for same sample material and size and test conditions such as magnetization and induction coils, the power supplied, and frequency [3]. Moreover, the current study is interested in drawing comparisons between the influences of sheet thickness, grain orientation, and blanking speed upon the cut edge deformation. Therefore, the measured flux density and hysteresis losses needed to be normalized.

There is a wide diversity of physical forms and magnetic circuits which can be applied to investigate the magnetic properties of electrical steel. Therefore, it is important to select a suitable physical form of tester that matches the standard principles. The apparatus used to measure magnetic properties in the current study is a type of single sheet tester (SST). The test was intended to measure the ES magnetic properties at DC power conditions to determine the specific hysteresis loss and general magneto-properties for tensile and blanked specimens in different cutting conditions.

The following considerations have been incorporated regarding the SST system design:

- The Small single sheet tester (SST) needs to be appropriate for determining the magnetic properties of samples when insufficient material is available for using other known testers such as the Epstein or ring test [141].

- Although the small specimen size is critical, the SST is not expected to achieve similar accuracy to the Epstein test methods. In addition to the specimen size consideration, there may be considerable variation in magnetic properties. Therefore, the test results, in general, represent averages of magnetic quality. This test method is suitable for specification acceptance, service evaluation, research and development and design [142].
- A double-yokes fixture was used to complete the magnetic circuit and prevent formation of eddy current pools in the strip. Yokes (cores) were constructed from grain-oriented electrical steels in the preferred grains orientation in thicknesses not exceeding (0.35 mm) to reduce flux losses [141].
- The number of turns in the primary and secondary windings should preferably be equal and wound in the same direction from a common starting point at one end of the coil form; the number of turns depends on the mass of specimen and test frequency [141].
- The test is used to determine the normal induction curve and the hysteresis loop (B-H loop) by rapid reversals of the direct current. Magnetic field strength and magnetic induction range from zero to flux saturation of the material [138].
- Temperature increase has a significant effect on the test measurements and it should not exceed 50C°. Therefore, cooling fans were used and the coil temperature was monitored using a temperature sensor or the thermocouple [143].
- Due to the small sheet volume represented by the cut area and material thickness, a slight change in the properties and loss was expected due to the blanking effect. To measure this loss, very sensitive flux meter devices were used with a micro-magnetic field measurement range accuracy. Two flux meters were used to validate results readings.

3.5.1 Design of the new SST apparatus

A new single sheet tester was designed and built according to the requirements of the project including samples sizes and magnetization field strength. The tester fixture can accommodate the flat rectangular shape of the blanked specimen ($50 \times 10 \text{ mm}^2$) and the tensile samples. The blanking dies were used to produce electrical steel sheet samples at different blanking speeds for the 0.2 and 0.35 mm thicknesses and in the RD and TD sheet

grain orientations. The magnetic properties and hysteresis losses of samples were then compared. Following the SST standards [138, 143], the new apparatus consisted of a pair of U cores, which were manufactured from grain oriented silicon steel. The first U core was fixed to the apparatus base, while the second could be moved up and down to allow the specimens to be inserted and removed, as shown in Figure 3.16a. Also, a pair of coils was built: a magnetization coil (N_1) was connected to terminal 1 for magnetizing the sample, which in turn was connected to the power supply circuit. In addition, an induction coil (N_2) was built and connected to terminal 2 to sense the change in created flux in the specimen, and then connected to a flux meter device. Both N_1 and N_2 were wound around special bobbins built by a 3D printing technique, as illustrated in Figure 3.16b. The air gap between the sample and the induction coil was designed to be very small so that its effect would not be significant.

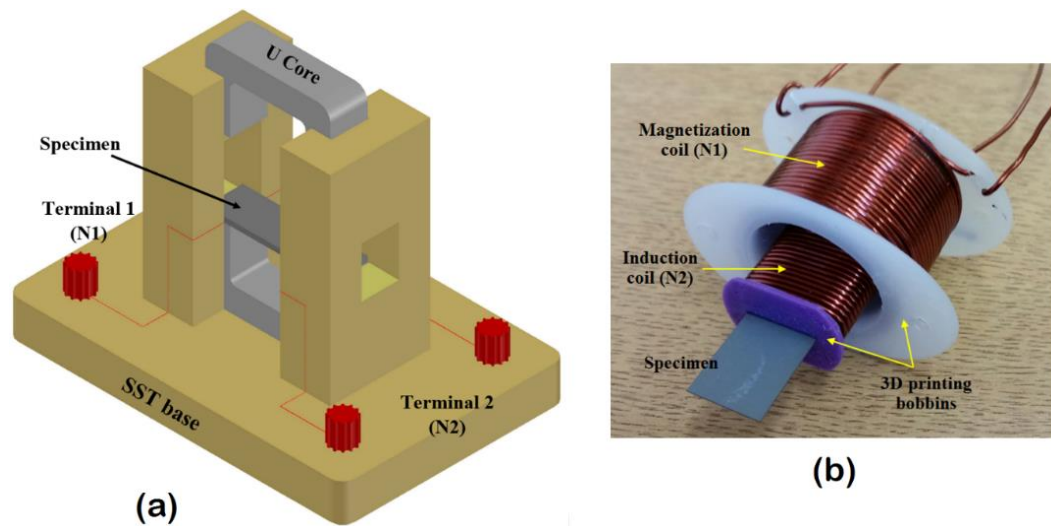


Figure 3.16: SST system design and coils arrangement.

The current in the coil produces a magnetic field around the sample. The parallel and closed field lines in this region exhibit a highly uniform and strong field. Field lines behave in a similar way to how a bar magnet would if it had a north pole at one end and South Pole at the other end. The strength of the magnetic field can be increased by increasing the current in the coil, increasing the number of coils in the solenoid, and using a soft iron core. The full magnetic flux path in the closed double yoke system and in ES sheet are shown in Figure 3.17.

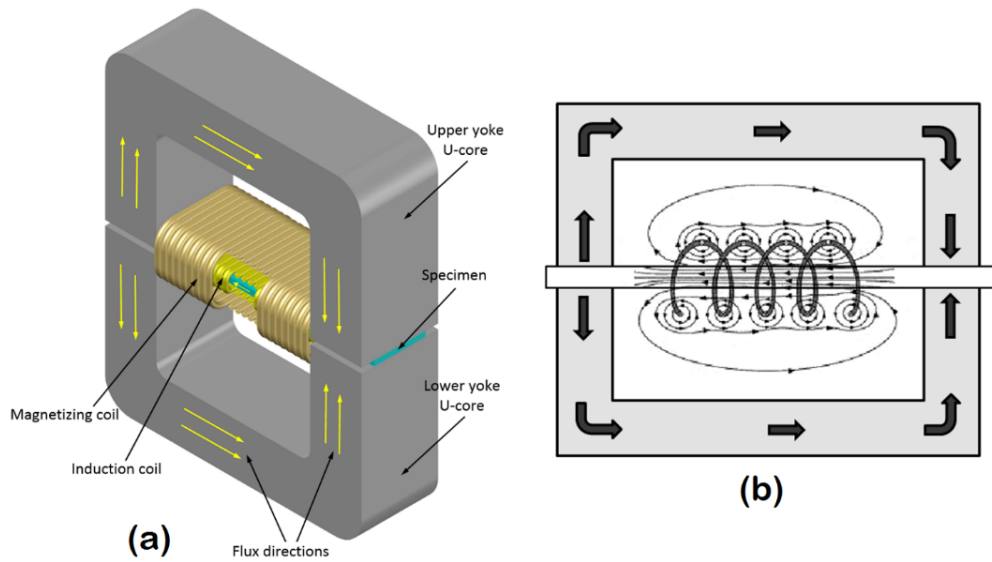


Figure 3.17: (a) Flux path in closed double yoke system, (b) Flux coil path in ES sheet.

The connections of both magnetizing and induction electrical circuits are shown in Figure 3.18. A stabilized D.C. power supply was used as the source of direct current E and connected with the current measuring device or Ammeter. Both were connected to a reversing switch $S1$ type (DPDT), then to the magnetizing winding N_1 on the SST specimen. When switch $S2$ is closed, the current in the magnetizing circuit is controlled by variable resistor R . The secondary circuit comprises of the secondary winding N_2 (B coil) connected to the flux integrator. Figure 3.19 shows the full design that comprising all the new single sheet magnetic tester parts. A point-to-point method according to [143] was followed to determine the complete hysteresis curve.

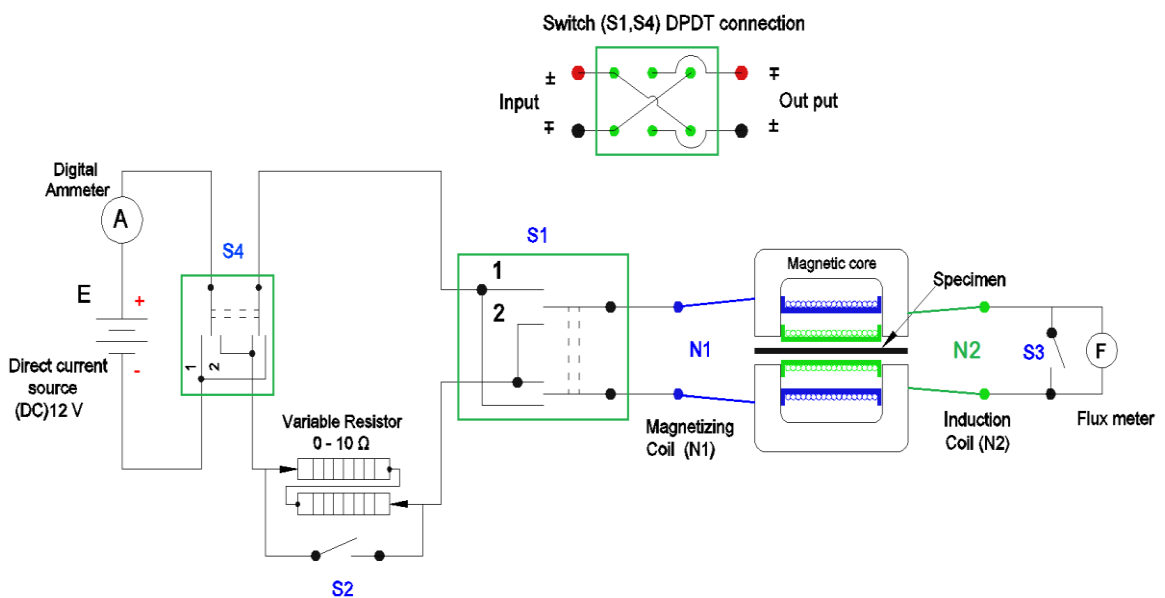


Figure 3.18: SST equipment parts connections and electrical circuit.

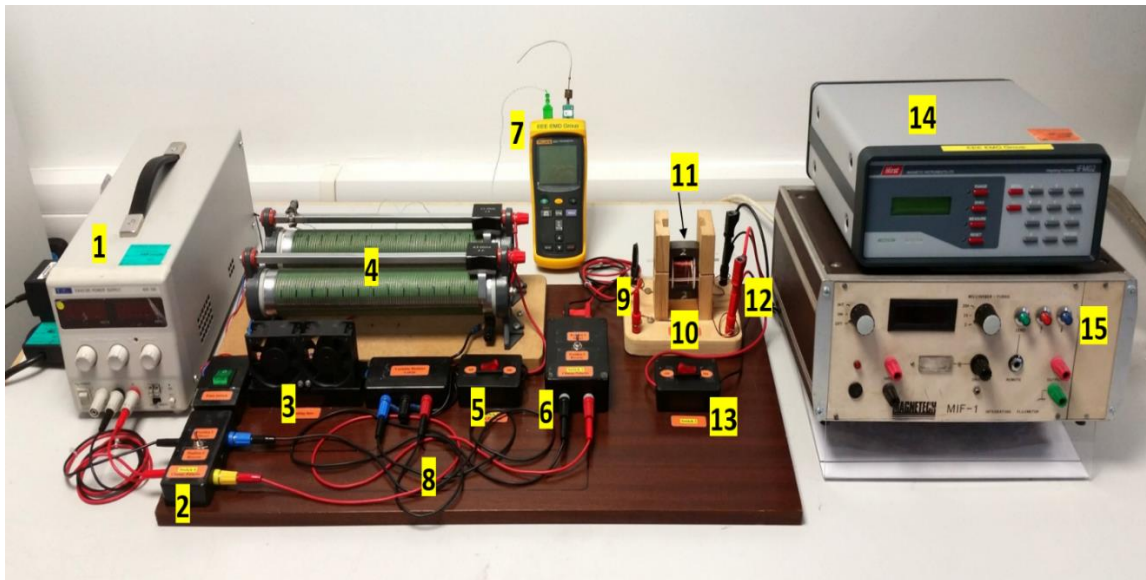


Figure 3.19: Full design of new single sheet magnetic tester, (1) Power supply, (2) Switch 4, (3) Cooling fans, (4) Variable Resistors, (5) Switch 2, (6) Switch 1, (7) Thermocouple, (8) Cables, (9) Terminal 1 for N1 coil, (10) SST System, (11) Double Yokes, (12) Terminal 2 for N2 coil, (13) Switch 3, (14) Flux meter 1, (15) Flux meter 2.

3.5.2 Determination of magnetization curve and hysteresis loss

The hysteresis magnetization loops can be achieved by applying several steps using the SST tester: First, a low current is passed through the magnetizing winding N1. The current is then reversed about ten times by reversing switch S1 to bring the material into a steady cyclic state. When switch S3 is opened, the flux integrator reading corresponds to the reversal of the magnetizing field is recorded. Here, the flux meter should be zeroed and then a current of value sufficient to produce the maximum magnetic field strength required shall be passed through the magnetizing winding N1. This current shall be slowly reduced to zero, then reversed and increased to its maximum negative value, reduced to zero, reversed again and increased to its maximum positive value.

Through this procedure, the corresponding values of the magnetic field strength (H) and the magnetic flux density (B) can be obtained, from which the points of the hysteresis loop were determined and plotted. After each measurement, the test specimen was de-magnetized from a magnetic field strength by means of repeated reversals of S1. A short time was allowed to elapse between each reversal to ensure that the magnetic field had completely penetrated the test specimen. The magnetizing current shall never

be decreased during the measurements, otherwise the test specimen shall be demagnetized before resuming measurements. Similar test details were reported in [143].

The values of magnetic field strength were calculated manually depending on the current values that varied with the change of resistor values, according to the following equation:

$$H \times L = N \times I \quad (3.4)$$

Where: H: is the magnetic field strength, in amperes per meter (A/m), N: is the number of turns of magnetizing winding, L: is the mean magnetic path length, in meters, and I is the magnetizing current, in amperes.

The magnetic flux density is obtained from the corresponding magnetic flux density and cross-section area of the specimen. Remanent flux density is the measured magnetic flux density value (in Tesla) when the magnetic field strength is zero on the hysteresis loop. Coercive field strength is the measured magnetic field strength value (in amperes per meter) when the magnetic flux density is zero on the hysteresis loop. The hysteresis energy can be obtained from half of a hysteresis loop [144, 145] as illustrated in Figure 3.20.

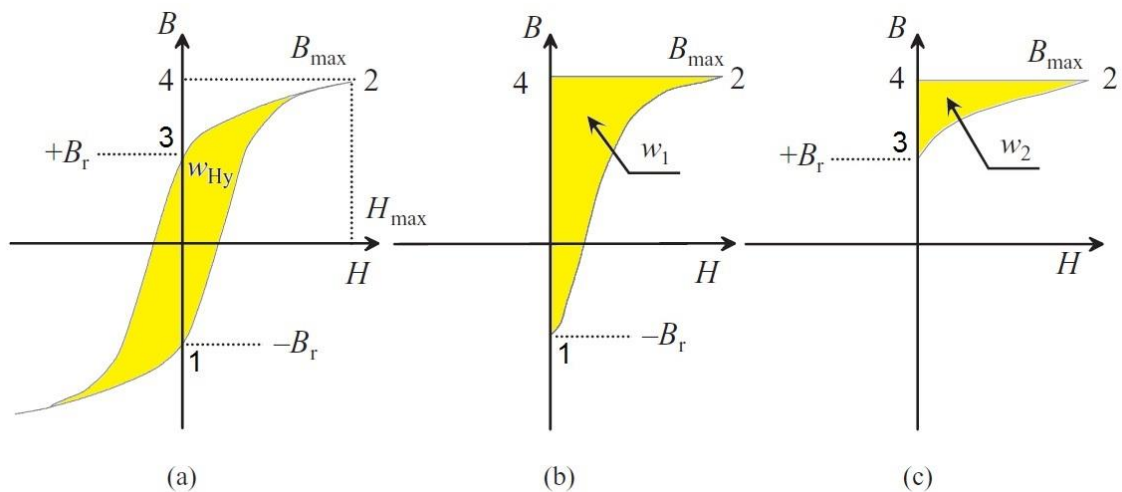


Figure 3.20: Determination of hysteresis loss: (a) entire hysteresis curve, (b) absorbed energy area w_1 , (c) dissipated energy area w_2 [145].

The shaded area between the BH curve and the B axis in Figure 3.21b represents the work done per unit volume of material. When H increases from zero to H_{\max} (from points 1 to point 2), the absorbed energy per unit volume is:

$$w_1 = \int_{-B_r}^{B_{\max}} H dB \quad (3.5)$$

While the dissipated energy in Figure 3.21c when H decreases from H_{\max} to zero is:

$$w_2 = \int_{B_{\max}}^{B_r} H dB \quad (3.6)$$

The total hysteresis loss is equal to the energy used to establish field minus energy released by the collapse of the field. Therefore, the energy required to magnetize the core represented by the area under the curve from points 1 to point 2 is more than the returns area under the curve from points 2 to point 3 [144,145].

From another view, the back of the electromotive force, also called the electromagnetic field (emf) differs from the generated one. As the emf is proportional to the change in flux, which means that the remaining flux changes less than the generated flux. Therefore, it can be concluded that the total power lost over one complete cycle is proportional to the area within the hysteresis loop.

According to the Steinmetz hysteresis law, the hysteresis loss per m^3 per cycle of magnetization of a magnetic material depends on the maximum flux density and the magnetic quality of the material [146].

$$W_h = K_h \times f \times B_{\max}^n \quad (\text{joule}/m^3/\text{cycle}) \quad (3.7)$$

Where K_h is Steinmetz hysteresis constant depending on the nature of the magnetic material, n is empirical index Steinmetz exponent equal to 1.6 when the B_{\max} is between 0.1 and 1.2 Wb/m^2 , f (Hz) is frequency of reversals of magnetization because the hysteresis loss changes with each cycle of the core, alternating from positive to the negative magnitude of B , which means the loss is directly proportional to the frequency of operation. Calculating the hysteresis power loss requires either dividing the hysteresis work over the specimen volume size to convert it to watts (joule/s), or converting the density of the material to watts/kg. Therefore, the formula for the hysteresis power loss will be:

$$P_h = W_h / \rho \quad (\text{Watt}/\text{kg}) \quad (3.8)$$

Hysteresis loss is essentially independent of the load current; it depends just on the flux and hence the voltage; thereby the efficiency of a transformer drops towards zero with the load current.

3.5.3 Uncertainty and limitations of determination the magnetization curve and complete hysteresis loop

According to the standard [143], there are two methods can be used to determine the normal magnetization curve and complete hysteresis loop when conducted SST: the continuous recording method and the point-by-point method.

To utilize the continuous recording method, additional equipment is required. For example, the output from the flux integrator meter should be connected to the Y axis of an X-Y recorder, plotter or computer interface. Also, the terminals of this resistor should be connected to the X-axis of the same devices. The system can be in overall give direct readings of magnetic flux density and the magnetic field strength in form of B-H loop. However, in the continuous recording method, the overall uncertainty may be increased depending on the resolution of the recorder system.

In addition, if digital control is performed, two signal digital-to-analogue converter with specific lab view software setting is required. Also, because the output signal from a digital-to-analogue converter is a stepwise waveform, so it required a low-pass filter to smooth the signal and reduce data noise as well.

All these additions will increase the complexity and cost of the tester. Therefore, to keep the tester as simple as possible, the point-by-point method has been used in the current SST measurements in spite of its limitation that could lead to increasing the measurements uncertainty, for example, the measurements data are recording manually result in a limit number of points. That was due to the many reasons such as the test time is short (the duration of test is approximately 12 ms). In addition, the reading flux value is corresponding to a specific value of the current at a specific resistor value. Also, sample shape, corner, cross-section, and hysteresis characteristics of yokes can affect the measurement. However, absolute accuracy is difficult to attain. Therefore, precautions must be taken to avoid the uncertainty in test accuracy.

In addition, the area inside the hysteresis loop represents the total hysteresis loss and equal to the energy required to magnetize the core. Thereby, determining the hysteresis loop by limited points could lead to reducing loops accuracy and thereby the loss is not accurately determined. Consequently, a problem could arise with the measuring of the area of the loops of the deformed samples and the calculation of the hysteresis loss will be affected.

3.6 Microstructural analysis

Material microstructures have a strong influence on the properties, therefore blanked samples microstructures were investigated at the deformed cut edge. Samples were prepared for microstructure analysis using a series of standard operations including sectioning, mounting, polishing, etching, and coating. Both optical and scanning electron microscopy (SEM) were used to examine the microstructure of the cut edge of blanked electrical steel thin sheet. In general, the microstructure preparation procedures of electrical steel are similar to those used for low-carbon steels [9]. In addition, different samples were prepared without etching and coating for Nano-indentation tests, whilst some further specimens, such as those used to examine the edge zones of the cut edge, were observed without preparation in order to assess the surface state.

3.6.1 Samples preparation

To prepare the samples for microstructure examination, several steps needed to be implemented including: sectioning, mounted, grinding, polishing, etching, conductive coating or silver painting. Each step depends on the material type and size. Care needed to be taken to ensure the preparation of the sample surface was done accurately according to the following steps:

Sectioning and mounting of the samples was conducted in such a way as to expose the cut edge profile and deformation [147]. The blanked samples were manually sectioned from the blanked sheet using the Tin cutter with great caution to prevent alteration of the structure of the metal or damage to the sample at the cut edge, as this would lead to erroneous results. Then the samples were cold mounted in order to provide the required support for mechanical grinding, polishing and hardness measurements and to identify the sample code.

In general, there are two mounting methods: hot mounting, also called compression mounting, and cold mounting. Hot mounting involves using Bakelite thermosetting material and applying heat of around 150-180 °C and high pressure around 290bar to the specimen [148]. The heating cycle may cause changes in the microstructure, or the pressure may cause delicate specimens to collapse or deform. Therefore, it was decided to use cold mounting because it does not involve application of pressure and heat to protect the thin sheet specimen edge and preserve the integrity of the material's surface

features during preparation. Cold mounting uses a mixture of resin and hardener [149]. The cold mounting powder was mixed with the liquid Acry-Kleer system in a ratio of 2:1. A system from Met Prep Company was selected because it is transparent, offers fast solidification and exhibits lower volume shrinkage. Figure 3.21 shows the prepared samples in the mould.

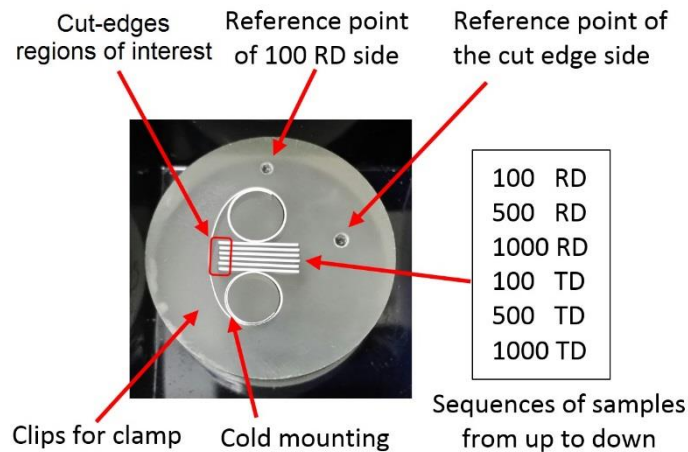


Figure 3.21: Arrangement of the cut samples in the cold mounting.

Grinding and polishing of the samples was carried out using a progressive sequence of abrading operations, from coarse abrasive paper of grade 400μ to a finer grinding paper of 1200μ . The microscopic structure of the electrical steel is very sensitive to water [9] and during grinding tends to oxidize quickly, within around 10 seconds, especially after removing the coating layer, because of the use of nitrogen gas in the heat treatment used in ES manufacturing. For this reason, water was avoided completely in the final stages of sample preparation and an oil-based diamond lubricant was used instead. Although this produced an acceptable surface, it was noted that there were some depositions of debris sticking to the surface caused by the oil's influence. Therefore, a polycrystalline diamond alcohol-based compound with the alcohol-based diamond lubricant was used instead. Isopropanol or ethanol solutions were used for washing samples. Gradually, polishing with a cloth was applied, starting with white cashmere cloth at 6 and 3μ and progressing to smooth Trounoire black cloth at 1μ .

This was followed by etching and coating, whereby the microstructure features were revealed through chemical etching using 2% Nital etchant at room temperature. The solution consists of a mixture of nitric acid HNO_3 and alcohol such as Methanol CH_3OH or Ethanol $\text{C}_2\text{H}_6\text{O}$ [9]. This etching solution was used to reveal the grain boundaries and

deformation bands. The best results in the current work were obtained by submerging the sample in Nital reagent for 40-50 S and then directly washing the sample using Isopropanol or ethanol.

When a small sample is surrounded by a relatively big non-conductive area such as cold mounting, the electrons with a negative charge will gather locally, causing specimen charge-up and thus preventing the emission of secondary electrons. The illumination of the electron beam in SEM will be affected directly by this charge-up and this will affect image quality in the form of abnormal contrast and shift in image [150]. Therefore, to reduce specimen charge-up, the specimen surfaces were coated with gold to a thickness of some microns using a gold coating machine type EMSCOPE, SC500 for two minutes. In addition, silver paint was applied to reduce charge-up and to give the specimen surfaces uniform conductivity. This conductive silver paint, type AGG3691 Agar quick drying silver paint suspension, was applied around the cold mounting and through the middle of the sample.

3.6.2 Microstructure examination

Optical light microscopy was performed using a Nikon Eclipse LV150 microscope to examine the cut edge microstructure. The microscope was equipped with Buehler OmniMet software for the image analysis and to determine the extent of the distortion areas at the cut edge and vicinity area. The line intercept method [151].

was used to measure the average grain size according to ASTM standard E112 standard by drawing a line across the sample image and marking each intersection between grains.

The edge surface created by the blanking process was observed under a scanning electron microscope (SEM), using a field emission gun Inspect F microscope, at an accelerating voltage of 20 kV and spot size of 4 μm , in the secondary electron (SE) imaging mode to observe the cut edge profile and vicinity area and microstructure features of fracture surface at higher magnification. In addition, it enabled expression of the edge surface topography and the different cutting phases including rollover, shear, fracture zones, and burr height directly without material preparation or etching. Inspect F was further used to investigate the Nano-hardness samples to observe the indents' positions in relation to the cut edge. The working distance (WD) was increased slightly under direct camera vision (CCD) by moving the sample platform down to reduce the charging effect

and to gain better image quality, although the change may have influenced the resolution of the image quality.

Energy dispersive spectroscopy (EDS) analysis was performed to quantify the chemical composition of the morphological reactions and elements distribution through the deformed cut edge. EDS was applied using the Inspect F electron microscope at accelerating voltage of 20 KV and spot size 4 μm and in the secondary imaging mode to observe the microstructural features. The EDAS Genesis software was used for the analysis and to chart the peaks of the elements.

3.7 Summary

Blanking experiments can provide insight into the cutting process mechanism and the local induced deformation at the cut edges. In addition, the testing of samples under a known production condition can allow the affected magneto-mechanical properties. Together, the three analysis elements including process, material, and testing can provide a complete range of information about the blanking process and the properties of the produced samples, which could lead to better understanding of this process.

This chapter provided a detailed explanation of the methodology used for the experimental works of the current study, including blanking procedures and the material types and specifications. In addition, it has provided in-depth specifics of the magneto, mechanical, and microstructure tests. For example, the technical specifications of the designed blanking dies. In addition, it has illustrated the DIC setup system and the camera types and recording frequency rates used. Furthermore, it has explained in full the design and manufacture of a new magnetic single sheet tester to suit the size of the samples and the setting of the conditions for the Nano-indentation tests and SEM and optical examinations. The uncertainty aspects and limitations for each used test have been mentioned as well.

The next chapter will present the results obtained by implementing the experimental tests described in this chapter.

4

Experimental results

4.1 Introduction

This chapter presents the experimental results obtained from the blanking process and the conducting of mechanical, microstructure, and magnetic characterizations for the tested material. Processes and tests settings and conditions were explained previously in the experimental work chapter. Generally, the results are divided into four main sections in order to report on the effect of material thickness of 0.2 and 0.35 mm as well as the loading orientations RD and TD. The investigation results for each of these categories are shown and linked through expressing their material properties and quantifying the deformation at the cut edge and the vicinity area in accordance with the objectives of the research.

4.2 Characterization of mechanical properties

4.2.1 Tensile tests

The tensile tests were carried out for standard tensile samples of electrical steel at different crosshead speeds of 1, 5, 10 mm/min at room temperature to find out the influence of variation in test speed on the mechanical properties of the material. [Figure 4.1a, b](#) show tensile engineering stress-strain curves for 0.2 mm thick materials at the RD and TD orientation subjected to different loading speed with strain rate from about 0.67 to $6.67 \cdot 10^{-3}$ /s. The figures illustrate that there is a limited dependency on the test orientation and the material behaviour seems to be more consistent at higher loading speeds. In addition, there are some differences in material properties when tested at lower

loading speeds, the lowest yield and tensile strength being observed at 1mm/min testing speed.

Figure 4.1c shows standard deviation error bars for the tensile results in Figure 4.1a and b regarding the yield stress and UTS values. Generally, results are less steady in the TD direction; this might be due to the grains structure in the local cross-section of the thin sheet.

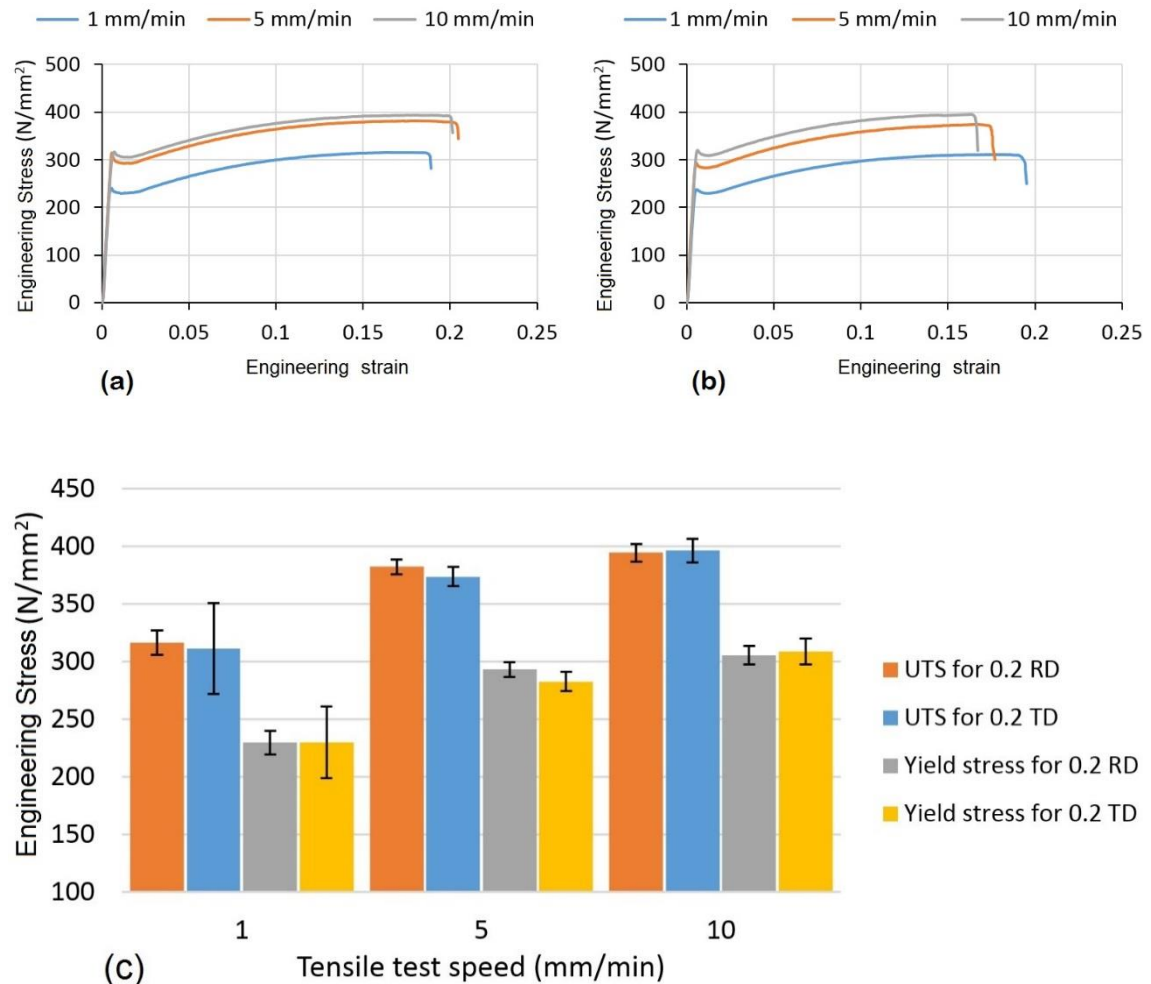


Figure 4.1: Tensile rate sensitivity at different test speeds, a) 0.2 RD, b) 0.2 TD, c) maximum UTS and yield stress values with standard deviation error bars.

Tensile tests were also done for 0.35 sheet thickness under the same tests conditions as for the 0.2 thick sheets to verify the influence of sheet thickness on the tensile results at different strain rates. Figure 4.2a, b show there is a little variation in the mechanical properties of the thicker material compared to the thinner one. The figures also show a limited dependency on the test orientation. However, the material's behaviour is still more consistent at higher loading speeds. Therefore, the speed 10 mm/min was

adopted in all tensile tests for the current research. Figure 4.2c shows more stability in the tensile results for 0.35 sheet thickness than the 0.2 in both sheet orientations; this could be confirmation of the influence of grains in the local cross-section of the sheet on the variation of tensile results.

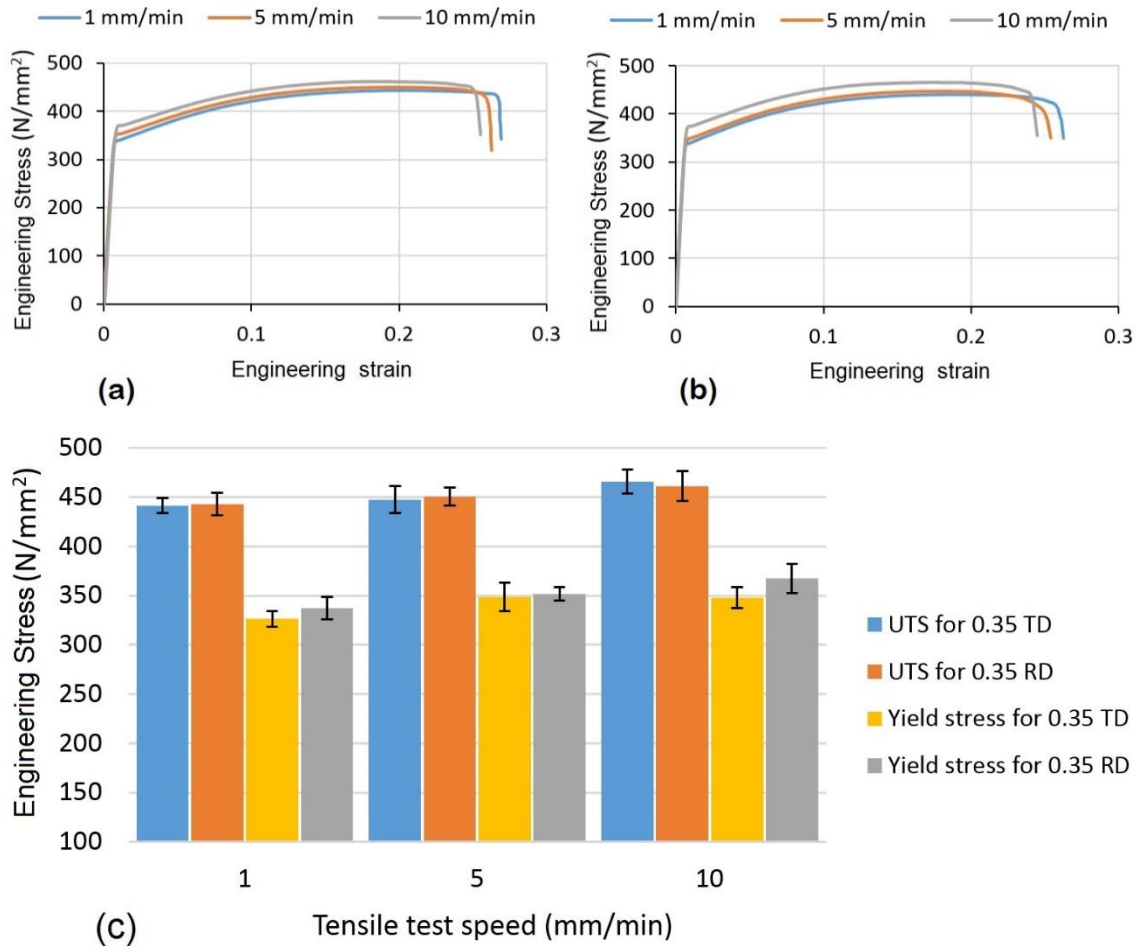


Figure 4.2: Tensile rate sensitivity at different test speeds, a) 0.35 RD, b) 0.35 TD, c) maximum UTS and yield stress values with standard deviation error bars.

4.2.2 Strain distribution in uniaxial loading

DIC technique was used to measure the strain distribution on the tensile samples tested at 10 mm/min. Figure 4.3 shows the stress-strain curves of electrical steel for the two sheet thicknesses and orientations. As it was expected, the graph illustrates higher extension for rolling direction than for the transverse direction due to the applied axial tensile load being parallel to the rolling direction.

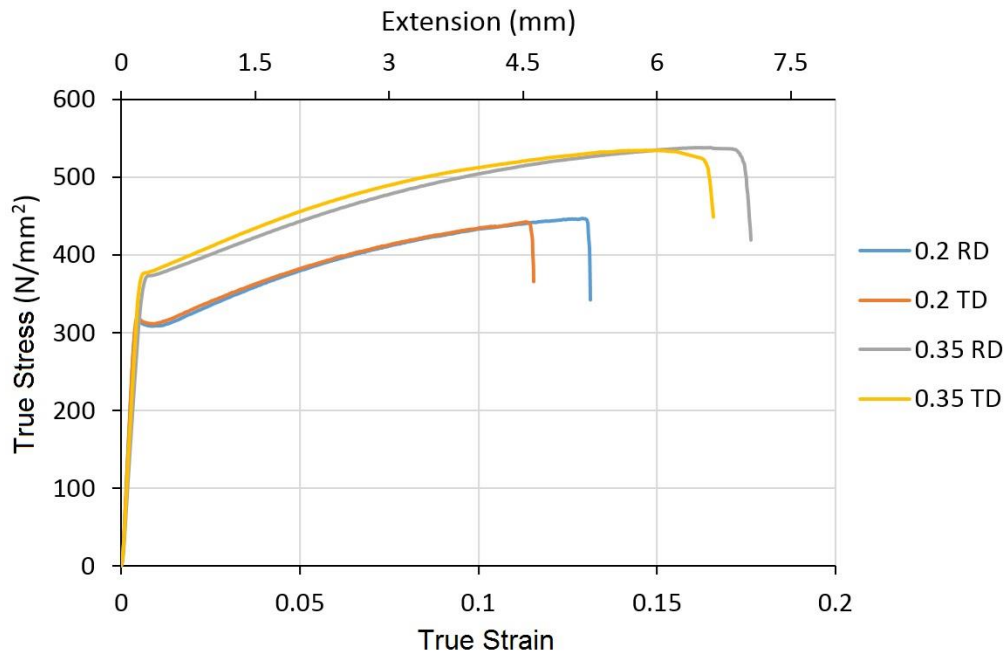


Figure 4.3: Stress-Strain curves for 0.2, 0.35 in RD, TD samples at 10 mm/min test speed.

Figure 4.4 shows the Macrograph of tensile samples at different plastic deformations. The figure illustrates formed of more deformation bands when increasing the material deformation that could reflect the affected of grains and texture in the local deformation.

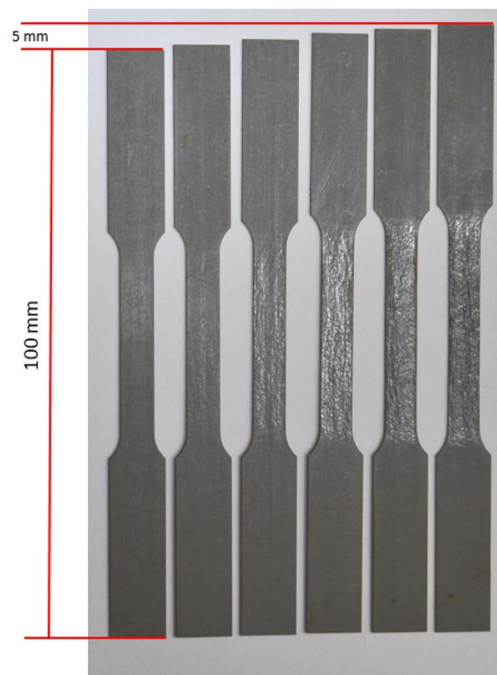


Figure 4.4: Macrograph of tensile samples at different plastic extensions.

In order to evaluate the DIC accuracy measurement, the error calculations have been made by analysis some un-deformed images or static images before applying loads of tensile specimens. Around 5 images have been taken with a time interval equal to the imaging time of the test have been analysed with DIC to quantify the maximum error in the measured strain values during tensile tests. Figure 4.5 shows that the resulting strain map with a maximum strain value of about 0.03, which is negligible compared to the strain values recorded during the test. Thereby, all values of the measured strains during tensile tests using DIC technique in the current study represent the absolute values of the true strains results including the error values.

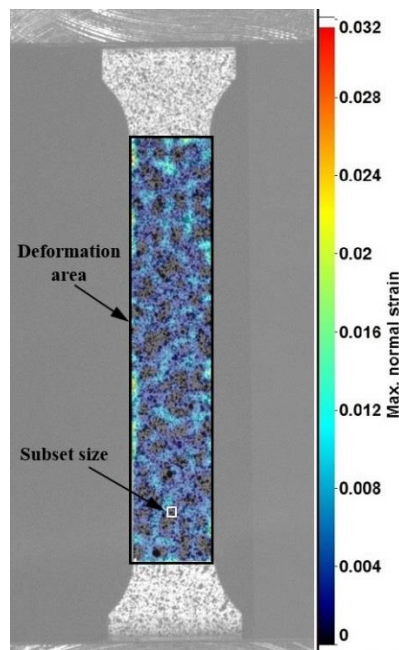


Figure 4.5: The strain error analysis for the tensile samples determined with DIC.

Figure 4.6 to 4.9 show the distribution of the local strains during different stages of the tensile test for both 0.2 and 0.35 mm sheet thickness in both RD and TD orientations of electric steel. The figures demonstrate that the deformation of samples is almost uniform all over the gauge section. Also, there is no clear local necking and the local deformation instantly results in a fracture. According to the local concentration areas of strain distribution, the figures illustrate that the crack begins to form at the edge of the samples in the late stages of the test. Then the crack propagates quickly to the fracture stage. That may be because of the small thickness of the sheet or because the sheet edges were affected by the induced HAZ due to the EDM process when preparing samples, where the stresses are concentrated and the local strain value rises significantly.

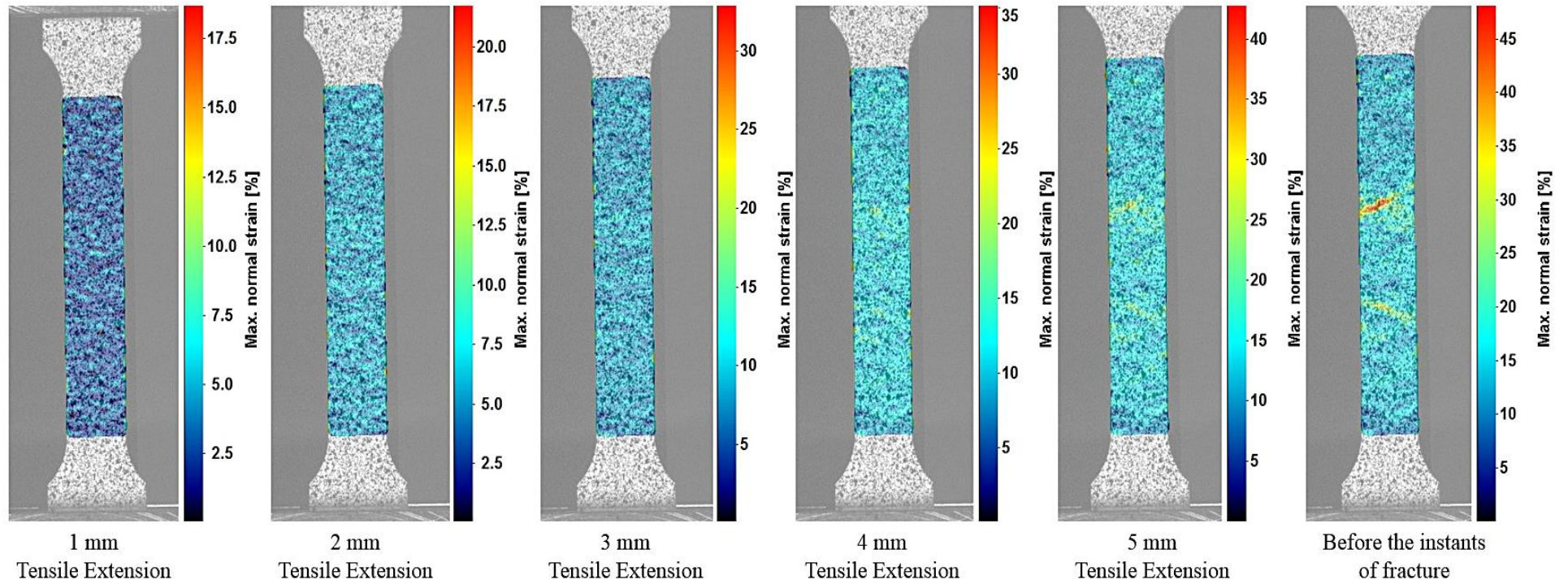


Figure 4.6: Maximum normal strain distribution of tensile samples at different stages of extension during the tensile tests of 0.2 RD.

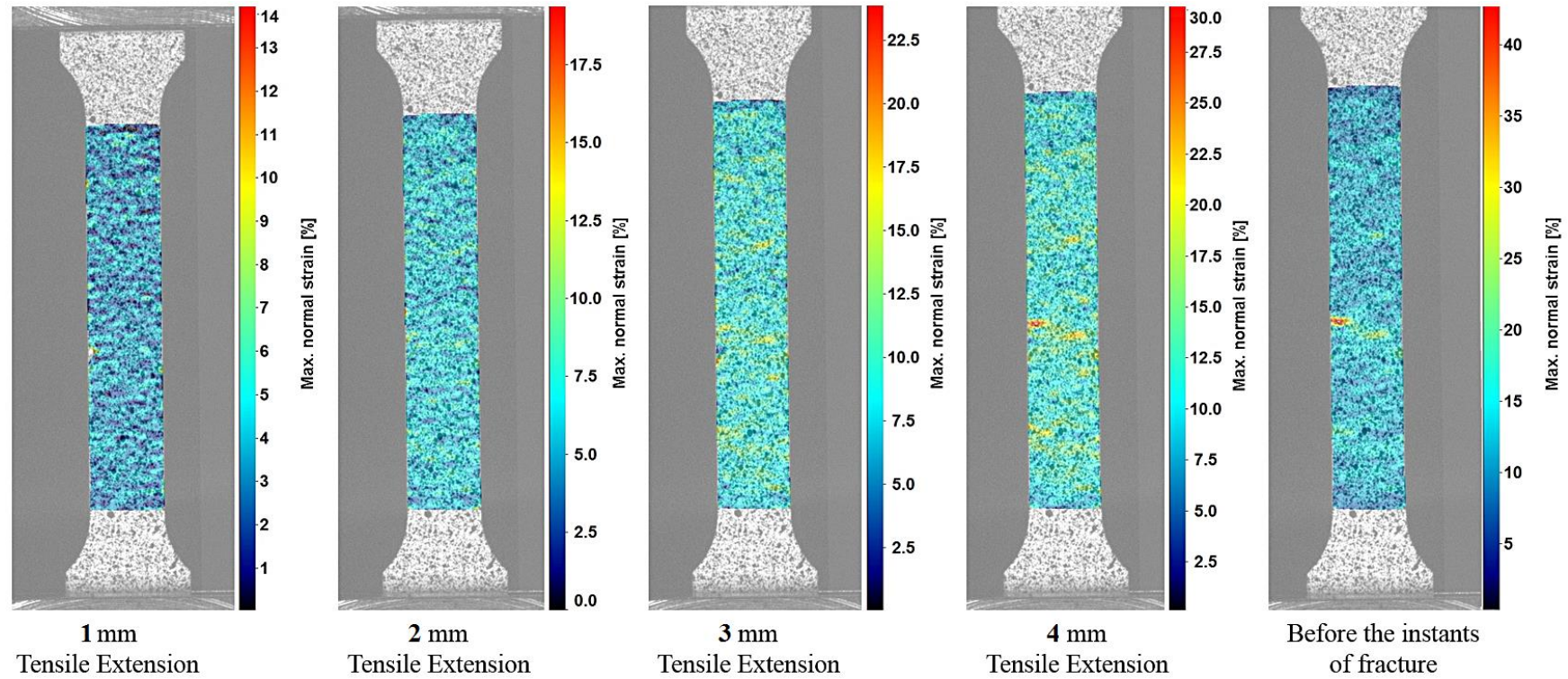


Figure 4.7: Maximum normal strain distribution of tensile samples at different stages of extension during the tensile tests of 0.2 TD.

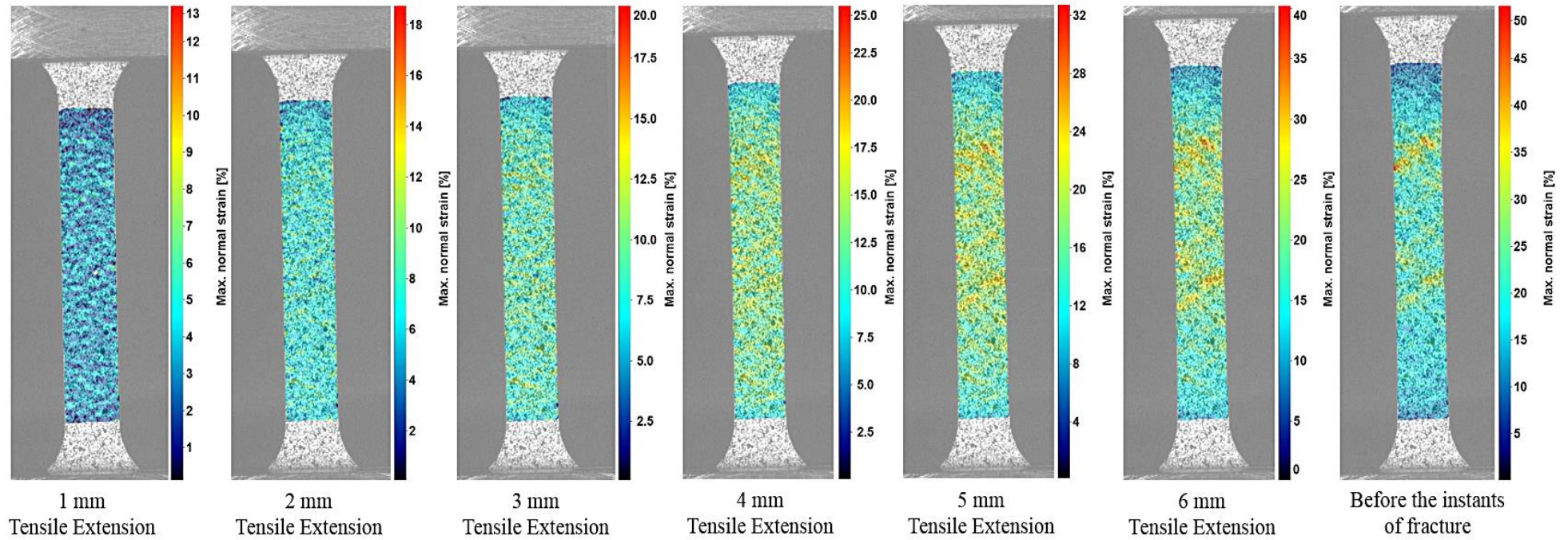


Figure 4.8: Maximum normal strain distribution of tensile samples at different stages of extension during the tensile tests of 0.35 RD.

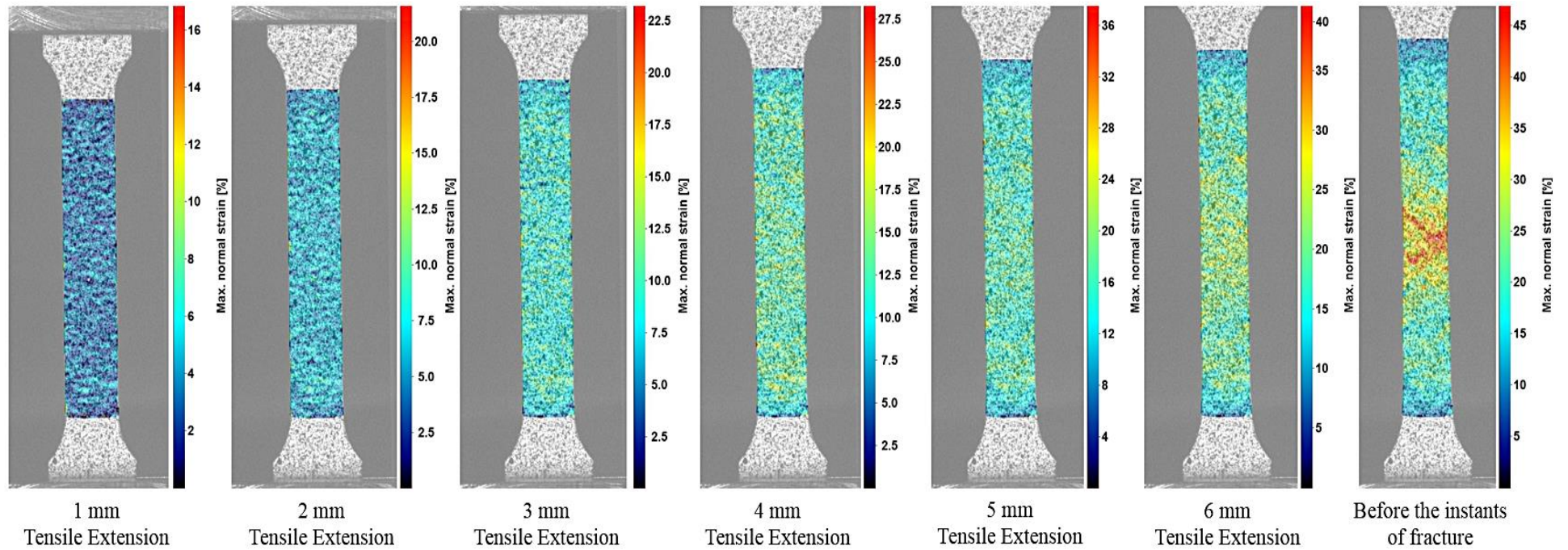


Figure 4.9: Maximum normal strain distribution of tensile samples at different stages of extension during the tensile tests of 0.35 TD.

4.3 Blanking process results

4.3.1 Blanking load stroke

During the blanking process, the cutting force value changes in a cutting cycle. Therefore, to measure the value of the force accurately, the cutting force evolution was constantly recorded by the load cell. When the punch moves down and touches the sheet surface, the cutting force values increase sharply and this is considered as the starting point of the actual sheet cut. Therefore, the actual force required to cut the sheet material was calculated by subtracting the maximum load from the value at the touch point. Figure 4.10 shows the blanking load-displacement for samples at the blanking speed of 100 mm/min.

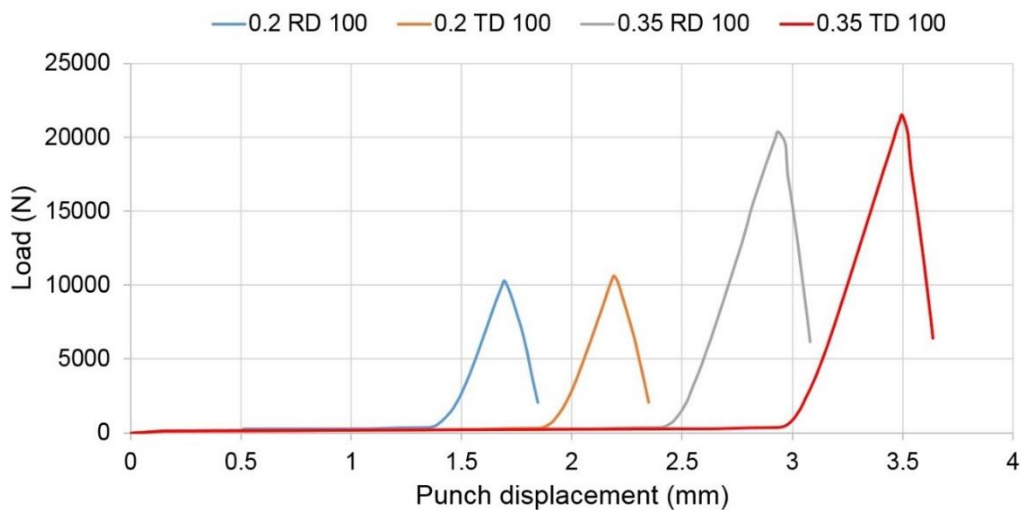


Figure 4.10: Blanking load-stroke displacements for 0.2 and 0.35, RD and TD samples.

Figure 4.11 shows the blanking forces at different test speeds for all ES tested samples. The figures show the cutting load is not affected by the sheet orientation, but there is a significant impact of the blanking speed on the required cutting force to accomplish the blanking process in the full die (type A). The force values were the greatest at the lower speed of 100 mm/min.

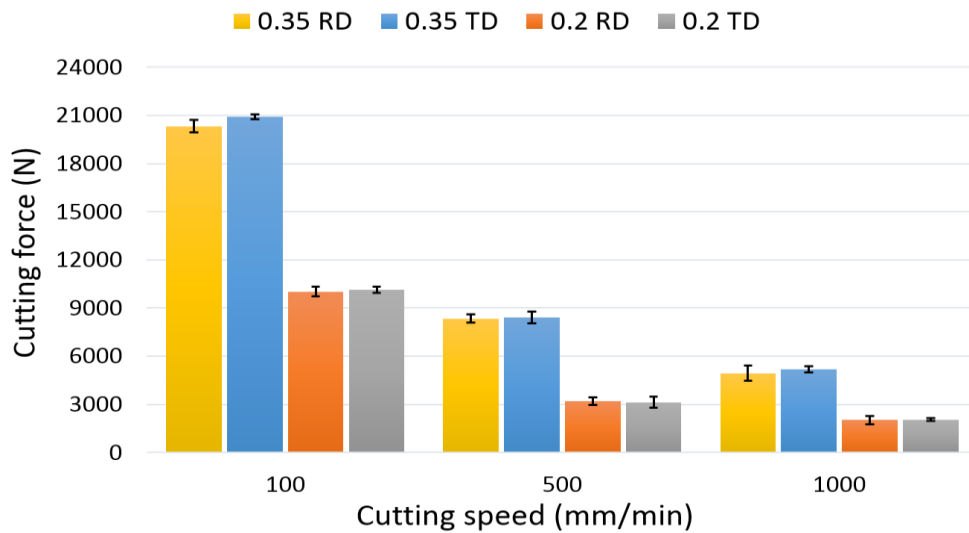


Figure 4.11: Maximum load stroke at different blanking speeds for full die.

Similar results were obtained when the die type B was implemented, but with lower force values because of the shorter cut length line as shown in [Figure 4.12](#). Generally, there is less variation in results when using die type A than with the die type B because of the uniform distribution of applied load on the sample during the cutting process in die type A. According to the results, the force values change with the change of speed even when the thickness and orientation are fixed.

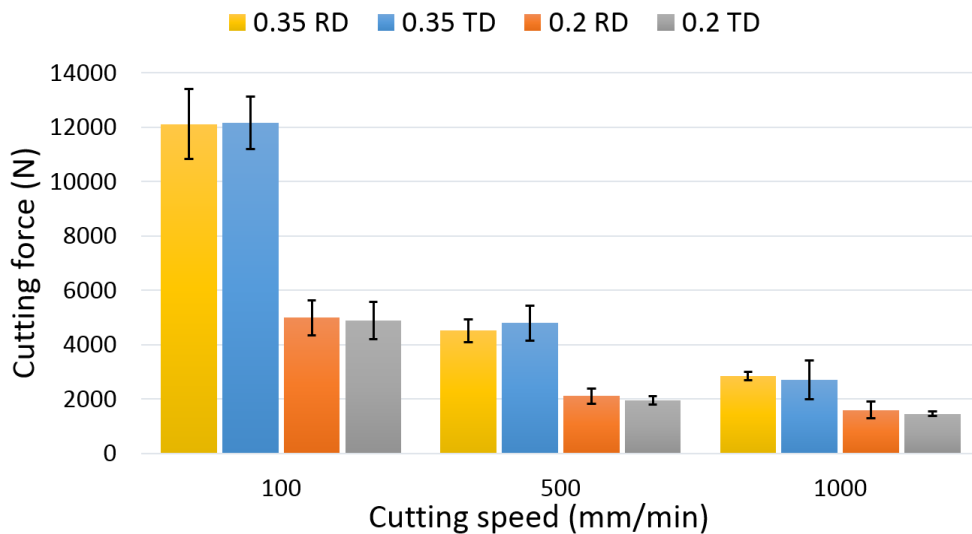


Figure 4.12: Maximum load stroke at different blanking speeds for the die type B.

4.3.2 Strain distribution in the blanking process

The DIC test was used to investigate the strain distribution in electrical steel sheets in-situ blanking process and suitable DIC set-up as explained in previous chapter.

To evaluate the DIC accuracy measurement of blanking tests, the error calculations have been made by analysis of 20 static images in the un-deformed conditions before applying loads with a time interval equal to the imaging time of the test. As it supposed to have no strain when the samples are not loaded, therefore any calculated strain is due to the systematic errors in image processing. These images have been analysed at different settings of DIC parameters to set the proper setting that can give the lower error. Figure 4.13 shows the maximum error in the measured strain values during blanking tests for the current settings. The resulting strain map illustrates a maximum strain value of 0.018, which can be considered as a small value (less than 10 % compared to the maximum strain values recorded during the blanking test). Thereby, all values of the measured strains in the current study represent the absolute values of the true strains results including the obtained error values.

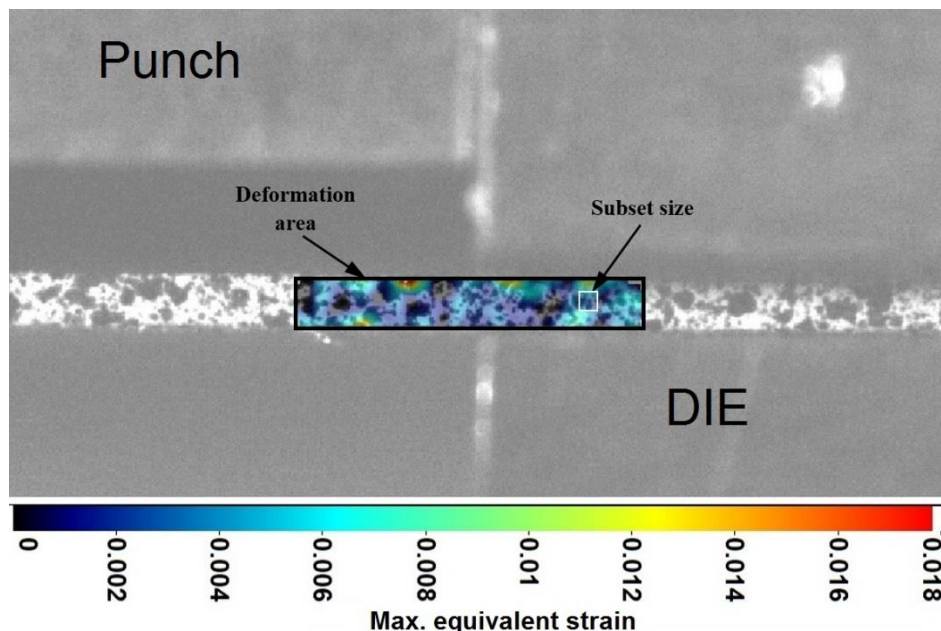


Figure 4.13: The strain error analysis for the blanking samples determined with DIC.

Analysing high-speed DIC tests results during the blanking process included many challenges. For examples, the difficulty of the timing of DIC image acquisition and the determining of the instant of beginning deformation because of the high rate recording

system and high-speed punch movement. In addition, there are differences in fracture moment between the sample because of the differences in applied speeds and blanking conditions. Therefore, it was unattainable to select specific images for the comparison between different samples at different blanking cases at exactly the same punch position.

However, regardless of the punch position, the last image before the fracture and separation of the blank from the sheet could show the state of the blanked part. Also, the seed point or reference point of analysis was localized in the die side only in order to stop the correlation when the separation occurs because disappearing of the speckles. Therefore, the last image before stopping the correlation was considered to represent the maximum deformation for the blanked sample. Several stages have been illustrated during the blanking process to show the mechanism of the process.

In addition, the state of the deformation varies from sample to another because it depends on the local grains and their orientations at the cut edge location. The following high-speed DIC results show the deformation that occurred during the blanking process for the current case study. However, the comparison has been avoided and each test was treated individually.

Figures 4.14 to 4.16 show the distribution of equivalent strains during the four stages of the blanking cutting process of 0.2 RD samples at three different cutting speeds. The first stage shows strains concentration on the sample surfaces at the contact points with the edges of each die and punch. The second stage shows the expansion of deformation with an increase in strain value due to the increase of punch load. Then, the deformation continues to increase in the following stage because of increased penetration of the punch in the sample. The last stage before the instance of fracture shows the largest value of strains and represents the final deformation at the cut edge in the blanking process. It is notable to mention that the deformation can concentrate on both sides of the sheet only when applying very small clearance [62]. Also, the punch, die, and the blank holder seems unclear or blurred because the DIC camera was focused only on the small deformation area of the sample.

Figure 4.14 shows the strain distribution of the 0.2RD100 sample, the maximum strain values increased from the beginning of the cutting process to reach about 45%. This equivalent strain value was decreased to 40% when the blanking speed increased to 500 mm/min as shown in Figure 4.15. The least strain value was resulted with highest blanking speed to be about 35% at 1000 mm/min, as illustrated in Figure 4.16.

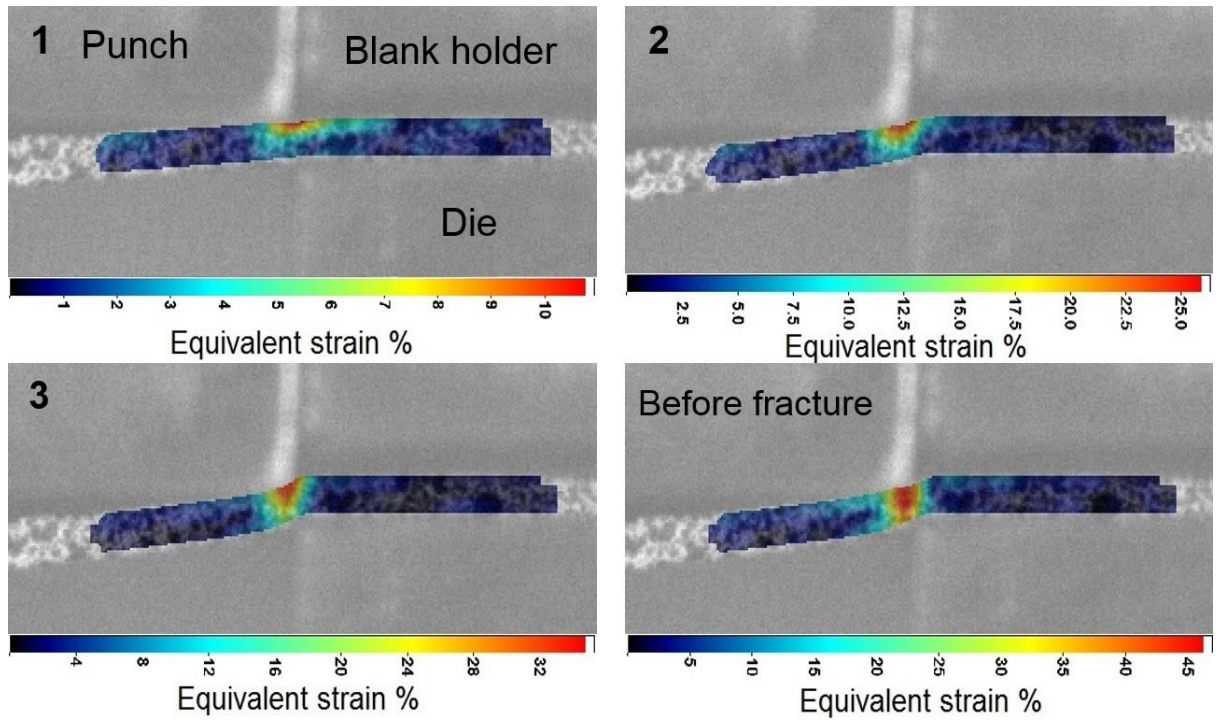


Figure 4.14: Maximum equivalent strain distributions during the blanking process in different stages at 100 mm/min for 0.2 RD 100 sample.

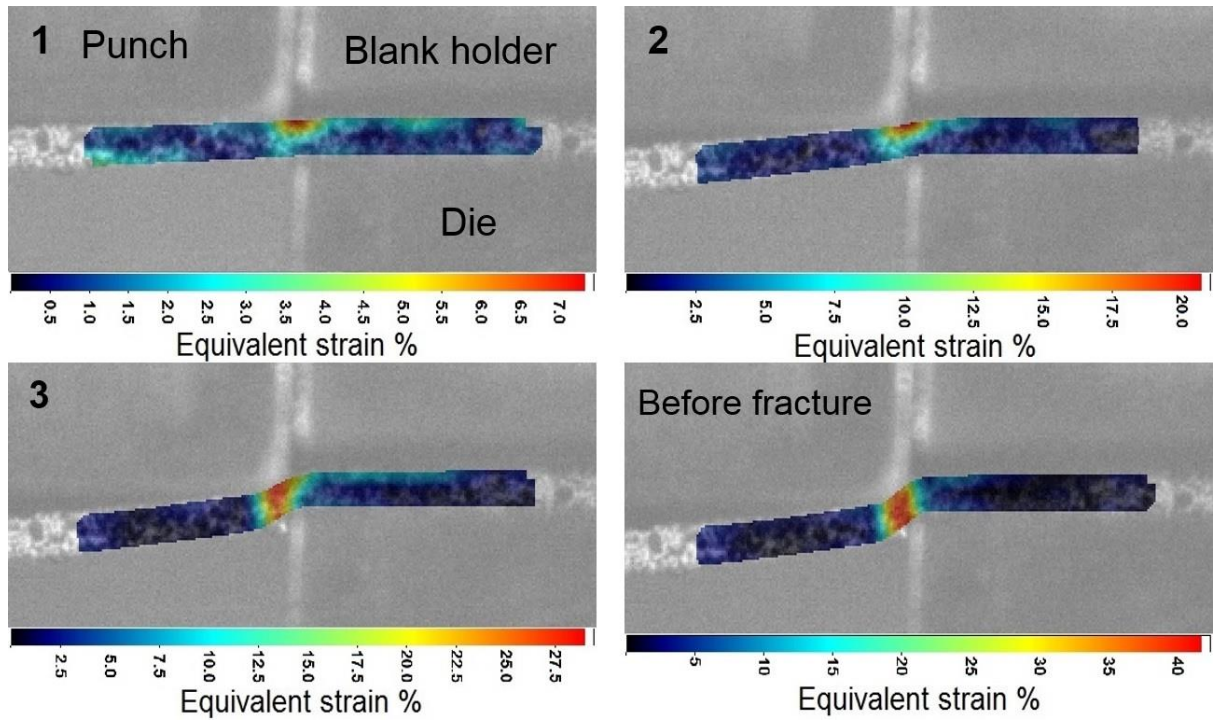


Figure 4.15: Maximum equivalent strain distributions during the blanking process in different stages at 500 mm/min for 0.2 RD 500 sample.

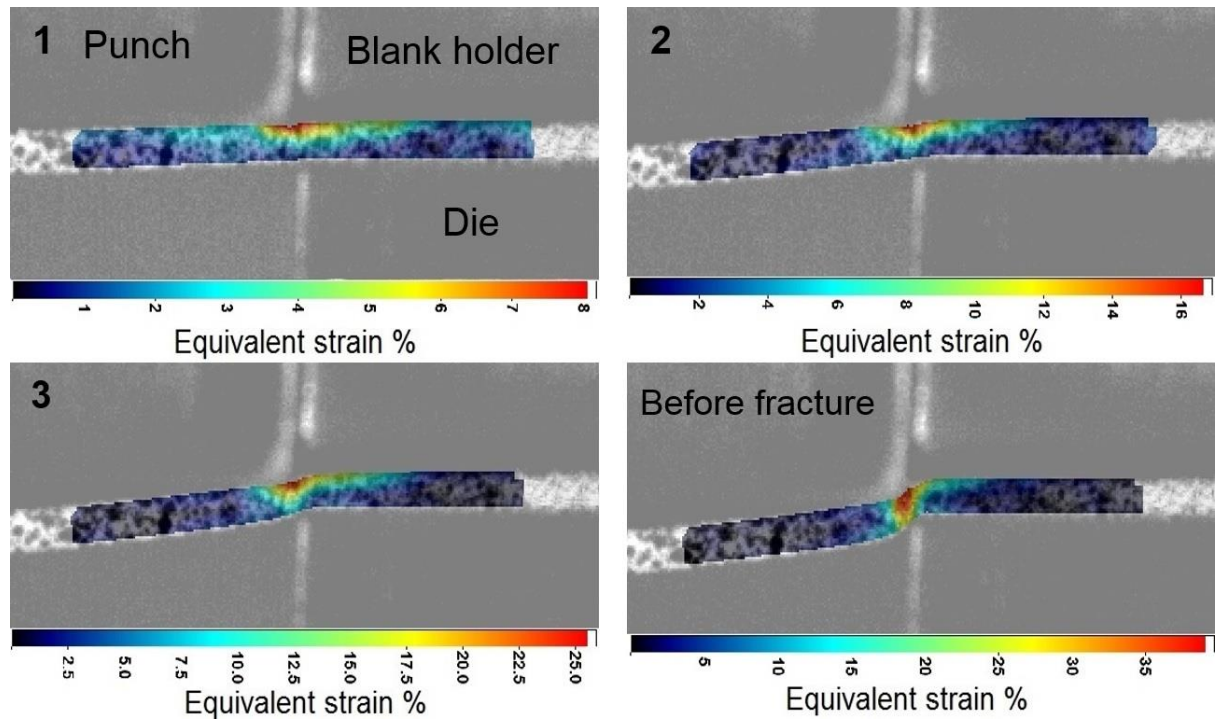


Figure 4.16: Maximum equivalent strain distributions during the blanking process in different stages at 1000 mm/min for 0.2 RD 1000 sample.

In general, a similar behaviour of material related to the mechanism of the process was observed for the equivalent strains distribution in the 0.2TD electrical steel samples as a result of applying the blanking process in the rolling direction. Figures 4.17 to 4.19 show relatively lower strain values to those in orientation RD even with the same sheet thickness and cutting condition. The highest value of equivalent strains with regard to cutting conditions was identified as about 40%. Both blanking speed and grain orientation have affected the deformation by means of changing the strain values.

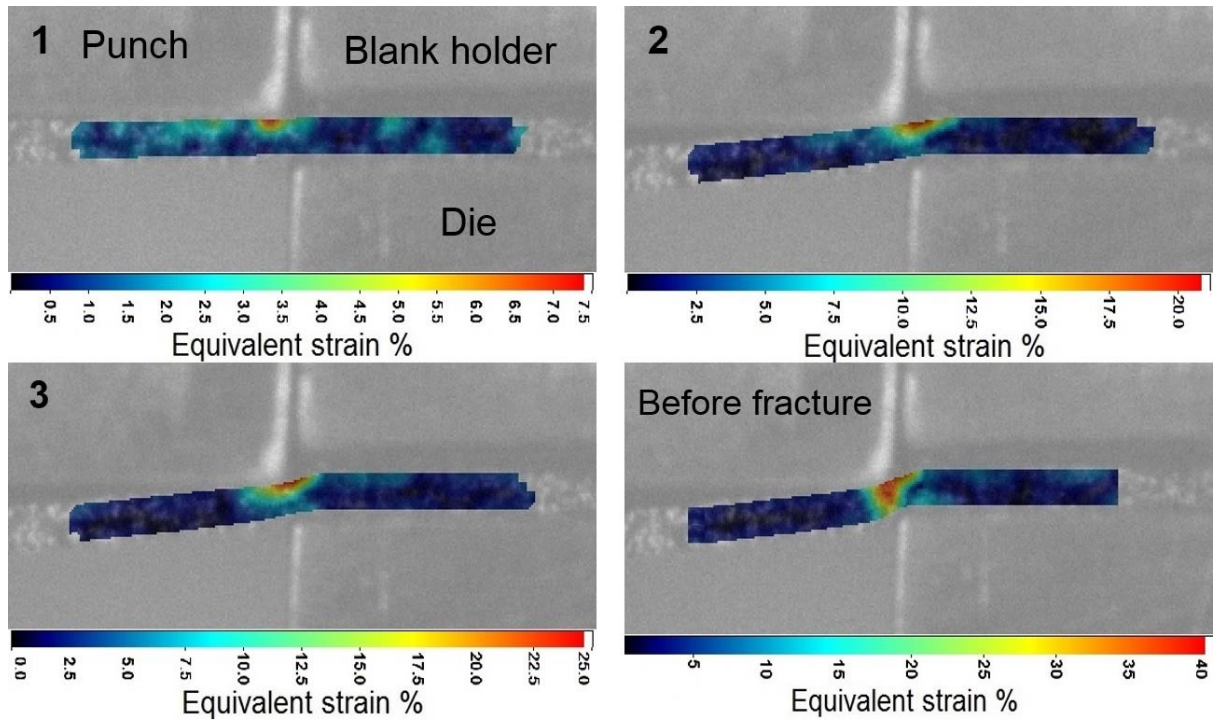


Figure 4.17: Maximum equivalent strain distributions during the blanking process in different stages at 100 mm/min for 0.2 TD 100 sample.

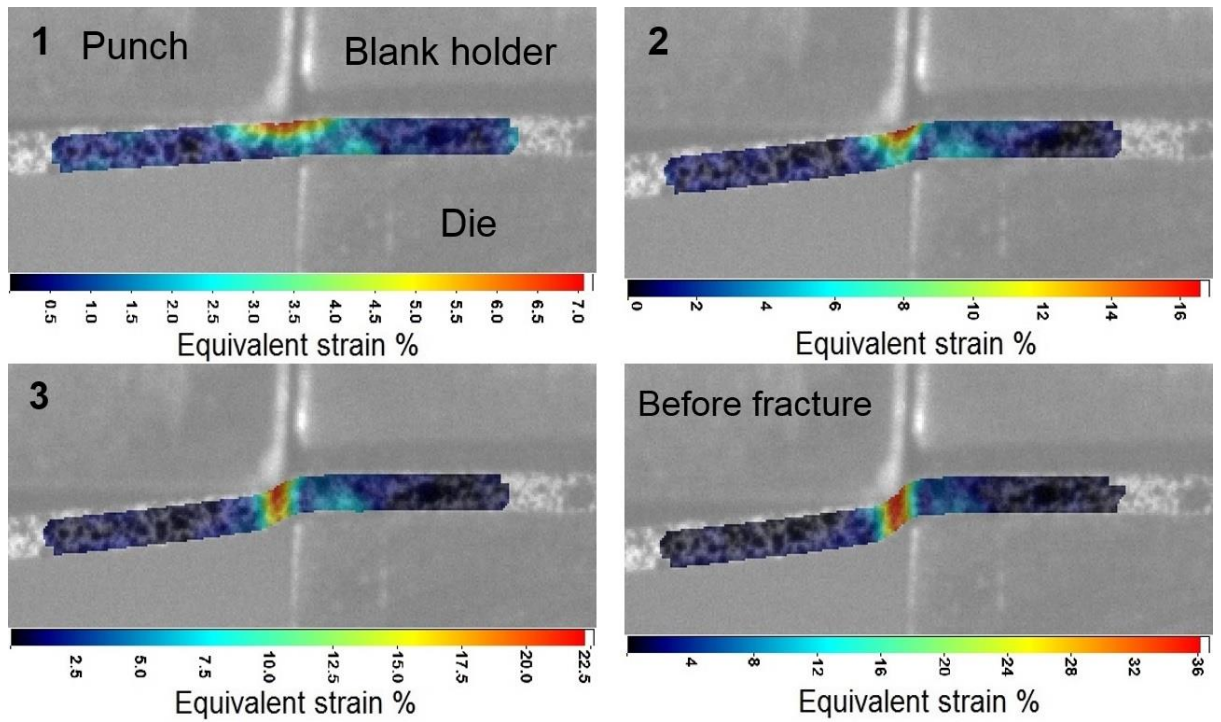


Figure 4.18: Maximum equivalent strain distributions during the blanking process in different stages at 500 mm/min for 0.2 TD 500 sample.

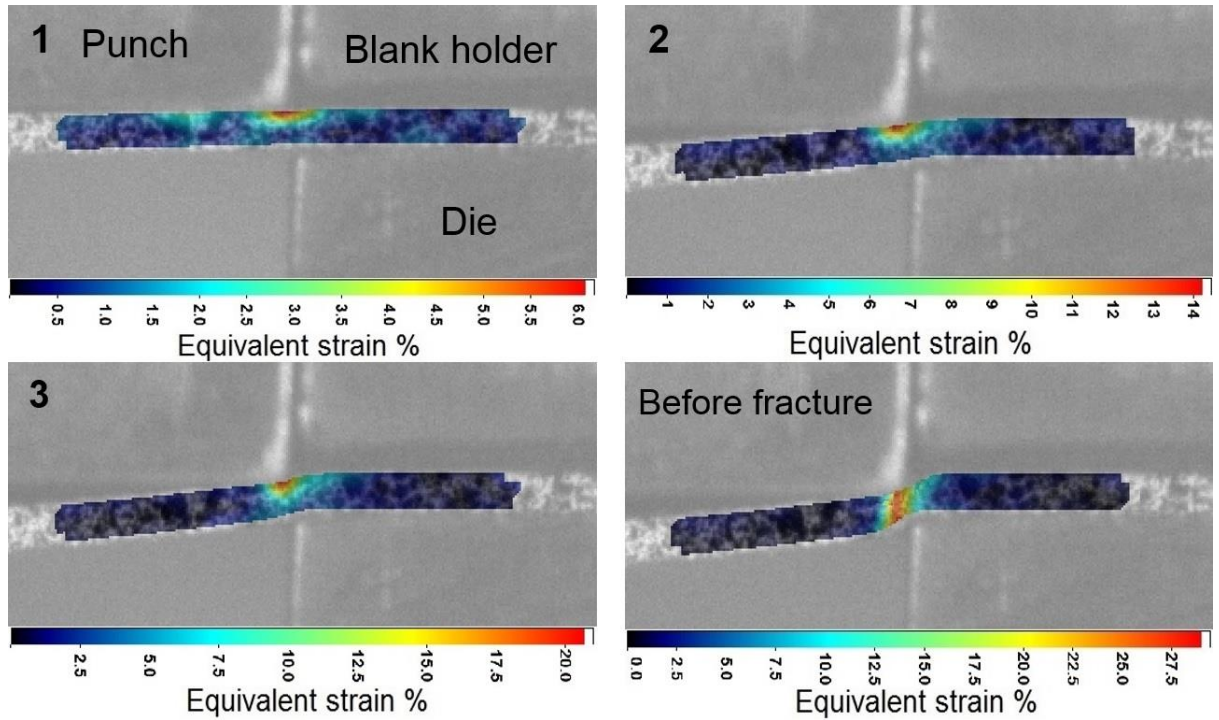


Figure 4.19: Maximum equivalent strain distributions during the blanking process in different stages at 1000 mm/min for 0.2 TD 1000 sample.

In order to investigate the effect of the sheet thickness, similar results were obtained to the 0.35mm electrical steel sheet thickness. Figure 4.20 to 4.22 show the distribution of equivalent strains of the 0.35RD samples in the cut-edge and vicinity area during the cutting process. Because the sheet sample was thicker (0.35 mm), the speckles in the cross-section of the sheet deformation area increased. This resulted in production of clearer images than for the 0.2 thick samples, due to the improved correlations between the subsets.

It seems that the mechanism of process is similar for both material thicknesses, as the deformation increase with increase the penetration of the punch in the material. Figure 4.20 shows the strain distribution of the sample 0.35RD100, the maximum strain values was increased during the process stages to reach about 40%. This equivalent strain value was decreased to the 36% when the blanking speed increased to 500 mm/min as shown in Figure 4.21. The least strain value was resulted with highest blanking speed to be about 32% at 1000 mm/min, as illustrated in Figure 4.22.

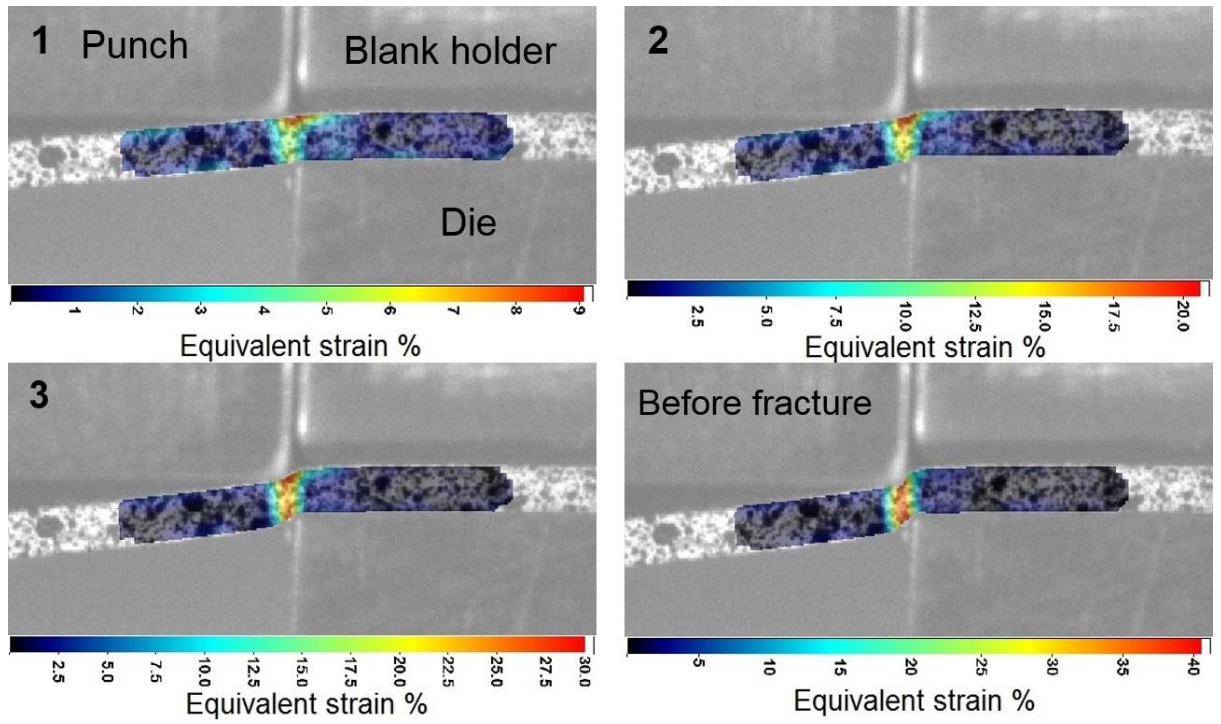


Figure 4.20: Maximum equivalent strain distributions during the blanking process in different stages at 100 mm/min for 0.35 RD 100 sample.

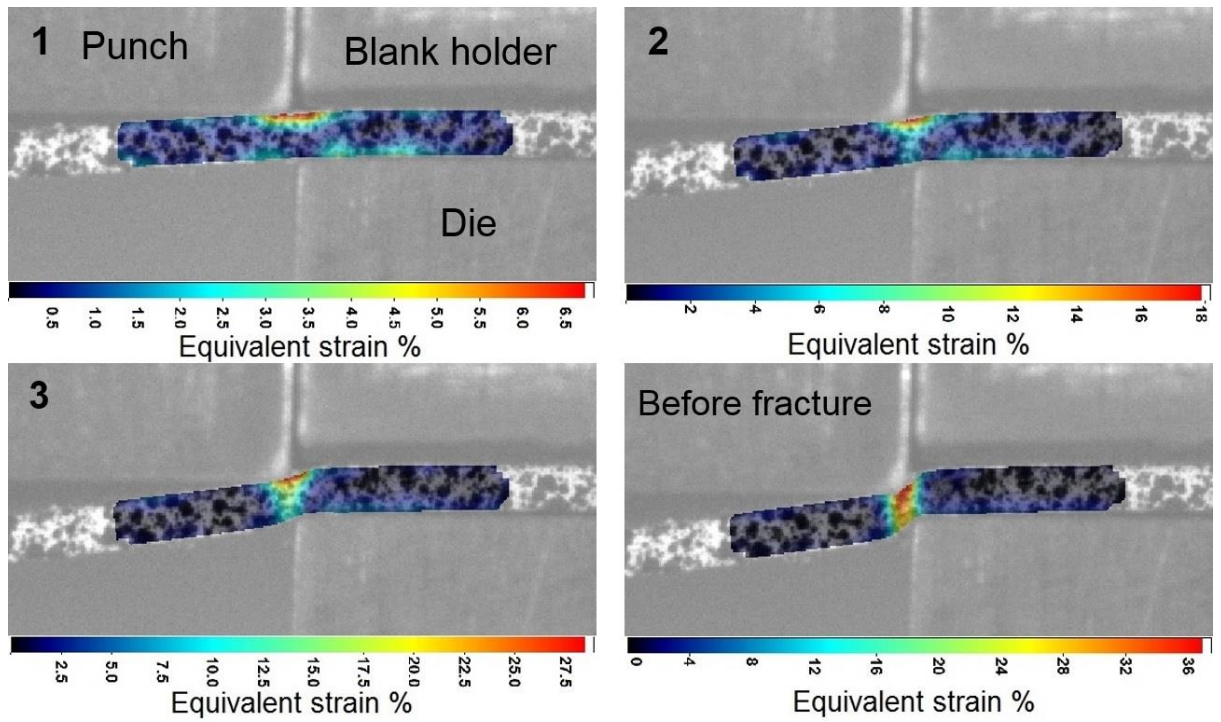


Figure 4.21: Maximum equivalent strain distributions during the blanking process in different stages at 500 mm/min for 0.35 RD 500 sample.

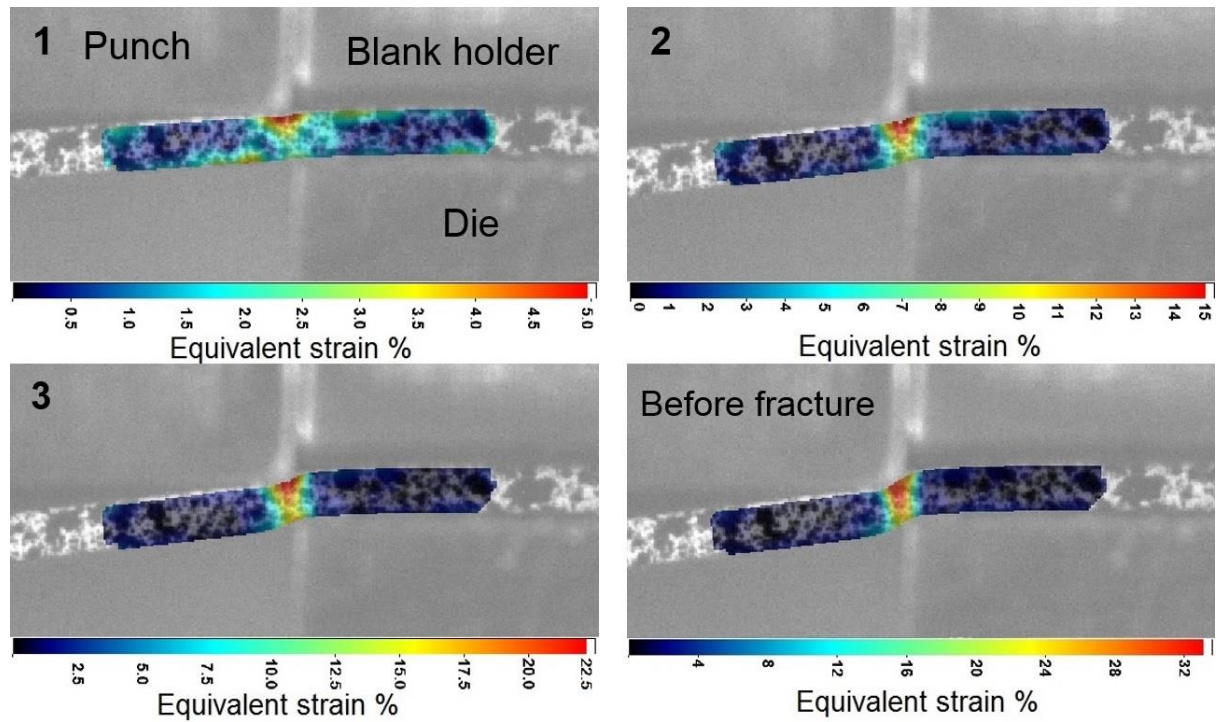


Figure 4.22: Maximum equivalent strain distributions during the blanking process in different stages at 1000 mm/min for 0.35 RD 1000 sample.

Figure 4.23 to 4.25 show the distribution of equivalent strains of the 0.35TD samples in the cut-edge deformation zone and the vicinity area. Similar material behaviour was observed to that in rolling direction, but lower strains values were produced. The highest value of equivalent strains regarding cutting conditions was about 36%.

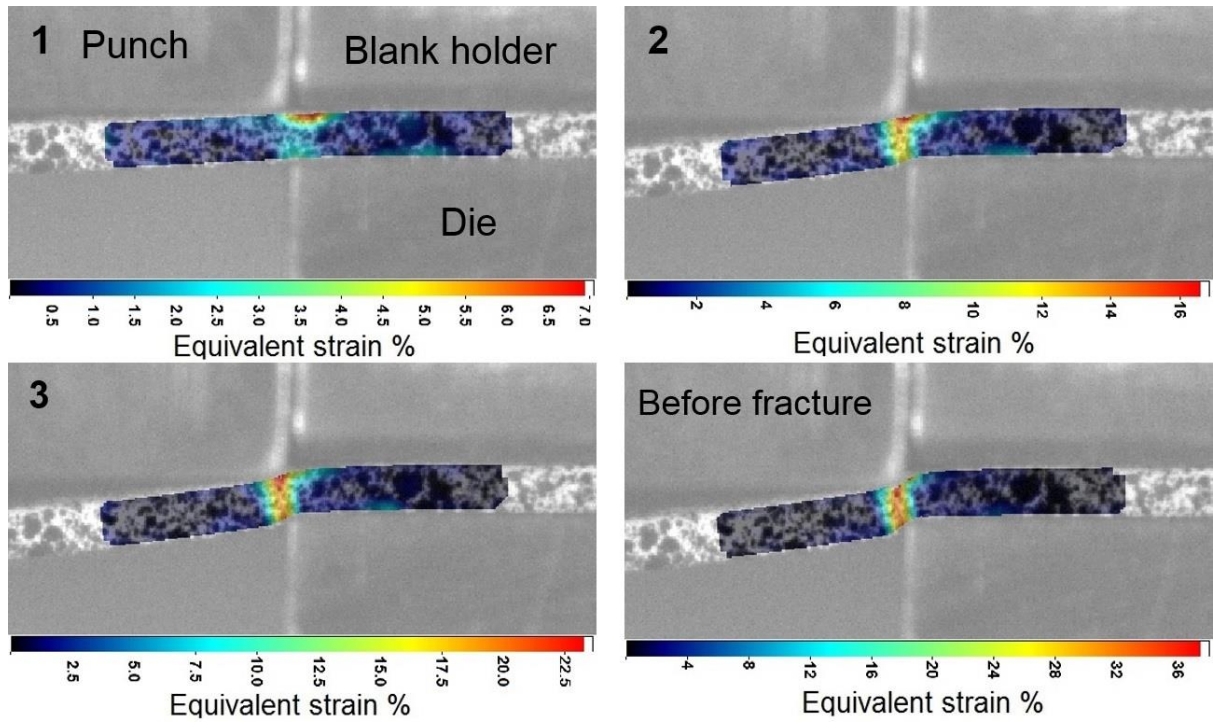


Figure 4.23: Maximum equivalent strain distributions during the blanking process in different stages at 100 mm/min for 0.35 TD 100 sample.

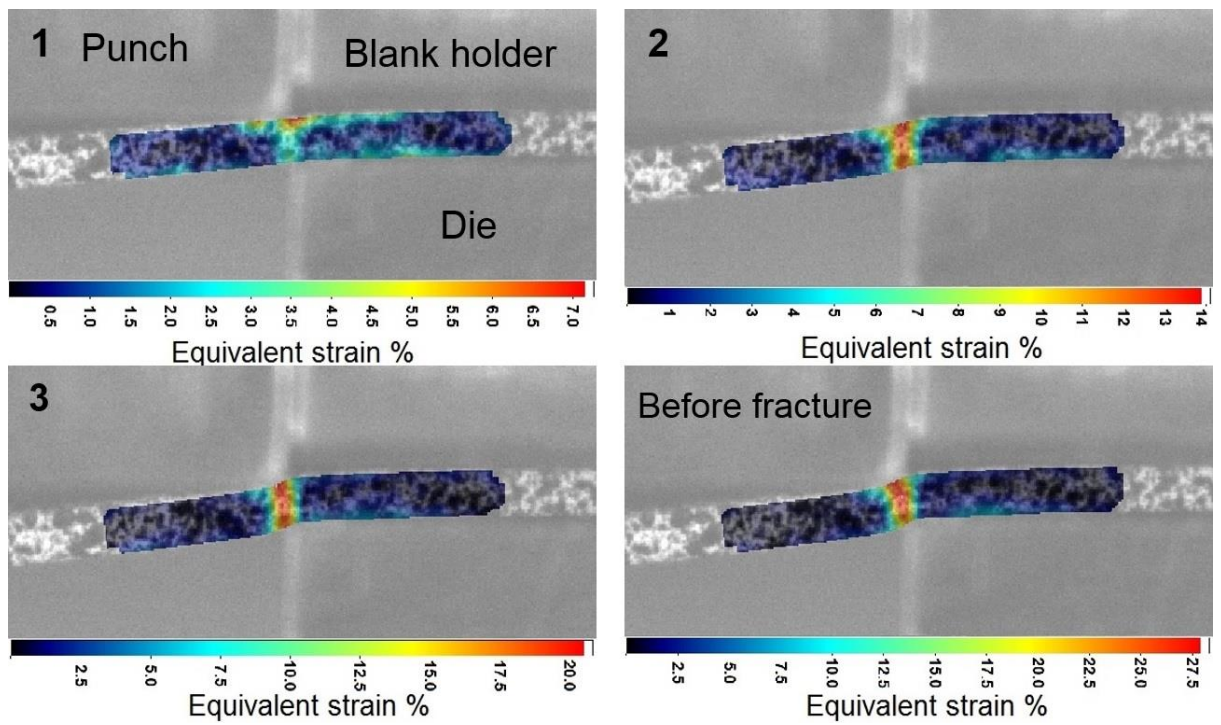


Figure 4.24: Maximum equivalent strain distributions during the blanking process in different stages at 500 mm/min for 0.35 TD 500 sample.

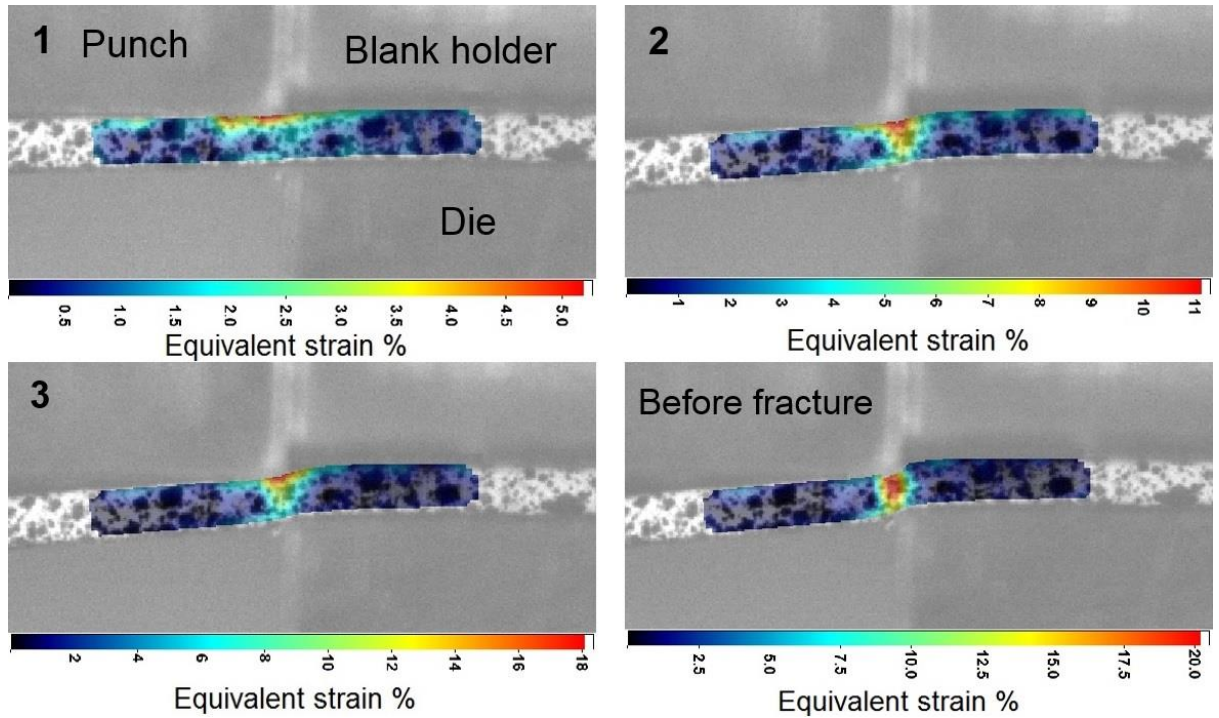


Figure 4.25: Maximum equivalent strain distributions during the blanking process in different stages at 1000 mm/min for 0.35 TD 1000 sample.

Figure 4.26 shows the general material behaviour during the blanking process, according to the maximum equivalent strain obtained in the current deformation case study. It can be seen that the larger deformation zone is obtained at the lower blanking speeds. In addition, transverse orientation produced lower strain than the rolling direction regarding the applied of the direction of cutting line.

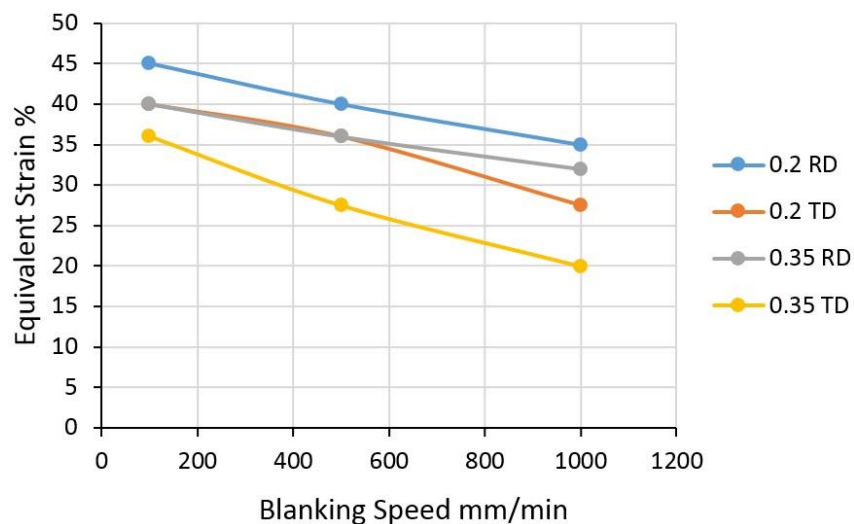


Figure 4.26: General effects of blanking speeds and sheet thickness, orientation regarding max. equivalent strain.

4.3.3 Characterization of local deformation using Nano-indentation

Nano indentation tests were conducted at the cut edge and the vicinity area to indicate the plastic deformation regarding the different cutting conditions. Tests were carried out in the middle of the cut edge using 50 indenters extend within a distance of about 150 μm from the cut edge.

A 3D distributions of measured Nano-hardness values as a function of distance from the cut edge and through-thickness distance are shown in Figures 4.27 and 4.28 for both 0.2 and 0.35 sheet thicknesses respectively. That was to illustrate the variation between hardness values for those indents at the same distance to the cut edge as they do not clearly appear in the 2D graphs. The figures show that the hardness values significantly increase toward the cut edge, in the case of both sheet thicknesses. The change in the hardness values could indicate the influenced of the cutting edge zone by the deformation due to the cutting process. This deformation causes strain hardening that leads to increasing material resistance to the penetration of the indenter. Therefore, the high value of hardness may be interpreted as a result of the existence of high deformation and strain hardening. The variance in hardness values could be explained by the effect on the indenter of impurities and grain boundaries [5].

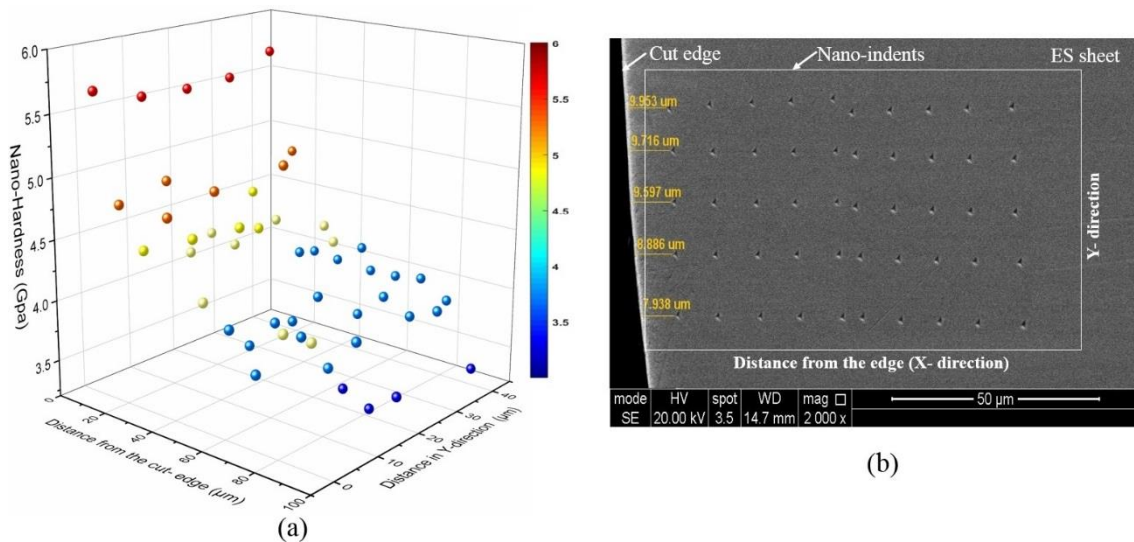


Figure 4.27: Nano-hardness distribution as a function of the distance from the cut edge for 0.2 RD 1000 sample, a) 3D distribution of hardness values b) SEM image of indents locations regarding the cut edge.

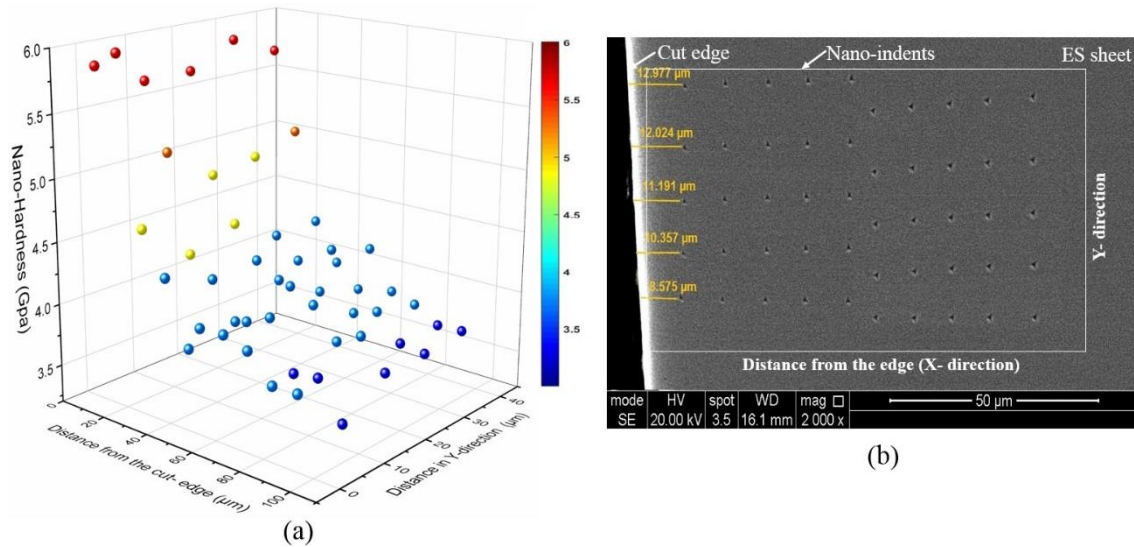


Figure 4.28: Nano-hardness distribution as a function of the distance from the cut edge for 0.35 RD 1000 sample, a) 3D distribution of hardness values b) SEM image of indent locations regarding the cut edge.

Generally, high hardness values are located in the area very close to the edge. This high value graduating in the vicinity area of the high affected zone. The lowest hardness values and located at the outer end of the deformation area when the hardness values are close to the hardness value of the general material. The average hardness value of the ES sheets away from the cut edge was measured using the Nano-indentation test as shown in [Figure 4.29](#). The average Nano-hardness value of the material was about 3.5GPa.

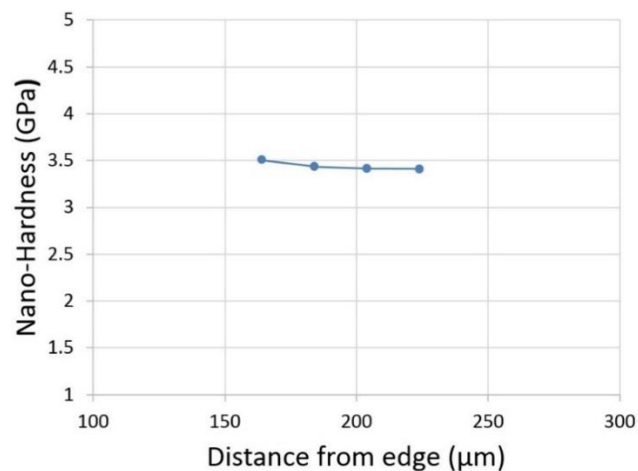


Figure 4.29: The average Nano-hardness value of the material.

[Figure 4.30](#) shows Nano-hardness values regarding the distance from the cut edge for the 0.2 mm thickness samples in both rolling and transverse direction at different

blanking speeds. Clear degradation can be observed in the hardness values in the form of very high values at the edge around 7GPa at 5 μm away from the edge and then sharp descended in the vicinity area until reaching the general sheet hardness value.

It is very difficult to identify the depth of the deformation area according to the hardness measurements because of the big variations. However, the position of the stability of the hardness values at the general hardness value of the sheet given in [Figure 4.29](#) was considered as the end of the deformation. According to the current results, the size of the plastic deformation zones is slightly varied depending on the deformation condition. The average extension of deformation for 0.2 ES samples were reached to around 100 μm in most cutting cases.

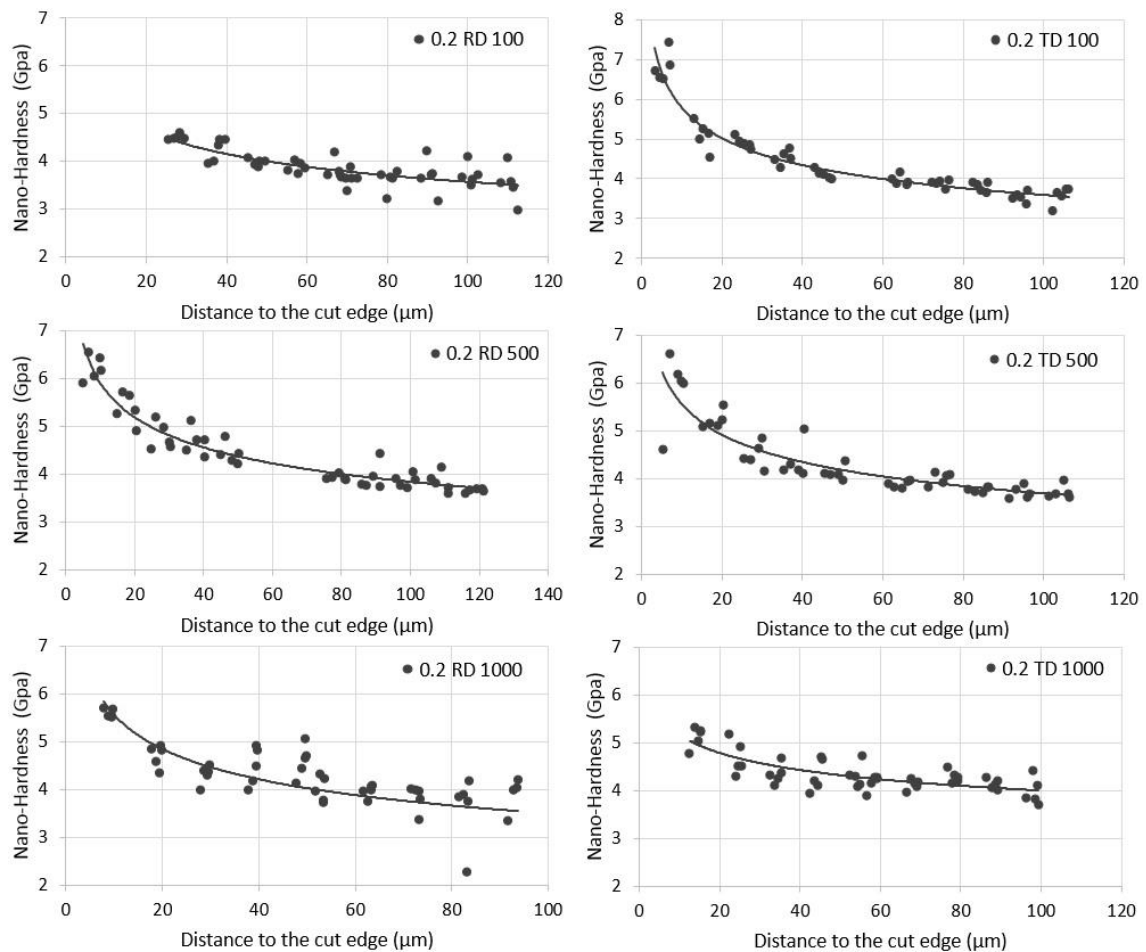


Figure 4.30: The distributions of Nano indentation values for 0.2 mm sheet thickness at different blanking speeds.

In order to show the effect of the blanking parameters against the hardness values, the average hardness values at distance between 25 to 30 μm for different parameters are illustrated in [Figure 4.31](#).

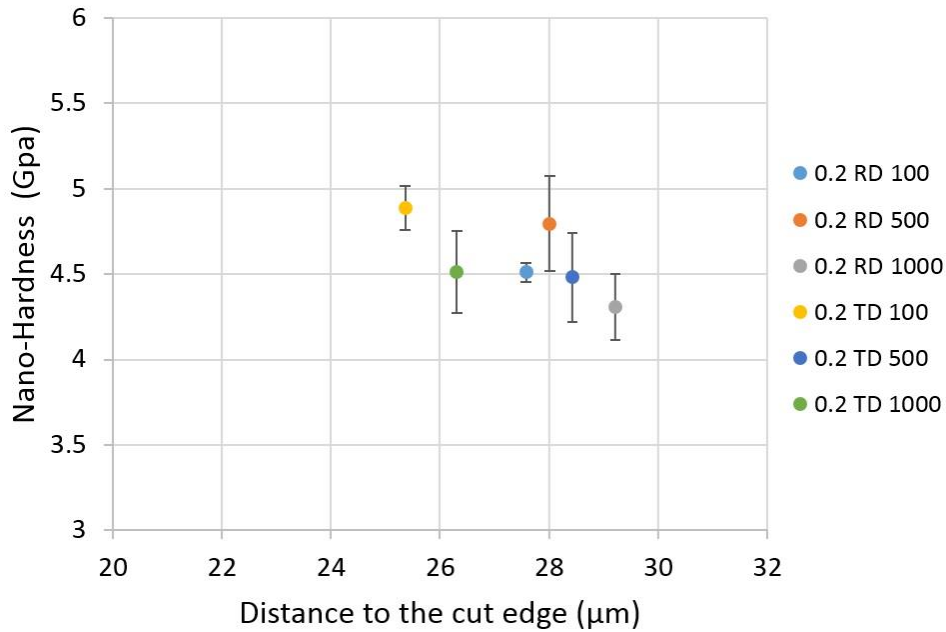


Figure 4.31: The effect of the blanking parameters against the hardness values of 0.2 ES sheet thickness at specific distance to the cut edge.

To investigate the influence of sheet thickness, the same strategy was applied to the 0.2 thickness sheet as on the ES sheet with 0.35 mm thickness. Generally, all cases show the deformation is distributed randomly around the cut edge. However, there is some variation in the hardness values in that they are higher close to the cut edge and descend gradually with increasing distance to the vicinity areas.

[Figure 4.32](#) shows Nano-hardness measurements regarding the distance from the cut edge for the 0.35 mm thickness samples in both rolling and transverse direction at different blanking speeds. A similar trend to the 0.2 samples was apparent in the form of high value at the cut edge and sharp descended in the neighbour area. However, a lower ranges of hardness values than 0.2 were observed around 6GPa at the edge. The average depth of the deformation area according to the current hardness measurements were around 80 μm in most cutting cases.

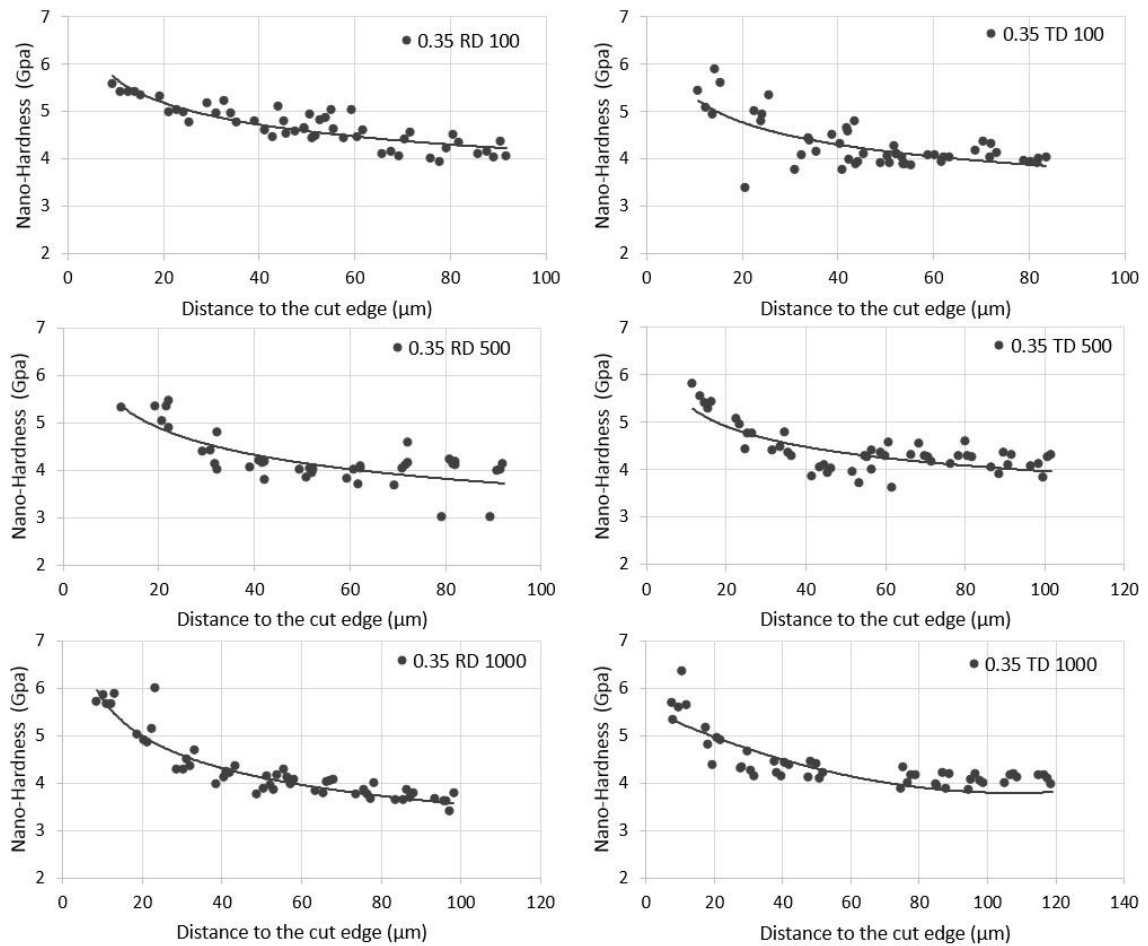


Figure 4.32: The distributions of Nano indentation values for 0.35 mm sheet thickness at different blanking speeds.

A similar results was obtained to show the effect of the blanking parameters of 0.35 mm ES sheet thickness against the hardness values, the average hardness values at distance between 25 to 30 μm for different parameters are illustrated in [Figure 4.33](#). The figures illustrate that the size of the plastic deformation zone is almost consistent in all of the samples, however, the total DAZ is varying depending on the deformation condition and local grains condition.

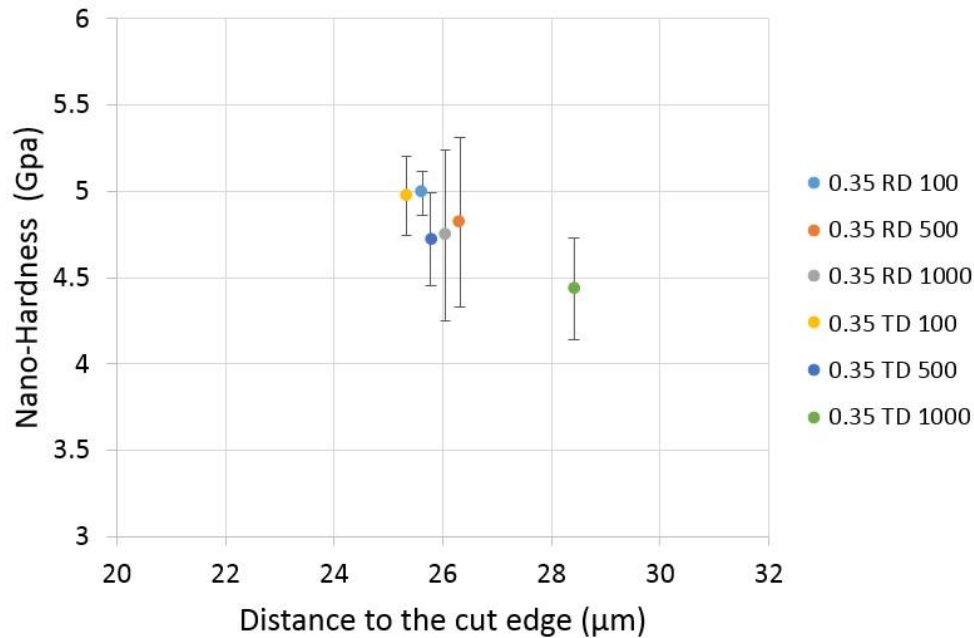


Figure 4.33: The effect of the blanking parameters against the hardness values of 0.35 ES sheet thickness at specific distance to the cut edge.

4.4 Magnetic properties outcomes

The dissipation of energy causes hysteresis loss because of the reversal of the material's magnetism. The magnetic hysteresis loops (B-H curves) were measured for all blanking samples in the current study to determine the effect on the magnetic properties caused by the induced deformation due to the blanking process at different conditions, which would reflect the blanked quality magnetically. Moreover, the magnetic properties under different plastic elongations of tension were investigated. The hysteresis losses can be estimated through the residual of induction flux density induced by the magnetizing field, i.e. the area under the hysteresis loop. Because of the current study is considered as a comparative investigation between blanking and tensile samples at different conditions. Therefore, the measured flux density values were normalized, because of the differences between the current test conditions and the standard test settings regarding the apparatus design and testing conditions.

4.4.1 Effect of uniaxial deformation on magnetic properties

The hysteresis loops were measured for the tensile samples at different plastic elongations by interrupting the tensile test with an increment of 1 mm until sample fracture. The

conditions of the magnetic tester or the single sheet tester were explained earlier in chapter three.

The area inside the hysteresis loop represents the total hysteresis loss. However, determining the hysteresis loop by limited points could lead to reducing loops accuracy and thereby the loss is not accurately calculated. Consequently, a problem could arise with the measuring of the area of the loops of the deformed samples and the calculation of the hysteresis loss will be affected. Therefore, only the type and size of loops by means of saturation points between the different samples will be investigated.

Figure 4.34 shows the hysteresis loops for 0.2 RD tensile samples. The figure shows the different sizes of the hysteresis loop for each elongation. Although the limited of measured points lead to not show the coercivity points clearly, the larger loop area was for the not deformed sample by means of saturation point. The size of the loops was reduced when increase in the elongation. The induced hysteresis loop at 5 mm was the smallest one and had lower saturation point.

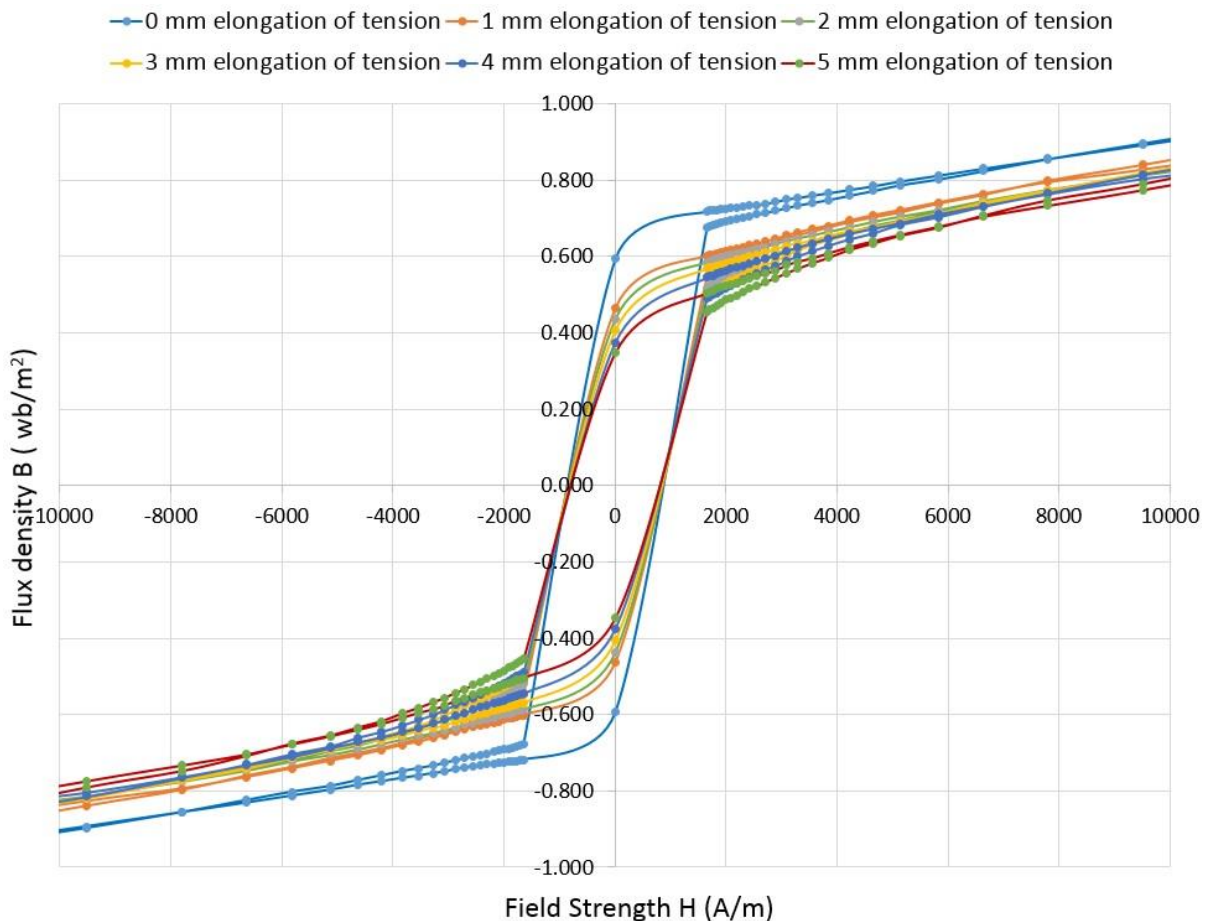


Figure 4.34: Hysteresis loops of 0.2 RD of ES samples at different elongations of tension.

Figure 4.35 shows hysteresis loops for 0.2 TD sample at each stage of elongation under tension. The figure also shows a bigger hysteresis loop for the not deformed sample than for the remaining deformed samples represented by a higher saturation point. The size of the loops decreased with increases in the elongation of deformation ranging from 1 mm to 5mm. Generally, the hysteresis loops exhibited similar shapes and trends due to the use of the same tests settings.

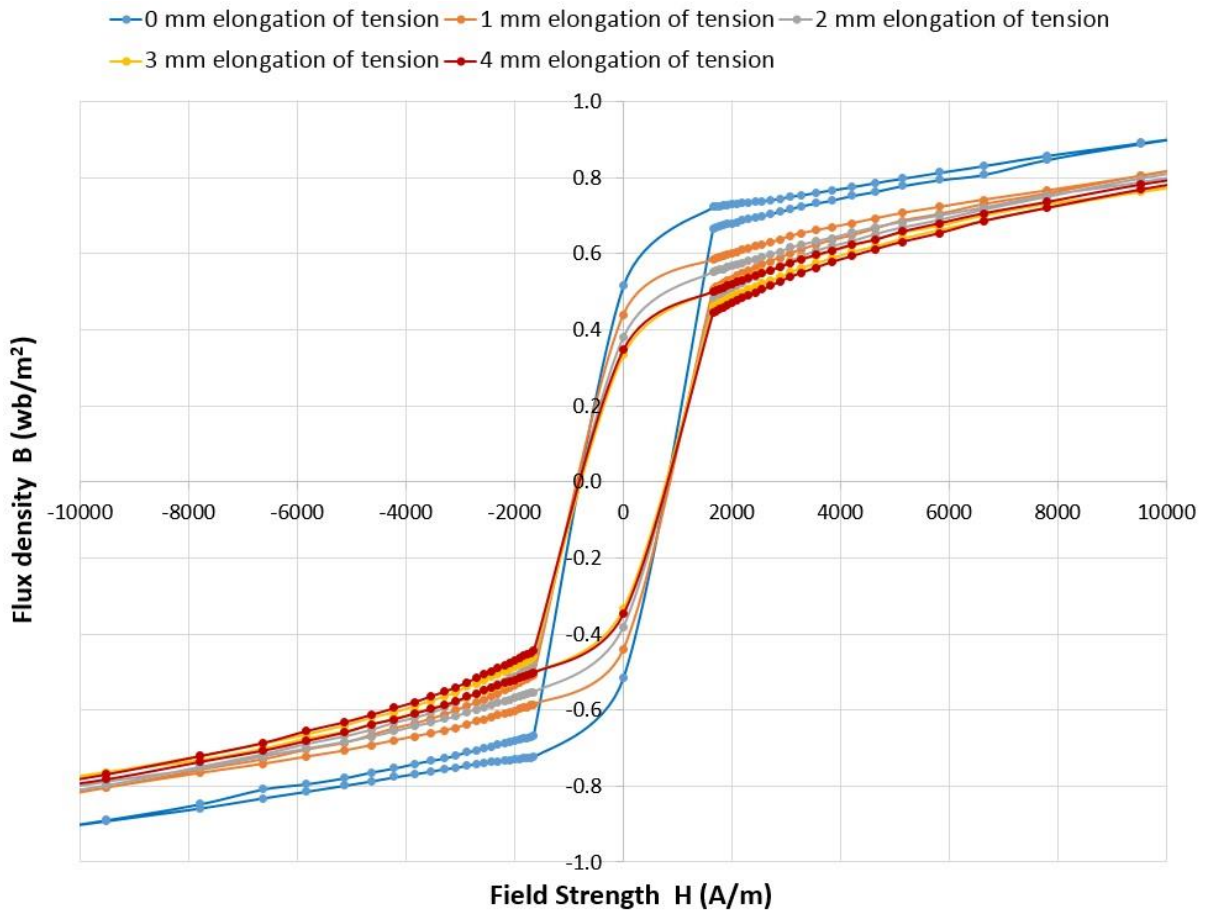


Figure 4.35: Hysteresis loops of electrical steel type 0.2 TD samples at different stages of elongations of tension.

Figure 4.36: shows that the B-H loops for all the elongations of the tension of the 0.35 RD electrical steel sample exhibit similar behaviour to the 0.2 RD sample regarding the existing differences between the deformed and undeformed samples, which means that sheet thickness has a little influence on the magnetic properties.

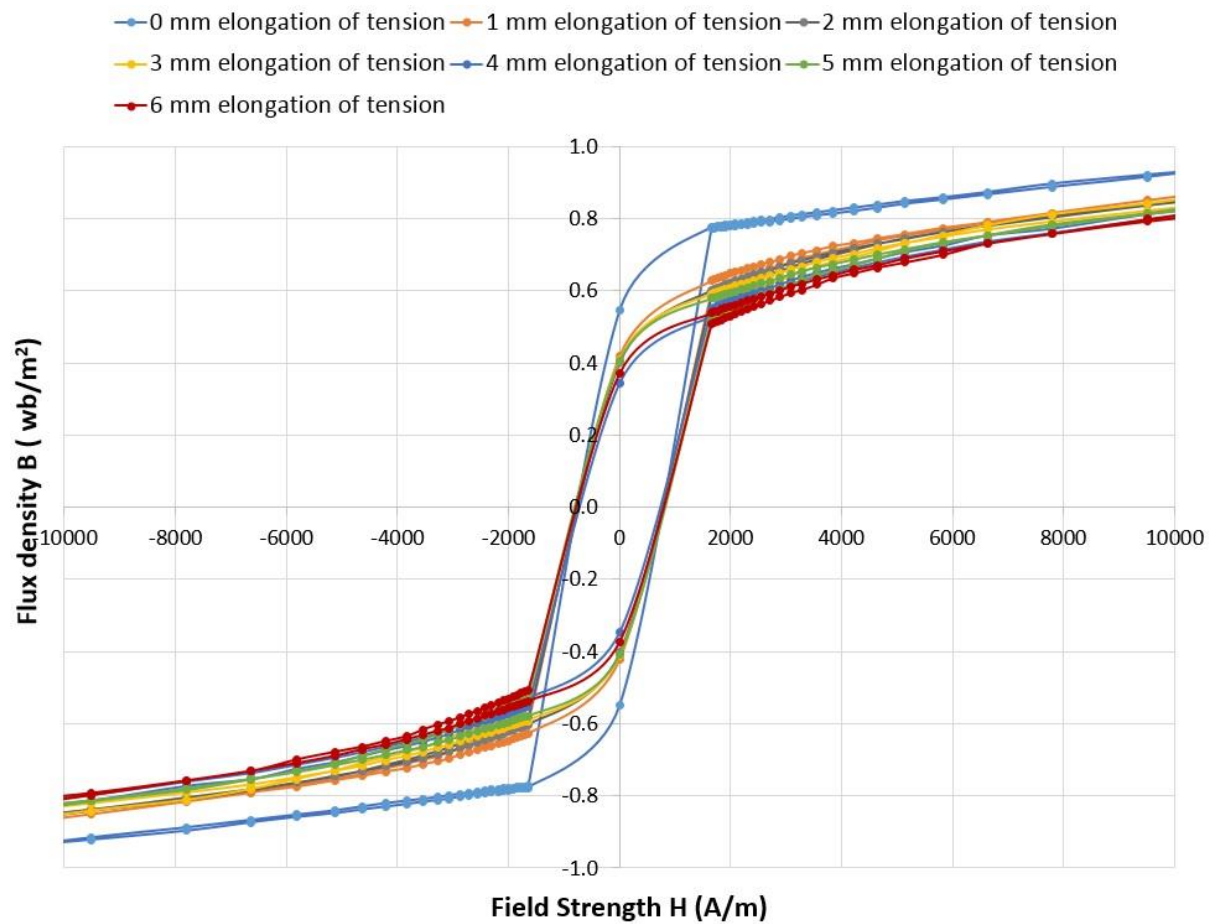


Figure 4.36: Hysteresis loops of electrical steel type 0.35 RD samples at different stages of elongations of tension.

Figure 4.37 shows hysteresis loops for the 0.35 TD sample at each stage of elongation under tension. The figure also present lower saturation point for higher elongation stage. All hysteresis loops were of similar shapes and trends due to use of the same test conditions. The not deformed sample induced a different hysteresis loop than the deformed samples which reflect the influences of the deformation upon the magnetic structure and domain wall movements.

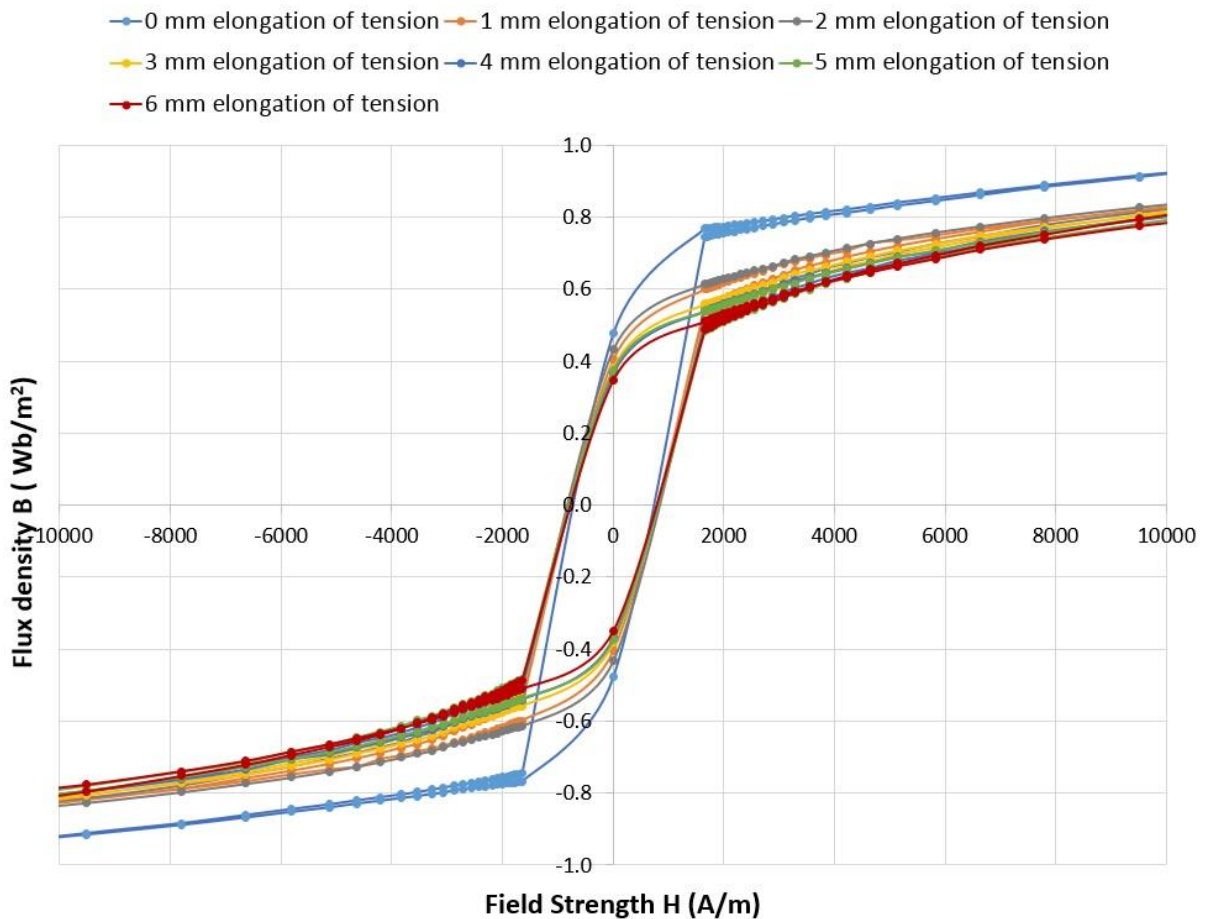


Figure 4.37: Complete hysteresis loops of electrical steel type 0.35 TD samples at different stages of elongations of tension.

Figure 4.38 shows a summary of the results that include the standard error bars of the variations in the measured results. The flux density expresses the subjected magnetic field required to magnetize the sample and reach the saturation point. A big convergence occurs between hysteresis loops of 0, 1, 2 mm tensile elongation and an approximately corresponding one between the 3 and 4 mm elongations. In addition, there are slight differences between the RD and TD samples. This could indicate the effecting of grain orientation on the magnetization process and induced hysteresis losses.

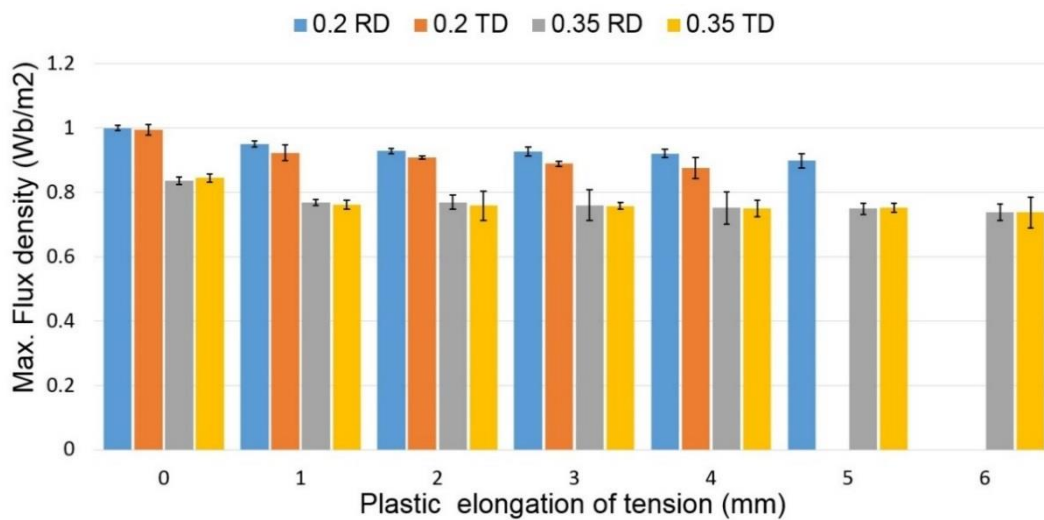


Figure 4.38: Maximum flux density at different stages of elongations of tension for the different electrical steel samples categories

4.4.2 Effect of induced blanking deformation on magnetic properties

The effect of the blanking process on the magnetic properties was investigated. The hysteresis loops were obtained, and hysteresis losses were calculated for the produced ES samples at a different cutting condition of the full die (die type A) using the single sheet tester. Figure 4.39 shows the complete hysteresis loops for the 0.2 RD samples at different blanking speeds. A small differences between the hysteresis loops can be observed because the loops had very close saturation levels. That may reflect the convergent effect of the variation of blanking speed on the magnetic properties of electrical steel. Hysteresis losses were calculated according to the loops areas because of presence a kind of identically loops shape. However, it can be seen that the hysteresis loop induced by the lower blanking speed of 100 mm/min was slightly wider, thereby causing a higher hysteresis loss.

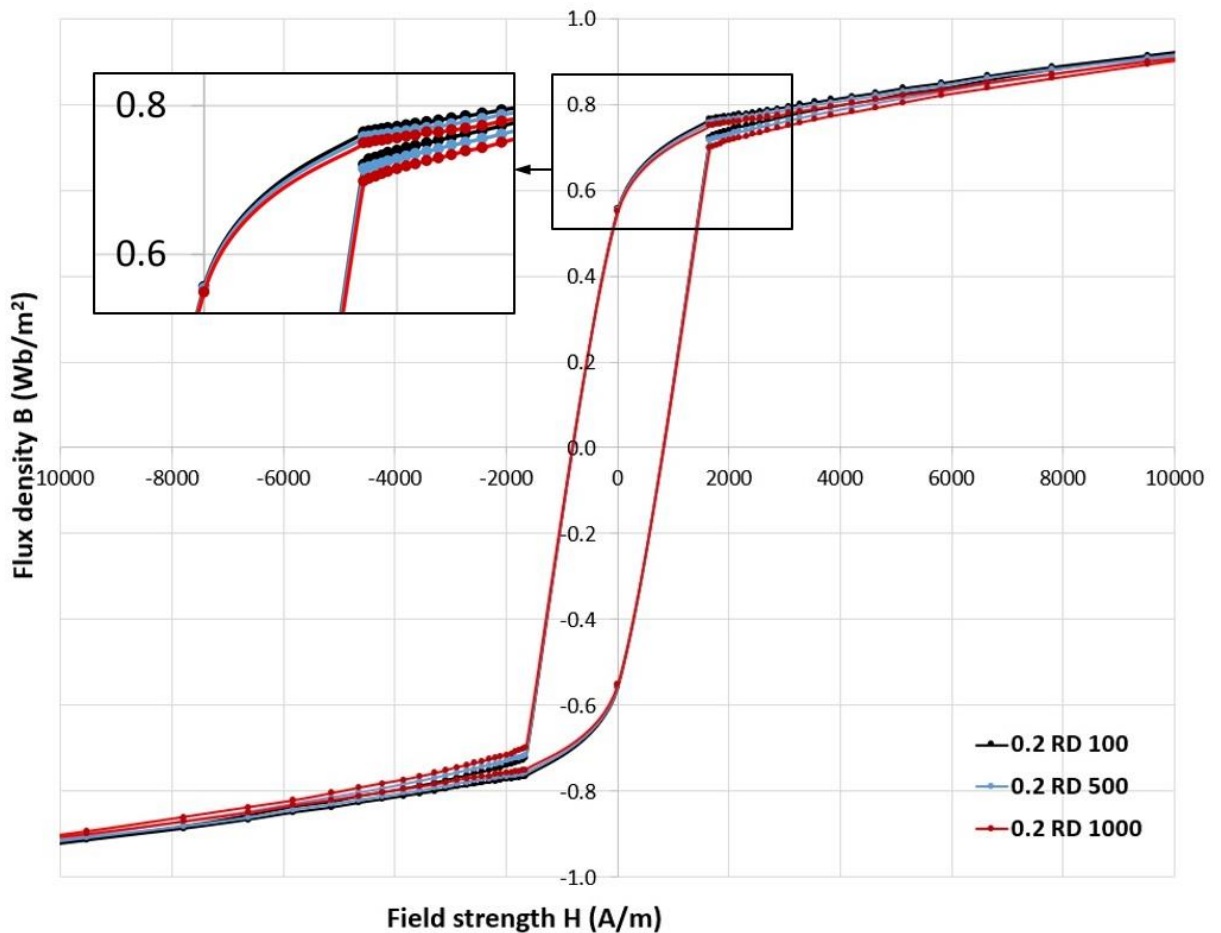


Figure 4.39: Hysteresis loops of electrical steel type 0.2 RD samples cut by blanking process at different blanking speeds.

Figure 4.40 shows hysteresis loops of 0.2 TD electrical steel samples cut at three different blanking speeds. The graphs show that the hysteresis loop of 100 mm/min blanking speed has higher (B_{\max}) and remanent flux density (B_r) than the rest of the samples which means more flux was applied to reach the saturation point and consequently there was more hysteresis loss. The coercive field strength (H_c) appear to be nearly the same for all specimens because the limited of measured points of the B-H loops. The hysteresis loops for the 500 and 1000 mm/min blanking speeds are nearly the same and lower than for the low blanking speed.

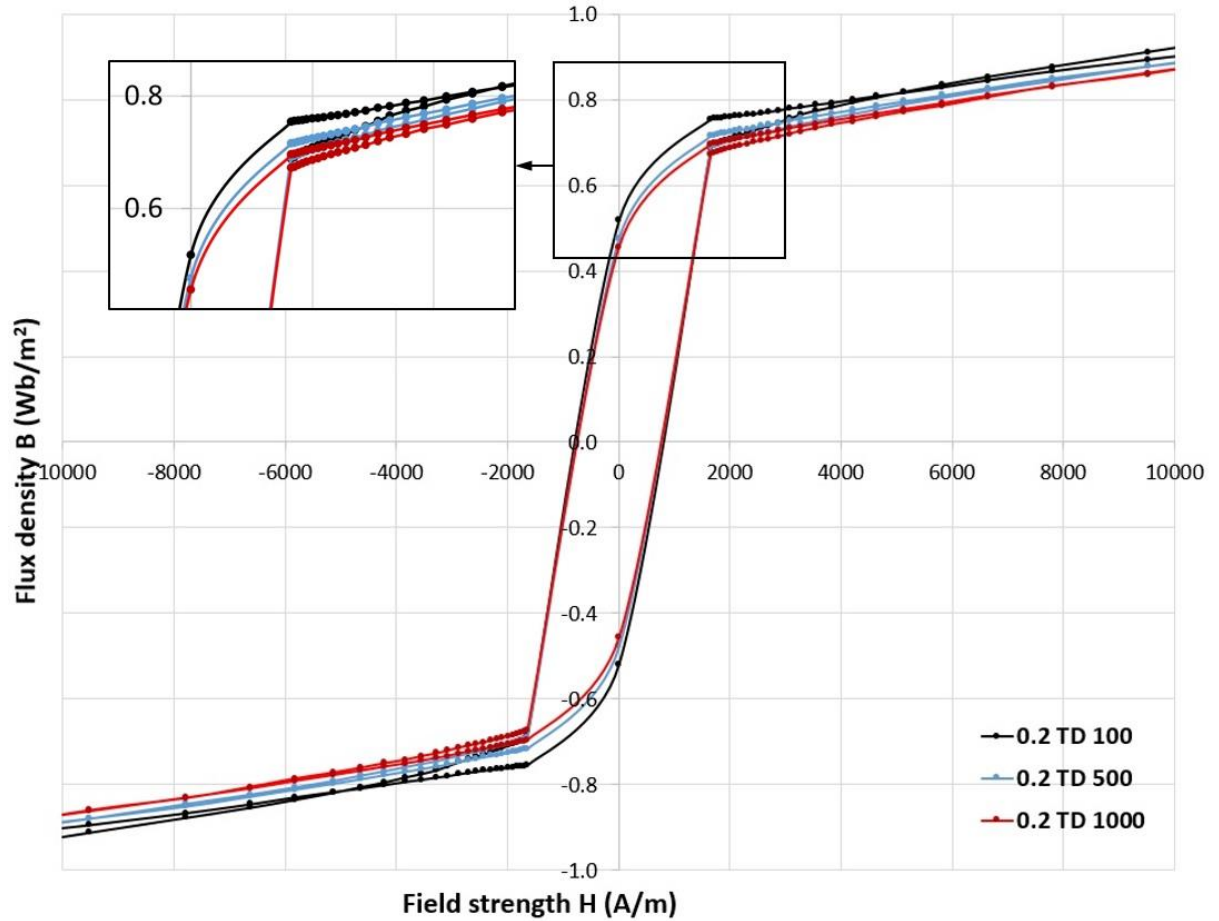


Figure 4.40: Hysteresis loops of electrical steel type 0.2 TD samples cut by blanking process at different blanking speeds.

Similar investigations were done on magnetic properties of electrical steel sheet with thickness 0.35 mm in both grain orientations, RD and TD, at different blanking speeds. Figure 4.41 shows the B-H loops of electrical steel type 0.35 RD samples cut at three blanking speeds, 100, 500, and 1000 mm/min. Similar behavior to that of the 0.2 samples was observed, resulting in similarly shaped hysteresis loops. Wider loops resulted from the lower blanking speed of 100 mm/min. Loop size decreased with increased blanking speed, reflecting less deformation of the affected cut edge.

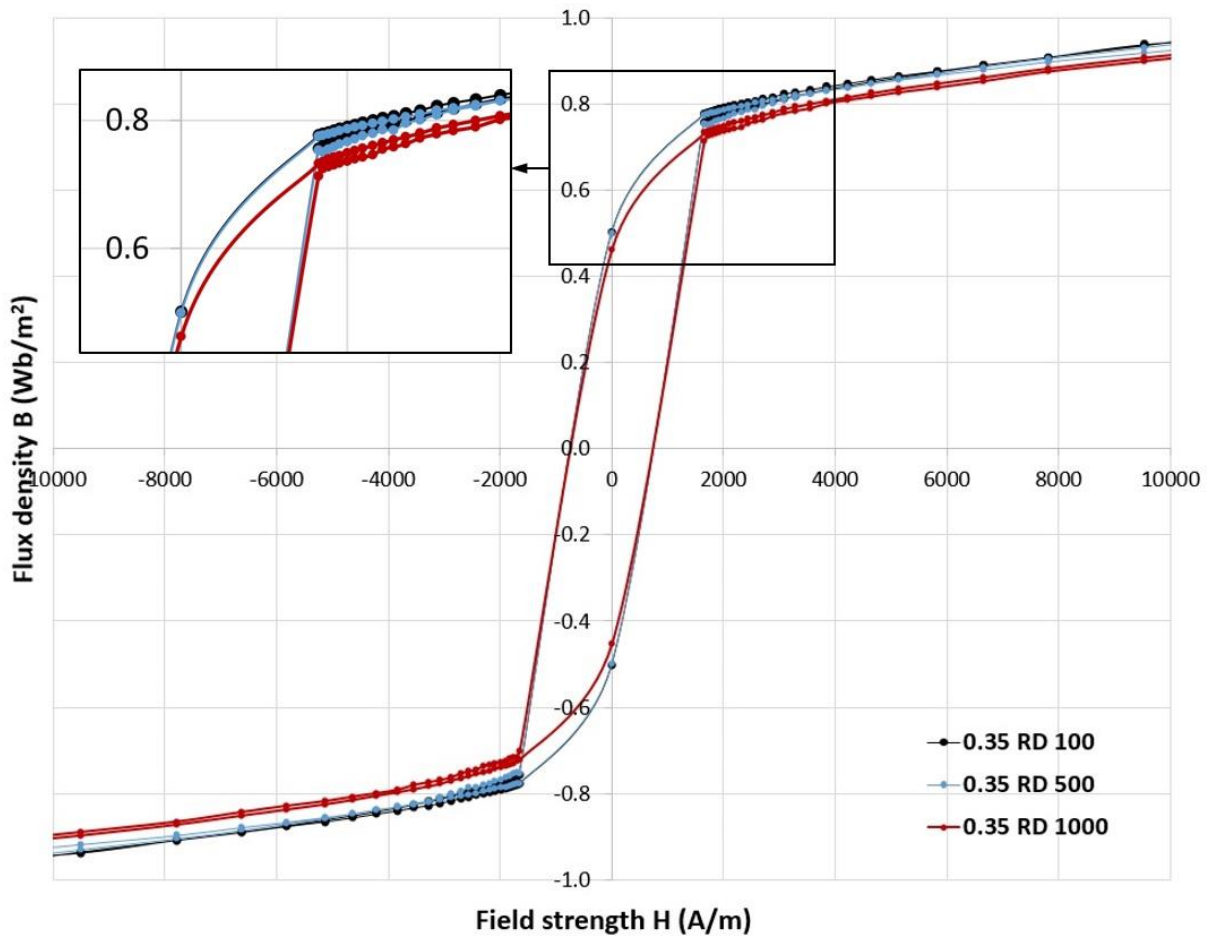


Figure 4.41: Hysteresis loops of electrical steel type 0.35 RD samples cut by blanking process at different blanking speeds.

Figure 4.42 shows the B-H loops of electrical steel 0.35 TD samples cut at different blanking speeds. Less differences was observed between 100 and 500 mm/min. Smaller loops resulted from the lower blanking speed of 1000 mm/min.

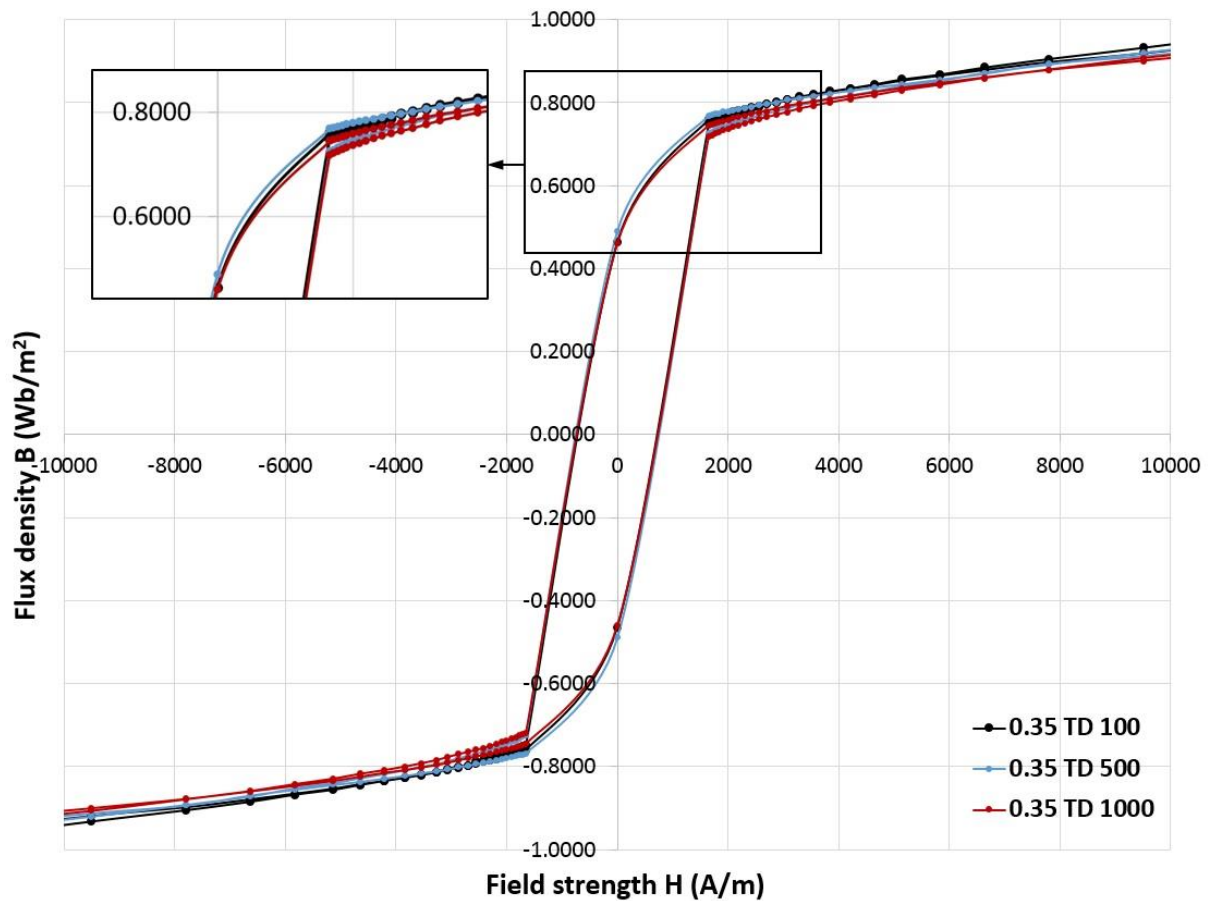


Figure 4.42: Hysteresis loops of electrical steel type 0.35 TD samples cut by blanking process at different blanking speeds.

Figure 4.43 illustrates the hysteresis power losses of electrical steel samples cut by blanking process with respect to the flux density. The hysteresis loss at 100 mm/min was slightly higher than the hysteresis losses at 500 and 1000 mm/min. This may indicate that increasing the blanking speed can reduce the cut edge deformation and minimize hysteresis power losses.

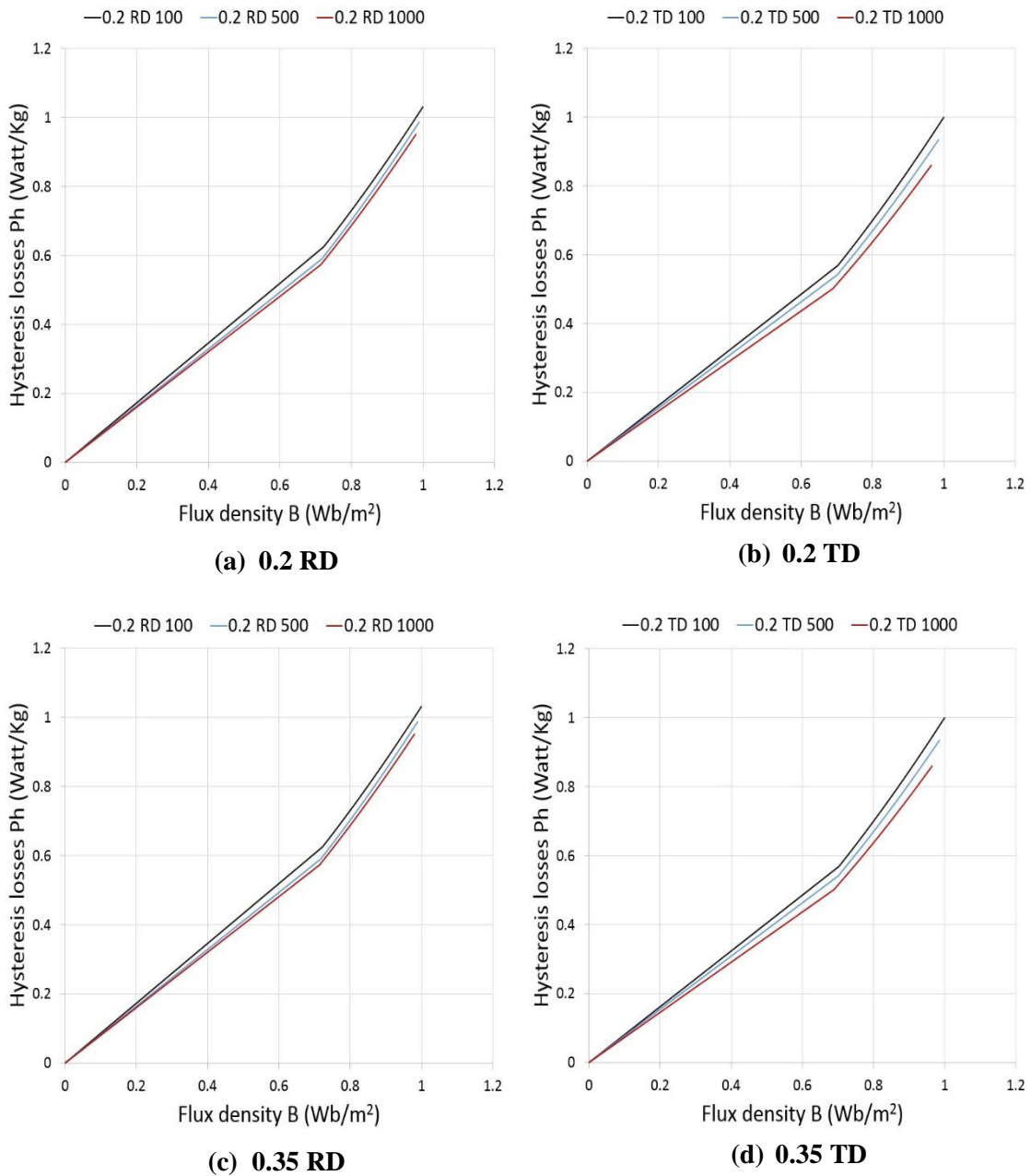


Figure 4.43: Hysteresis losses of electrical steel samples cut by blanking process at different blanking speeds.

Figure 4.44 shows the maximum flux density at different blanking speeds for all electrical steel samples with standard deviation error bars. The figure illustrates that the generated flux density is less in the 0.35 thick samples. Also, high induced flux density was induced at the low blanking speed samples and it is higher for RD than TD. Also, the variations in the values of the flux density were more for the thin sheets. As the thickness increases the variations become smaller.

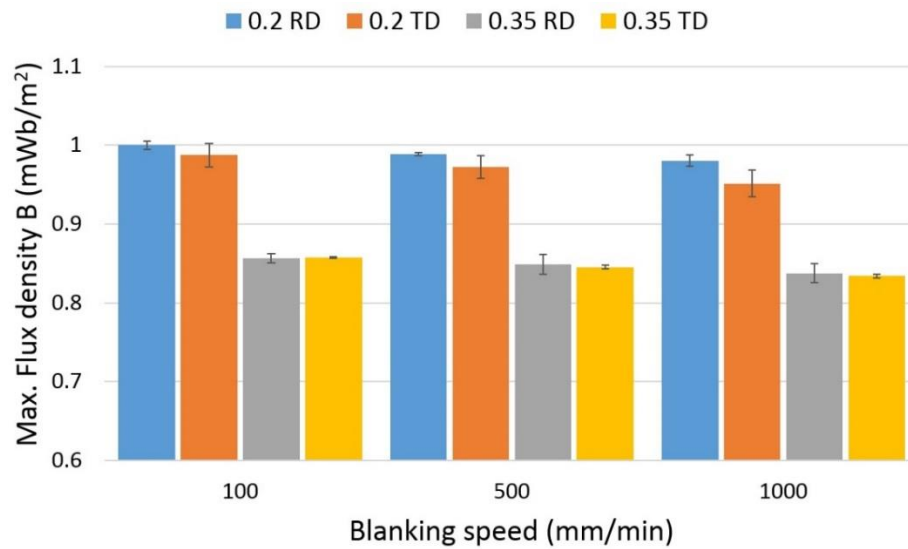


Figure 4.44: Standard error bar for the maximum flux density at different blanking speeds for the different electrical steel samples categories

4.5 Microstructural analysis of the cut edge

The microstructure and fracture surface at the cut-edge for different blanking conditions were analysed using optical and SEM microscope in order to determine the effect of applied blanking processes on the microstructural morphology of the sheets. The location and analysis of the microstructure imaging was explained in chapter three in [Figure 3.8](#). The results were derived from SEM and optical imaging and EDS test analysis.

4.5.1 Investigation of the induced cut edge fracture surface

All the produced cut-edge surfaces in the tested samples were examined at the same position with respect to the blanking die to illustrate the generated zones in the fracture surface including the rollover, shear or burnish, fracture or rupture, and burr zones. The samples were tested directly after the cutting process without any microstructure preparation in order to maintain the resulting edges. A 1000 μm long section at the middle of the sample's width was selected for all the analysed samples for the sake of consistency.

[Figure 4.45](#) shows the SEM micrographs of the fracture surfaces produced by blanking of 0.2RD samples using different blanking speeds. All the four zones are clearly

visible in the cut edge surface in spite of the small sample section size. In addition, some black areas spotted on the fracture surface which may have formed due to the rapid staining of the material and the contaminants after the blanking process. These black sections were neither treated nor cleaned in order to avoid modifying the induced cut edge surface. The figure also shows that the proportion of shear zone to fracture zone increases at the low blanking speed of 100 mm/min (sample A), which indicates greater penetration of the punch inside the material. This proportion reduces at the higher blanking speed of 1000 mm/min (sample C). That means the fracture zone increases when the blanking speed is increased, which may reflect the fact that the material sheet fails faster at high-speed cutting.

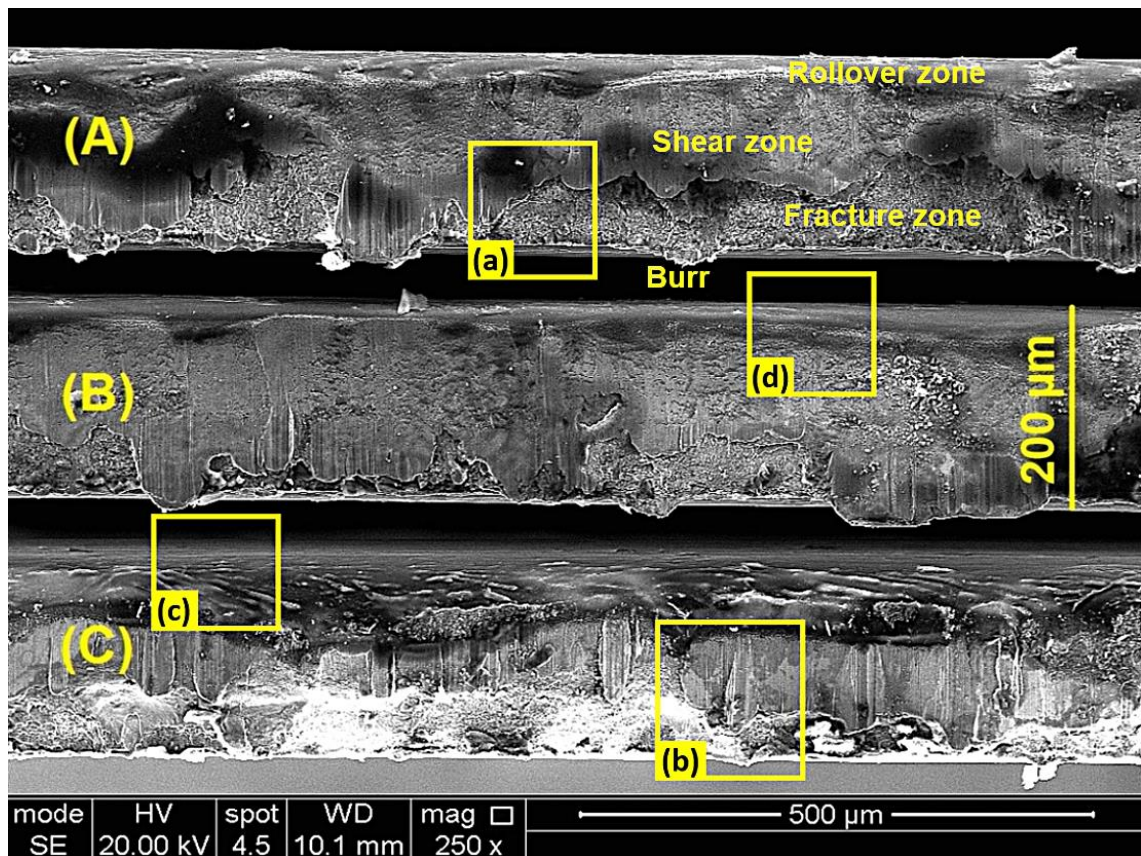


Figure 4.45: SEM image for induced blanking cut edges of 0.2 RD samples at different blanking speeds, A) 100 mm/min, B) 500 mm/min, C) 1000 mm/min.

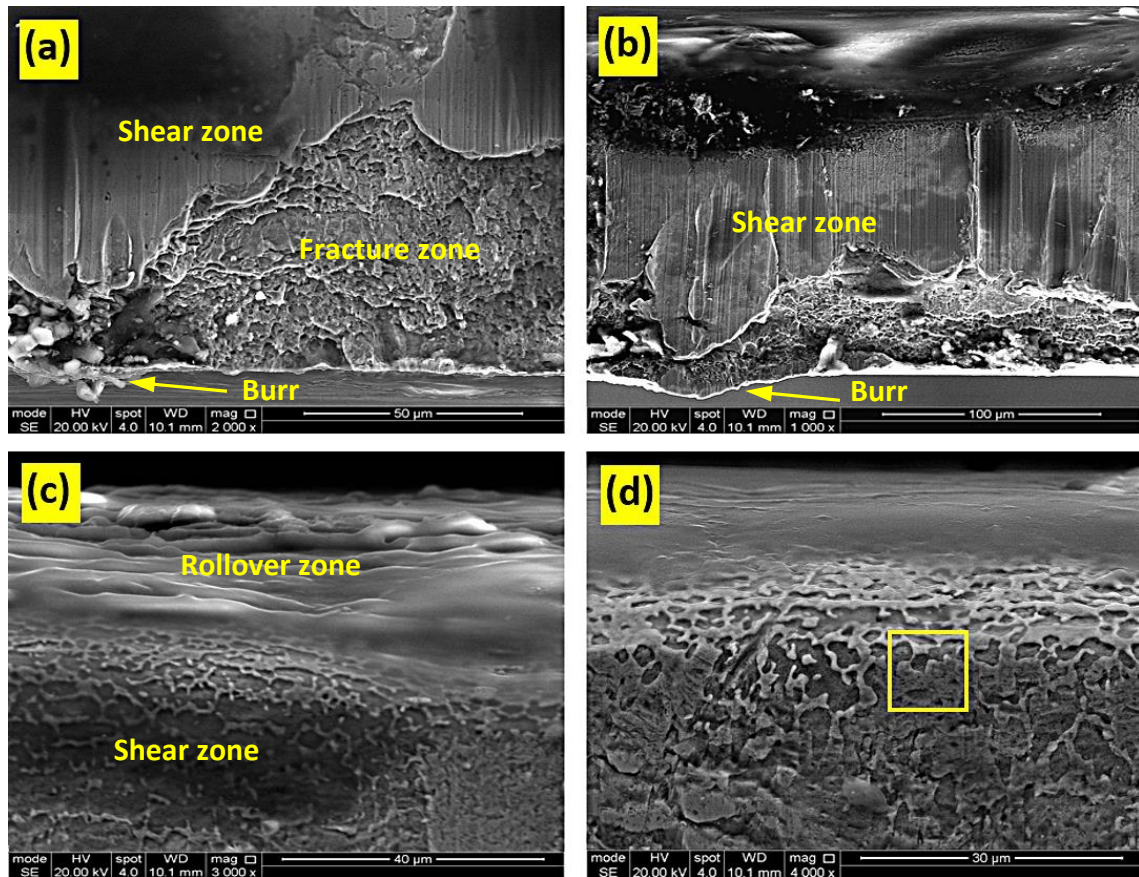


Figure 4.46: Microstructure at higher magnification of some selected areas in Figure 4.45 a,b) At shear and fracture zones, c,d) At rollover and shear zones.

Figure 4.46 shows high magnification micrographs of the selected areas of the 0.2 RD samples in Figure 4.45. Shear, fracture, and burr zones can be observed in Figure 4.46 a, b in different regions. The shear area appears as a smooth, flat surface, with some scratch lines apparent in the shear zone that are potentially the result of friction caused between the blanked material and the die cavity wall when the punch pushes the material out of the die cavity. The fracture area is located below the burnished area and their surfaces appear as a rough and ruptured area. Meanwhile, the burr zone resembles an extension of the material at the bottom of the edge. Figure 4.46 c shows the rollover zone which located at the top of the cut surface. While Figure 4.46 d shows the shear zone next to the rollover zone. Due to the applied plastic deformation in the rollover zone, the sheet coating has been broken and separated from the surface and created those features on the surface.

Figure 4.47 shows elemental analysis by EDS test of the selected area in Figure 4.46 d. The analysis reveals the presence of the main elements such as Fe, Si, and

Al in the ES sheet material's composition in addition to the high percentage of O and C elements relating to the polymer material that makes up the coating layer.

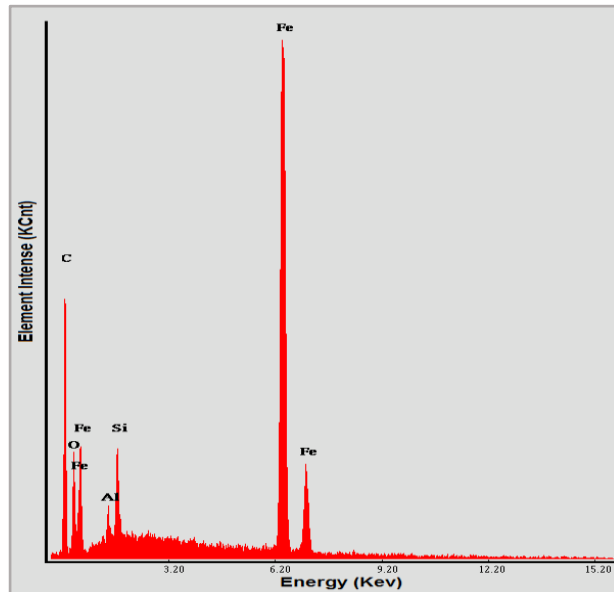


Figure 4.47: EDS analysis for the square part indicated in the Figure 4.46 d.

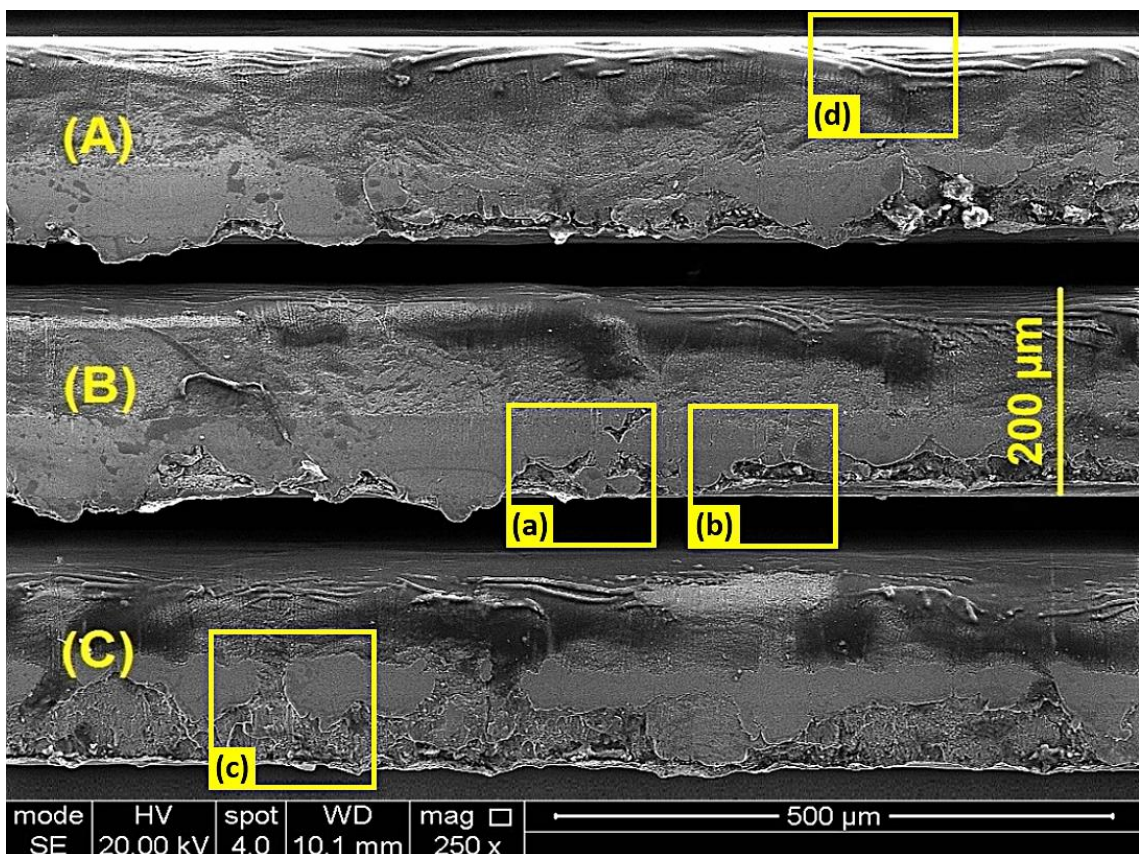


Figure 4.48: SEM image for induced blanking cut edges of 0.2 TD samples at different blanking speeds, A) 100 mm/min, B) 500 mm/min, C) 1000 mm/min.

Figure 4.48 illustrates the cut edge zones for 0.2 TD samples at three blanking speeds. Generally, similar behaviour to the 0.2 RD and all of the four zones is exhibited in the cut edge surface. However, there is a bigger shear zone and smaller fracture zone compared with the 0.2 RD samples at all blanking speeds. This means there was more penetration of the punch inside the material before fracture of the material.

Figure 4.49 shows high magnification micrographs of selected areas of the 0.2 TD sample shown in Figure 4.48. The shear and fracture zones are illustrated in Figure 4.49 a, b. Also, the shear surface can be recognized as a flat, burnished, and smooth surface, while the fracture zone surface is rough and ruptured. Figure 4.49 c, d show the burr and rollover zones respectively. The burr appears as an area of small ridges and rough protrusions, the structure being similar to that of the fracture area.

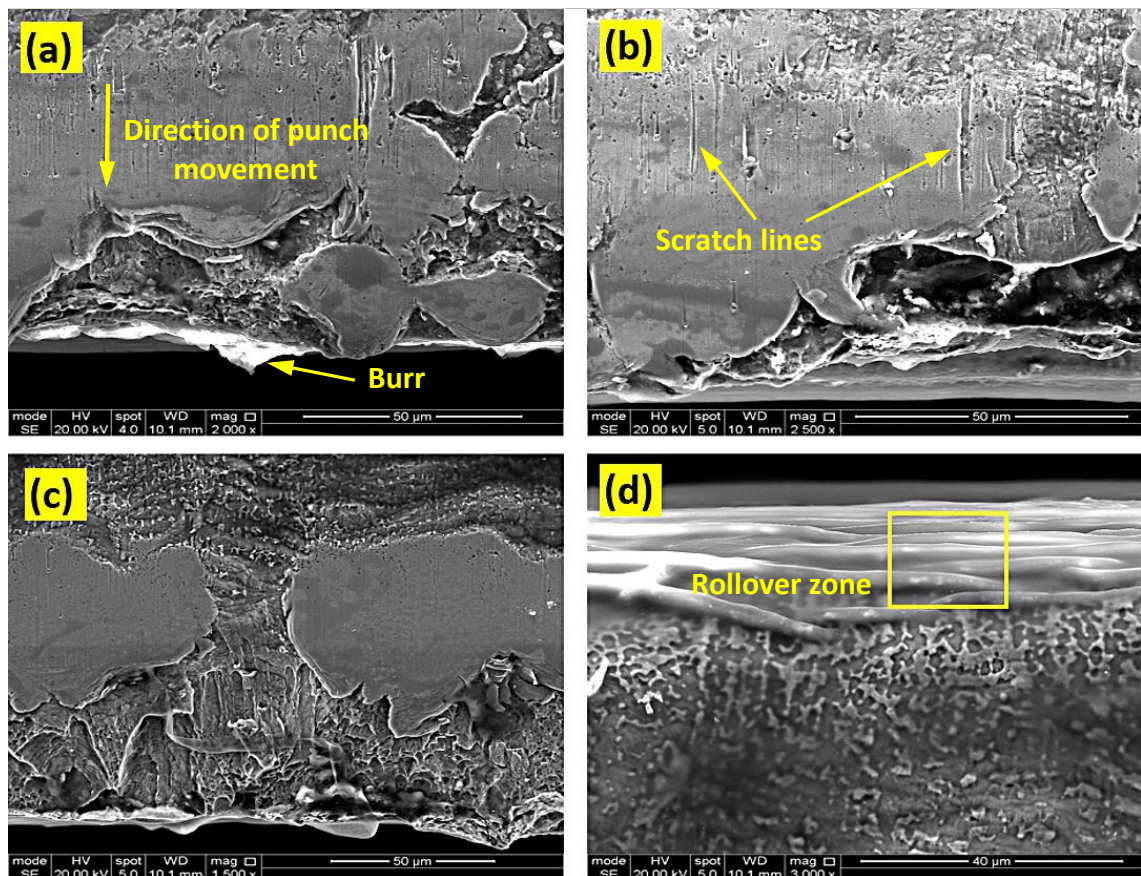


Figure 4.49: Microstructure at higher magnification of some selected areas in Figure 4.48 of 0.2 TD samples. a,b) At shear and fracture zones, c) at fracture and burr zones, d) At rollover and shear zones.

Figure 4.50 shows the elemental analysis by EDS test for the selected area in figure 4.60d. The analysis displays the presence of the main elements such as Fe, Si, and Mn in ES sheet material composition in addition to the high percentage of O and C elements relating to the polymer material that makes up the coating layer and is not within the original material structure.

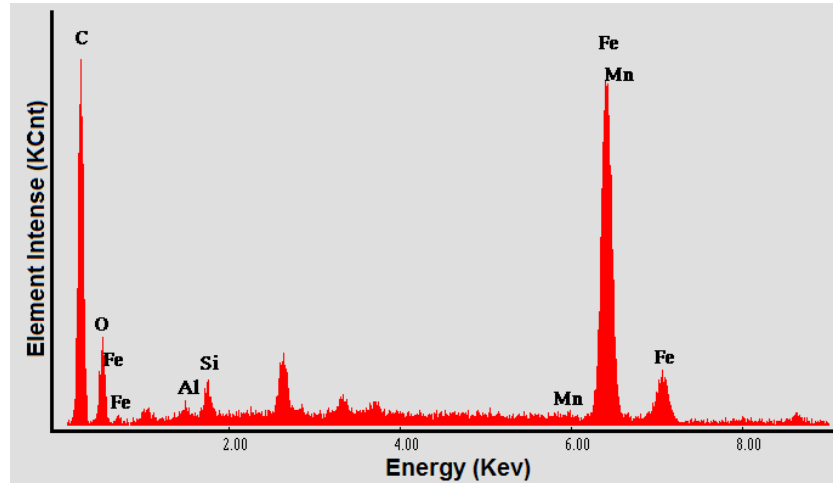


Figure 4.50: EDS analysis for the square part indicated in the Figure 4.49d.

The sheet thickness 0.35 mm was investigated to show the influences of sheet thickness on the induced cut edges zones and their features. Figure 4.51 shows the cut edge surface zones formed by blanking process for 0.35 RD samples at three blanking speeds, 100, 500, and 1000 mm/min. The zones are wider and the boundaries between them are clearer and sharper compared with the 0.2 mm sheet thickness. A significant increase is observed in the shear area and a decrease in fracture area size.

Figure 4.52 shows magnification of the selected area of the 0.35 RD sample in Figure 4.51. The shear and fracture zones can be shown in the Figure 4.52a where the smooth shear surface extends somewhat regularly along the edge surface. The fracture zone surface is generally similar to that of the fracture area in the 0.2 mm sheet thickness. Figure 4.52b shows the rollover zone, where some clusters are apparent due to peeling of the coating layer.

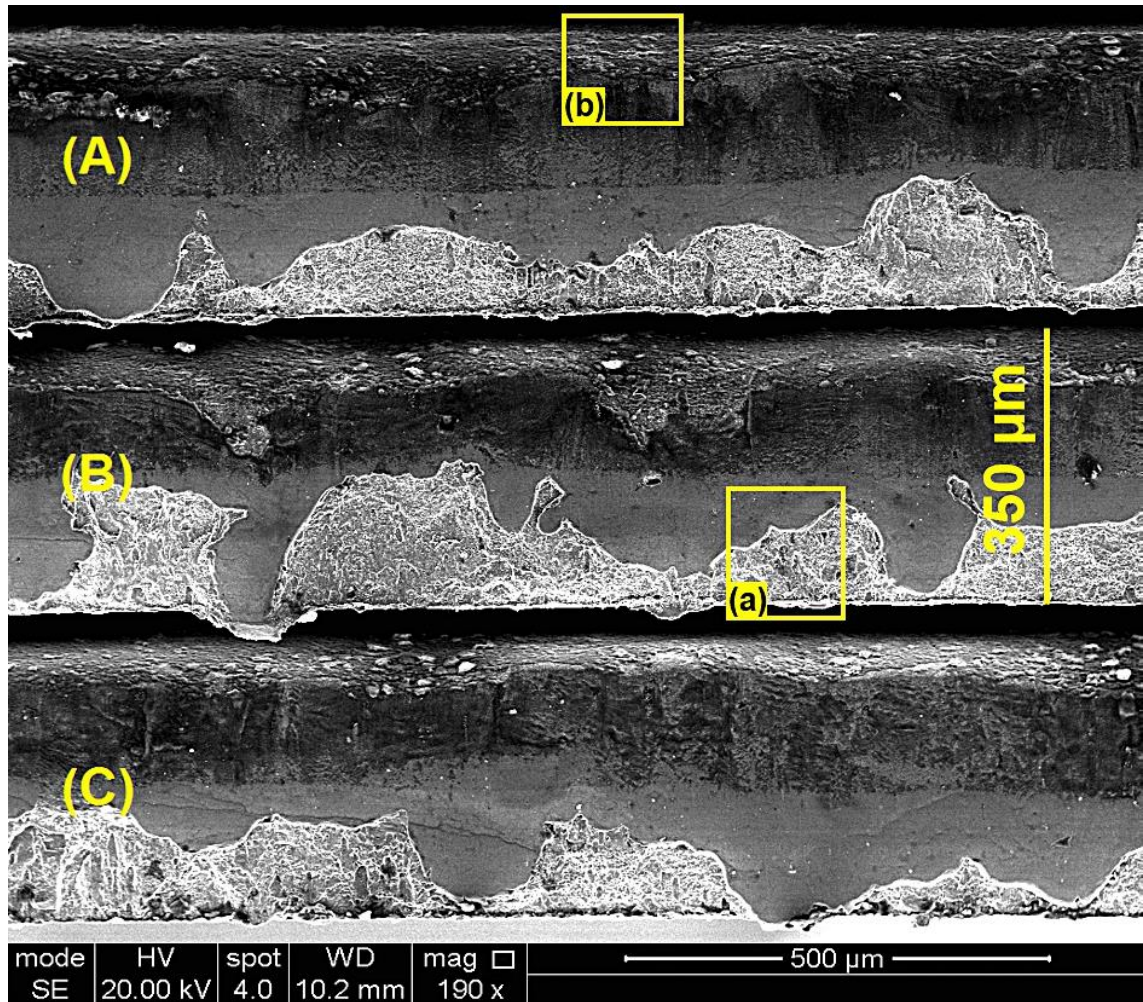


Figure 4.51: SEM image for induced blanking cut edges of 0.35 RD samples at different blanking speeds, A) 100 mm/min, B) 500 mm/min, C) 1000 mm/min.

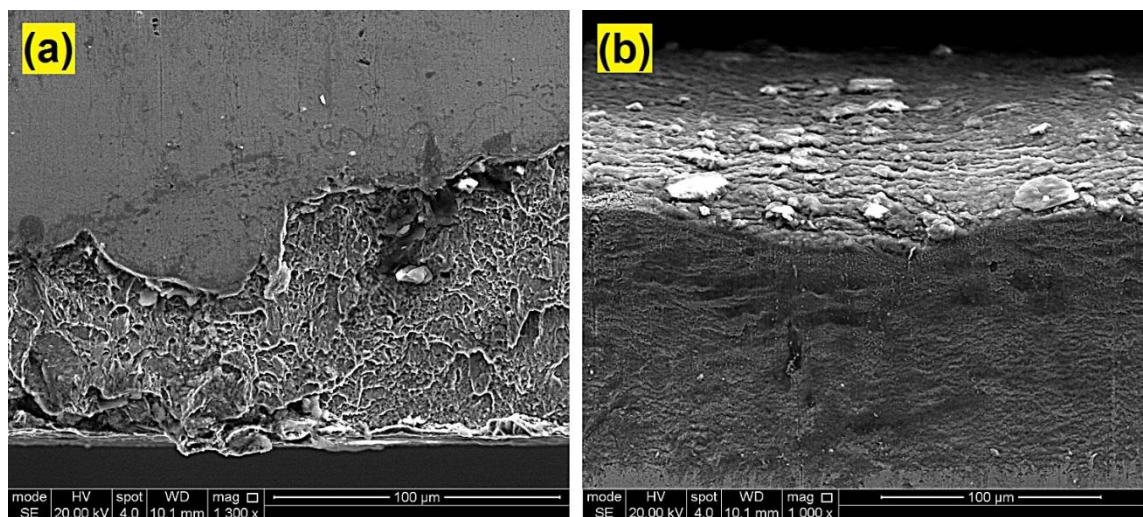


Figure 4.52: Microstructure at higher magnification of some selected areas in Figure 4.51 of 0.35 RD samples. a) At shear and fracture zones, b) At rollover and shear zones.

Figure 4.53 shows the cut edge surface zones formed by blanking process for 0.35 TD samples at different blanking speeds. The figures illustrate an increase in the fracture area and reduction in the shear area compared with the rolling orientation at the same thickness, behaviour reflecting that faster failure of the material can occur under this cutting condition. There is a small difference in the zones' features in both grain orientations, RD and TD, for 0.35 mm sheet thickness as shown in Figure 4.54a, b at higher magnification of the selected areas of the shear, fracture, and rollover zones.

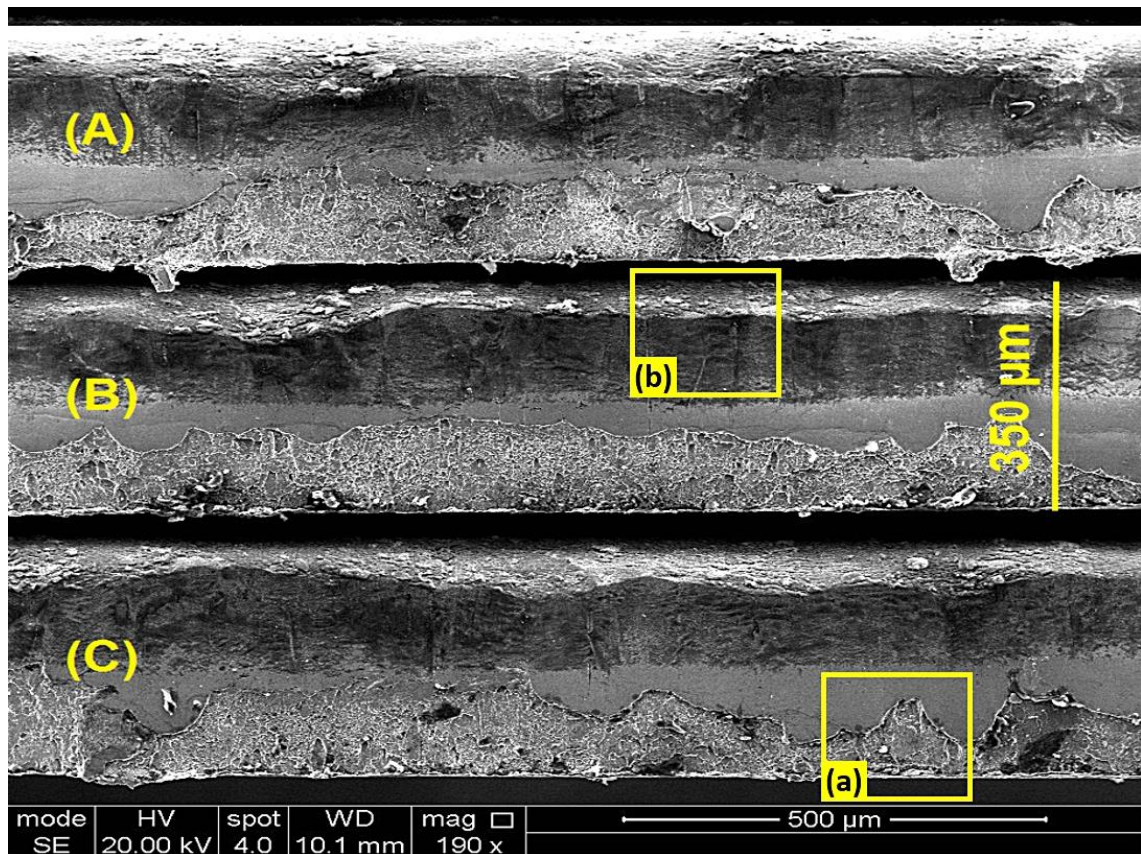


Figure 4.53: SEM image for induced blanking cut edges of 0.35 TD samples at different blanking speeds, A) 100 mm/min, B) 500 mm/min, C) 1000 mm/min.

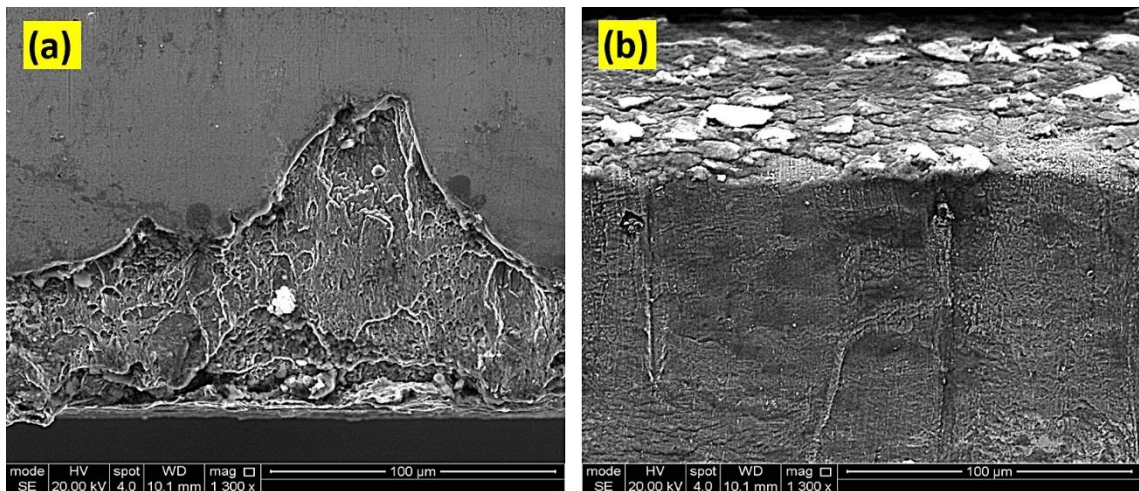


Figure 4.54: Microstructure at higher magnification of some selected areas in Figure 4.53 of 0.35 RD samples, a) At shear and fracture zones, b) At rollover and shear zones.

It is worth mentioning that the microstructure of the cut edge induced by wire EDM method is different from that induced by blanking method. Tensile samples and the initial sheets for blanking process were cut by wire EDM method. Figure 4.55 illustrates the absence of the four regions formed by blanking process. Instead, the EDM cut edge surface has only a single microstructure which is similar to the fracture zone produced in the blanking process.

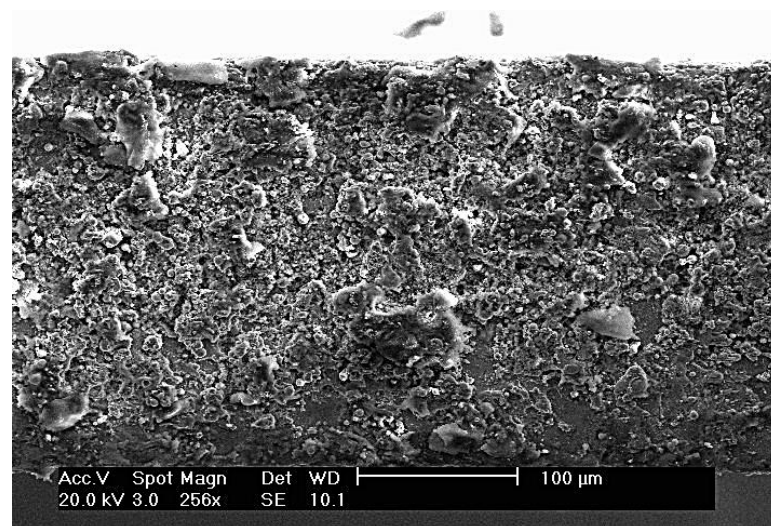


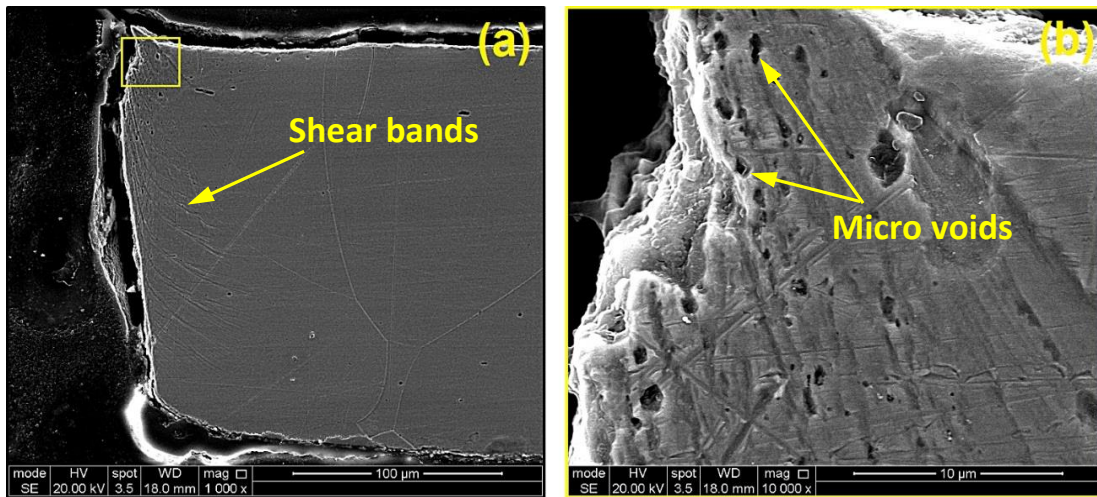
Figure 4.55: SEM image for cut edge surface induced by EDM method used to prepare ES samples.

4.5.2 Deformation analysis of cut edge fracture

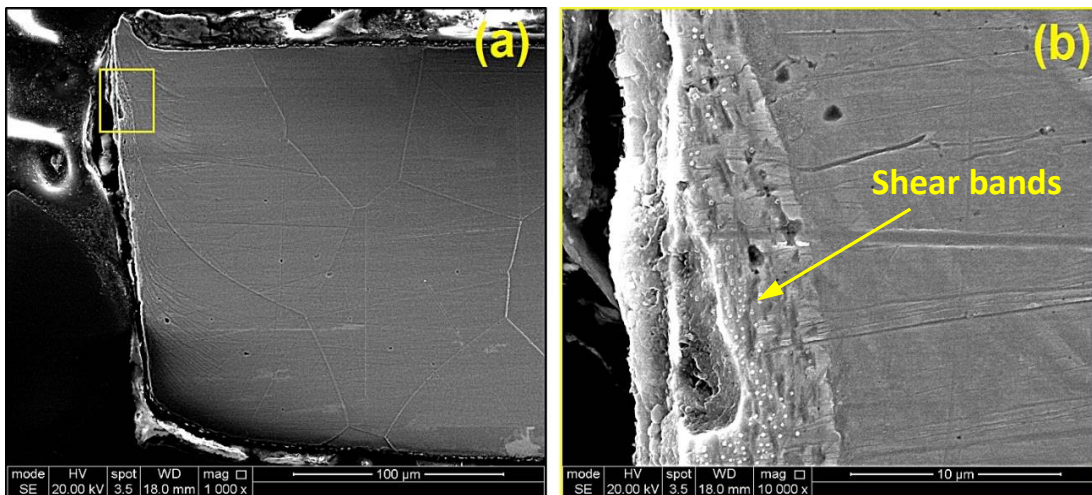
The burnished zone is formed purely by plastic flow of the material, as there is no crack formation or propagation in this region. However, the crack initiates and is propagated in the rupture zone during the blanking process. Therefore, a rough surface is produced by material splitting. After production of the burnished zone, the material undergoes a combined loading of shear and tension resulting in initiation of cracks and then the fracture surface is created. The latter cause separation of material during the cutting process. The fracture zone has many features such as small dents, pits, micro-cracks, and micro-voids. The method used to modify the material's texture and the distortion of the cut edge could have a significant impact on the material's behaviour and the quality of the cut edge produced in the blanking process.

Figure 4.56 shows the fracture surface features for 0.2 RD samples at different blanking speeds of 100, 500, and 1000 mm/min. All micrographs on the left side of the figures illustrate a full cut edge profile at low magnification, while part (b) of the figures demonstrate the selected affected areas of the fracture surfaces at high magnification as indicated by the square shapes in the micrographs (a). Plastic shear bands at the cut edge can be observed at the fractured edge, especially near to the burr zone. The figures show the voids generated during the final stages of the blanking process where the material undergoes mixed tensile-shear failure mode. It seems that the void concentration is higher closer to the burr formation zone.

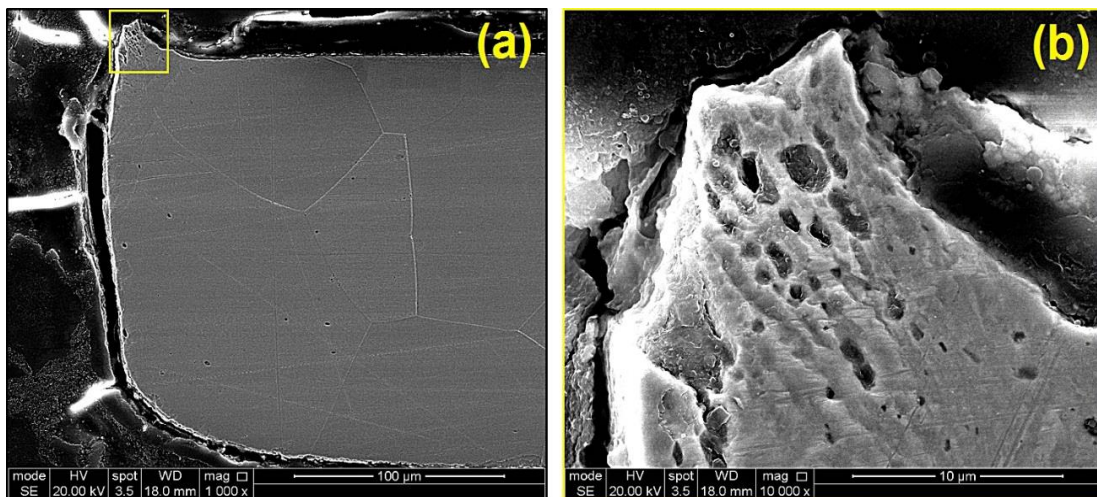
Figure 4. Figure 4.57 show fracture types for 0.2 TD samples at blanking speeds of 100, 500, and 1000 mm/min. Generally, a similar trend of fracture deformation is apparent in the transverse grain orientation samples to that seen in the rolling grain orientation samples. However, the figures show less affected areas, although some large voids near to the cut edge can be observed in figures (b).



I. 0.2 RD 100 sample at blanking speed 100 mm/min.

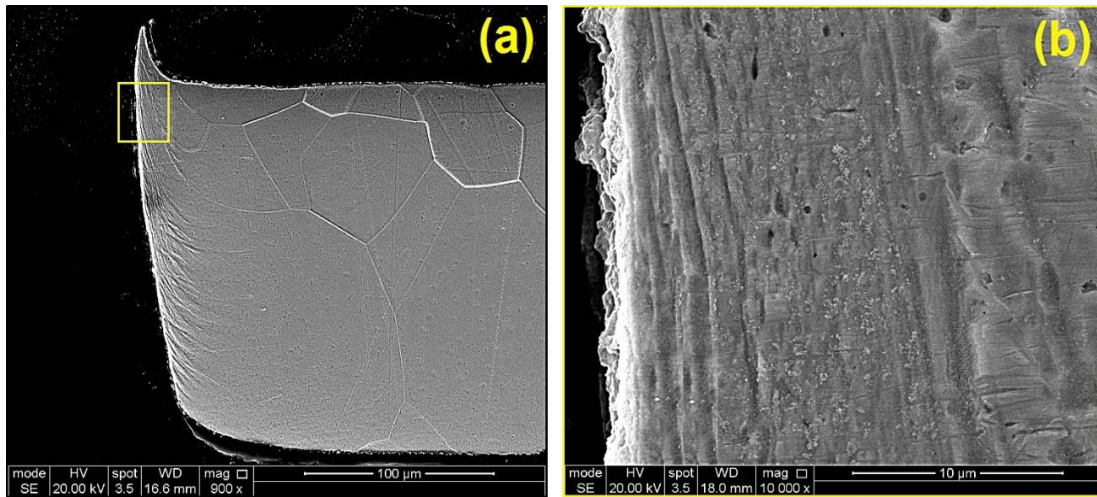


II. 0.2 RD 500 sample at blanking speed 500 mm/min.

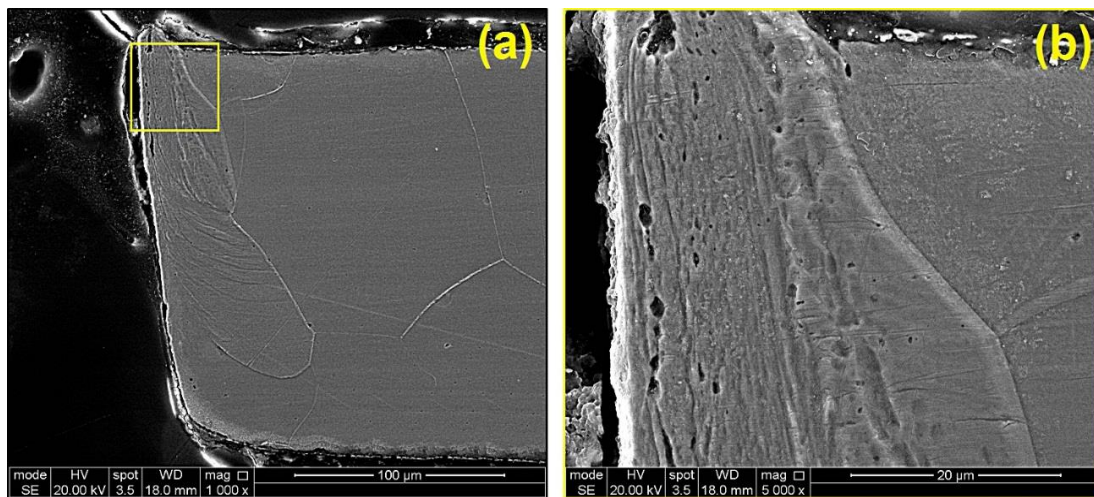


III. 0.2 RD 1000 sample at blanking speed 1000 mm/min.

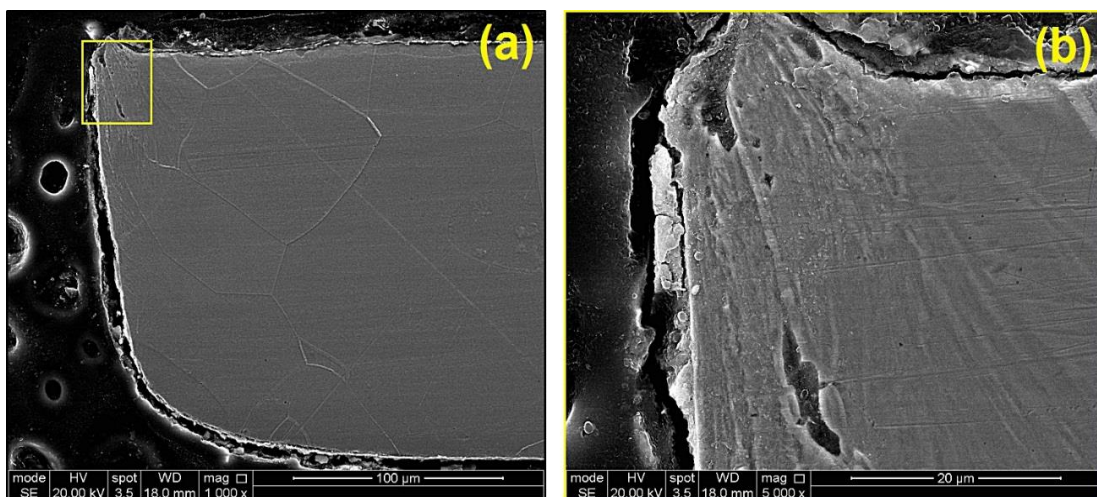
Figure 4.56: Cut edge fracture surface for 0.2 RD sample at different blanking speeds.



I. 0.2 TD 100 sample at blanking speed 100 mm/min.

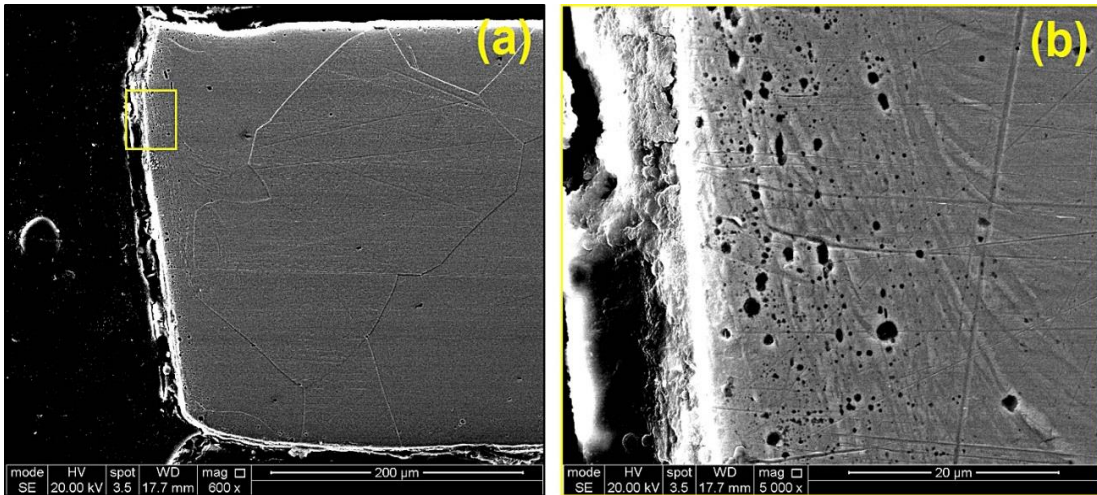


II. 0.2 TD 500 sample at blanking speed 500 mm/min.

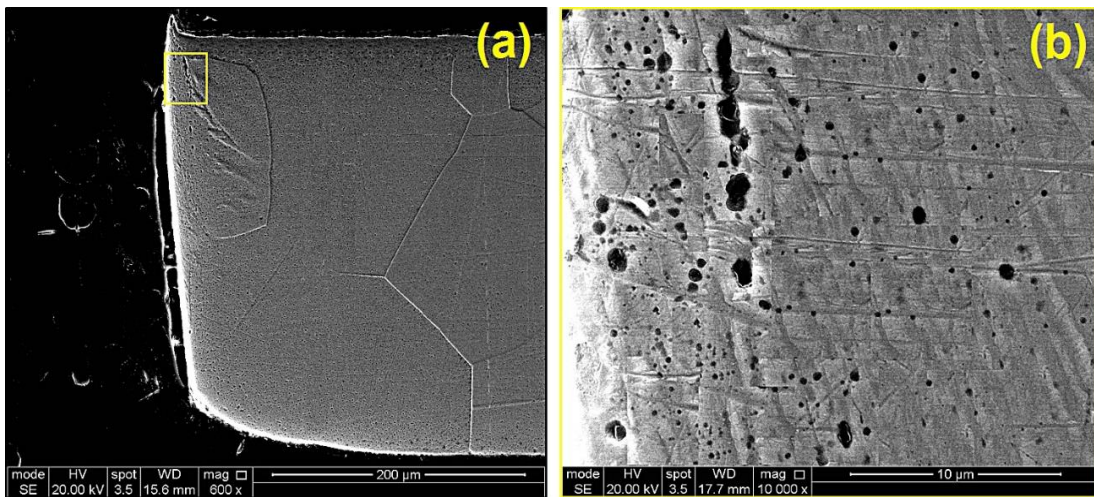


III. 0.2 TD 1000 sample at blanking speed 1000 mm/min.

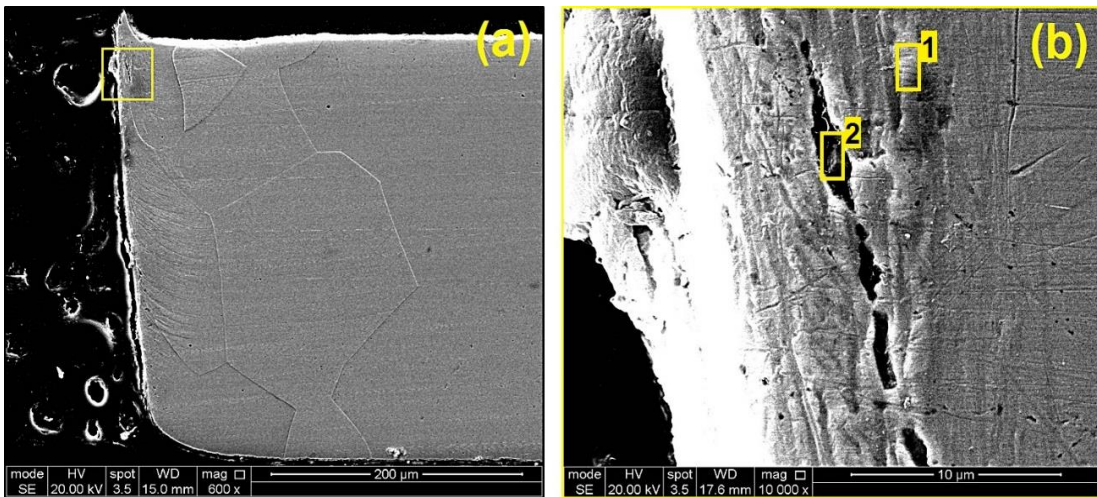
Figure 4.57: Cut edge fracture surface for 0.2 TD sample at different blanking speeds.



I. 0.35 RD 100 sample at blanking speed 100 mm/min.



II. 0.35 RD 500 sample at blanking speed 500 mm/min.



III. 0.35 RD 1000 sample at blanking speed 1000 mm/min.

Figure 4.58: Cut edge fracture surface for 0.35 RD sample at different blanking speeds.

Figure 4.58 show fracture types for 0.35RD samples at different blanking speeds of 100, 500, and 1000 mm/min respectively. Generally, a large number of voids can be observed, with some elongated voids in the shear deformation gathering to form something similar to cracks. Some defects are shown also in the area near to the edge.

Figure 4.59 shows elemental analysis by EDS test for the selected area in Figure 4.58 III b. The analysis displays a high percentage of O, C, and N elements in the indicated area 1 besides the main electrical steel alloy elements, relating to the coating layer ingredients. Meanwhile, no clear elements can be seen in area 2, although the test searched for elements within the body and not just the shell (The letter K after an element symbol refers to a body element, whereas the letter L refers to elements found in the shell). The results of the analysis may indicate the presence of deep voids, which may have resulted due to the applied plastic deformation.

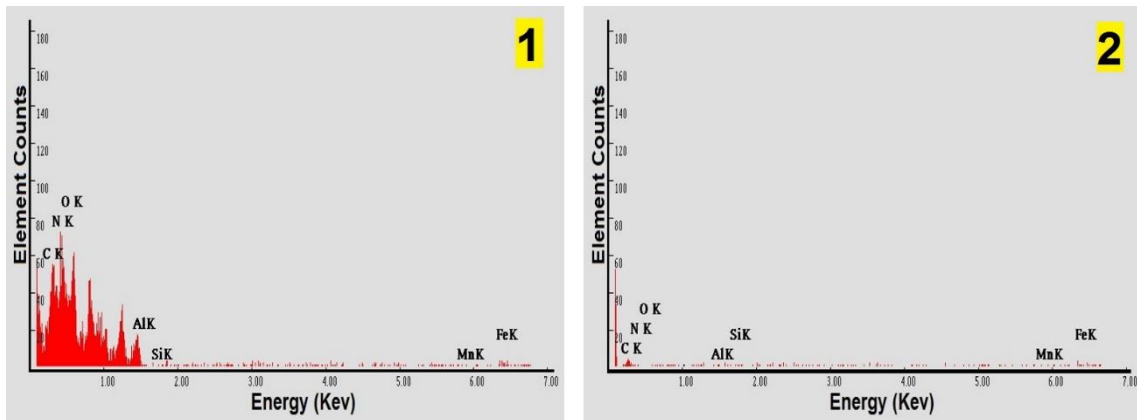
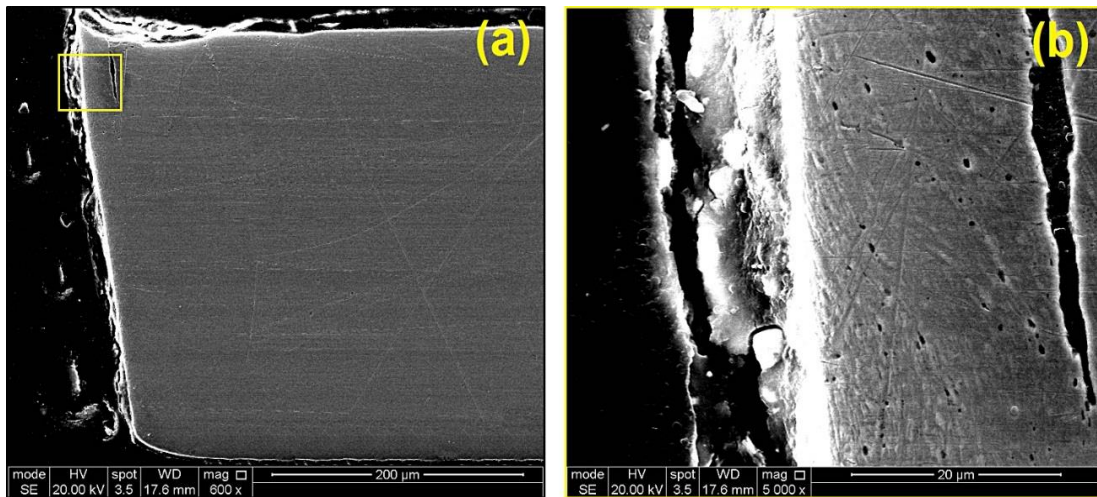
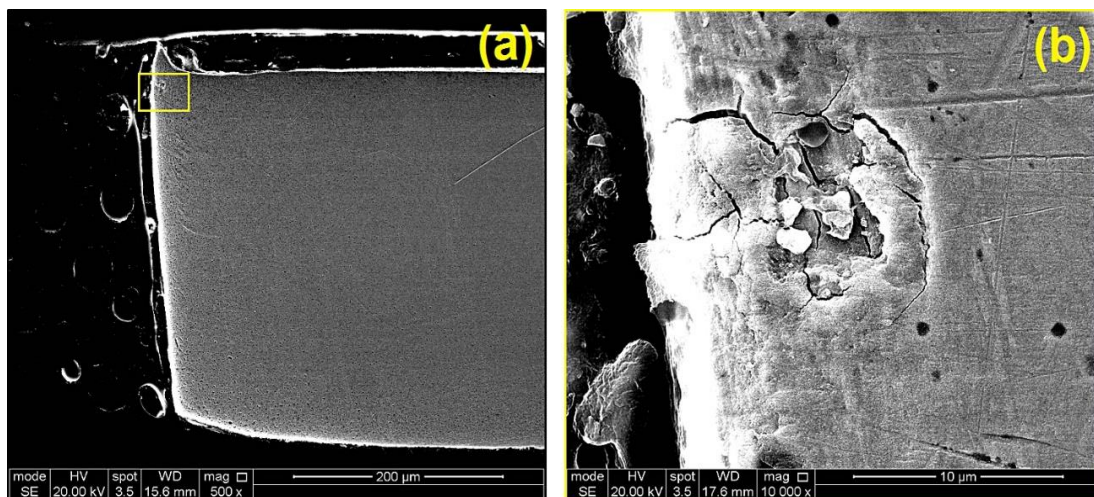


Figure 4.59: EDS analysis for the square parts indicated in the Figure 4.58 IIIb.

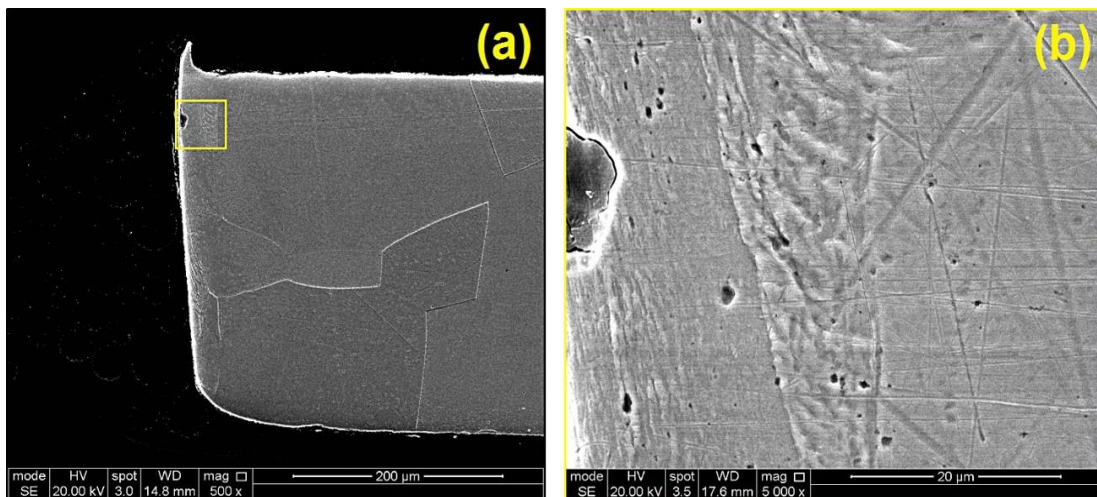
Figure 4.60 show fracture types for 0.35 TD samples at different blanking speeds of 100, 500, and 1000 mm/min respectively. Figures (a) on the left side illustrate a full cut edge profile at low magnification of SEM observation, while the micrographs (b) on the right side demonstrate high magnification of the indicated fracture area in the micrographs (a). Generally, less number of voids can be seen for 0.35 TD compared with 0.35 RD samples. The cutting process produced less distortion regarding these parameters, which was concentrated in specific locations. The characteristics of these areas are similar to those seen in the previous samples. Moreover, in all cases, the fracture angle is much larger for the low speed, as is more obvious with the thicker material.



I. 0.35 TD 100 sample at blanking speed 100 mm/min.



II. 0.35 TD 500 sample at blanking speed 500 mm/min.



III. 0.35 TD 1000 sample at blanking speed 1000 mm/min.

Figure 4.60: Cut edge fracture surface for 0.35 TD sample at different blanking speeds.

4.5.3 Estimation of the depth of cut edge deformation

Optical micrographs were used to determine the extension of deformation from the cut edge by indicating the limits of shear bands deformation. Moreover, they would indicate the grain number over the deformation area.

Figure 4.61 shows the optical microscopic micrographs of the sample 0.2 RD at different speeds. The crystalline boundaries appear clearer and show the presence of only two grains at the cut edge area. All the deformation expansions were within the large grains and shear bands are more visible in larger grains at the vicinity of the cut edge. In addition, the deformed grains pointed towards the punch movement direction when moving from the rollover area to the burr area which means the grains are stretched in the direction of cut. However, the extension of deformation still random and depends on the size of local grains at the cut edge.

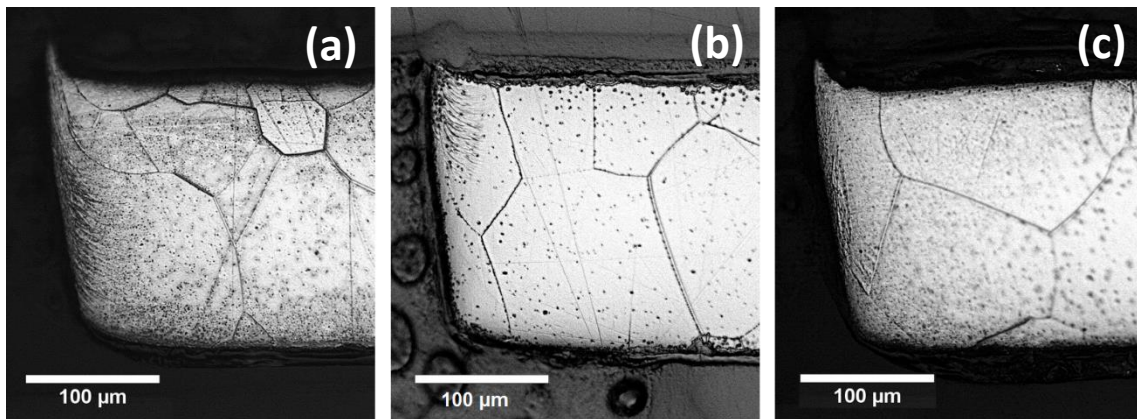


Figure 4.61: Optical micrographs for induced blanking cut edges of 0.2 RD samples at different blanking speeds, a) 100 mm/min, b) 500 mm/min, c) 1000 mm/min.

Figure 4.62 shows the optical microscopic micrographs of the sample 0.2 TD at different speeds and indicates the presence of only two to three grains at the cut edge area. The extension of plastic deformation seems to be concentrated at the fracture zone more than the rollover and shear zones. The deformed grains were also pointing towards the punch movement direction. The expansion of deformation seems to have stopped at the grain boundaries.

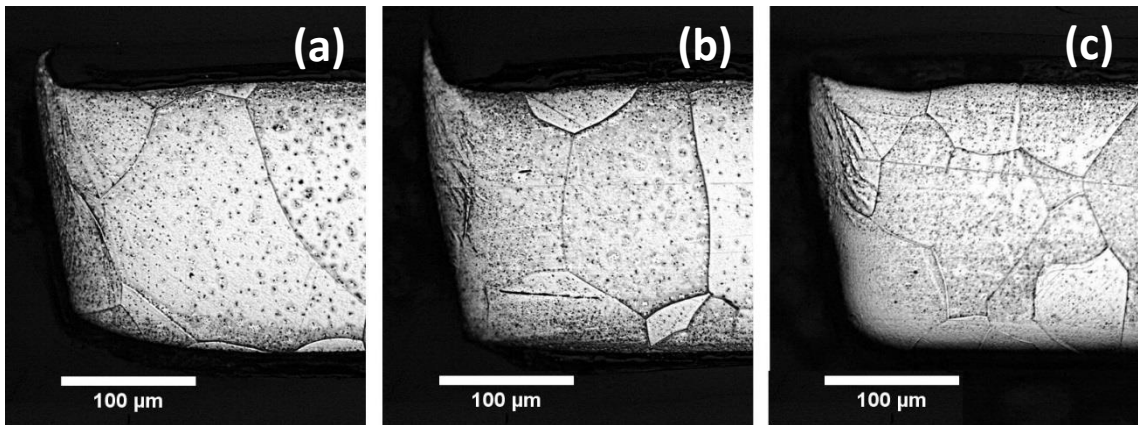


Figure 4.62: Optical micrographs for induced blanking cut edges of 0.2 TD samples at different blanking speeds, a) 100 mm/min, b) 500 mm/min, c) 1000 mm/min.

Figure 4.63 shows the optical microscopic micrographs of the sample 0.35 RD at different speeds. Also, about 2-3 grains are present at the cut edge area. The deformation is less relative to the thickness of sample and concentrated in specific locations along the cut edge line, possibly because of the increase in the sample thickness.

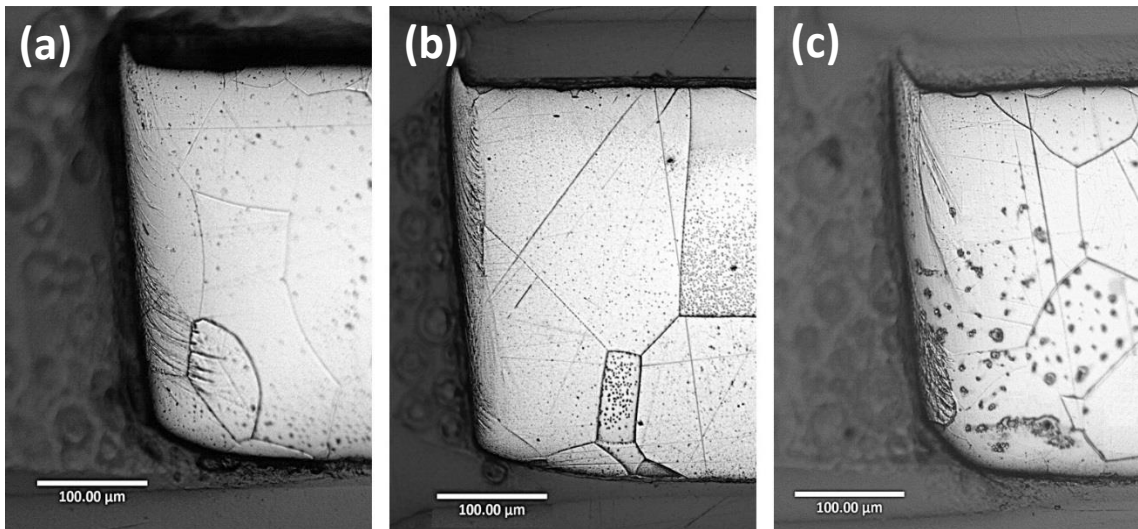


Figure 4.63: Optical micrographs for induced blanking cut edges of 0.35 RD samples at different blanking speeds, a) 100 mm/min, b) 500 mm/min, c) 1000 mm/min.

Figure 4.64 shows the optical microscopic micrographs of the sample 0.35 RD at different speeds. About 2-3 grains are present at the cut edge area. The extensions of plastic deformation are distributed along the cut edge, but it does not extend much from the edge. It should be noted that it is very difficult to measure or even estimate the amount

of the extension because it represents a variable state that depending on the case of the sample.

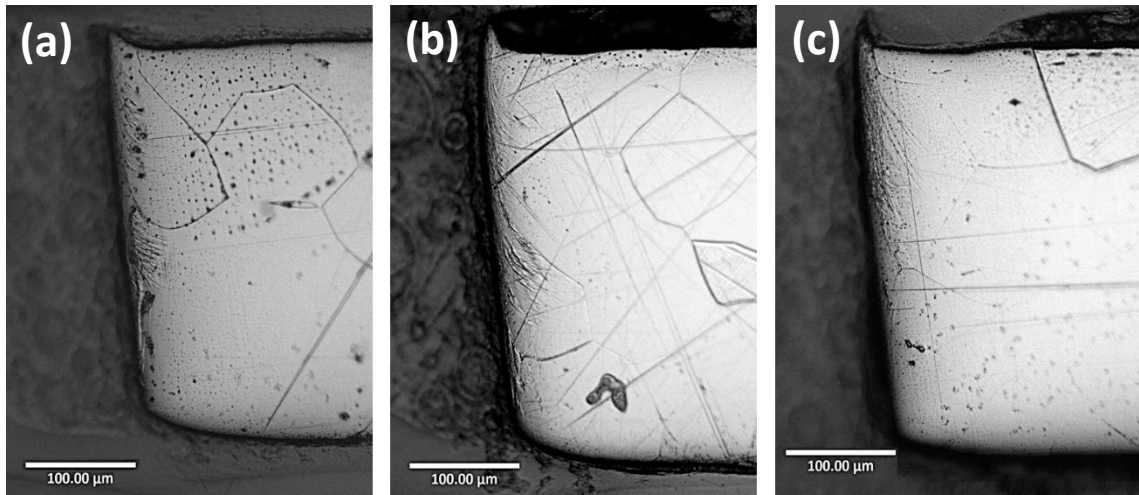


Figure 4.64: Optical micrographs for induced blanking cut edges of 0.35 TD samples at different blanking speeds, a) 100 mm/min, b) 500 mm/min, c) 1000 mm/min.

The micrograph results can prove that the defects are depending on the texture and grain dimension at the cut edge. It seems that if the cutting line occurs inside the grain, the deformation will extend further, especially if the grain size is very big. That means that the expansion of deformation could be impeded by the grain boundaries. Thereby the grain size and location play the key roles in deformation extension.

4.5.4 Estimation of the grain size and number over the sheet thickness

The size of the grains in the sheet material is very important in the blanking process because of the small number existing over the sheet thickness. Therefore, grain size can cause changes in the edge quality and the type of edge fracture. Generally, the effect of grain size on the cutting process increases when the sheet thickness is reduced.

Figure 4.65 a, b illustrates the number of grains existing for both the ES sheet thicknesses, 0.2 and 0.35 mm. The number of grains across the thickness of the material was limited to 2-3 and 4-5 for the 0.2 mm and 0.35 mm thicknesses, respectively. Therefore, the local grains features at the cut edge are playing an important role in the mechanics of deformation of blanking process of the thin sheet samples. According to the figure, the average grain size for the 0.2 mm thickness samples was approximately 103 μm , whereas it was about 140 μm for the 0.35 mm thickness (see appendix B).

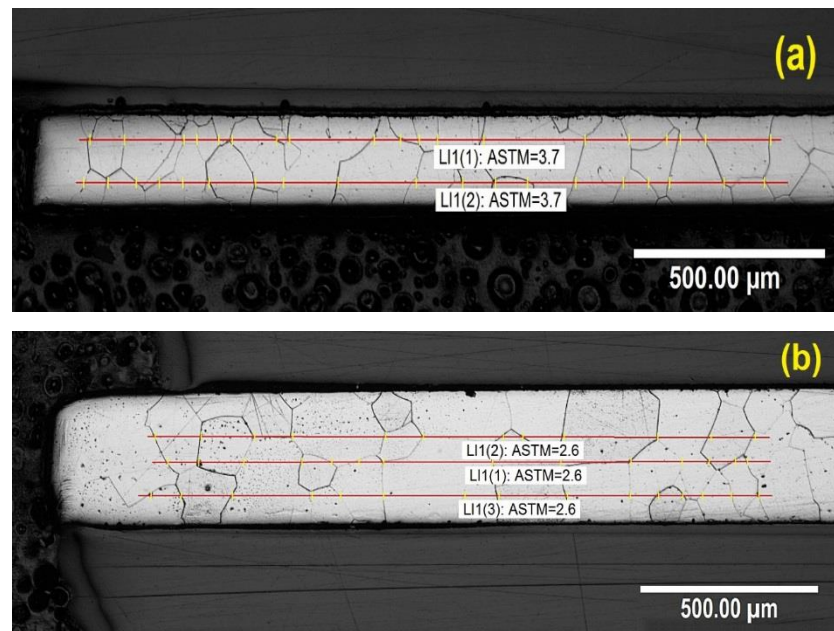


Figure 4.65: Optical micrographs for the (a) 0.2 mm and (b) 0.35 mm electrical sheet thicknesses at low magnification of 20X.

4.6 Summary

Electrical steel sheets were successfully cut using the blanking process for two different thicknesses, 0.2 and 0.35 mm, and two-grain orientations, RD and TD, at three different blanking speeds of 100, 500, and 1000 mm/min. The following experimental tests, which presented quite serious challenges due to the small sheet thickness of the produced samples, were carried out:

- Mechanical properties for ES sheets and cut edge area were characterized using tensile tests, DIC technique, and Nano indentation tests.
- Material microstructure and cut edge fracture and zones deformation were examined using SEM, optical and the EDS tests.
- Magnetic properties and hysteresis losses in both tension and blanking condition were investigated using a single sheet magnetic tester.
- Strain distribution due to both tensile and blanking deformation was tested using DIC technique.

The results of these experiments tests were presented. The importance of these investigations lies in identifying the deformation distributed around the cut edge. The results proved that the methods used were effective to give a clear conception of the effect

of the edge deformation on the material's properties. The analysis of the results also indicated of uncontrolled nature of the deformation because it depends on the type and size of a limited number of grains that exist in the cut area that can change the blanking deformation according to the cutting location. The next chapter will attempt to establish links between some of the most important findings in order to reach accurate conclusions and provide further discussion related to the cut edge deformation, in particular those aspects that are most influential regarding cut edge deformation.

5

Discussions and statistical analysis

5.1 Introduction

The results of the characterization of cut edge deformation and the effects on magneto-mechanical properties reported in the previous section will be discussed in this section. Moreover, the potential errors and limitations of the developed and applied methods with a critical analysis of the results obtained will be discussed. This will be done in order to establish a relationship between blanking parameters and outcomes of deformation which could provide further explanation and understanding of the consequences of the deformation. In addition, the statistical analysis of the results will be used to determine the most statistically significant operational parameters in terms of the cut-edge quality.

5.2 The critical influences of the cut edge microstructure

The current study presents the effects of a possible case study of the blanking deformation with microstructure images of the cut edge grains for specific blanking parameters on the magnetic and mechanical properties of the blanked thin sheet of ES. The induced deformation plays an important role in the evolution of the final blanking product. Using thin sheets of electrical steel led to reducing the number of local grains at the cut edge region. These small number of grains could be different in size and shape. Also, the position of cutting line is varied and cannot be controlled as the sheets are

randomly feeding to the blanking dies. That can lead to rising several critical issues regarding the analysis of induced deformation of the blanking process, for examples, the deformation will vary from sample to sample even with same blanking setting and therefore it is very difficult to determine the effects of the induced deformation or specify any fixed trend regarding the process parameters.

The grain size has a significant influence on the blanking process, when there are only a few grains cross the sheet thickness, even the fracture type by means of crack initiation and propagation may differ and thereby the deformation depth could increase or decrease and also the cut edge zones will change along the cutting line, that was well reported in [72, 73].

As a result, characterized blanking induced deformation behaviour and the cut edge quality may not only relate to the blanking parameters as reported in [116, 117]. These are also influenced by the condition of the grains at the cut edge where the presence of few grains across the thickness can show a strong variation not only in the cut edge profile but also in blanking deformation distribution.

The grains orientation and coordination also play a crucial role in shear deformation. With the decrease of sheet thickness, the number of grain in the cross section of the sheet decreases and possibly grains size become bigger that will lead to increase the anisotropy of the local deformation mechanisms and individual grains become key players on affecting the local shear deformation in blanking as mentioned in the literature [74]. However, as it is explained previously the finer grains in the microstructure increases the number of active grains during deformation, therefore statistically there may be more favourable deformation orientations in the critical zone. Where the blanking deformation of fine-grained in sheet specimen takes place with the most favourable grain sliding systems. This will result in a more uniformly distributed deformation conditions as shown by [74]. While in the coarse-grained sheet specimen, the grain crystal orientation varies and the slipping systems are oriented differently with the blanking direction. The grains with an unfavourable orientation towards the blanking direction may lead to shear deformation more difficult. That makes the orientation of these grains very important, especially for the cutting direction, these differences are related to the variation of deformation behaviour during the blanking process.

The microstructural results (Figures 4.45, 4.48, 4.51, and 4.53) for the cut edge surface demonstrated that the cut edge surface consists of four distinct regions: rollover, burnished, rupture, and burr zones. This is a typical condition in all sheet metal blanking

operations as reported in [63, 64]. These SEM images showed that the cut edge zones occur sequentially and the size of each zone is affecting by the sheet thickness. According to the cut edge fracture results (Figure 4.45 to 4.54). The larger shear zones at lower blanking speed indicate more penetration of the punch into the material. Therefore, the fracture zone is expected to increase, at the expense of smaller shear zone when the blanking speed is increased. This indicates that the material fails more quickly due to possible faster crack initiation and propagation because of the applied kinetic energy [4].

The shear bands are formed due to the applied elongation and shear stress/deformation. According to the images of cut edge fracture analysis (Figure 4.56 to 4.60), the shear deformation is concentrated with just a few grains that confined by the punch and the die. Also, the shear bands are propagating and elongating in alignment in parallel to the direction of punch movement. The qualitative analysis of the SEM micrographs indicates that the density of the shear bands are higher close to the cut edge and the bands are densely packed in a narrow zone. This can indicate that the severe plastic deformation occurred within a narrow zone because of excessive the punch penetrated into the sheet thickness lead to exposing the material to more shear and compression stresses and results in more dislocations. This shows the severity of the plastic deformation in these regions that could be linked to the measured plastic strains and the high hardness values obtained from the Nano-indentation results.

Moreover, the higher amount of shear bands visible at the low blanking speeds support the theory that the punch penetration is higher for this testing condition as the larger punch penetration should be compensated by more material deformation and flow around the punch to facilitate the blanking process. In contrast for the higher speeds, the crack propagations will take the dominant role, as already explained, therefore less material will deform in these cases.

The observed cut edge deformation in the current study are in a good agreement with the literature findings [152, 153]. The shear band becomes more obvious with greater penetration of the punch because of the involvement of more grains in the shearing process. While the shear bands become less visible with a decreasing number of grains in the shared area as seen in Figure 4.61 to 4.64. Similar findings are also reported in the literature [154]. In addition, a few large-sized grains appeared over the sheet thickness section as shown in Figure 4.65. That can prove the big role of the individual local grain on the mechanics of deformation at the cut edge of thin sheet samples. The anisotropic property of the single grain makes the deformation inhomogeneous and the slipping

direction of the grain may not be in the blanking direction [154]. Moreover, it may not be accurate to generalize the process of thin sheet analysis according to the thick sheet analysis, as it seems the material behaviour may be different because increasing the number of local grains at the cut edge will increase the stability for grains effects.

5.3 Plastic strain and magnetic properties under uniaxial tension

The tensile testing at different rates was conducted to verify the rate sensitivity of used two different thicknesses (0.2 and 0.35 mm) at different grain orientations (RD and TD) of the thin steel sheets. The tensile results (Figures 4.1 and 4.2) show that the samples strength has a limited dependency on the test orientation and the material behaviour is more consistent at higher loading speeds. Also, the increase of tension test speed led to slightly higher tensile strength regardless of the specimen orientation. The material properties were affected when reducing the sheet thickness and led to varying the mechanical properties, for example, the yield stress was decreased for thinner sheets similar trend was reported by [155].

Moreover, the material properties slightly changed when tested at lower loading speeds by means of lowering the tensile yield. This behaviour could be attributed to the small thickness and grain size of the sample [133, 156]. The other possible reason is the effect of the machine's stiffness/compliance on the results. Lower strain rate can cause less stiff (more compliant) testing machine [157].

The tensile results in Figure 4.3 also showed that the samples elongation was affected by the applied tension direction with the higher extension for rolling direction which is well documents in the literature [155]. This is due to the application of the axial tensile load parallel to the rolling direction. The anisotropy and grain orientation have a great impact on the plastic deformation, the flow stress tends to decrease when the thickness of the sheet decreases [155]. The figure also showed some differences in the tensile results for the selected material having sheet thicknesses, which could be attributed to slight variation in the chemical composition and the effects of the manufacturing and rolling processes. Also, grain size may play the main role in crack initiation and propagation. Also, the existing of few grains in the local deformation zones may affect the strength of bonding between the grains orientation [155, 156].

The conducting of the DIC technique during the tensile tests gave a vision of the strains distribution in each stage of the test. The local strain distribution in uniaxial loading was reported in [Figure 4.6 to 4.9](#) during different stages of interpreting the tensile test. A uniform deformation of samples all over the gauge length was observed.

However, the processing analysis of the captured images using the Davis software includes several parameters could affect the accuracy of the analysis results. For examples, the image resolution and the selection of the proper subset and step size that directly related to the speckles number and size inside the deformation zone. The measured strain errors associated with the DIC technique results due to the uncertainty in pinpointing the intersections of the deformed grids to measure the strain distribution and the error associated with the correlation parameters and algorithms used in DIC [158]. Additionally, a small difference in the selected gauge size for strain calculation can also introduce errors in the obtained results.

[Figure 4.5](#) illustrating the error values in the measured strain values distributed over the analysed region, the figure shows a maximum error value of about 3%, this value can be negligible compared to the large strain values measured during the tensile test about 45%. Consequently, the error analysis results proved of the presence of acceptable error percentage, about less than 10% regarding the maximum amount of deformation applied during the tensile tests of ES steel. Similar error levels are reported in the literature even for smaller applied strain [159].

The strain distribution images illustrated that there is no local necking and the fracture occurs instantly, where the fast crack formation and propagation caused through concentration of stress at the crack edge. The micrographs in [Figure 4.4](#) also confirms that. This may be attributed to the high percentage of silicon in the ES material that can increase the material brittleness and affect the fracture type [155].

To investigate the effect of plastic deformation on the magnetic properties, the tensile test was interrupted with an increment extension 1 mm plastic deformation where each elongation is corresponding to a strain value that provided precisely by DIC test. Each deformed tensile sample was measured using the magnetic single sheet tester.

The increase of the dislocation at larger deformation causing to increase the spacing between domains and lead to facilitate of domain wall movement and achievement of the saturation state [22]. Dislocations in crystal lattice are the major pinning centres for domain wall movement. Whenever the dislocation density increases will cause more hindering of domain wall movement and result in large magnetic losses.

Figure 2.32 could prove this idea by showing the development of simple dislocations into wavy slip bands when increasing plastic deformation [13].

The hysteresis loops (Figures 4.34 to 4.37) were shrunk when applied plastic deformation during tensile tests. This was more evident at the saturation level and minimal variations were observed at the coercivity points due to the limitations of the applied method. The change of the hysteresis loop is reported to be directly linked to the applied deformation will change the stress state and distance of the active domains in the samples [101]. Additionally, the variations observed between the RD and TD curves could be explained by the material tends to deformation and local grain orientation across the tested regions.

The changing in the magnetic hysteresis loops are mainly due to domain walls motion when applying a magnetic field [21]. Therefore, the domain theory about the aligning domain and the motion of the domain wall consider as a suitable tool for providing a physical explanation of the stress effect in electrical steels [20]. A free-stress condition can be described as a small number of large domains oriented inside each grain close to the rolling direction [23]. Applying tensile stress seems to improve the domain structure because it leads to the refining of the wall spacing of main domains that results in an almost ideally oriented domain structure [22]. This may be because the thinner sheet could contain a larger number of grains along sample length, and thereby more grain boundaries. Each grain boundary is considered as a big domain wall that may contain many regions of small domains. Therefore, this creates more pinning sites of domain movements and thereby causes more loss [9]. The results proved that hysteresis loops are highly influenced by the sheet thickness and less by the grain orientation.

5.4 Defects evolution during the blanking process

Blanking process was reported as the preferred method and the most desirable way to produce the final shape of the stator and rotor laminations because it can be used for mass production at lower cost [43, 46]. Moreover, it was concluded that electrical steel sheet is the most common material used as a lamination material due to its relatively good magnetic properties, such as high permeability and lower loss [11, 3].

However, several effects can be induced by the blanking process, for example, as the blanking process is implemented under cold working conditions, it produces a region of residual stress that spreads some distance from the sheared edge, as shown in [Figure 4.30 to 4.33](#) and reported in studies [3, 4]. Additionally, although the small deformation zones and the effect of built-up compression could suppress the generation of fracture zones in the shear surface and minimize the crack size [61], the increased dislocations density due to blanking induced plastic deformation [6] could affect the local mechanical and magnetic properties of the sheet [13]. Accumulations of these dislocations generate pin sites restrain domain walls movements and impair permeability and increase power loss [3]. The microstructural defects of the cut edge surface can be observed in [Figure 4.45 to 4.54](#) of the cut edge surface fracture.

These results showed that cut edge geometry defects were affected by the implemented blanking conditions, which in turn can influence the magnetization process and the distribution of flux around the cut edge [3] that reflected in the different hysteresis loops size as shown in [Figure 4.39 to 4.42](#). The magnetic properties represented by the hysteresis loops and losses in the current study was changed due to the blanking effects that could increase or decrease according to the changing of process parameters. Consequently, all the above-reviewed blanking effects can prove the affected the magneto-mechanical properties of the cut edge. For example, the production of burrs may cause electrical contact between the laminations of the core. Soft steel could produce long burrs that lead to an increase in magnetic loss [1].

The results of the cutting force were recorded by a load cell attached to the upper plate of the die are shown in [Figures 4.11 to 4.12](#). The study showed that the speed of the deformation significantly affects the blanking force. Where the study found that conducting the process at higher speeds caused a reduction in the punching force and improved the quality of the part edge as represented in a larger shear zone, smaller burr height, and rollover area. Also, at different blanking speeds, the cut material can show different behaviour which can result in a diverse cutting force as reported in [89], that because it also depends on the condition of local grains at the cut edge and fracture type.

The cutting force was decreased as a result of increasing the blanking speeds even when the thickness and orientation are fixed for all produced sample in both used blanking dies. That matched the finding by some of the previous researches [86], although others noticed some variation in the relation between them [82]. There are conflicting data concerning the effects of shearing speed on the energy requirement for shearing [82]. That

because each study implement the cutting process in different blanking speeds some at very slow up to 10 mm/s and others at very high speed up to 10 m/s. That could be attributed to the fact that the higher speeds may result in less plastic deformation that could cause higher kinetic energy and therefore quicker shear crack initiation, propagation, and fracture [87]. That means a reduction of shear area and increase of the fracture zone as shown in [Figures 4.45 to 4.54](#). In other words, the energy required for plastic deformation is lower, therefore there is higher stored elastic energy that could facilitate shear crack propagation [5, 82]. Other possible interpretation is the thermal conduction and distribution of heat to the vicinity of the cut area by. In high punch velocity, the limited balancing of temperature causes a higher temperature at the deformed cutting edge. In contrast, at slow punch velocity, the heat is dissipated out of the shearing zone because there is enough time for thermal conduction to occur [80]. Accordingly, the other mentioned reason is that the short time of high blanking speed can lead to concentration of generated heat in the material, causing a thermal softening and reduction of the force required to cut the sample [80, 81].

However, because the speeds used in the blanking process in the current study were not very high, the reason for the decrease in cutting force could fluctuate between the two mentioned explanations. In addition, the blanking force measurements also show that the increase of thickness leads to an increase of the force value, which occurs because of the increase of the deformed area due to the larger thickness.

5.5 Blanking local strain and the depth of deformation

The evolution of local plastic deformation in electrical steel has been studied using a DIC technique in-situ blanking process and the Nano-indentation test at the cut edge. Tests were performed using a specially blanking die and suitable DIC set-up. Implementing this test was associated with big challenges because of the very small deformation zone represented by the thickness of the sample and the high-speed punch movement.

Maximum equivalent strain were extracted for blanking samples because the deformation region undergoes a combined loading of shear, tension, and compression during the blanking process [63]. Therefore, the strain values could include axial strains components in addition to the shear strains components. Thereby, the equivalent strain could better express the strain in blanked material than the normal strain as it is a resultant of both principle and shear strains.

The strain distribution around the sheared edge was measured through tracking the initiation and evolution of damage over the thickness of the sheet at different stages of the process using DIC tests. According to the DIC results, the observed deformation was started from the contact point between the punch and the sheet surface, then grew towards the die side, as shown in most of DIC results during the blanking process, this trend was also reported by K.wang [99]. Sometimes, the deformation may concentrate on both sides of the sheet when applying very small clearance may reach 2% of sheet thickness [62, 137]. Which is not the case on current cutting condition as the clearance is around 10%t, therefore the figures 4.14 to 4.25 showed the strain starts concentrated from the punch side. That because of the breakoff angle of the cracks between the punch and die sides will not meet when extended because applying insufficient or excessive clearance [62]. Consequences the cutting zone and lead to extend or narrow the deformation effect. The obtained results illustrated the cut edge zones and stages for the mechanism of blanking process starting when the punch touches the sheet surface then shear and crack formation until the fracture stage and separation. However, the analysis process of induced blanking strain in a thin sheet of ES using the digital image correlation (DIC) technique includes many issues that could affect the analysis results. For examples: the results showed that there are differences in fracture moment between samples due to the applied diverse blanking speeds that can cause different impact energy which results in different material resistance and thereby different yield points. In addition, the high-speed movement of the punch and the induced vibrations due to the impact with the sheet surface lead to the difficulty of the determining of the instant of touching blanking tool (Punch) to the sheet surface because of the high rate recording system and high-speed punch movement. Moreover, the low thickness will lead to reducing the possibility of generating speckles across the sheet thickness. Also, the small deformation zone will lead to reducing the image resolution.

The individual analysis of the blanking test cases because of the difficulty in the timing of DIC image acquisition at different blanking speeds, and regardless of the punch position, the last image before the fracture and separation of the blank from the sheet showed the state of the part after blanking which can represent the maximum deformation for the blanked sample. In addition, although the state of the deformation may vary from sample to another because it depends on the local grains and their orientations at the cut edge location. The high-speed DIC results showed the deformation that occurred during the blanking process for the current case studies.

The processing analysis of the captured images using the Davis software also includes several parameters could affect the accuracy of the analysis results. For examples, the image resolution and the select of the proper subset and step size that directly related to the speckles number and size inside the deformation zone. The measured strain errors associated with the DIC technique results due to the uncertainty in pinpointing the intersections of the deformed grids to measure the strain distribution and the error associated with the correlation parameters and algorithms used in DIC [158].

Implementing the high-speed DIC technique during relative high-speed blanking process resulting in significant challenges and problems in strain measurements especially with triggering, timing, spatial resolution and errors. The error analysis of the DIC technique has revealed that the existence of error though small in strain distribution patterns obtained from DIC. An average error of about 1.8% in strain values was found over the entire analysed area of the blanking process as shown in [Figure 4.13](#). This value can be negligible compared to the large strain values measured during the process. However, the DIC technique under-determines the strain values with an average error of about 5% for the amount of deformation applied during the blanking tests of ES steel.

In spite of the uncertainties associated with the applied DIC measurement technique, a qualitative comparison of the measured strain maps showed a larger deformation zone is generated for lower blanking speeds. In addition, transverse orientation produced lower strain than the rolling direction regarding the applied of the direction of cutting line. This trend could be due to the increased plastic deformation and the time required for the material to flow around the cut edge. Also the grains orientations in a parallel direction to the cutting line led to increasing of the extent of deformation.

The Nano-indentation test was implemented for the thin sheet electrical steel material at the cut edges and vicinity area to identify the mechanical properties and show the distribution of residual stress on the sheared edge and the nearby area. It is known that there is a strong relationship between hardness and tensile strength [5]. Therefore, the deformation could be estimated based on the hardness results through the correlations between the indenter penetration depth and true contact area. Also, Nano-scale can allow the investigation to be conducted very close to the end of the cut edge. However, the high variability of the Nano-indentation measurements makes it difficult to pick out clear trends regarding process parameters.

Figures 4.30 to 4.33 showed that the local hardness of at the vicinity of the cut edge changes dramatically with values as high of about 6.5 to 3.5 Gpa at a distance of 100

microns from the cut edge where the value reached the average hardness of the bulk material. Such a large variation of the local hardness could be related to the strain hardening effect as the material experiences large plastic strains, showed by the DIC maps, as well as the presence of residual stresses around the plastically affected zones. The residual stresses affect the penetration load of the indenter and therefore the Nano-indentation measurements read higher values for the loading part of the curve. The obtained hardness profile could, therefore, be an indicator of residual stress depth as also reported in [3, 4].

However, the change in the hardness values between those close and far from the cut edge proved the influences the cutting-edge zone by the deformation resulting from the blanking process as shown in Nano-indentation results (Figures 4.30 and 4.32) . That because of the deformation can causes strain hardening and leads to increasing hardness values due to increased material resistance to the penetration of the indenter [103, 104]. As the higher values of hardness were observed concentrated near to the cut edge and widely distributed, that could lead to conclude that the impact of the plastically deformed zone on the mechanical properties is greater than that of the stressed area as shown in all obtained results. These results matched the finding by [5].

It is very difficult to identify the depth of the deformation area according to the hardness measurements because of the variations. However, the position of the stability of the hardness values regarding the general hardness value of the sheet could be considered as the end of the deformation. According to the current results, the size of the plastic deformation is varied between samples depending on the deformation condition. The average extension of deformation for 0.2 ES samples was reached to around 100 μm in most cutting cases and slightly less for 0.35 ES samples. Also, there is no clear trend to explain the effect of the rolling and transverse orientation regarding the hardness values

Moreover, in order to show the variation of hardness values at a specific distance from the cut edge regarding the blanking parameters, the average hardness values at distance between 25 to 30 μm for different samples as illustrated in Figure 4.31. A similar result was obtained to show the effect of the blanking parameters of 0.35 mm ES sheet thickness against the hardness values as illustrated in Figure 4.33. The figures illustrate proved the high variation of hardness results even at same position to the cut edge, however, the total DAZ is varying depending on the blanking condition and local grains condition.

5.6 The effects of blanking induced plastic deformation on magnetic properties

The link between the electrical steel material and the magnetic applications means that the edge deformation could directly correlates with the magnetic properties. It is already shown that the induced plastic deformation due to the blanking process causes residual stresses, thereby having a harmful effect on the magnetic properties of the material [113] and resulting in much larger B-H loops and a high energy loss [114]. These locked-in stress areas can affect the magnetizing process of the material and impair permeability and increase power loss [3,116]. In addition, dislocations of the crystal lattice are the major pinning centres for domain wall movement. Therefore, the increase of the dislocation density will cause more impeding of domain wall movement and result in a large increase in energy loss [54, 56].

It is already reported that the applied plastic deformation and locked-in stresses could increase the hysteresis losses [3] due to the higher amount of energy required to break the barrier developed by the induced dislocations [13] and magnetize the material. The effects of the blanking process on the magnetic properties were demonstrated through measuring the hysteresis loops of blanked samples at different cutting conditions applied in the current study. The hysteresis losses were calculated from loops for electrical steel samples by subtracting the absorbed energy from the dissipated energy [144, 145].

Figures 4.39 to 4.42 showed that for the applied cutting conditions the loops changes in way of its size which can indicate the affected magnetic properties by these changes in the cutting process and material conditions as reported in [114]. However, this could be considered with caution as there were not enough data points, due to the limitations of the applied technique to determine the full hysteresis loop, especially around the coercivity points. The changing in the cutting parameters can affect the size of the hysteresis loops in a complicated way due to the interaction between these parameters. For example, the increasing of the blanking speed could reduce the hysteresis loss as shown in Figure 4.43. Additionally, the effect of blanking speed is well visible in the graphs in which higher speed reduces the loss. This is well linked the aforementioned theory about the observed plastically deformation zone and the energy required for the blanking since the higher speeds induce less plastic deformation, therefore the magnetic domains are less disturbed, leading to reduced hysteresis losses.

The trend is also reported in the literature, according to [5, 63], the die clearance can lead to increase or decrease the stressed area and thereby affect the magnetic properties. Figure 5.1 shows the links between the calculated magnetic losses and the induced blanking-DIC strain of the same sample regarding the blanking speeds and material thickness. The figure illustrates a logical trend of hysteresis losses with the maximum measured strain by DIC, wherein higher losses are attributed to the larger measured strains. In addition, there is a proportional relation between the induced strain and the magnetic losses, or, in other words, when the strain is being increased, the hysteresis losses will increase as well. Also, it is noticeable that increasing the blanking speed can lead to the reduction of hysteresis losses because the induced deformation is less at high speed as shown in the DIC results.

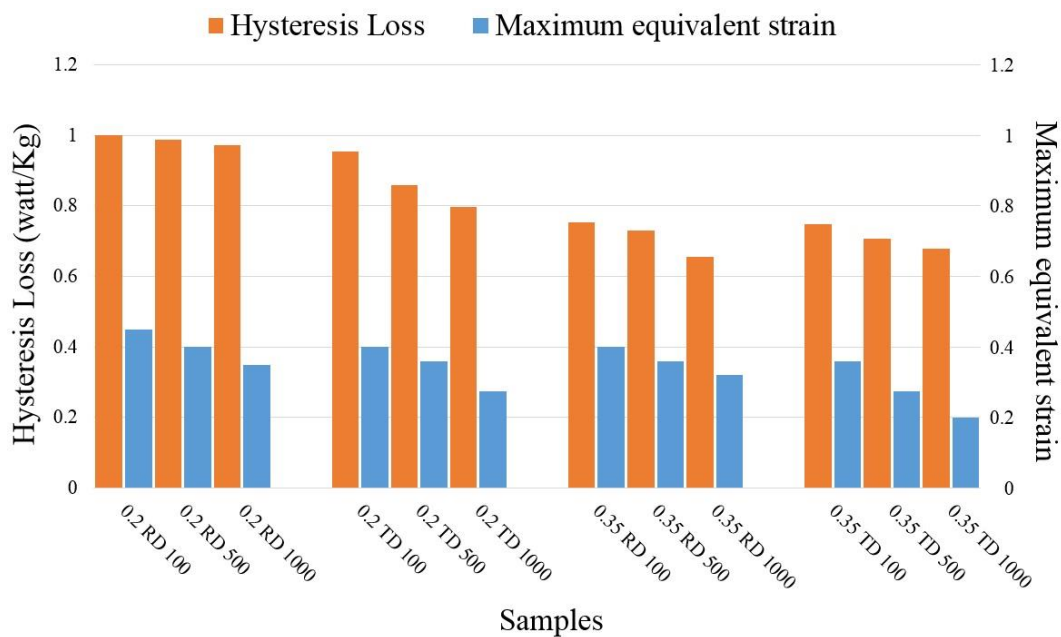


Figure 5.1: Magnetic hysteresis losses and the induced blanking strain regarding blanking conditions.

In addition, the figure shows that sheet thickness has a significant influence on the hysteresis losses and magnetic properties, where the hysteresis losses being higher at the low sheet thickness. Although the general known trend is that the thinner the sheet is better the magnetic properties [7, 30], and the power loss generally decreases at lower thickness because the eddy current loss component tends to decrease linearly with reducing the thickness [30, 31]. Contrary, the hysteresis losses component tends to increase with decreasing the sheet thickness [31]. This is because the hysteresis loss results due to the irreversible nature of the magnetization process of a magnetic material,

whereas the eddy loss occurs due to the currents flow in the opposite direction to the electromotive force (emf) induced in the material due to the magnetic field [29]. There is a discrepancy between the sum of hysteresis and classical eddy current loss when compared to the specific total loss in a material. This difference is due to anomalous losses [29].

Several factors appear to be responsible for the reductions in energy losses with decreasing thickness of ES sheet such as the change in the material's permeability. The other factor that could influence the energy loss of the thin sheet is the domain wall spacing on sample thickness because of reducing the grains number [32]. The increase in the number of domain walls because of the increase in grain boundaries along the length of the sheet (see Figure 3.17 for the flux flow path and Figure 4.65 for grains number along the ES sheets) with a lower thickness results in reduced domain wall velocity and thereby reducing the flow of magnetic flux and affect the magnetization process.

Moreover, the flux density is more intensive in the thinner sheets because the applied magnetic field is constant and the cross-sectional area is smaller. The losses are increased at high flux density [160].

According to Figure 4.44, the flux density in the thinner sheets is higher than the thicker one because the applied magnetic field is constant and the cross-sectional area is smaller for thin sheet. The high flux density can associate with a higher hysteresis loss as reported by [160]. This is due to the amount of flow flux density is related to the absorbed energy. The evidence for this is that when domain wall movement is high, the absorbed energy will be less and thereby the hysteresis loss is less. Conversely, deformation will lead to slow the domain wall movements, in consequence, more flux are needed to absorb more energy to overcome the constraints and thereby increase the dissipated energy and cause high loss [19].

5.7 Statistical Analysis

The results of the experimental tests can be analysed to obtain meaningful information through establishing the conditions in the process and estimating the contribution and significance of individual parameters and their interactions.

The statistical software Minitab 18 was used to analyse the results. Analysis of variance (ANOVA) was adopted to analyse experimental data to identify the important parameters, and the statistical results and ANOVA statistics (R-square, adjusted R-square, standard error) were examined to find out whether the model fits and is

acceptable. Usually, the ANOVA models are used with the design of experiments (DOE) to design and analyse cases that involve a response change as a function of one or more independent variables [161]. However, the current work only used the statistical model to analyse the obtained experimental results and not as a prediction model to determine the impact strength of outputs regarding the process conditions by linking the input variables with the results of one or more outputs [162].

5.7.1 Interaction between parameters and response

The input variables, also called parameters, are values that change and provide an output, and can be divided into quantitative and qualitative variables [163]. In the current study, the input variables are the cutting process and material conditions which comprises two electrical sheet thicknesses: 0.2 and 0.35 mm, two sheet orientations: RD and TD, and three blanking speeds: 100,500, 1000 mm/min, and one clearance 10% from the thickness. The response, meanwhile, is also the output variable of the experiment. The response of this study is the quantities of the cut edge properties and deformations. The interaction between parameters occurs when the response of one variable differs at different levels from that of another variable [163]. The goodness of the ANOVA model depends on the residual of the difference between the response value (the output variable) and the predicted value [163].

5.7.2 Analysis of Variance (ANOVA)

The analysis of variance (ANOVA) was used to determine the significance of cutting parameters on the cut edge deformation and properties results. ANOVA analysis includes terms such as [163]:

- The source: represents the main parameters (independent variables) and the interactions that have effects on the response (dependent variable).
- F-value: is a statistical test used to find out how close the parameter is with the dataset. The F critical value is around 4 of the slope of the normal distribution of data analysis. When the variable is smaller than 4, it is an insignificant factor. Conversely, the higher F-value indicates a significant effect [163].
- P-value: indicates whether the results are statistically significant. Therefore, it provides a clear and concise summary of the significance of the experimental

results. The range of the P-value is from 0 to 1. The confidence level or the significance level of the parameter interaction is considered as a significant factor when the P-value is less than the confidence level 5% [163].

- Standard deviation (S): is a function for measuring the goodness of the fit and is calculated in the units of the response. The standard error represents the average distance of the observed values from the fitted line. Thus, the smaller the value of the standard error, the closer the observations are to the line of best fit.
- R-squared (R-sq.): also known as the coefficient of determination and indicates the goodness of the data fit in the model and ranging from 0 to 100%. The model fit of the analyzed data becomes better when the R-squared is high. The adjusted R-squared (adj.-R-sq.) is used when the model is complex and has many independent variables that related to each other and it is always less than R-squared. While the predicated R-squared (pred.-R-sq.) is used to indicate the acceptance of the model fitting by predict responses for new observations data.

5.7.3 The impact strength of the maximum equivalent strain versus sheet thickness, blanking speed, and sheet orientation

Differentiation of the impact strength between variables of the blanking process was implemented to find out the strength of affected parameters such as sheet thickness, grain orientation, and blanking speed on the deformation outcomes. This differentiation could be employed in industry during the blanking process. Due to the few values and the simple model level, the general linear fitting statistical model was used in ANOVA analysis to find the relationship between all factors of the blanking process and material conditions for each response, including maximum strain, cutting force, the extension of deformation, and magnetic losses.

The statistical model was applied to investigate the effect strength of blanking and material factors on the induced equivalent strain of all electrical steel samples. Table 5.1 shows the model summary and information of factors effect on the induced strain values in the sheets during the blanking process. The analysis of variance shows that the effect of the grain orientation factor has a larger F-value (32.87), thereby it is considered to have a more significant effect than the other factors on the value of strain. Next is the blanking speed factor, while the least important factor is the thickness of the sheets. The table

summarizing the model illustrates that the model has good quality of fit due to the high value of R-squared components.

Table 5.1: ANOVA model for plastic strains versus blanking parameters.

Factor Information:				
Factor	Levels	Values	F-Value	P-Value
Sheet thickness	2	0.20, 0.35	11.66	0.011
Blanking speed	3	100, 500, 1000	29.35	0.000
Grain Orientation	2	RD, TD	32.87	0.001
Model Summary:				
	S	R-sq.	(adj.-R-sq.)	(pred.-R-sq.)
	2.36668	93.65%	90.02%	81.34%

The graph of ANOVA analysis to determine the tendency of the significant impact of cutting parameters on blanking strain is shown in [Figure 5.2](#). In such graphs, the higher slope expresses the significant effect of this factor. The mean value line passing through the mid-line of the plots illustrates good quality of the analysis model. The model results indicate that the effect of sheet orientation is greater than those of sheet thickness and blanking speed.

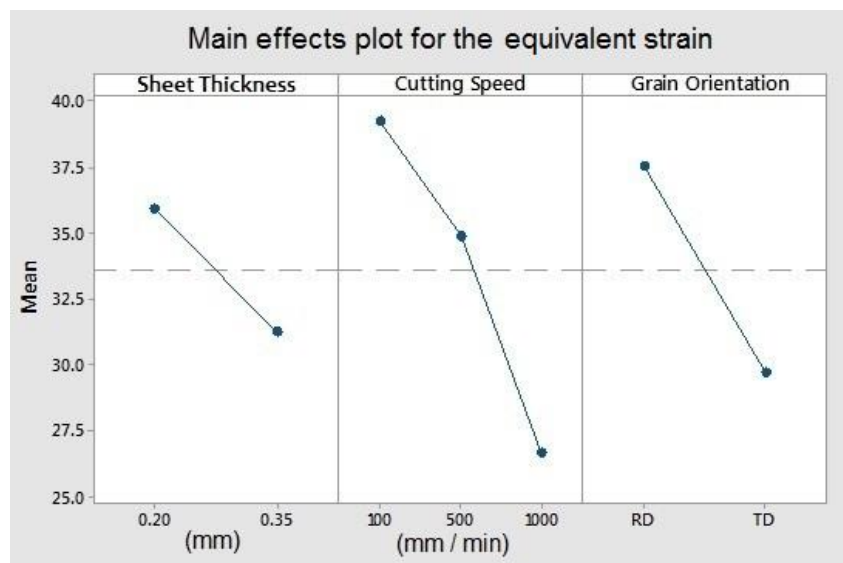


Figure 5.2: Effect of blanking and material factors on the induced equivalent strain.

5.7.4 The impact strength of the maximum cutting force of the full die versus sheet thickness, blanking speed, and sheet orientation

Table 5.2 shows the model summary and information of the impact of blanking and material parameters on the maximum measured cutting force values during the blanking process. The factor information shown in this model is the same as in the previous model due to the use of the same input parameters. The analysis of variance shows a higher F-value 36.8 for the blanking speed factor; thereby it is considered to have a more significant effect than the other factors on the cutting force value. This is followed by the sheet thickness factor with 27.53 F value, while grain orientation is not an important factor and does not affect the cutting force according to the very small F-value. The model summary also illustrates good quality of the model due to the high value of R-squared components.

Table 5.2: ANOVA model for the cutting force versus blanking parameters.

Factor Information:				
Factor	Levels	Values	F-Value	P-Value
Sheet thickness	2	0.20, 0.35	27.53	0.001
Blanking speed	3	100, 500, 1000	36.80	0.000
Grain Orientation	2	RD, TD	0.02	0.893
Model Summary:				
	S	R-sq.	(adj.-R-sq.)	(pred.-R-sq.)
	2.06688	93.53%	89.83%	80.98%

Figure 5.3 shows the stronger effect of blanking and material factors on the measured maximum cutting force values. The second part presents the effect of blanking speed on the force values; the sharp decline explains the significant effect of this factor. The level grain orientation slope reflects a very low effect. Also, the mean value line passing through the mid-line of the plots illustrates good quality of the analysis model.

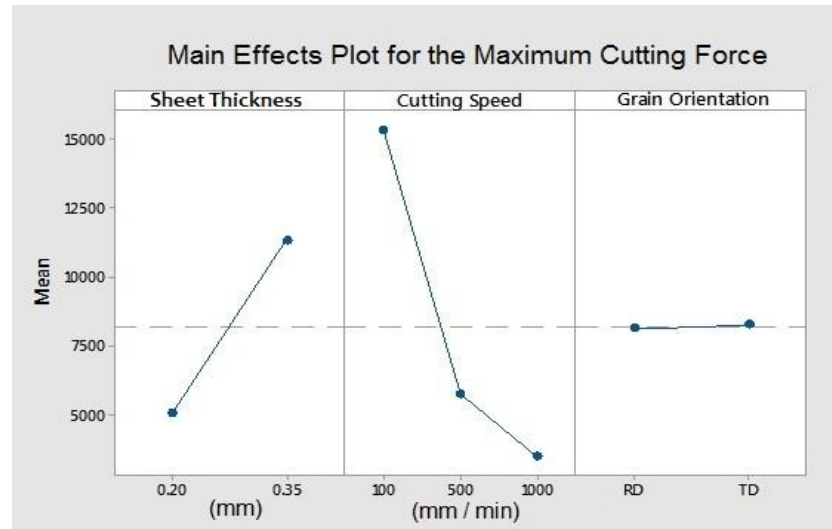


Figure 5.3: Effect strength of blanking and material factors on the induced cutting force.

5.7.5 The impact strength of the maximum hysteresis loss versus thickness, blanking speed, sheet orientation

Table 5.4 shows the model summary and information of blanking and material parameters on the maximum hysteresis losses values calculated for blanking samples using magnetic SST test. The factor information shown in the model is the same as that in the previous model due to use of the same input parameters. The analysis of variance shows a larger F-value (67.59) of the sheet thickness factor; thereby it is considered to have a more significant effect than the other factors on the value of cutting force, followed by the grain orientation factor. The least effective factor is blanking speed.

Table 5.3: ANOVA model for the hysteresis losses versus blanking parameters.

Factor Information:				
Factor	Levels	Values	F-Value	P-Value
Sheet thickness	2	0.20, 0.35	67.59	0.000
Blanking speed	3	100, 500, 1000	3.74	0.079
Grain Orientation	2	RD, TD	4.99	0.061
Model Summary:				
	S	R-sq.	(adj.-R-sq.)	(pred.-R-sq.)
	0.045531	91.96%	87.36%	76.37%

Figure 5.4 shows the impact strength of blanking and material factors on the calculated maximum hysteresis losses values. The first part presents the effect of sheet thickness on mean hysteresis losses values. The factor has a sharp slope which explains the significant effect of this factor, while convergence between the slopes of blanking speed and grain orientation reflects convergence in the strength level of the effect. The mean value line passing through the mid-line of the plots illustrates good quality of the analysis model.

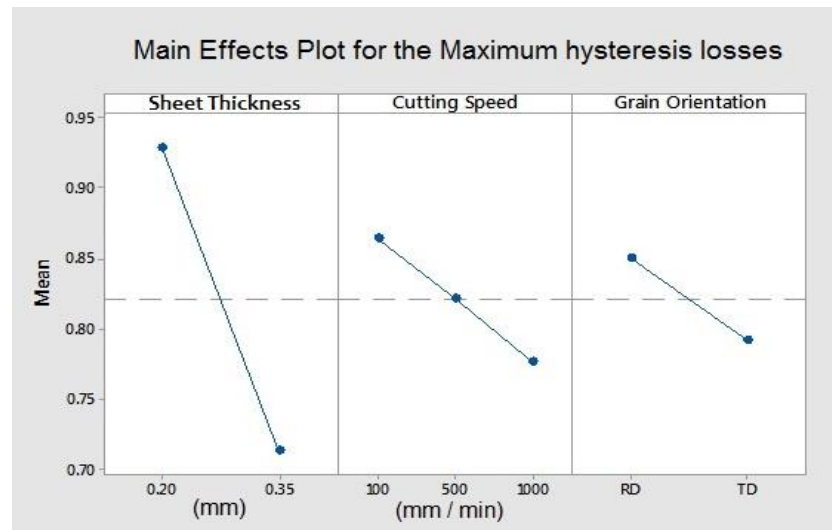


Figure 5.4: Effect strength of blanking and material factors on the hysteresis losses.

Table 5.5 summarizes the strength effects of the blanking parameters on the blanking results according to the calculated F-Value of the statistical model. The results show that the blanking speed plays an important role in all blanking results. There are variations in effect between the input and output parameters, therefore it is difficult to achieve optimization between these factors.

Table 5.4: Summary of ANOVA models of the factors' impact strength on the blanking results

Results \ Factor	Sheet thickness	Blanking speed	Sheet Orientation
Max. equivalent strain	**	**	***
Max. cutting force	**	***	*
Max. hysteresis loss	***	**	**
*** Very important factor, ** Important factor, * Not important factor			

5.8 Summary

This chapter has discussed the results produced on the cut edge deformation of NGO electrical steel sheets and linked some of the most important results regarding the changes induced during the blanking process. The deformation features of each sample were characterized and an ANOVA statistical analysis model was applied to investigate the strength of the affected parameters of the blanking process and material conditions. Material behaviour was discussed in each case to give a description of the cut edge deformation and characterize the blanking induced magneto-mechanical and modified edge texture of the cut edge defects in non-oriented electrical steel. Also, the most critical issues affecting the stage of blanking deformation were also discussed including grains conditions at the cut edge and the limitations associated with the testing techniques.

6

Conclusions and future works

6.1 Conclusions

In this study, the effect of the blanking operation on the local magnetic and mechanical properties and local deformation at the cut edge and vicinity area of the non-grain orientation electrical steels thin sheet has been experimentally investigated. The cutting process conditions were two thin sheets of thicknesses 0.2 and 0.35 mm, about 10% clearance between the punch and die, three blanking speeds of 100, 500, and 1000 mm/min, and two grain orientations of ES sheet, in rolling and transverse directions. These conditions were chosen to produce different cut samples. Then, samples were tested using different methods including tensile tests, digital image correlation technique during both blanking and tensile testing, and Nano-Indentation was used to evaluate the mechanical properties. SEM and optical microstructure examinations allowed evaluation of the integrity of the structure. The magnetic single sheet tester was used to investigate the magnetic properties.

Based on work conducted, the data collected from these tests, the main conclusions are drawn as follows:

- According to the microstructure examinations, there are a small number of grains across the thickness of the sheet around 2 to 3 grains because of the low sheet thickness. Therefore, the cut edge deformation was heavily influenced by the local grains' location and size at the cut edge leading to the high variation in the results. Also, this can indicate that grain size and location play the key roles in deformation extension. Thereby, the sample to sample variability is very high and the effects of blanking parameters are therefore too difficult to determine.
- Generally, the methods used in this study are effective, but the efficiency of their results depends on the conditions of the process applied to it. Thereby, due to the sensitivity of applying these techniques on the blanking process of thin sheets involving many challenges, errors, and limitations. Therefore, the maximum possible accuracy of performed tests for the investigation and analysis should be taken into account in order to minimize results errors.
- The results demonstrated that blanking and material parameters had a significant effect on the cut edge quality. However, the high variation in the results means any investigation in the blanking deformation on thin sheets representing one of the possible deformation cases. In other words, the obtained results in each case cannot be generalized on the general behaviour of the material. Therefore, it is preferred to avoid comparisons and each test treated individually.
- The current design of blanking dies produced good edge geometry of the cut edge. This cut edge had different characteristics at different cutting conditions. That can indicate the influencing of the process parameters such as the blanking speed, sheet thickness and grain orientation. The impact strength of these conditions varies according to the type of deformation.
- According to the results of blanking force measurement, sheet orientation has little influence, while blanking speed has a significant impact on the cutting load, with higher force recorded at the lower speed of 100 mm/min.

- The measurements of the local strains distribution on the cut edge using the digital image correlation (DIC) technique enabled to investigate and visualize the mechanism of the high-speed blanking operation in a thin sheet of ES. However, the analysis process of induced blanking strain using this technique includes many issues that could affect the analysis results. For examples, the difficulty in the triggering, timing of DIC image acquisition at a specific moment of blanking process. Moreover, the spatial resolution of captured images led to the analysis error because of the small deformation zone and high speed of punch movement.
- The Nano- indentation test is usually used to indicate stresses and strains induced in the deformed areas. Although the results for applying hardness test on the blanking process showed very high values close to the cut edge then reducing with increasing distance from the edge. However, the variability of the Nano-indentation measurements makes it impossible to pick out clear trends with process parameter.
- The magnetic properties deteriorated due to the blanking effects caused by changes in the domain structure and divergence between domain walls due to the dislocations deformations. The results show that sheet thickness has a significant influence on the hysteresis losses and magnetic properties. Despite the higher thickness of the 0.35 mm samples, the hysteresis losses were less than for the low sheet thickness of 0.2 mm. Moreover, there is a clear impact for the blanking speed on the hysteresis losses, where the cutting at high-speed can reduce this magnetic loss.

6.2 Recommendations for future work

Further investigations could be conducted to carry out related work that we did not have time to do. These investigations could focus on the cutting process or the methods for characterization of mechanical and magnetic properties, or even quantifying the deformation of the cut edge and vicinity area. Although the current study produced positive results, the results could be enhanced and more precise results produced by carrying out additional work. These works could provide details to supplement the current

study results. The following proposals present some main points of interesting ideas aligned with the current research that could provide a starting point for future studies:

- Experiments could be conducted using a different selection of electrical sheet thicknesses, for example, 0.1 and 0.5 mm, to establish the effect of sheet thickness on the cut edge deformation.
- The blanking process could be implemented with different clearances between the die and the punch to investigate the effect of small and large clearance on the deformation zone.
- Magnetic single sheet tests could be performed by applying AC power supply for the purpose of comparison with the current results and the test could be conducted using different current frequencies.
- Electron Backscatter Diffraction (EBSD) could be used to observe the grain orientation, grain morphology and the crystal deformation at the edge zone.
- Finite element analysis models in 2D or 3D could be tested under the flux field condition to investigate the effect of the cut edge on the magnetic properties for a wide range of blanking variables, such as clearance, tools edge, sheet thickness, which might be difficult to carry out using experimental procedures.
- Development of a damage-failure model for the blanking process to predict magneto-mechanical damage at the cut edge and investigate the interaction of multiple variables of the blanking process.
- Different types and grades of electrical steel material could be used, such as oriented electrical steel or different types of coating layer.
- The blanking process could be carried out using a lubricant during the operation or under a different heat condition (higher than the room temperature but below the recrystallization temperature).

It might be useful for future researchers to take into consideration the following challenges and limitations that were faced during this study:

- The blanking process occurs in a closed and tiny area, especially in the case of the thin sheets, which makes it difficult to access the deformation zone during the process.
- The variation of cut edge deformation increases the difficulty of conducting precise evaluation. Also, testing and analysis in the current study were made more difficult by the fact that all tests were conducted in a specific area at the end of the cut edge.
- The very small differences between the cases of the study made it difficult to distinguish them easily and increased the required accuracy of the tests.
- Expansion of investigation into blanking parameters is very difficult experimentally. For example, using different clearance between the punch and die means manufacturing more dies. Because two sheet thicknesses were used, two more dies for each additional clearance were required. Therefore, there were higher cost and time requirements due to the doubling of all tests.
- Conducting sensitive edge tests meant the procedures had to be more sophisticated, starting from taking samples from the blanking die, and then cold mounting with highly precise identifying of the position of the cut edge.
- Because the material is very sensitive to water it is very hard to prepare samples with less than 1μ surface roughness. Moreover, to keep the cut edge safe from thermal stresses and high-pressure effects it was necessary to use cold mounting with conductive gold coating and silver paint to enhance the sample surface's conductivity in order to obtain high quality SEM images.

References

- [1] Wei Tong, "Mechanical Design of Electric Motors," Radford, Virginia. 2014
- [2] AK Steel, "Selection of Electrical Steels for Magnetic Cores," Elements, pp. 1–28, 2007.
- [3] P. Beckley, "Electrical Steels for rotating machines." Institution of Engineering and Technology, London, 2002.
- [4] T. Altan, A.E. Tekkaya, "Sheet metal forming processes and applications," ASM International, ISBN-10: 0-61503-844-2, 2012.
- [5] S Kalpakjian and S R Schmid, Manufacturing engineering and technology, sixth edition, Pearson education, Inc. 2010.
- [6] D. Jiles, "Introduction to Magnetism and Magnetic Materials," First edition 1991
- [7] D. S. Petrovi, "Non-Oriented Electrical Steel Sheets," vol. 44, pp. 8, 2010.
- [8] S. Tumanski, "Hand book of magnetic measurements," Taylor and Francis group, 2011.
- [9] Vander Voort and W. Baldwin, "Metallography and Microstructures Handbook," ASM Int., vol. 9, p. 2733, 2004.
- [10] B. Frederic, W. Thierry, and F. Hervé, "The use of iron-nickel and iron-cobalt alloys in electrical engineering, and especially for electrical motors," EEIC 2007, pp. 394–401, 2007.
- [11] J. M. D. Coey, "Magnetic materials," J. Alloys Compd., vol. 326, no. 1–2, pp. 2–6, 2001.
- [12] <http://www.dfliq.net/optimizing-electrical-motor-efficiency> and [http:// www.eilamination.com/tag/silicon-steel-lamination](http://www.eilamination.com/tag/silicon-steel-lamination).
- [13] C. Schayes, "Low cycle fatigue of the Fe-3Si steel: damage mechanisms and strain localisation by EBSD," p. 206, 2016.
- [14] W. M. Arshad et al., "Incorporating Lamination Processing and Component Manufacturing in Electrical Machine Design Tools," 2007 IEEE Ind. Appl. Annu. Meet, pp. 94–102, 2007.
- [15] H. Baker, ASM handbook, Alloy Phase Diagrams. Int., vol. 3, p. 1741, 1998.
- [16] B. L. Bramfitt and A. o. Benschoter, Metallographer's Guide - Practices and Procedures for Irons and Steels. 2002.
- [17] D. Steiner Petrovic, B. Markoli, and M. Ceh, "The nanostructure of non-oriented electrical steel sheets," J. Magn. Magn. Mater, vol. 322, no. 20, pp. 3041–3048, 2010.
- [18] <https://cogent-power.com/products>, grain-oriented, non-oriented -electrical-steel.
- [19] K. Atallah, "Iron losses in brushless permanent magnet DC-machine," 1993.
- [20] D. Fang, F. Li, B. Liu, Y. Zhang, J. Hong, and X. Guo, "Advances in Developing Electro-mechanically Coupled Computational Methods for Piezoelectric /Ferroelectrics at Multi-scale," Appl. Mech. Rev., vol. 65, no. 6, p. 060802, 2013.

- [21] Roy A. Colclaser, S. D.-N. Materials and Devices for electrical engineer and physicists. Network: McGraw-Hill 1985.
- [22] A. Hubert, R. Schafer, "Magnetic domains, the analysis of magnetic microstructures," 1998.
- [23] V. Permiakov, "1D and 2D Magnetization in Electrical Steels under Uniaxial Stress," ISBN 90-8578-022-5, NUR 961, 967, 2005.
- [24] D. Jiles, Introduction to Magnetism and Magnetic Materials, Chapman & Hall, 1991.
- [25] Springer handbook of materials measurement methods, vol. 9, no. 7–8. 2006.
- [26] H. Kronmuller and S. Parkin, "Handbook of Magnetism and Advanced Magnetic Materials, Volume 1: Fundamentals and Theory," John Wiley & Sons, Ltd. ISBN: 978-0-470- 02217-7, 2007.
- [27] A. Krings, J. Soulard, "Overview and Comparison of Iron Loss Models for electrical Machines," J. Electrical. Eng., vol. 10, pp. 162–169, 2010.
- [28] Reuben Lee, "Electronic Transformers and Circuits - Core Materials," Fast Spectr. React, vol. 9781441995, pp. 1–9, 2012.
- [29] S. Ramanathan, "Study of dislocations from continuous flattening anneal and its effect on magnetic properties of grain oriented electrical steel," thesis," 2013.
- [30] S. D. Washko, R. F. Miller, "Sheet thickness effects on energy losses in 3% silicon-iron," J. Magnetism. Magnetic. Material, vol. 19, no. 1–3, pp. 361–364, 1980.
- [31] K. Takeda and T. Yamaguchi, "Magnetic properties in thinned oriented Si-Fe sheet," IEEE transactions on magnetics, VOL.MAG-23, NO. 5, pp. 3233–3235, 1987.
- [32] P. W. Neurath, "Hysteresis and Eddy Losses in Silicon Iron as a Function of Sheet Thickness," J. Appl. Phys., vol. 30, no. 4, pp. S88–S89, 1959.
- [33] J. Barranger, "Hysteresis and eddy current losses of a transformer lamination," NASA, TN D-3114, Lewis Research Centre, E-2992, November 1965, 2018.
- [34] M. Mikulec, "Accuracy of single sheet testers," vol. 112, pp. 112–114, 1992.
- [35] B. Naas, D. Hachi, H. Hammache, B. Naas, and D. Moussaoui, "Measurement of the Magnetic Field in the Single Sheet Tester 500 * 500 mm²," no. 3, pp. 58–61, 2014.
- [36] J. P. Schlegel, N. J. Batistela, N. Sadowski, J. P. A. Bastos, M. Rigoni, A. A. De Espíndola, and L. V. Dokonal, "Testing strategies to evaluate non-oriented electrical steels losses," J. Microwaves, Optoelectron. Electromagn. Appl., vol. 11, no. 2, pp. 304–315, 2012.
- [37] Elemír Ušák, Jan Bydžovský, Volodymyr Stoyka, František Kováč "ANALYSIS OF CAPABILITIES OF SMALL DOUBLE-YOKE SINGLE SHEET TESTER," vol. 59, no. 7, pp. 21–24, 2008.
- [38] T. Nakata, N. Takahashi, K. Fujiwara, and M. Nakano, "Study of horizontal-type single sheet testers," J. Magn. Magn. Mater, vol. 133, no. 1–3, pp. 416–418, 1994.

- [39] N. Takahashi, D. Miyagi, F. Inoue, and M. Nakano, "Novel measurement method of DC magnetic properties having freedom of specimen shape," *J. Appl. Phys.*, vol. 109, no. 7, pp. 1–4, 2011.
- [40] M. Enokizono, H. Matsuo, "A measurement system for 2D DC-biased properties of magnetic materials," *Journal of Magnetism and Magnetic Materials* 254–255, 39–42, 2003.
- [41] N. Takahashi et al. "Development of the 2D single sheet tester using diagonal exciting coil and the measurement of magnetic properties of GO electrical steel sheet, *IEEE transactions of magnetics*, Vol 47, 2011.
- [42] J.R. Duflou, and W. Dewulf, "On the complementarity of TRIZ and axiomatic design," *Procedia Engineering*, 9, pp.633–639, 2011.
- [43] S.P. Bhise, and M.Y. Shinde, "Study of Process Parameters Used in Wire-electric Discharge Machining," *IJRASET journal*, volume 4, pp.485–489, 2016.
- [44] M. F. Handbook and S. B. Heidelberg, "Metal Forming Handbook," vol. 3, and no. c. 1998.
- [45] P. P. Badgujar and M. G. Rathi, "Abrasive Waterjet Machining-A State of Art," *J. Mech. Civil Eng.*, vol. 11, no. 3, pp. 59–64, 2014.
- [46] Y. Demir, O. Ocak, Y. Ulu, and M. Aydin, "Impact of lamination processing methods on the performance of permanent magnet synchronous motors," *Int. Conf. Electrical. Mach.*, pp. 1218–1223, 2014
- [47] S. Bayraktar and Y. Turgut, "Effects of different cutting methods for electrical steel sheets on performance of induction motors," *Proc. Inst. Mech. Eng. Part B J. Engineering Manufacturing*, 2016.
- [48] V. Manescu, G. Paltanea, and H. Gavrilă, "Some Important Effects of the Water Jet and Laser cutting methods on the Magnetic Properties of the Non-oriented Silicon Iron Sheets," *ATEE*, pp.451-455, 2015.
- [49] Y. Kurosaki, H. Mogi, H. Fujii, T. Kubota, and M. Shiozaki, "Importance of punching and workability in non-oriented electrical steel sheets," , vol. 320, pp. 2474–2480, 2008.
- [50] H. Naumoski, B. Riedmüller, A. Minkow, and U. Herr, "Investigation of the influence of different cutting procedures on the global and local magnetic properties of non-oriented electrical steel," *J. Magn. Mater.*, vol. 392, pp. 126–133, 2015.
- [51] S. Steentjes, G. Von Pflingsten, and K. Hameyer, "An application-oriented approach for consideration of material degradation effects due to cutting on iron losses and magnetizability," *IEEE Trans. Magn.*, vol. 50, no. 11, pp. 2–5, 2014.
- [52] T. Bulín, E. Svabenska, M. Hapla, C. Ondrusek, and O. Schneeweiss, "Magnetic properties and structure of non-oriented electrical steel sheets after different shape processing," *Acta Phys. Pol. A*, vol. 131, no. 4, pp. 819–821, 2017.

- [53] R. Siebert, J. Schneider, and E Beyer, "Laser Cutting and Mechanical Cutting of Electrical Steels and its Effect on the Magnetic Properties," *IEEE transactions on magnetics*, pp. 2001904, VOL. 50, 2014.
- [54] A. Belhadj, et al. "Effect of laser cutting on microstructure and on magnetic properties of grain non-oriented electrical steels," vol. 256, no. 5, pp. 20–31, 2003.
- [55] M. Emura, F. J. G. Landgraf, W. Ross, and J. R. Barreta, "The influence of cutting technique on the magnetic properties of electrical steels," *J. Magn. Magn. Mater*, vol. 254-255, pp. 358–360, 2003.
- [56] G. Paltanea, and G. Horia, "The effect of mechanical and electrical discharge cutting technologies on the magnetic properties of non-oriented silicon iron," 2017.
- [57] E. G. Araujo, et al. , "Dimensional Effects on Magnetic Properties of Fe–Si Steels due to Laser and Mechanical Cutting," *IEEE*, VOL. 46, pp213-216, 2010.
- [58] P. Lazari, K. Atallah, and J. Wang, "Effect of Laser Cut on the Performance of Permanent Magnet, Assisted Synchronous Reluctance Machines," vol. 51, no. 11, 2015.
- [59] G. Loisos and A. J. Moses, "Effect of mechanical and Nd:YAG laser cutting on magnetic flux distribution near the cut edge of non-oriented steels," *J. Mater. Process. Technol.*, vol. 161, no. 1–2 SPEC. ISS, pp. 151–155, 2005.
- [60] P. Baudouin, A. Belhadj, F. Breaban, A. Deffontaine, and Y. Houbaert, "Effects of Laser and Mechanical Cutting Modes on the Magnetic Properties of Low and Medium Si Content Non-oriented Electrical Steels," *Magn. Int. Conf.*, vol. 38, no. 5, pp. 3213–3215, 2002.
- [61] M.P. Groover, "Fundamentals of Modern Manufacturing, Materials, Processes and Systems," 4th edition, John Wiley & Sons, Inc. 2010
- [62] J R Paquin, R E Crowley, *Die design fundamentals*, Second edition, industrial press, Inc. 1987.
- [63] S.L. Semiatin, *Forming and Forging*, ASM Handbook, Volume 14 of the 9th Edition Metals Handbook, 1993.
- [64] V. Boljanovic, "Sheet metal forming processes and die design," *Technol. Eng.*, 2nd edition, industrial press Inc. 2014.
- [65] E. Al-Momani, I. Rawabdeh "An Application of Finite Element Method and Design of Experiments in the Optimization of Sheet Metal Blanking Process" *JJMIE*, *Jordan Journal of Mechanical and Industrial Engineering*, V2, N1, ISSN 1995-6665, P53 -63, 2008.
- [66] R. Hambli, "Design of experiment based analysis for sheet metal blanking processes optimisation," *Int. J. Adv. Manuf. Technol.*, vol. 19, no. 6, pp. 403–410, 2002.
- [67] C. Husson, Correia, J. P. M., Daridon, L., & Ahzi, S "Finite elements simulations of thin Copper sheets blanking: Study of blanking parameters on sheared edge quality. *Journal of Materials Processing Technology*, 199(1-3), 74-83, 2008.

- [68] R. Wiedenmann, Sartkulvanich, P., & Altan, T. "FEA on the effect of sheared edge quality in blanking upon hole expansion of advanced high strength steel" IDDRG 2009.
- [69] S. Subramonian, T. Altan, B. Ciocirlan, and C. Campbell, "Optimum selection of variable punch-die clearance to improve tool life in blanking non-symmetric shapes," *Int. J. Mach. Tools Manuf.*, vol. 75, pp. 63–71, 2013.
- [70] S. K. Maiti, A. A. Ambekar, U. P. Singh, P. P. Date, and K. Narasimhan, "Assessment of the influence of some process parameters on sheet metal blanking," *J. Mater. Process. Technol.*, vol. 102, no. 1–3, pp. 249–256, 2000.
- [71] A. I. O. Zaid, "Blanking and piercing theory, applications and recent experimental results," *IOP Conf. Ser. Mater. Sci. Eng.*, vol. 60, p. 012065, 2014.
- [72] K. H. Shim, S. K. Lee, B. S. Kang, and S. M. Hwang, "Investigation on blanking of thin sheet metal using the ductile fracture criterion and its experimental verification," *J. Mater. Process. Technol.*, vol. 155–156, no. 1–3, pp. 1935–1942, 2004.
- [73] A. M. Goijaerts, L. E. Govaert, and F. P. T. Baaijens, "Evaluation of ductile fracture models for different metals in blanking," *J. Mater. Process. Technol.*, vol. 110, pp. 312–323, 2001.
- [74] F. Gréban, G. Monteil, and X. Roizard, "Influence of the structure of blanked materials upon the blanking quality of copper alloys," *J. Mater. Process. Technol.*, vol. 186, pp. 27–32, 2007.
- [75] J. Qin, P. Yang, W. Mao, and F. Ye, "Punchability and Punching Fracture Behavior of High Silicon Steel Sheets," *J. Iron Steel Res. Int.*, vol. 22, no. 9, pp. 852–857, 2015.
- [76] J. Xu, B. Guo, C. Wang, and D. Shan "Blanking clearance and grain size effects on micro deformation behavior and fracture in micro-blanking of brass foil" *International Journal of Machine Tools and Manufacture*, V60, Pages 27-34, 2012.
- [77] B. Y. Joo, S. H. Rhim, S. I. "Micro-hole fabrication by mechanical punching process, *Journal of Materials Processing Technology* 170 (3), 593–601, 2005.
- [78] J. Xu, B. Guo, D. B. Shan, Size effects in micro blanking of metal foil with miniaturization, *International Journal of Advanced Manufacturing Technology* 56, P5–8, 515–522, 2011.
- [79] D. Zakariya Lubis and M. Mahardika "Influence of Clearance and Punch Velocity on the Quality of Pure Thin Copper Sheets Blanked Parts" *Materials Science and Engineering* 157, 012012 doi:10.1088/1757, 2016.
- [80] P. Demmel, H. Hoffmann, R. Golle, C. Intra, and W. Volk, "Interaction of heat generation and material behaviour in sheet metal blanking," *CIRP Manufacturing Technology* 64, 249–252, 2015.
- [81] S. Subramonian, T. Altan, C. Campbell, and B. Ciocirlan, "Determination of forces in high speed blanking using FEM and experiments," *Journal of Materials Processing Technology* 213, 2184–2190, 2013.
- [82] T. A. C. Stock and A. L. Wingrove, "The energy required for high speed shearing of steel," *Journal of mechanical engineering science*, Vol. 13 No 2, pp 110-115, 1971.

- [83] H. Marouani, A. Ben Ismail, E. Hug, M. Rachik” Rate-dependent constitutive model for sheet metal blanking investigation” *Materials Science and Engineering*, 162–170, 2008.
- [84] Grunbaum et al, Influence of high cutting speeds on the quality of blanked parts. Report No. ERC/NSM- S-96-19, Centre for Precision Forming, Columbus, 1996.
- [85] M Hirsch, P Demmel, R Golle, and H Hoffmann” Light Metal in High-Speed Stamping Tools. *Key Engineering Materials*, 473, 259-266, 2011.
- [86] A. M. Goijaerts, “Prediction of Ductile Fracture in Metal Blanking,” The Eindhoven University of Technology, doctoral thesis 1999.
- [87] C. Gaudilliere, N. Ranc, A. Larue, A. Maillard, and P. Lorong, “High Speed Blanking: An Experimental Method to Measure Induced Cutting Forces,” *Exp. Mech.*, vol. 53, no. 7, pp. 1117–1126, 2014.
- [88] M. Grunbaum, J. Breitling, and T. Altan, “Influence of high blanking speeds on the quality of blanked parts,” *ERC Rep.*, pp. 5–96, 1996.
- [89] S. Krrabaj, B. Bytyqi, and H. Osmani, “Influence of Blanking speed on the Quality of Blanked Parts,” *15th Int. Research Mach. Assoc. Technol.*, no. September, pp. 817–820, 2011.
- [90] X. Chen, X. Xie, J. Sun, and L. Yang, “Full Field Strain Measurement of Punch-stretch Tests Using Digital Image Correlation,” *SAE Int. J. Mater. Manuf.*, vol. 5, pp. 345–351, 2012.
- [91] T. J. Liutkus, “Digital Image Correlation in Dynamic Punch Testing and Plastic Deformation Behavior of Inconel 718,” 2014.
- [92] S. Daly, “Principles and Techniques of Digital Image Correlation,” *Microsc. Microanal.* vol. 17, no. S2, pp. 1946–1947, 2011.
- [93] S. Yoneyama, “Basic principle of digital image correlation for in-plane displacement and strain measurement,” *Adv. Compos. Mater.*, vol. 3046, no. February, pp. 1–19, 2016.
- [94] B. Pan, J. Yuan, Y. Xia, “Strain field denoising for digital image correlation using a regularized cost-function,” *Optics and Lasers in Engineering* 65 pp9-17, 2015.
- [95] L. Yang, L. Smith, a. Gothekar, and X. Chen, “Measure Strain Distribution Using Digital Image Correlation (DIC) for Tensile Tests,” pp. 1–27, 2010.
- [96] A. M. Goijaerts, Y. W. Stegeman, L. E. Govaert, D. Brokken, W. A. M. Brekelmans, and F. P. T. Baaijens, “Can a new experimental and numerical study improve metal blanking?,” *J. Mater. Process. Technol.*, vol. 103, no. 1, pp. 44–50, 2000.
- [97] V. Rratus, F. Kosel, and M. Kovac, “Determination of optimal cutting edge geometry on a stamped orthotropic circular electrical steel sheet,” *J. Mater. Process. Technol.*, vol. 210, no. 2, pp. 396–407, 2010.
- [98] J. Slavic, S. Bolka, V. Bratus, and M. Boltezar, “A novel laboratory blanking apparatus for the experimental identification of blanking parameters,” *J. Mater. Process. Technol.*, vol. 214, no. 2, pp. 507–513, 2014.

- [99] K. Wang and T. Wierzbicki, "Experimental and numerical study on the plane-strain blanking process on an AHSS sheet," *Int. J. Fract.*, vol. 194, no. 1, pp. 19–36, 2015.
- [100] Y. H. Wang et al., "Whole field sheet-metal tensile test using digital image correlation," vol. 34, no. 2, pp. 54–59, 2010.
- [101] N. Leuning, S. Steentjes, M. Schulte, W. Bleck, K. Hameyer, "Effect of elastic and plastic tensile mechanical loading on the magnetic properties of NGO electrical steel" *Journal of Magnetism and Magnetic Materials* 417, 42–48, 2016.
- [102] F. J. G. Landgraf, "Nonoriented electrical steels," *Jom*, vol. 64, no. 7, pp. 764–771, 2012.
- [103] V. E. Iordache and E. Hug "Effect of mechanical strain on the magnetic properties of electrical steel," *J. Opto. Electron Adv. Mater.*, vol. 6, no. 4, pp. 1297–1303, 2004.
- [104] M. Fukuhara, T. Yonamine, F. J. G. Landgraf, and F. P. Missell, "Evolution of magnetic properties and crystallographic texture in electrical steel with large plastic deformation," *J. Appl. Phys.*, vol. 109, pp. 23–26, 2011.
- [105] F. J. G. Landgraf, M. Emura, K. Ito, and P. S. G. Carvalho, "Effect of plastic deformation on the magnetic properties of non-oriented electrical steels," , vol. 215, pp. 94–96, 2000.
- [106] J.M. Makar and B.K. Tanner, "The effect of plastic deformation and residual stress on the permeability and magnetostriction of steels" *Journal of Magnetism and Magnetic Materials* 222-304, 2000.
- [107] J.M. Makar and B.K. Tanner, "The effect of stresses approaching and exceeding the yield point on the magnetic properties of high strength pearlitic steels" *NDT&E International*, Vol. 31, No. 2, pp. 117-127, PII: SO963-8695(97)OOOO8-X, 1998.
- [108] V. G. Kuleev, T. P. Tsar'kova, E. Yu. Sazhina, and A. S. Doroshek, "The Influence of Plastic Deformations of Low Carbon Ferromagnetic Steels on the Changes in the Shapes of Their Hysteresis Loops and the Field Dependences of the Differential Permeability," *Journal of Nondestructive Testing*, Vol. 51, No. 12, pp. 738–749, 2015.
- [109] A. Schoppa, J. Schneider, and C. D. Wuppermann, "Influence of the manufacturing process on the magnetic properties of non-oriented electrical steels," , vol. 215, pp. 74–78, 2000.
- [110] D. Singh, A. Belahcen, and A. Arkkio, "Effect of Manufacturing on Stator Core Losses," pp. 106-110.
- [111] K. Senda, M. Ishida, Y. Nakasu, and M. Yagi, "Influence of shearing process on domain and magnetic properties of non-oriented electrical steel," vol. 304, pp. 513–515, 2006.
- [112] A. Peksoz, S. Erdem, and N. Derebasi, "Mathematical model for cutting effect on magnetic flux distribution near the cut edge of non-oriented electrical steels," *Comput. Mater. Sci.*, vol. 43, no. 4, pp. 1066–1068, 2008.
- [113] A. Kedous-Lebouc, B. Cornut, J. C. Perrier, P. Manfé, and T. Chevalier, "Punching influence on magnetic properties of the stator teeth of an induction motor," *J. Magn. Magn. Mater.*, vol. 254–255, pp. 124–126, 2003.

- [114] A. J. Moses, N. Derebasi, G. Loisos, and A. Schoppa, "Aspects of the cut-edge effect stress on the power loss and flux density distribution in electrical steel sheets," *J. Magn. Magn. Mater.*, vol. 215, pp. 690–692, 2000.
- [115] A. Schoppa, J. Schneider, and J. Roth, "Influence of the cutting process on the magnetic properties of non-oriented electrical steels," , vol. 216, pp. 215–217, 2000.
- [116] R. Rygal et al., "Influence of cutting stress on magnetic field and flux density distribution in non-oriented electrical steels," *J. Magn. Magn. Mater.*, vol. 215–216, pp. 687–689, 2000.
- [117] H. A. Weiss et al., "Influence of shear cutting parameters on the electromagnetic properties of non-oriented electrical steel sheets," *J. Magn. Magn. Mater.*, vol. 421, pp. 250–259, 2017.
- [118] H. Cao et al., "The influence of punching process on residual stress and magnetic domain structure of non-oriented silicon steel," *J. Magn. Magn. Mater.*, vol. 406, pp. 42–47, 2016.
- [119] Wego Wang, "Reverse engineering, technology of reinvention," Taylor and Francis Group, LLC, 2011
- [120] E. Broitman, "Indentation Hardness Measurements at Macro, Micro, and Nanoscale: A Critical Overview," *Tribol. Lett.*, vol. 65, no. 1, pp. 1–18, 2017.
- [121] J. Menscik, "Simple models for the characterization of the mechanical properties by nanoindentation," vol. 5. 2011.
- [122] C. Anthony, F. Cripps, "Nanoindentation," Third edition springer, 2011.
- [123] M. A. Meyers and K. K. Chawla, "Mechanical Behaviour of Materials," 2009.
- [124] A. Pulnikov, P. Baudouin, and J. Melkebeek, "Induced stresses due to the mechanical cutting of non-oriented electrical steels," *J. Magn. Magn. Material*, vol. 254–255, pp. 3, 2003.
- [125] A. Ben Ismail, M. Rachik, P. E. Mazeran, M. Fafard, and E. Hug, "Material characterization of blanked parts in the vicinity of the cut edge using nanoindentation technique and inverse analysis," *Int. J. Mech. Sci.*, vol. 51, no. 11–12, pp. 899–906, 2009.
- [126] W. C. Oliver and G. M. Pharr, "An improved technique for determining hardness and elastic modulus using load and displacement sensing indentation experiments," 1992.
- [127] Y. L. Shen and X. H. Tan, "On the correlation between hardness and yield strength in multilayered elastic-plastic materials," *J. Mater. Sci.*, vol. 40, no. 17, pp. 4683–4686, 2005.
- [128] A. E. Giannakopoulos and S. Suresh, "Determination of elastoplastic properties by instrumented sharp indentation," *Scr. Mater.*, vol. 40, no. 10, pp. 1191–1198, 1999.
- [129] T.A. Venkatesh, K.J. Van Vliet, A.E. Giannakopoulos and S. Suresh, "Determination of elastoplastic properties by instrumented sharp indentation: guidelines for property extraction," *Scripta mater.* 42 (2000) 833–839, Pergamon, elsevier, 2000.
- [130] B. Poon, D. Rittel, and G. Ravichandran, "An analysis of Nano indentation in elastic-plastic solids," *Int. J. Solids Struct.*, vol. 45, no. 25–26, pp. 6399–6415, 2008.

- [131] C. Heinrich, A. M. Waas, and A. S. Wineman, "Determination of material properties using Nano indentation and multiple indenter tips," *Int. J. Solids Structure*, vol. 46, no. 2, pp. 364-376, 2009.
- [132] P. Zhang, S. X. Li, and Z. F. Zhang, "General relationship between strength and hardness," *Mater. Sci. Eng. A*, vol. 529, no. 1, pp. 62–73, 2011.
- [133] ASTM Int., "Standard Test Methods for Tension Testing of Metallic Materials 1," ASTM, no. C, pp. 1–27, 2009.
- [134] M. J. Sablik, T. Yonamine, F. J. G. Landgraf, "Modelling plastic deformation effects in steel on hysteresis loops with the same maximum flux density," *IEEE Transaction of Magnetics*, Vol. 40, pp. 3219-3226, 2004.
- [135] H. Lemmen and R. Alderliesten, "The power of Digital Image Correlation for detailed elastic-plastic strain measurements," *Emeseg*, pp. 73–89, 2008.
- [136] M. A. Sutton, J. J. Orteu, and H. W. Schreier, "Image Correlation for Shape, Motion and Deformation Measurements, Basic Concepts, Theory and Applications" Springer Science, ISBN: 978-0-387-78746-6, 2009.
- [137] C Donaldson, G H Lecain, and V C Goold, *Tool Design*, Third edition, Tata McGraw-hill edition, 35th 2005.
- [138] ASTM, A341/ A341M, "Standard Test Method for Direct Current Magnetic Properties of Materials Using D-C Parameters and the Ballistic Test Methods," pp.1–13, 2011.
- [139] A. S. for T. and Materials, "Standard practice for labelling art materials for chronic health hazards," 1984 Annu. B. ASTM Stand., vol. 94, no. Reapproved, pp. 956–960, 1984.
- [140] W. D. Callister, D. G. Rethwisch, "Materials Science and Engineering, an Introduction," Eighth Edition, Wiley Inc., 2010.
- [141] ASTM, A1036-04, "Standard Guide for Measuring Power Frequency Magnetic properties of Flat-Rolled Electrical Steels Using Small Single Sheet Testers," pp. 1–5, 2009.
- [142] ASTM, A804/A804M-04 "Standard Test Methods for Alternating-Current Magnetic Properties of Materials at Power Frequencies Using Sheet-Type Specimens," pp. 1–15, 2009.
- [143] B. S. En 60404-4, "Magnetic materials –Methods of measurement of D.C magnetic properties of magnetically soft material," pp. 1–26, 1997+A2 2008
- [144] F. Barrell, "Capacitors, Magnetic Circuits and Transformers," *Electronics and Power*, vol. 12, no. 1. p. 17, 1966.
- [145] D. F. O. R. Development and D. D. I. E. C. Ts, *Rotating electrical machines*. 2002.
- [146] B.L. Theraja, A.K. Theraja, "Electrical technology," Volume I, S. Chand and company LED. 2005
- [147] E3-11, "Standard Guide for Preparation of Metallographic Specimens 1," ASTM, vol. I, pp. 1–12, 2011.

- [148]K. Geels, W. Kopp, and M. Ruckert, "Metallographic and Material graphic Specimen Preparation, Light Microscopy, Image Analysis and Hardness Testing. 2007.
- [149]Buehler Sum-Met, "A Guide to Materials Preparation & Analysis. 2004.
- [150]Jeol, "A Guide to Scanning Microscope Observation," Image Rochester NY, pp. 1–36, 2004
- [151] M. Shabani and A. Mazahery, "Prediction of mechanical properties of cast A356 alloy as a function of microstructure and cooling rate," Arch Metal Mater, vol. 56, pp. 671-675, 2011.
- [152]Z. H. Chen, L. C. Chan, T. C. Lee, and C. Y. Tang, "An investigation on the formation and propagation of shear band in fine-blanking process," J. Mater. Process. Technol., vol. 138, no. 1–3, pp. 610–614, 2003.
- [153]Y. Wen, Z.H. Chen, and Y. Zang, "Failure Analysis of a Sheet Metal Blanking Process Based on Damage Coupling Model," JMEPEG, 3288-Volume 22 (11) Journal of Materials Engineering and Performance , 2013.
- [154] M. Wang, W. Lun, "Micro-scaled Products Development via Micro-forming," Springer, ISBN 978-1-4471-6325-1, 2014.
- [155] H. Hoffmann, S. Hong, "Tensile Test of very thin Sheet Metal and Determination of Flow Stress Considering the Scaling Effect," Vol. 55(1), pp.263-266, 2006.
- [156] T.A. Kals, Ralf Eckstein, "Miniaturization in sheet metal working," 103, pp.95-101, 2000.
- [157] ISO 6892-1:2016, BSI Standards, Ambient Tensile Testing of Metallic Materials, pp.1-5. Available at: www.instron.com.
- [158]H. Ghadbeigi & C. Pinna & S. Celotto" Quantitative Strain Analysis of the Large Deformation at the Scale of Microstructure: Comparison between Digital Image Correlation and Microgrid Techniques" Society for Experimental Mechanics, 52:1483–1492, 2012.
- [159]Sutton MA, Turner JL, Bruck HA, Chae TA" Full-field representation of discretely sampled surface deformation for displacement and strain analysis. Experimental Mechanics, 31(2):168–177, 1991.
- [160]D. Miyagi, Y. Aoki, M. Nakano, and N. Takahashi, "Effect of Compressive Stress in Thickness Direction on Iron Losses of Non-oriented Electrical Steel Sheet," IEEE Transactions on Magnetics, VOL. 46, NO. 6, pp 2040-2043, 2010.
- [161] R. L. Mason, R. F. Gunst, and J. L. Hess, Statistical Design and Analysis of Experiments. 2003.
- [162]P. G. Mathews, Design of Experiments with MINITAB. ASQ Quality Press, 2005.
- [163]R. K. Roy, Design of experiments using the Taguchi approach: 16 steps to product and process improvement. John Wiley & Sons, 2001.
- [164]Davis Software, Manual, V8.4, LaVision, 1005, 1003001, DaVis-D84, 2017.
- [165]Strain Master, help, LaVision, 1003017, StrainMaster-D84, 2017.

Appendix A

The normal strain (also called principle strain) represents the strain component E_{xx} , or E_{yy} in a rotated coordinate system, the bigger value is called maximum normal strain, the smaller minimum normal strain. The maximum shear strain is the shear in a coordinate system 45° , where the residual shear becomes maximum. The Local strain coordinate system is shown in the Figure 0.5.

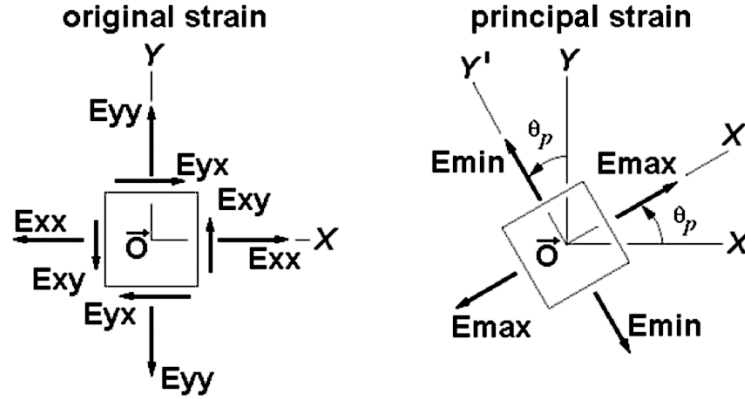


Figure 0.1: local strain coordinate system [164].

The 2D strain components can be calculated using the following matrix, where each parameter value for which a differential equation under given conditions [165].

$$\begin{vmatrix} E_{xx} & E_{xy} \\ E_{yx} & E_{yy} \end{vmatrix}$$

The following formulas express the calculation of the maximum and minimum normal strain modes. In addition to the shear and equivalent strains [164, 165]:

$$E_{\max} = \frac{E_{xx} + E_{yy}}{2} + \sqrt{\left| \frac{(E_{xx} - E_{yy})^2}{4} + \frac{E_{xy} + E_{yx}}{2} \right|}$$

$$E_{\min} = \frac{E_{xx} + E_{yy}}{2} - \sqrt{\left| \frac{(E_{xx} - E_{yy})^2}{4} + \frac{E_{xy} + E_{yx}}{2} \right|}$$

$$E_{\text{shear}} = \sqrt{\left| \frac{(E_{xx} - E_{yy})^2}{4} + \frac{E_{xy} + E_{yx}}{2} \right|}$$

The equivalent strain can be calculated according to the following equation:

$$E_{eq.} = \frac{2}{3} \sqrt{\frac{3(e_{xx}^2 + e_{yy}^2 + e_{zz}^2)}{2} + \frac{3(\gamma_{xy}^2 + \gamma_{yz}^2 + \gamma_{zx}^2)}{4}}$$

where e and γ are the engineering and shear strains respectively.

Appendix B

According to the Figure 4.84, the grain size was estimated using the following formula:

$$\text{Average grain size} = \text{line length} / \text{numbers of grains over the line}$$

Table 0.1: Grains size calculations for both ES thickness 0.2 and 0.35 mm.

0.2 mm Sheets thickness					
	line	No. of grains	Length (μm)	Average Grain size (μm)	ASTM G
	LI (1)	18	1839	102.16	3.7
	LI(2)	18	1869	103.8	3.7
Sum:			3708	205.96	7.4
Mean:			1854	102.98	3.7
Std dev			21.21	1.1597	
Min:			1839	102.16	3.7
Max:			1869	103.8	3.7
0.35 mm Sheets thickness					
	line	No. of grains	Length (μm)	Average Grain size (μm)	ASTM G
	LI (1)	11	1747	158.8	2.6
	LI(2)	13	1736	133.5	2.6
	LI(3)	14	1781	127.2	2.6
Sum:			5264	419.5	7.8
Mean:			1755	139.83	2.6
Std dev			23.46	16.7	
Min:			1736	127.2	2.6
Max:			1781	158.8	2.6